Nanoscopic Surface Modification for Biomimetic Surface Preparation in Biomedical Applications

A
Thesis Submitted
in Fulfillment of the Requirements
for the Degree of
DOCTOR OF PHILOSOPHY
by

ABSHAR HASAN

Under the Supervision of

Dr. Lalit M. Pandey

Department of Biosciences and Bioengineering
Indian Institute of Technology Guwahati
May, 2018

DECLARATION

This is to certify that the thesis entitled **"Nanoscopic surface modification for biomimetic surface preparation in biomedical applications"**, submitted by me to the *Indian Institute of Technology Guwahati*, for the award of the Doctor of Philosophy, is a bonafide work carried out by me under the supervision of Dr. Lalit M. Pandey. The content of this thesis, in full or in parts, have not been submitted to any other University or Institute for the award of any degree or diploma. I also wish to state that to the best of my knowledge and understanding nothing in this report amounts to plagiarism.

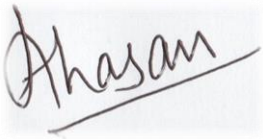

Abshar Hasan
Department of Biosciences and Bioengineering,
Indian Institute of Technology Guwahati,
Guwahati-781039, Assam, India.

Date: 14-11-2018

CERTIFICATE

This is to certify that the thesis entitled **"Nanoscopic surface modification for biomimetic surface preparation in biomedical applications"**, submitted by Abshar Hasan (146106020), a PhD student in the *Department of Biosciences and Bioengineering, Indian Institute of Technology Guwahati*, for the award of the degree of Doctor of Philosophy, is a record of an original research work carried out by him under my supervision and guidance. The thesis has fulfilled all requirements as per the regulations of the institute and in my opinion has reached the standard needed for submission. The results embodied in this thesis have not been submitted to any other University or Institute for the award of any degree or diploma.

Supervisor: Dr. Lalit M. Pandey
Department of Biosciences and Bioengineering,
Indian Institute of Technology Guwahati,
Guwahati-781039, Assam, India.

Date: 14-11-2018

ACKNOWLEDGEMENTS

First and foremost, I want to thank my PhD supervisor, Dr. Lalit M. Pandey, for believing in me and providing this opportunity. It has been an honor to be his first PhD student. He has taught me, both consciously and unconsciously, the importance of hard work and patience. I appreciate all his contributions of time, ideas, and suggestions to make my research experience productive and stimulating. The joy and enthusiasm he has for his research was contagious and motivational for me, even during tough times in the PhD pursuit.

Besides my advisor, I would like to thank the rest of my doctoral committee: Dr. Debasish Das (committee chairman), Dr. Nitin Chaudhary, and Dr. Soumen Maiti, for their insightful comments, suggestions and encouragement, but also for the hard questions which incented me to widen my research from various perspectives.

My special thanks to the Department of Biosciences and Bioengineering (BSBE), Indian Institute of technology Guwahati for giving me a chance to be a part of this prestigious Institute. The faculty members and staffs of BSBE are also acknowledged for their help and support. I am also highly thankful to the Central Instrument Facility (CIF), IIT Guwahati for letting me use all the sophisticated instruments that add up to my work.

Commonwealth commission, UK is highly acknowledged for providing me Commonwealth Split-site fellowship that financially helped me to carry out research for 12 months at University of Strathclyde, UK. I would like to express my special appreciation and thanks to my UK supervisor, Dr. King Hang Aaron Lau, you have been a tremendous mentor for

me. I would like to thank you for encouraging my research and for allowing me to grow as a research scientist. Thank you for accepting me for the exchange program, your advice on both research as well as on my career have been invaluable.

My time at Guwahati was made enjoyable in large part due to the many friends and groups that became a part of my life. I am grateful for their support and love through all my good and bad times. Faheem, Suraj, Tasleem, Adil and Ishani Chakrabartty hold special places in my life for being friends-cum-family. Evening tea with you all at near-by Dhabaas will be missed.

I thank my fellow labmates: Varun, Poulami, Sakshi, Swati, Gyan, Rahul, Aquib, Gayatri, and Abhishek for the stimulating discussions, for the sleepless nights we were working together before deadlines, and for all the fun we have had in the last four years. Especially Varun, who has taken care of all the IIT Guwahati formalities during my stay in UK. I also extend my sincere gratitude to Dr. Ishani Shukla for her generous support and valuable suggestions, without which this thesis wouldn't have been in this form.

I am also thankful to my postdoc at Strathclyde University, Dr. Kunal Tewari for being like my elder brother and introducing me to all new world of Synthetic Chemistry. Without you it would have been very difficult to grasp new concepts. I am thankful to my UK labmates: Marwa, Ana Sousa, Alasdair for helping me in various forms during my research.

Finally, but by no means least, thanks go to dad, mother, and family for almost unbelievable support and their trust in me. They are the most important people in my world and I dedicate this thesis to them. I would like to thank Almighty Allah for giving me determination and strength to do my research.

Sincerely
Abshar Hasan

ABSTRACT

Physicochemical interactions of proteins with surfaces mediate the interactions between implant and biological system. Surface chemistry of implants is crucial as it regulates such events at interfaces. The objective of this thesis was to explore the performances of the modified surfaces for such interactions relevant to various biomedical applications. The entire thesis has been divided into five main sections. The first section deals with surface modification via silanization and their in-depth characterization using high end techniques. With the wide range of surface wettability, we aimed to study serum proteins (BSA, FB, and IgG) behavior (i.e. conformations changes and their packing) during protein adsorption from single and binary solutions, which are comprised in the second section of this thesis. The change in surface functionalities resulted in variation in the physio-chemical properties such as roughness, wettability and energy that in turn regulated the protein behavior such as adsorbed mass, secondary structure, and protein orientation during single and competitive protein adsorption. The third section deals with the effect of adsorbed proteins on initial cell adhesion kinetics using mammalian fibroblast cell line (L929). Thereafter, the developed and characterized silanization technique was implemented to biomedically relevant Ti6Al4V surface for its possible application in bone tissue engineering. We also explored the adsorption pattern of cell adhesive fibronectin (FN) protein on these modified surfaces. We have reported that their cell binding motifs (RGD), which are enclosed in turns, gets more exposed on hydrophobic surfaces as compared to hydrophilic surfaces. These findings will help the surface scientists to design biocompatible surfaces with such carefully controlled surface properties for better cell adhesion. The fifth and the final section of the thesis

comprise of the synthesis and characterization of the novel peptidomimetics “peptoid” molecules for antifouling applications. These peptoids can be immobilized on the above modified surfaces to impart the additional antimicrobial features.

Contents

List of Figures

List of Tables

Abbreviations

SAMs	Self-assembled monolayers
TEOS	Triethoxyoctylsilane
APTES	Aminopropyl triethoxysilane
OTS	Octadecyltrichlorosilane
APTMS	3-Aminopropyl trimethoxysilane
MPTS	3-mercaptopropyl trimethoxysilane
PFS	Polytetrafluoroethylene
HAI	Hospital-acquired infections
PEG	Polyethylene glycol
PVP	Polyvinyl pyrrolidone
PEO	Polyethylene oxide
PU	Polyurethane
PDMS	Polydimethylsiloxane
PMPC	Poly-2-methacryloyloxyethyl phosphorylcholine
PMEMA	Poly-2-methoxyethyl methacrylate)
PLGA	Polylactic-co-glycolic acid
SPR	Surface plasmon resonance
QCM	Quartz crystal microbalance
XPS	X-ray photoelectron spectroscopy
HREELS	High-resolution electron energy loss spectroscopy
WCA	Water contact angle
FTIR-ATR	Fourier-transform infrared spectroscopy-attenuated total reflectance

ITC	Isothermal titration calorimetry
EDS	Energy-dispersive X-ray spectroscopy
FESEM	Field emission scanning electron microscopy
AFM	Atomic force microscopy
PBS	Phosphate buffer saline
FBS	Fetal bovine serum
FN	Fibronectin
IgG	Immunoglobulin-G
FB	Fibrinogen
HAS	Human serum albumin
BSA	Bovine serum albumin
ECM	Extracellular matrix
BCA assay	Bicinchoninic acid assay
MIC	Minimum inhibition concentrations
WPPCP	Water-phase precipitation copolymerization
ATRP	Atom transfer radical polymerization
SDS-PAGE	Sodium dodecyl sulfate polyacrylamide gel electrophoresis
FAK	Focal adhesion kinase
AMPs	Antimicrobial peptides
TDS	Thermal desorption spectroscopy
CVD	Chemical vapor deposition
PVD	Physical vapor deposition
VCAM-1	Vascular Cell Adhesion Molecule-1

ICAM	Intercellular Cell Adhesion Molecule
μM	Micromolar

Chapter 1

Introduction

When a biomaterial comes in contact with the biological environment, interactions of macromolecules at interfaces take place at the interface. These interactions decide the fate of biomaterials. Physical and chemical characteristics of a biomaterial implant surface such as surface potential, nanoscale surface chemistry, physical structure, wettability, and surface topology, etc. play a vital role in the above interactions [1-5]. These parameters have a huge impact on protein adsorption and repulsion, protein aggregation, protein displacement, cell adhesion and differentiation, and platelet adhesion and activation [2, 6]. Irrespective of the nature of the material (metallic, ceramic, polymeric, or composite), nonspecific protein adsorption is the first process observed at surface–biological system interfaces *in vivo* [7, 8], which adversely affects subsequent cellular interactions. This leads to deleterious cellular processes such as nonspecific immune cell attachment, platelet adhesion and activation, and finally host response [9]. This results in the loss of the sole function/purpose of the biomaterial and more over cause inflammatory responses due to rejection. Therefore, it is important to design (modify) surfaces of the bulk material in such a way that they become acceptable by the living body with a minimal host response. Various physical, chemical and biological approaches had been used till date to modify surfaces. The physical process, such as plasma treatment suffers from uncontrolled surface modification whereas biological processes involve immobilization of target biomolecules which struggles from stability issues. Chemical modification offers salient features to overcome

issues of stability, user friendly modification process and is relatively cost effective hence, has attracted huge attention of surface engineers in the material science field.

Silanization is becoming one of the most widely used functionalization techniques for modifying silica based surfaces via self-assembled monolayers (SAMs). It is often used to modify the physical and chemical properties of surfaces without affecting the bulk properties of materials. These modified surfaces find wide applications in surface science, microfluidic systems for nano/biosensors, surface patterning, drug delivery, immobilization of biomolecules, and many other fields [1-3, 6, 7, 9, 10]. Organosilanes are among the widely used organic molecules that can modify intrinsic properties of silica substrates by forming self-assembly via covalent linkage. An organosilane molecule basically consists of 3 parts (i) surface-reactive head group (-OR), which covalently attaches to surface silanol groups (-SiOH) via siloxane (Si-O-Si) bond formation, (ii) alkyl chain, which serves as a hydrocarbon chain spacer and (iii) terminal group (X) that imparts functionality to a silica surface. Although this process seems to be a simple reaction, but the actual process is very complex due to uncontrolled reactions and its sensitivity to reaction conditions such as temperature, moisture percentage, type of solvent, reaction time, concentration and solution age [11]. Due to the availability of a wide range of silanes with huge library of different functional head group, it is easier to prepare the desired functional moiety on surfaces. Although silanization is a widely used process for surface modification, its kinetics of surface modification is still uncertain and hence various researchers have reported different time constants. Due to this disparity among different researchers about the time constraints in SAM formation kinetics, we studied SAM formation of triethoxyoctylsilane (TEOS) on a silica substrate to determine the time constant of molecular attachment and re-orientation.

Bacterial colonization on implantable biomedical devices (e.g. catheters and orthopedic implants) and the consequent infections contribute to 40-70% of hospital-acquired infections (HAI). Various coatings have been reported for regulating bacterial fouling (e.g. antifouling polymers such as polyethylene glycol (PEG), immobilized antibiotics, and antimicrobial peptides). In spite of some successes, they suffer from short lifetime, susceptibility towards protease degradation, difficulty to synthesize and cytotoxicity. Recently, Lau et al. pioneered surface-grafted polypeptoid brushes that inhibited non-specific protein adsorption and bacteria attachment [12, 13]. Various antimicrobial peptoids sequences were synthesized and characterized using mass spectrometry and their antimicrobial activity was investigated.

1.1. Objectives

With the aim to bridge the knowledge lacuna as reviewed in Chapter 2 and to provide deeper insight into the processes of protein adsorption and cell adhesion on surfaces, the five thesis objectives are as follows:

1. Synthesis and characterization of modified substrates with varying wettability using different organosilanes for the formation of mono, mixed and hybrid SAMs.
2. Study of the adsorption behavior of serum proteins from mono and binary protein solutions on the above modified surfaces.
3. Adhesion of fibroblast cells on the above modified surfaces with and without pre-adsorbed proteins.
4. Modification of titanium surfaces with different SAMs and study of cell adhesive protein adsorption and subsequent cell adhesion.

5. Synthesis and characterization of antimicrobial peptoids for antifouling applications in biomedically relevant surfaces.

1.2. Thesis Outline

The thesis has been organized into eight chapters based on the above five objectives. A chapter-wise thesis outline is as follows:

Chapter 2

This chapter is dedicated to critical reviewing of the existing literature about surface modification and its effect on protein adsorption and cell adhesion behavior. Various types of modifications based on polymers have been mentioned while SAMs of alkanethiols and organosilanes have been majorly discussed.

Chapter 3

This chapter discusses the modification of silica substrates using silanization method. Surfaces were modified with the aim of generating wide range of wettability by forming mono, mixed and hybrid SAMs. Modified surfaces were physically and chemically characterized in terms of surface functional groups, wettability, surface energy, roughness and morphology. We also studied the kinetics of SAM formation on silica substrate using triethoxyoctylsilane as a model silane coupling agent.

Chapter 4

This chapter focuses on the performances of the modified surfaces for interactions relevant to various biomedical applications. With a wide range of surface wettability, we aimed to study protein behavior (i.e. conformations changes and their packing) during competitive protein adsorption. Three serum proteins (bovine serum albumin, BSA; fibrinogen, FB; and immunoglobulin G, IgG) were tested for their conformational changes and orientation upon adsorption on hydrophilic (COOH and amine), moderately hydrophobic (mixed and hybrid) and hydrophobic (octyl) surfaces. Side-on and end-on orientations of adsorbed protein molecules were analyzed using theoretical and atomic force microscopy (AFM) analysis. A theoretical analysis was also used to determine the percent (%) secondary structures of competitively adsorbed proteins from BSA/FB and BSA/IgG binary protein solutions.

Chapter 5

In this chapter, we described the effect of previously silanized five different (amine, octyl, mixed, hybrid and COOH) surfaces on fetal bovine serum (FBS) protein adsorption and initial cell adhesion (upto 6 h) under three different experimental conditions: (a) with FBS in media, (b) with pre-adsorbed FBS on surfaces and (c) incomplete media, i.e., without FBS. Cell features such as cell morphology/circularity, cell area and nuclei size were studied for the above stated conditions at different time intervals.

Chapter 6

This chapter discusses about the surface modification of the biomedically relevant titanium alloy (Ti6Al4V) and their potential scope in tissue engineering applications. Different

modified surfaces resulted in different behavior of cell adhesive fibronectin (FN) protein in terms of adsorbed mass and secondary structure. Secondary structure of adsorbed FN was found to play major role in fibroblast cells adhesion and spreading.

Chapter 7

In this chapter, we synthesized and characterized antimicrobial peptoids sequences with N and C terminal modifications. The sequences were successfully tested against *E.coli* and *P.aeroginosa* and exhibited low minimum inhibition concentrations (MICs) values.

Chapter 8

This chapter summarizes the contributions and also gives directions for future research.

Chapter 2
Literature Survey

This chapter reviews existing literature on various methods of surface modification of biomaterials and their implications on protein adsorption and subsequent cell adhesion. Different types of SAMs and factors governing their formation on surfaces are reviewed in depth. At the end, the effects of organosilanes SAMs surfaces on protein adsorption and cell adhesion are discussed.

2.1. Biomaterials and the Need for Surface Modification

A biomaterial may be defined as any foreign material, irrespective of its origin (naturally derived or artificially synthesized), that interacts with biological systems for the analysis of human physiological parameters (for example blood glucose level) and the replacement and treatment of damaged tissues and organs, which improves the quality of life. Various applications of such materials are well known and few are still in the process of improvement on many aspects. Based on applications, they have been designed separately for example soft and hard tissues and dental materials (Figure 2.1) require a sufficient load-bearing capability. Moreover, depending on the functions and biological environment, hemo-compatibility and osseo-compatibility are crucial to *in vivo*. Biomaterials of the macro- and nanoscale size (Figure 2.1), can be administered orally or by intravascular/intramuscular injections. Site specific drug

delivery systems have enabled to deliver the drugs in a prescribed manner in order to enhance the drug effectiveness with reduced side effects [14].

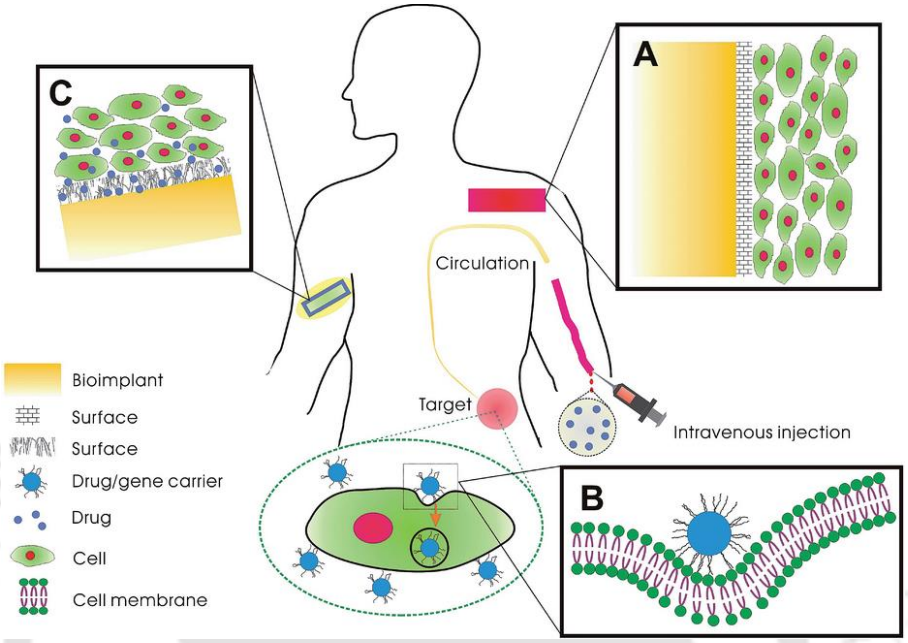

Figure 2.1. Roles of biomaterials. Adapted from ref. [14] with permission from The Royal Society of Chemistry.

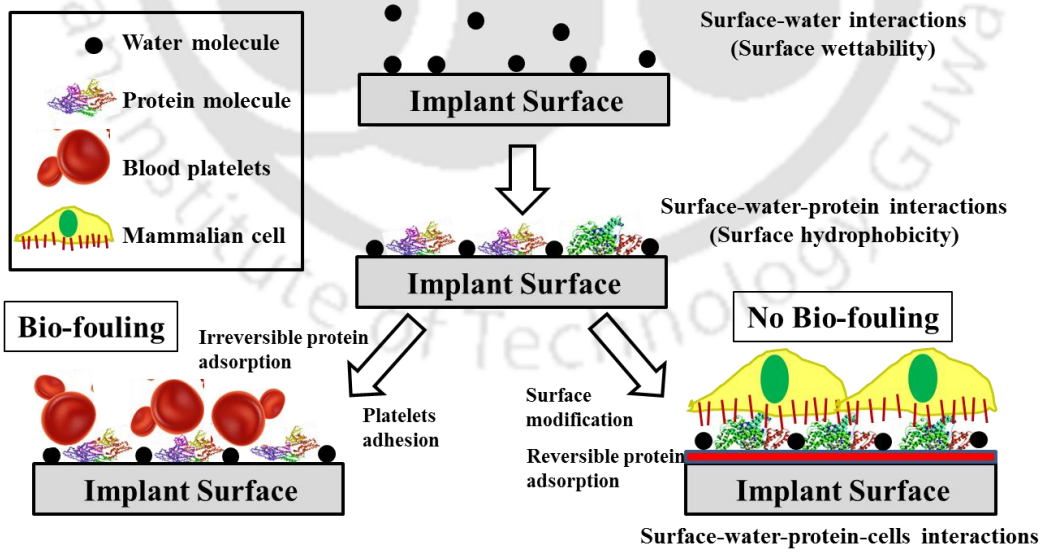

Figure 2.2. Schematic representation of implant's surface bio-fouling and its prevention after surface modification.

Consistent improvements and innovations in the material science over the last few decades had huge and sustainable impact in the progress of biomaterials and resulted in advanced medical devices and implants [15, 16]. When an implant or any other biomaterial comes in contact with the biological environment, it is the surface and not the bulk material that interacts with the body fluids. At these interfaces, a cascade of reactions/processes take place such as protein adsorption and displacement, cell adhesion and platelet adhesion etc. These biomolecules have huge recognition power down to molecular level due to specificity towards foreign materials via various binding interactions arising because of surface topology, nanoscale roughness and chemical properties. Still, many of the biomolecules undergo physical adsorption process on solid surfaces without any specific interactions known as nonspecific adsorption. Such a process may result in loss of the functionality of the interface that may finally lead to biofouling. For example, the nonspecific adsorption of proteins initiates unwanted biological responses that favors platelets adhesion and activation and may result in immunological reactions leading to the implant failure (Figure 2.2).

Therefore, in order to avoid such nonspecific interactions, interfaces are to be designed in such a way that they promote specificity so that the sole purpose and function of the implant remains intact. Understanding the basic underlying principle behind such process at the interface is the key to design a successful biocompatible material. Physiochemical properties of the biomaterial surfaces like surface roughness, surface potential, hydrophobicity and surface chemistry regulate such processes taking place at surface-biological system interfaces. Such properties can be tuned by carefully tailoring surfaces via physical, biological and chemical modification routes.

The physical methods for surface modifications mainly include plasma and laser treatment. The other techniques which are also employed are (Ultra Violet) UV irradiation, γ-ray, flame and plasma treatment, electron beam, corona discharge, and ion beam treatments etc. The major drawback associated with physically modified surfaces is a short aging time (poor stability) due to loss of modified surface characteristics when exposed to environments like air and blood [17]. Biological methods include physical adsorption of molecules via hydrophobic or Van der waal interactions, cross-linking and immobilization of biomolecules (such as proteins, cells, enzymes, DNA/RNA and polysaccharides etc.). They also suffer from the same issues of poor stability due to a short aging time. Chemical methods have shown promising stability due to covalent attachment of molecules on the surfaces resulting in a longer shelf life. SAM is one of the most widely employed methods which have attracted huge attention among surface chemists around the globe. Self-assembly of molecules upon adsorption on solid or liquid surfaces from solution or gases state results in the formation of SAM [18]. Surface modified with such one-molecule-thick layer provides excellent systems for studying the phenomenon and reactions taking place at interfaces. They have been divided into two major groups based on molecules used for the SAM formation. One group includes small molecules (eg. thiols, silanes etc.) while the other group includes long chain of macromolecular constituents with surface recognizing/binding units.

2.2. Polymers as Surface Modifying Agents

Polymers such as poly(vinyl pyrrolidone) (PVP), poly(ethylene glycol) (PEG), polyethylene oxide (PEO), polyurethane (PU), PDMS (polydimethylsiloxane), poly(2-methacryloyloxyethyl phosphorylcholine) (PMPC), and poly(2-methoxyethyl methacrylate)

(PMEMA) and their copolymers, etc. have been exploited for modifying biomaterial surfaces due to their one or the other property which are essential in producing protein repellent surfaces and antifouling surfaces [19-24]. Surfaces which inhibit non-specific protein adsorption, bacterial and platelet adhesion are referred as antifouling surfaces. Figure 2.3 shows the representation of surface modification using polymers, modified polymers and SAMs for antifouling applications.

PVP has been widely used in various fields such as pharmaceutical tablets, disinfectants, hydrogels, and drug delivery systems due to its excellent solubility in water (being hydrophilic) [25, 26]. Modified PVP such as PAN-g-PVP [27] and crosslinked PVP [28] have shown promising antifouling property and are comparable to PEO and PEG. Wan et al. showed the increasing antifouling property of PAN-g-PVP due to the introduction of PVP in copolymer synthesized via water-phase precipitation copolymerization (WPPCP). Decrease in water contact angle measured by goniometer clearly confirmed the hydrophilic nature of copolymeric surface responsible for reduced protein adsorption [27].

In another study, atom transfer radical polymerization (ATRP) method was employed to initiate the polymerization of vinylpyrrolidone on silicon substrate to yield low fouling surfaces grafted with PVP. PVP of 15.06 nm thickness and with contact angle (θ) of 24° was found to be most effective in reducing the adsorption amount of fibrinogen (FB), human serum albumin (HSA), and lysozyme by 75, 93, and 81%, respectively [29].

Telford et al. were first to synthesize and report thermally induced cross-linked PVP method for better antifouling coatings [28]. It was suggested that the C-H group present on the pyrrolidone ring and on the backbone chain undergoes homolytic cleavage to generate radicals that form interchain C-C bonds resulting in cross-linking. Polymer density, thickness and

viscosity could be easily tailored by changing temperature. Antifouling properties of modified PVP are comparable to PEG modified surfaces and hence, it finds its wide application area in biosensors and biochips, central venous catheters, hemodialysis and blood purification units [30-32].

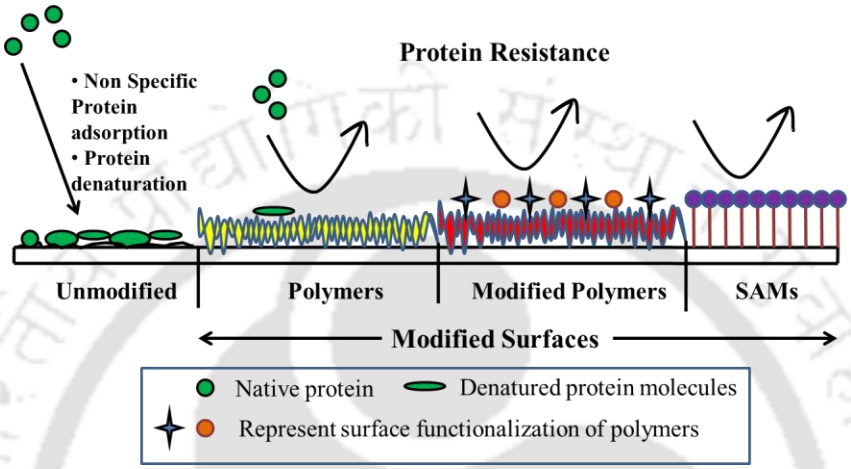

Figure 2.3. Pictorial representation of surface modification using polymers and SAMs for antifouling surface preparation.

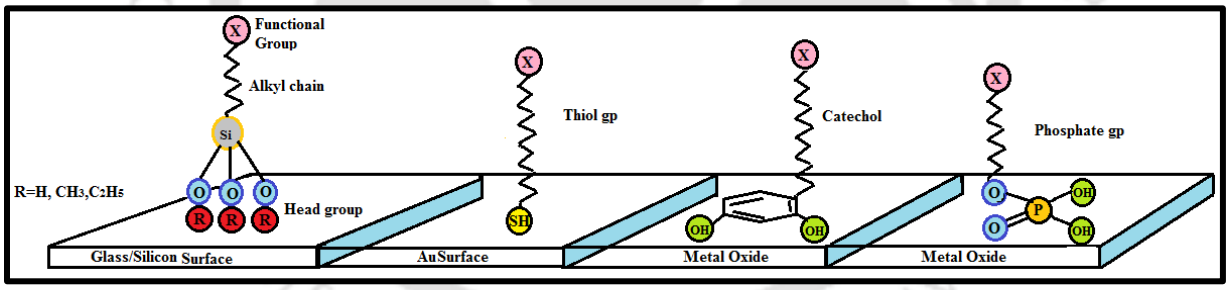

Figure 2.4. Typical representation of SAM formation on glass/silicon oxide, gold, and metal oxide substrates showing end group attached to substrate, alkyl chain, and functionalized head group (X) exposed on the surface.

The major drawback in using PVP is its poor stability and polymerization problems which limits its boundaries for its short term applications. The major polymerization problems associated with PVP are (i) physical coating of PVP goes off with time, (ii) low graft density by UV-initiated graft polymerization method, (iii) loss of mechanical properties by γ-radiation

method, (iv) loss of biocompatibility due to plasma treatment method [33]. Various polymers and co-polymers have been tabulated along with their applications and results on protein adsorption in Table 2.1.

Table 2.1. Various polymers and copolymers as surface-modifying agents, their methods of application, and salient results

Polymer(s)	**Method(s)**	**Protein(s) studied**	**Reaction condition (s)**	**Surface analysis**	**Measuring method**	**Results**	**Ref.**
PAAm, PMEMA, and PAAm–PMEMA modified Si substrate and silica particles	Atom transfer radical polymerization (ATRP)	Bovine serum albumin (BSA)	Phosphate buffer (PBS) containing BSA (0.50 mg/ml) for 2 h at 37ºC	FTIR, XPS, WCA	UV spectrometry	Higher resistance for protein adsorption was observed for the PMEMA- and PAAm–MEMA-modified particles.	[6]
PAN-b-PVP	Water-phase precipitation copolymerization	BSA	2 and 5 g/l in PBS (pH 7.4, 30°C, 24 h)	Copolymer was characterized by FTIR, ^{1}H NMR and DSC and membrane by WCA	Spectrophotometric method	Remarkable suppression in BSA adsorption was observed.	[27]
PDMA	SI-ATRP	Europium labelled HAS	Dynamic-equilibrium and Static equilibrium protein binding	XPS	QCM-D	1) Dynamic-equilibrium results showed no protein adsorption to the grafted QCM crystal. 2) Static-equilibrium protein binding assays showed decreased protein adsorption with increasing molecular weight.	[34]
PDMVSA, PDMMSA and PMPC	Polymers were grafted onto cellulose membrane via ATRP	platelet-poor plasma (PPP) made from fresh blood	2mL of PPP at 37 ◦C for 90 min	ATR-FTIR, XPS, WCA and TGA	Bicinchoninic acid (BCA) protein assay	All zwitterionic substrates exhibited better resistance to nonspecific protein adsorption and platelet adhesion.	[22]
PDMVSA, PDMMSA and PMPC	Modification via SI-ATRP on	Platelet-poor plasma	Substrates were contracted	XPS, WCA, AFM	BCA assay	Reduction in amount of protein absorbed at modified-SR than	[35]

	Silicone Rubber (SR)	(PPP)	with PPP for 90 min, 37°C			pristine-SR.	
PEG	Grafting on aldehyde activated glass or polished silicon wafer	BSA, Fibronectin (FN)	30 µg/ml FITC-labeled Fn at 37°C, 2 h	XPS and VASE	Ellipsometry, fluorescence microscopy and radio-labeling techniques	Initially protein adsorption decreased with increasing PEG chain density until 0.12 chains/nm^2 PEG, and then increased for 0.29chains/nm^2PEG.	[19]
PEG	APPLD and APPECVD	BSA and Fibrinogen (FB)	0.1 mg/ml protein solution in PBS (pH 7.4, RT) for 2h	ToF-SIMS, XPS	XPS, ToF-SIMS and radiolabelled techniques	90% protein reduction on APPLD-PEG surfaces while on APPECVD-PG shows 50 to 85% reduction.	[36]
Dendronized Poly-PEG brush	Polymerization via SI-ATRP on PDMS substrate	Labelled protein (BSA, chicken egg albumin and lysozyme)	1mg/ml protein in PBS (pH 7.4, 37°C, 1 h)	ART-IR, XPS,	Fluorescence microscopy	PolyPEG brush grafted PDMS showed significant reduction in protein adsorption in comparison to pristine PDMS.	[37]
PEG-Methoxy group	Covalent binding of PEG on polyaniline film	BSA and γ-globulin	2 mg/ml BSA solution in PBS(pH=7.4), 25°C, 24 h	XPS, AFM, WCA	UV-visible spectroscopy	Modified surface showed lesser BSA and γ-globulin adsorption ability of 0.2 and 0.51 µg/cm^2 respectively in comparison to control (BSA and γ-globulin, 1.0 and1.8 µg/cm^2, respectively).	[21]
PEG like gradient {diethylene glycol dimethyl ether (DG) as a monomer}	PECVD	HSA and FBS	HSA(0.1 mg/ml) and FBS (1.02mg/ml) in PBS, pH 7.4, 37°C, 1 h and 24 h incubation	XPS	XPS and ToF-SIMS	1) Amount of adsorbed HSA increased with decreasing ether (PEG-like) film chemistries. 2) XPS revealed significant protein adsorption at surface ether concentrations of less than 70% in the gradient films.	[38]
PEO	Polyaniline film was grafted with PEO via chlorosulfonation	BSA	BSA (0.2 mg/ml) in a NaAc/HAc buffer (pH 7.1), 4°C, 24 h	XPS and WCA	Coomassie brilliant blue method using UV spectrophotometer	BSA adsorption was reduced by more than 80%.	[39]

	method						
PEG -g-SEBS	SEBS film membranes modified with PEG through plasma treatment and UV-irradiated	BSA and FB	Protein (1 mg/ml) in PBS (pH 7.4, 2h, RT)	XPS and WCA	QCM-D	Protein adsorption reduced to 493 and 1205 ng/ml for BSA and fibrinogen, respectively for SEBS-g-PEG-1 and further to 45 and 237 ng/ml for SEBS-g-PEG-2 from 427 and 2002 ng/ml of pristine SEBS.	[40]
Chitosan backbone grafted with PEO	Polymers were attached to gold surface via solution adsorption, covalent coupling, and microcontact printing (μCP)	BSA and FB	Protein solutions were prepared in HBS-EP buffer at pH 7.4, 37°C	INE, DLS and SANS	Surface plasmon resonance (SPR) and INE	1) Protein adsorption decreased on increasing polymer layer thickness via all three mentioned methods. 2) PEO-density for protein suppression: Electrostatic adsorption>covalent coupling>μCP.	[41]
P(*n*EOMA) modified silica particles	Surface initiated polymerization	BSA	0.40 mg/mL of BSA/PBS, at 37°C, 2 h	ESR and FT-IR	UV-Spectrophotometer	BSA adsorbed for polymer density is shown as 1.5±0.2μg cm^{-2} (n = 1), 1.8±0.2μg cm^{-2} (n = 2), 2.2±0.2μg cm^{-2} (n = 3)	[42]
PHEMA and PDMAEMA brushes on PVDF	PVDF surfaces modified via SI-ATRP	BSA	BSA (1g/L) stock solution for 30 min	FTIR, XPS, SEM, AFM, WCA	Cross-flow membrane filtration and fouling reversibility experiments	Modified PVDF membrane with PHEMA and PDMAEMA showed higher antifouling property than unmodified PVDF.	[43]
PIBS, PS	Electrospinning and Compression Molding	Insulin, Ubiquitin and Lysozyme	Protein solution containing 10pmol/μL of each protein in 0.01M ammonium acetate(pH =4.4,5.4 and6.9), 37°C, 100 rpm	SEM and WCA	MALDI-ToF MS	1) Electro-spinned fibers showed higher hydrophobicity and surface-to-volume ratio than compression molded flat surfaces leading to higher protein adsorption. 2) Comparatively PIBS fiber mat showed higher protein adsorption than PS fiber mat due to thin polyisobutylene layer to the fiber surface.	[44]
PLA, PGA	Chemical	BSA	4 ml of	Single	BCA assay	1) Co-polymer brushes	[45]

and PCL brushes and their co-polymer brushes with methoxy/hydroxyl OEG	grafting		PBS (pH 7.4, 37°C, containing different concentration of BSA)	wavelength ellipsometer		with a polyester as the first layer and OEG as the outer layer showed increased resistance to protein adsorption 2) Maximum resistance to protein adsorption was found for PGA on mixed OEG-OMe and OEG-OH substrates.	
PMPC, PCBMA, PSBMA and PHEMA	Polymers grafted on silicon substrate via Surface-initiated(SI)-ATRP	Proteins relative to 100% Fetal Bovine Serum (FBS)	100%, FBS, 37°C, 30 min	XPS, Ellipsometry, AFM, WCA	Quartz crystal microbalance with dissipation (QCM-D)	Thick zwitter ionic polymer-grafted substrates showed less protein adsorption than nonionic polymer-grafted substrates.	[20]
PMPC and PHEMA	SI-ATRP	FB	AFM cantilever contacted with 1 mg/ml Fibrinogen (PBS, pH 7.4, 37°C, 0.5h)	AFM, ellipsometry,	AFM	Adsorptive force between fibrinogen immobilized cantilever and polymer brush layers was measured by f-d curve. Increasing Mw of polymer increased protein repulsive force.	[46]
PMPC	PMPC was grafted on silicon substrate via SI-ATRP	FB	^{125}I radiolabeled fibrinogen in TBS buffer(pH 7.4, 23°C), 2h	WCA, XPS, AFM and ellipsometry	Radiolabeling method	Significant decrease in fibrinogen adsorption on increasing graft density and chain length. Protein level <10 ng/cm^2 at graft density 0.29 chains/nm^2 and chain length ≥100 units.	[47]
P(SBMA-b-NaSS) and P(SBMA-co-NaSS)	PSf surface modification via SI-ATRP	BSA, BSF	BSA and BFG,1mg/ml each in PBS (pH 7.4, 37°C) 2 h	FE-SEM, ATR-FTIR, XPS,WCA	BCA assay	The lowest adsorbed protein amounts were 2.7 and 2.4 µg/cm^2 for BSA and BFG, respectively.	[48]
PSBMA	PSf surface modification via SI-ATRP	BSA, BSF	BSA and BFG,1mg/ml each in PBS (pH 7.4, 37°C) 2 h	SEM, AFM, ATR-FTIR, XPS, WCA	BCA assay	The amount of adsorbed BSA and BSF were ~2µg/ml for PSBMA-PSf in comparison to 19 and 17.5µg/ml at pristine PSf and PSf-Chloride, respectively.	[49]
PSBMA, PCBMA	Polymers were	FB and FN		ESCA and WCA	Enzyme-linked	1) PSBMA and PCBMA conjugated surfaces	[50]

with Carboxyl as terminal groups	grafted on TLP films Via carbodiimide reaction.				immunosorbent assay (ELISA)	almost inhibited protein adsorption at pH 3 and 6.5. 2) Polymer density and length of PSBMA didn't produce much protein resistance.	
PU modified with PMA, PST, PEO	Blending followed by solution casting	HSA, IgG and FB	PBS (pH 7.2), containing 35 g/ml Fg, 5 mg/ml HSA and 0.1 mg/ml IgG	WCA and Surface tension measurement, XPS	Perfusion model and radio labeled assay	Protein adsorption reduced at modified surface than unmodified surfaces with PMA showing minimum adsorption.	[3]
PVP	PES/PES-NH^2 surface modification via SI-ATRP	BSA, BSF	BSA and BFG,1mg/ml each in PBS (pH 7.4, 37°C) 1 h	ATR-FTIR, SEM-EDS, WCA	BCA assay	Suppression in protein adsorption; lowest values for BSA and BFG were 4.25 and 4.1 $\mu g/cm^2$ respectively.	[51]
PVP-b-PMMA-b-PVP Triblock	RAFT	BSA	BSA,1mg/ml in PBS (pH 7.4, 37°C) 2 h.	TGA, XPS, FRIR, SEM	BCA assay	BSA adsorption was reduced to a large extent with minimum BSA adsorption of ~10$\mu g/cm^2$	[52]

PEG is highly hydrophilic and increases the water uptake capacity of the modified matrices resulting in the minimum protein adsorption [53] hence, well known for its protein repellent property. Factors such as PEG molecular weight (Mw), chain density, chain length and chain topology also effects protein adsorption at matrices [19, 54-56]. Lower PEG chain density yields mushroom confirmation while a higher density predominantly produces brush confirmation [57]. Malmesten et al. reported that an increasing chain density increased protein repelling capacity irrespective of grafting method for higher Mw PEG and was maximum for 0.1 chain/nm^2 [58]. Recently, Sun et al. reported decreased adsorption of FITC labeled FB until PEG density reaches 0.12 chains/nm^2 but adsorption slightly increased for 0.29 chain/nm^2 PEG [19]. Highest PEG grafted surface showed more BSA adsorption than FB, probably due to higher Mw of FB over BSA. Another study also revealed that PEG copolymer with poly lactic-co-glycolic

acid i.e. PLGA (PLGA/PEG diblock) having higher Mw PEG (5000) caused more protein adsorption comparatively than PLGA/PEG (750, 2000). Bulky PEG (5000) causes more matrix swelling effect, increasing protein adsorption [53]. Numbers of ethylene oxide units per chain (i.e. chain length) also affect protein adsorption and found an inverse relationship with protein adsorption to some extent. It was found that at a chain length of 2-7 oligomers terminated-SAM attached on gold surface showed maximum protein repulsion [59] while Lee and Laibinis reported maximum protein repulsion for 2-3 oligomers long chains [60]. Donna group synthesized PEG like gradient by DG monomer via PECVD method and using electrode at 5W and 30W load power. 5W gradient showed no HSA adsorption in comparison to higher adsorption at 30W gradient. Moreover, higher PEG like gradient chemistry showed less adsorption of HSA and bovine serum [38].

However, stability of coated polymer is also important along with antifouling property. Decrease in antifouling activity with time is the major concern for PEG (co)polymers coated biomaterials [61]. For example, PDA substrate coated with thiol-terminated methoxy-poly(ethylene glycol) (mPEG-SH) could exhibit antifouling properties against mammalian cell for 2 days. While Ding et al. synthesized PEG-b-cationic polycarbonate diblock copolymers which showed negligible amount of blood protein adsorption and inhibited *S. aureus* biofilm for a period of 7 days [62]. PolyPEG was able to produce significant reduction in protein adsorption even after 30 days of membrane synthesis [63]. Tendency to undergo oxidation at physiological conditions and thermal instability [64] make PEG unsuitable for most of the applications and hence need modifications.

2.3. Self-Assembled Monolayers (SAMs)

SAMs are highly oriented, ordered and two-dimensional molecular arrangements (as shown in Figure 2.3) formed on the surfaces (in the form of thin films) due to high specificity towards substrate resulting in spontaneous adsorption of the SAM molecules. Preparation of organic thin films by the deposition of long-chain carboxylic acids on solid surfaces was first studied by Blodgett in 1935 [65, 66]. Zisman et al. in 1946 demonstrated the formation of self-assembly of long chain hydrocarbons containing polar groups during surface modification [67]. Later in years 1978 and 1980, Polymeropoulos and Sagiv recognized the usefulness of these monolayers and were able to synthesize uniformly ordered monolayers of organosilanes on the silicon oxide surfaces from solution via the dip casting method [68, 69]. "Self-assembled monolayer" was termed by Sagiv et al. in 1983 due to the property by virtue of which monomers assemble themselves into monolayers [70].

Pioneer works on silane and thiol based monolayers by Sagiv [69, 70] and Nuzzo and Allara [71] on the glass and gold substrates, respectively have introduced a wide area for research and development in the field of surface science. Analysis of such monolayers has been made easier with inventions of tools around that time, which can analyze surfaces at the microscopic level such as scanning probe microscopies and grazing-incidence X-ray diffraction. Great interest among researchers for such systems was developed due to their salient features like: easy to prepare, tailoring surface properties by changing surface chemistry at nanoscale level, immobilization of biomolecules and other chemical functionalization on such monolayer systems, and patterning of surfaces for multifunctional moieties preparation for different applications [72].

Generally, preparation of SAMs (Figure 2.4) involves amphiphilic molecules which comprise of three parts: (i) the head group, (ii) molecular spacers (eg. alkyl chain) and (iii) free terminal functional group. The head group has specific affinity for substrate which helps in adsorbing and packing of molecules in an edgewise fashion. The molecular spacer lies between the head and terminal functional groups having a typical length of 1-3 nm, which determines the SAM thickness. The functional group at the end of the SAM molecule remains free and available for further modifications and mostly determines the physical and chemical properties of the modified surfaces. Another category of SAMs has also been used for surface modification which is based on arrangement of macromolecular chains. They contain specific surface active units which help them in attachment to different substrates on the basis of their specificity.

SAMs have been widely exploited for carefully altering surface properties of glass, silica, metals and polymers as shown in Figure 2.4. It finds huge applications in the synthesis of biomaterials for various biomedical purposes and also in semiconductor industries as well. Gold and other metal surfaces are modified by thiolsilanes while silicon/glass surfaces are modified by alkylsilanes for various applications in the biomedical field. Promising role of SAMs in fabricating materials of any shape and size (particularly nanomaterials) has helped in improving knowledge in nanoscience and nanotechnology for associating molecular level structures to macroscopic phases [73].

2.3.1. Chemical Modification of Gold Surfaces by SAMs

Gold has been the most widely used substrate for SAM preparation and application due to various characteristic properties which may or may not be offered by other metal substrates. These properties include: (a) inertness; due to which it does not get oxidized with atmospheric oxygen and react with other chemicals and thus provides easiness in sample preparation, (b)

highly biocompatible, (c) can easily form thin films which serves as substrates for a number of existing sophisticated analytical techniques like surface plasmon resonance (SPR), quartz crystal microbalance (QCM) and ellipsometer etc. (d) easy to pattern using different lithographic techniques [18]. "Bottom-up" approach has been used for creating complex 2D-structures on gold surfaces by adsorption of various sulfur containing molecules via chemical bonding (thiolate-metal bonds in case of thiols) with surfaces. Surfaces modified by thiolate assemblies had been widely used in various fields such as biotechnology, electrochemistry, medicine (therapy), micro/nano-fabrication of biosensors, electronic and other optically active devices [74-76].

2.3.1.1. SAMs Preparation and Structure

Gold surfaces show high affinity towards the attachment of alkanethiols without forming any substitutional sulfide interphase [71]. Gold and other noble metals (eg. silver) surfaces can be modified by adsorption of organosulfur containing compounds such as thiols (HS-R-X), dialkyldisulfides (X-R_1-S-S-R_2-X), and dialkylsulfides (X-R_1-S-R_2-X), exposing the functional group (X) away from surface (R represents alkyl group) as shown in Figure 2.5. More details about other SAM systems can be seen elsewhere [18, 77].

The formation of SAMs of alkanethiolates on gold surfaces takes place due to strong chemisorption of these sulfur containing molecules via Au-thiolate bond formation. This Au-S bond is quite strong with hemolytic bond strength of roughly 40 kcal mol^{-1}. The reaction starts with the oxidative addition of the S-H bond to Au surface, followed by removal of hydrogen molecule by reduction process, as shown in expression 2.1 [77].

$$R - S - H + Au_n^0 \rightarrow R - S^- Au^+ \cdot Au_n^0 + {}^1/_2\, H_2 \qquad (2.1)$$

Structure formed by these monolayers is well established and involves the sulfur atoms to coordinate to the threefold sites of Au (111) surface giving 30º tilted trans conformation to the well-ordered and closely packed alkyl chains [78]. This 30% tilt in the alkyl [$(CH_2)_n$] chains with surface normal helps in minimizing the free volume and maximizing the van der Waals interactions between alkyl chains. Studies from X-ray photoelectron spectroscopy (XPS),high-resolution electron energy loss spectroscopy (HREELS), and thermal desorption spectroscopy (TDS) revealed that S-S bond in dialkyldisulfides gets cleaved at room temperature resulting in Au-S bond formation with S-C bond tilted away from normal [79-81]. Unlike alkanethiols and disulfides, dialkylsulfides gets attached to the surface by dative bonds.

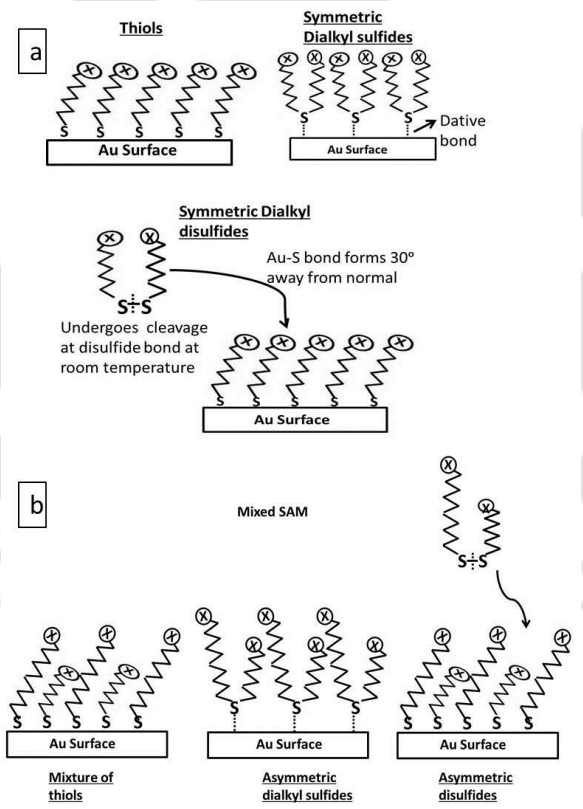

Figure 2.5. (a) Mono/single SAM of thiols, dialkylsulfides, and disulfides. (b) Preparation of mixed SAMs using mixture of thiols, asymmetric sulfides, and asymmetric disulfides. Adapted from Ref. [82].

Figure 2.6(b) shows the structure of alkanethiol containing terminal functional group exposed away from the surface, which controls the properties of the interface. If the size of the functional group is smaller or equals to the size of methyl group then it hardly affects the structure of SAM. X ray diffraction studies by Fenter et al. [83] suggested that chemisorption of alkanethiols takes place in the form of dialkyl disulphides due to dimerization. Although, this unusual reaction was not supported by any other such evidences.

The preparation of the SAMs takes place spontaneously due to adsorption either from liquid or vapor phase (under high vacuum) [18]. Preparation of organosulfur SAMs on metal surfaces from solution is simple and requires dipping of cleaned substrate in ethanol solution, containing these monomeric molecules (in mM concentration) for 12-24 hrs. 'Single SAMs' are generally prepared by immersing substrate in an ethanolic solution having a single type of compound (molecules), whereas 'mixed SAM' are prepared either by coadsorption of different types (mixture) of alkanethiols (HS-R-X) in the same ethanolic solution or from adsorption of asymmetric disulfides (RSSR') or asymmetric dialkylsulfides (RSR') [84-86].

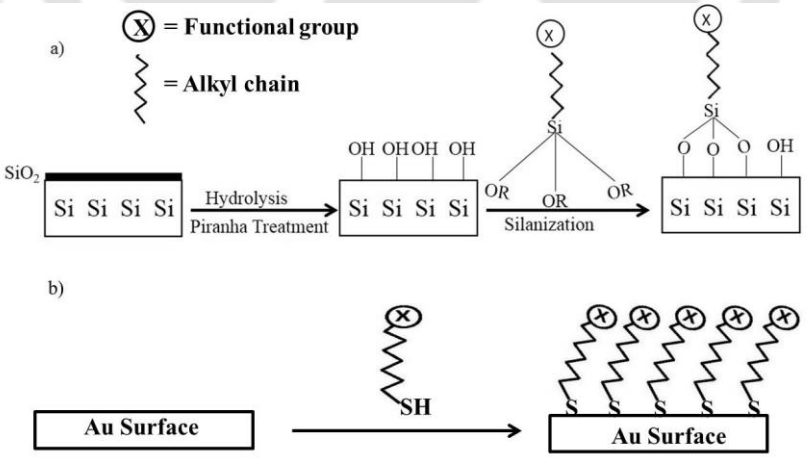

Figure 2.6. (a) SAM formation of organosilane on silicon surface and (b) Adsorption of alkanethiol on gold surface for SAM formation. Adapted from Ref. [82].

2.3.1.2. Single/Mono and Mixed SAMs

Single SAMs (for ex. thiolate SAMs) are easy to prepare and requires immersion of clean surfaces in ethanol solution having a single type of adsorbate. The commercially available gold surfaces or thin films deposited on silicon, glass or mica substrates are used as substrates. Thin films are deposited using one of the different available techniques like chemical vapor deposition (CVD), physical vapor deposition (PVD), or electrodeposition [87, 88]. The SAM formation starts spontaneously when such adsorbate in an appropriate concentration comes into contact with the freshly prepared and clean substrates. Attachment of alkanethiols results not only from the formation of Au-thiolate bond but also from the weak interactions (van der Waals and hydrogen bonding) with other adjacent molecules. Mixed SAMs are synthesized either from a mixture of alkanethiols ($R_1SH + R_2SH$) in the same solvent or from asymmetric disulfides and dialkylsulfides. Mixed SAMs offer the advantage of synthesizing gradients of interfacial composition for further studies like protein adsorption and cell adhesion. Experimental conditions such as the choice of solvent can affect the ratio of the adsorbing molecular components constituting the SAM. Chain length also plays an important role in the formation of the mixed SAMs. Alkanethiols with longer chains are found to be present at higher concentrations than a shorter alkanethiol. Mixed SAMs prepared from thiols are generally more stable than those prepared from disulfides and dialkylsulfides due to poor solubility [89]. Moreover, the SAMs synthesized from disulfides and dialkylsulfides also exhibit more defects than those formed by thiols [90]. The mechanism of the single and mixed SAM formation is shown in Figure 2.6(a).

2.3.2. Organosilane Based SAMs on Silicon Surfaces

The SAMs based on alkylsilanes are obtained by direct adsorption of organosilane via covalent attachment on hydroxylated surfaces from solution/vapor (shown in Figure 2.6(a)). Hydroxyl groups on silicon surfaces are generated by treatment with piranha solution or by oxygen plasma. Such hydroxyl terminated surfaces are highly hydrophilic and rapidly forms thin film of water which helps in the formation of well-packed monolayers [91-93]. The first report on the SAM formation by self-assembly of octadecyltrichlorosilane (OTS) on SiO_2 surface was published by Sagiv in 1980 [69]. He investigated the effect of water molecules on the SAM formation and revealed that adsorbed water molecules on surfaces play an important role in hydrolyzing OTS molecules. These hydrolysed molecules form polymeric network by further undergoing condensation reaction with other molecules and hydroxyl groups present on SiO_2 surface. There have been huge arguments on the mechanism of SAM formation on silica surfaces in the late 1980s and 1990s due to lack of appropriate instruments and techniques for verifying the SAM formation. Later in 1986, the view by Finklea et al. [94] further supported Sagiv's view on the ground that the SAMs of OTS can be prepared on surfaces without hydroxyl groups (eg. gold surface). They found well assembled OTS layer formed by siloxane linkage (Si-O-Si) on adsorbed water film on a gold substrate. This mechanism of the SAM formation was further confirmed by Silberzan et al. in 1991. Their report stated the formation of intermolecular siloxane bonds with few bonds attached to hydroxyl exposed surfaces resulting in the development of cross-linked polymeric network with terminal functional groups [95].

Complete absence of OTS silanization was observed during the SAM formation at room temperature on silica surfaces in carbon tetrachloride in deficiency of water [91, 96]. Wang et al. [97] reported the effect of solvent condition on the growth of a highly smooth SAM on

hydroxylated SiO_2. A very slow formation of the SAM resulted during 'dry preparation' in which water only in the form of thin layer was present on surface while solvent was hydrophobic and did not even contain traces of water. While during 'wet preparation', OTS undergoes fast hydrolysis in the presence of water molecules in solution and quickly condenses to form aggregates which gets adsorbed onto the surface. Surface modified due to such aggregate formation was although a very quick process but did not result in smooth coverage throughout the substrate as compared to 'dry' preparation.

Chemical vapor deposition (CVD) method of organosilane SAM formation [98] is also in much demand due to its several advantages over liquid based SAM deposition such as: less chances of multilayers formation due to controlled experimental factors, monolayers formed are of high quality and well-ordered with minimal defects, requires less volume of reagents. The monolayer film formation by CVD of organosilane depends on partial pressure, which can be obtained either by heating the system or reducing the pressure of the synthesis chamber by a vacuum pump. Table 2.2, shown below elaborates various reaction conditions on the SAM formation by different organosilanes.

Table 2.2: CVD of different organosilanes and the reaction parameters

Organo-silane	Substrate	Surface preparation	Temp. (°C)	Pressure	Time (h)	Ref.
APTMS	Glass	Piranha	NA	670 Pa	16	[99]
MPTS	SiO_2	Sulphuric acid/sodium peroxydisulphate	100	NA	NA	[100]
	Si	Piranha, oxygen Plasma	NA	1 mTorr	4	[101]
	Silica	Piranha, UV ozone	NA	200 mBar	0-120	[102]
OTS	Si	UV irradiation	150	NA	0.5-8	[103]
PFS	Si	UV irradiation	150	NA	0.5-8	[103]
	Si	$NH_4OH/H_2O_2/H_2O$ (1:1:4)	45	NA	3	[104]

Similar to alkanethiols, organosilanes also follow two stages kinetics for SAM formation. The initial fast adsorption of adsorbate molecules on surfaces undergoes phase transition from a lying down to a standing up phase. FTIR studies have revealed that 1mM concentration of OTS silane resulted surface coverage in 90 minutes [105].

2.3.3. Factors Governing the Formation of SAMs

2.3.3.1. Reproducibility

It is an important factor in the preparation of any kind of the SAM with the desired characteristic properties. Although, most of the experimental conditions yield reproducible SAMs but there still exist various defects and poorly ordered structure during preparation. There are a number of experimental factors that affect these structures and rate of the SAM formation.

2.3.3.2. Choice of Solvent

Studies revealed that the choice of solvent may affect the structure, assembly and rate of the SAM formation. The effect of solvent on the SAM formation kinetics is complex and not clearly understood even after four decades of research in this field. Ethanol is the most widely used solvent for alkanethiols due to its properties like availability in high purity grade, non-toxic, inexpensive and ability of solvating different alkanethiols irrespective of chain length. The rate of alkanethiol SAM formation was found to be higher than ethanol in certain non-polar solvents like hexane and heptanes. It was also seen that thiols SAMs formed from non-polar organic solvent resulted in poorly organized SAMs as compared to those from ethanol as solvent [84, 106]. Solvent-adsorbate and solvent-substrate interactions may obstruct the rate of SAM formation. For instance, adsorbate with more affinity towards the solvent will be attracted less

towards the substrate and also solvent having more affinity towards substrate need to be displaced prior to thiol adsorption. Hence, in such cases the rate of formation gets affected.

2.3.3.3. Concentration of Adsorbate Molecules and Dipping Time

These both parameters are inversely related as it takes less time for the SAM formation at a higher concentration. Temperature speeds up the rate of SAM formation with minimal defects, which are prepared at temperature above 298 K [107]. Factors such as purity of thiols, oxygen content and cleanliness of substrates also play critical role in preparation of highly ordered SAMs assemblies. These factors explained in more detail in the review article by Love et al. [18].

The SAMs formation of organosilanes on surfaces occurs by forming small homogenous islands distributed unevenly throughout the surface. Later, these islands like structures extend themselves depending on immersion time and concentration (immersion time reduces with increasing adsorbate concentration) resulting in complete coverage [108]. Initially, it was suggested that partially formed OTS monolayer comprises of islands structures which are heterogeneous in nature [109, 110]. Later various researchers, due to advancement of technology, concluded that these partial monolayers are although disordered but homogeneous [93, 111, 112]. OTS adsorption on glass, silicon oxide surface and mica was studied separately and confirmed the islands formation using AFM [113, 114].

2.3.3.4. Water

Water plays an important role in synthesizing a high quality SAM and its amount should be carefully controlled. Both deficiency as well as excess of moisture in solution can disturb the

structure and formation of the SAM. The absence of water results in incomplete formation of the SAM. While the excess moisture may cause polysiloxane formation within the molecules, resulting in adsorption of such structures with a lot of irregularities and defects [115]. Due to this reason, McGovern et al. [116] optimized the quantity of moisture (0.15mg/100ml of solvent) which should be present in the solvent for the formation of a highly ordered and packed monolayers. They suggested that hydrolysis of silanes into silanols is the initial step which is followed by condensation of silanols with surface, as a mechanism of the SAM formation. It was supported by Tripp and Hair [93] by describing conversion of methylchlorosilanes to methylsilanols by the thin layer of water present at a silica surface. Using FTIR analysis of amino modified silicon surfaces (using APTES, aminopropyltriethoxysilane), Kim et al. reported the fast condensation reaction between the head group (ethoxy, CH_3CH_2O-) of adjacent silane molecules and hydroxyl group (OH) present on piranha treated silicon substrates. This condensation reaction removes ethanol molecule and results in covalent attachment of silane molecule with silicon surface via siloxane (Si-O-Si) bond formation [117]. Banga et al. [114] studied the effect of open environment on deposition of octadecyltrichlorosilane (OTS) and (perfluoroalky1)trichlorosilane on silicon and glass surfaces. Using AFM, they reported the average surface roughness (R_a) was higher for a sample prepared in open atmosphere in comparison to closed clean room conditions. Moreover, the surfaces synthesized were not reproducible.

2.3.3.5. Temperature

The role and importance of temperature in the SAM formation was first demonstrated by Zisman et al. [67]. Soon after this report, they gave a brief account on the existence of threshold

temperature (*Tc*) above which the monolayer formation gets completely inhibited [118]. It was also observed that the bond formation was favored at a lower temperature. T_c is an intrinsic property (and do not depend on type of solvent) of a silane molecule below which a dense and ordered SAM formation takes place. This was further investigated by other researchers and concluded that temperature close to threshold temperature regulates the close packing of a high quality SAM formation in OTS [119, 120]. The rate of formation decreases with a decrease in temperature which results in a highly ordered self-assembly with minimal thermal defects and higher van der Waal's interactions [121]. It was also reported that for T_c to be function of the length of the alkyl chain; higher for longer chains and lesser for shorter chains [95]. Pasternack et al. [122] gave a contradictory report on the effect of temperature on monolayer formation. Higher solution temperature yielded denser aminopropyl silane (APS) film with well-structured and ordered monolayer. Conflict among various research groups about island-type growth or homogenous growth still exists in literature. It is also believed that islands-type growth pattern for the SAM formation takes place below the *Tc*. Whereas no islands-type SAM deposition was observed in reaction conditions having temperature higher than the *Tc*.

2.3.3.6. Solvent

The rate of monolayer formation can be widely affected by changing the solvent. With the help of in situ ellipsometry, Hoffmann and coworkers were able to determine the effect of solvent on the SAM kinetics. The rate of SAM formation varied by utmost factor of 50 when prepared from different solvents [123]. McGovern et al. [116] reported that an optimized quantity of water that should be present in the solvent to drive the rate of formation due to hydrolysis of silanes. They were the first to report that the hydrolysis process takes place in

solution and not on the surface. Moreover, solvents which can extract moisture from surfaces such as anhydrous toluene, enhances the rate of formation of ordered and densely packed SAMs.

2.4. Behavior of Biomolecules on Silane SAMs Modified Surfaces

2.4.1. Protein Adsorption

Attachment of biomolecules such as proteins and cells etc. to solid surfaces is a complicated process and is controlled by various factors such as physico-chemical properties of substrate, properties and structures of proteins, and environmental conditions. There are numerous reports on the behavior of proteins towards different surfaces [124]. Surface properties mainly wettability, is considered as an important factor that majorly controls protein adsorption and their conformational changes upon adsorption. Hydrophilic surfaces are known to exhibit poor protein adsorption while hydrophobic surfaces favor this process. Hydrophobic interactions between surfaces and hydrophobic domains of protein result in the release of bound water, this step is energetically favored due to less steric hindrance offered from almost no water molecules on hydrophobic surfaces [125]. On the other hand, hydrophilic surfaces have a layer of adsorbed water which offers steric hindrance for protein adsorption. Nonspecific protein adsorption is a curse to any material as it causes deleterious effects on its working efficiency and properties. It takes place due to tendency of proteins to adsorb physically on surface without any specific recognition and binding. Such nonspecific process triggers a cascade of reactions (such as foreign body reactions) that finally results in complete loss of the material.

Various other factors also participate in controlling protein behavior towards different surfaces such as wettability, surface potential and roughness. Hence, alkylsilanes have been extensively used for carefully tailoring surface hydrophobicity, roughness and other necessary

properties based on applications. Effect of different silane modified silicon surfaces on protein adsorption and cell adhesion has been presented in Table 2.3.

Table 2.3. Effect of different covalently functionalized silicon surfaces on surface properties and subsequent regulation of the biomolecules behavior at interface

Functional groups of alkylsilane SAMs	**Analytical technique(s) used**	**Surface properties (WCA)**	**Protein(s) studied**	**Cells used**	**Results**	**Ref.**
CH_3, CH_2=CH_2, Br, NH_2, COOH, PEG, OH	WCA, ellipsometry, AFM, SDS-PAGE	CH_3, CH_2=CH_2, Br →θ>80º NH_2, COOH →θ=48-62 º PEG, OH →θ<35º	Bovine serum	Fibroblasts	AFM confirmed nanoscale smoothness of modified surfaces. SDS-PAGE showed less protein adsorption on PEG and OH than to CH_3, NH_2 and COOH. Best cell growth, spreading and fibrinogen formation was observed at NH_2 and COOH due to enhanced activity of integrins on these surfaces.	[126]
OH, NH_2 and COOH	WCA, ellipsometry, FTIR, XPS, SEM	NH_2>COOH >OH>SiO_2	FB	MC3T3-E1	Calcium phosphate (Ca-P) was deposited on SAM modified surfaces. FB monolayer coverage was more on Ca-P coated-NH_2 SAM. But ALP activity was higher for Ca-P coated-OH and COOH SAM.	[127]
OH, CH_3, NH_2 and COOH	Ellipsometry, AFM	CH_3>NH_2> COOH>OH	Fibronectin (FN)	K562 Erythroleukemia cell	Effect of adsorbed Fn layer was investigated on integrin $\alpha_5\beta_1$ interactions. Fn adsorbed on COOH an OH surfaces showed better $\alpha_5\beta_1$ interaction than CH_3 and NH_3 surfaces.	[128]
OH, CH_3, NH_2, COOH, and C_6H_5	WCA, SEM	OH→ 52.8º COOH→54.7º NH_2→69.8º C_6H_5→92.3º CH_3→96.6º	NA	Saos-2	Cells showed slow proliferation rate on CH_3, OH, and C_6H_5 while COOH and NH_2 did not affect cell growth. Cells were also tested for	[129]

					apoptosis and expression of bone cell differentiation markers- osteonectin and osteopontin	
PEG	WCA	PEG→32º	FB and IgG	Fibroblasts and macrophages	PEG gold patterned silicon surfaces showed high resistivity towards protein adsorption and cell adhesion. This approach can be used for fabricating silicon based bioMEMs devices.	[130]
SOx, NH_2, $N^+(CH_3)_3$, –SH, and $–CH_3$	WCA, XPS and ATR-FTIR	SOx→7º NH_2→37º $N^+(CH_3)_3$→23º SH→63º CH_3→92º	NA	MC3T3-E1	Cells adhesion: SH> SOx≈CH_3> $N^+(CH_3)_3$≈ NH_2. SH surfaces exhibited least cell migration than $N^+(CH_3)_3$ and CH_3 surfaces. Cell area was least on SH surface and highest on $N^+(CH_3)_3$ and CH_3 surfaces.	[131]
CH_3, NH_2, COOH, and epoxide	WCA, XPS, ellipsometry and AFM	CH_3→103º NH_2→41.6º COOH→27.2º Epoxide→44.3º	RGD tripeptide	K100 erythroleukemia cells	Cell adhesion strength: CH_3<COOH ≈ epoxide<< NH_2 Cell adhesion strength increased in presence of immobilized RGD.	[132]
CF_3, CH_3, COOH, and NH_2	WCA	CF_3→110º CH_3→97.2º NH_2→51º	Fetal bovine serum	SV-40 human corneal epithelial cells	Surface chemistry influenced cell proliferation. Serum level did not affect cell behavior on modified surfaces.	[133]
$NH_2(CH_2)_2NH$- and CF_3	WCA, XPS	$NH_2(CH_2)_2NH$→32º CF_3→92º	FN	Endothelial cells	$NH_2(CH_2)_2NH$ with and without FN showed similar abilities to support adhesion, spreading, and proliferation of endothelial cells. Heparin sulfate on $NH_2(CH_2)_2NH$ inhibited cell adhesion.	[134]
EDA-[$NH_2(CH_2)_2NH$-]	WCA, XPS and ellipsom	EDA→8-32º PEDA→48-54º	NA	HUVECs	Cell surface area, shape, f-actin distribution, and adhesion strength of	[135]

PEDA-$[NH_2(CH_2)_2NH CH_2C_6H_5-]$	etry				HUVECs were investigated on EDA and PEDA. Cells on PEDA showed less spreading with round morphology and less tightly bound while EDA showed better cell spreading with tightly bound cells.	
CH_3, CF_3 and OH	WCA,TIRF	CH_3→109-111º CF_3→115-116º OH→54-56º	BSA and FB	NA	Single and competitive protein adsorption kinetics was investigated on hydrophobic surfaces. Both proteins from single protein adsorption show increased spreading rates with increasing hydrophobicity. From mixed protein solutions, initially proteins spreading continued till 2 h but later slowed down dramatically.	[136]

Wertz and Santore demonstrated the effect of hydrophobicity (CF_3>CH_3>>OH modified surfaces) on adsorption of BSA and Fibrinogen (FB) proteins from single solution as well as from mixed competitive environments [136]. Adsorption kinetics of single protein revealed increased spreading rate for initial 15 minutes, analyzed using TIRF. An increase in substrate hydrophobicity increased this rate from 0.02 to 0.16 nm^2/molecule and from 0.04 to 0.26nm^2/molecule for BSA and FB, respectively. Less spreading on hydrophilic surfaces resulted in more protein adsorption with minimal protein unfolding in comparison to hydrophobic surfaces. Both end-on and side-on orientation of protein adsorption was observed in the initial phase indicating no effect of hydrophobic and hydrophilic interactions until the proteins get

attached. Spreading rate was observed at a constant rate for competitive adsorption till 2 hrs, which later slowed down dramatically.

Silicon surface modified with thin layer of PEG was first put forward by Zhang et al. [137] using covalent attachment (siloxane bond) of PEG-O-$SiCl_3$ with surface silanols after hydrolysis. Later, various researchers used PEGylated silane for modifying surface with one step mechanism yielding uniform thickness (1-2 nm) throughout the substrate [138, 139]. Thickness can be regulated by varying molecular weight (chain length, OCH_2CH_2=2-17) of PEG. Lee and Laibinis tested various proteins ranging from low to high molecular weight (Mw) and reported that PEG monolayers could not resist high Mw proteins while they were quite effective against smaller proteins [60]. Moreover, PEG with longer chains offer great resistance for protein adsorption and cell adhesion in comparison to PEG with smaller chains.

Pandey and Pattanayek [140, 141] reported the effect of surface wettability and roughness on protein adsorption. A new surface called 'hybrid SAM' (formed by reaction between -NH_2 terminal groups of the SAMs and -NCO group of p-Tolyl isocynate, which contains a short hydrophobic and hydrophilic group in the same molecule) was also synthesized and compared with a single (amine, octyl) and mixed (amine-octyl, 1:1 v/v) SAM for physico-chemical properties and protein adsorption. The roughness parameter ($R_a = 1/n \sum_{i=1}^{n} |z_i|$, where z_i is the height of surface features) for clean, octyl, amine, mixed (amine-octyl, 1:1) and hybrid surfaces was 0.18 ± 0.1 nm, 0.83 ± 0.1 nm, 0.63 ± 0.1 nm, 1.61 ± 0.2 nm and 0.67 ± 0.1 nm, respectively. Using QCM, it was concluded that the adsorbed amount of protein on hybrid SAM was lower than hydrophobic (octyl) surface and close to amine surfaces. Structure/conformation of adsorbed BSA was shown to be preserved on hybrid SAMs, indicating their potential application for biomaterials. In another study, based on QCM analysis, the linear relationship

between wetting effect (difference of wetting tension of a solution and solvent) and adsorbed mass of protein/polymers on different SAMs was shown [142].

2.4.2. Cell Adhesion

Cell adhesion is a complex but an important event which regulates many cellular processes like cell migration, differentiation, proliferation, and cell signaling etc. for proper implant functioning. The adhesion of cells takes place via secretion of ECM protein on substrates which are recognized by cell membrane bound proteins called integrins. Integrins are trans-membrane heterodimeric (α and β subunits) proteins which bind to ECM proteins, cellular receptors like vascular cell adhesion molecule-1 (VCAM-1) and the intercellular cell adhesion molecule (ICAM) family to assemble actin cytoskeleton for signal transduction for different cellular functions [143-145]. Integrins bind ECM proteins via RGD (Arginine-Glycine-Aspartate) tripeptides. Cell adhesion on solid surfaces is either specific or nonspecific and is regulated by various parameters such as wettability, surface tension, surface potential/charge, roughness, surface chemistry (i.e. functional groups) and adsorbed protein etc. Surface chemistry plays a significant role in modulating cellular behavior and can be carefully tailored by using different SAMs (alkanethiols, organosilane and other polymeric) via surface modification.

Silane based surface modification delivers a tunable platform for providing different functionalities and their effects on cellular behavior. Various examples are presented in Table 2.3, to bring a clear image on how changes in functionality affect wettability and consequently protein adsorption and cell adhesion. The initial study on cell adhesion upon differently modified glass surfaces (having terminal groups-CH_3, SH, $SCOCH_3$, NH_2 and SO_3H) was carried out in 1990 and 1992 [146, 147]. They studied the adsorption mechanism of FB protein and later

interaction of fibroblasts and neuroblastoma cells with surfaces having adsorbed protein. Tzoneva et al. [148] studied the cellular behavior of endothelial cells on hydrophilic (cleaned glass, θ=24º) and hydrophobic (CH_3 modified, θ=86º) surfaces with FN and FB proteins. They demonstrated how wettability controlled cell adhesion and cytoskeletal arrangement of endothelial cells. Hydrophobic surfaces promoted cell-cell cohesion while hydrophilic surfaces promoted strong cell-surface attachment. Faucheux et al. [149] studied the effect of surface chemistry on fibrillar adhesions. Aminosilane and carboxysilane modified glass coverslips, having fibrinogen coating were investigated for fibrillar adhesion in fibroblast cells. Fibroblasts grown on NH_2 surfaces showed no focal contact segregation while this was favored on COOH grown cells indicating better adhesion on NH_2 modified surfaces. Moreover, cell migration was higher on COOH terminated surface further confirming poor adhesion on them.

Phillips et al. [150] described the effect of different surface chemistry on cell growth, morphology, proliferation, and differentiation of human mesenchymal stem cells (hMSC). They observed that the NH_2 SAMs coated with FN protein promotes differentiation of hMSCs into osteogenic and adipogenic lineages. While FN coated OH SAMs were highly permissive for osteogenic lineage and inhibited dipogenic differentiation. Moreover, FN adsorption also promoted cell adhesion to surfaces (CH_3) which were previously shown to resist cell adhesion. This implies that FN indirectly plays an important role in mediating cell adhesion for differentiation of MSCs to specific lineages. Other researchers have also reported the effect of surface topology, immobilized peptides, chemical functionalities, and the presence of induction medium on the controlled differentiation of MSCs [151, 152].

2.4.2.1. Role of Integrins in Cell Adhesion

Cell adhesion on surfaces is a receptor mediated process that involves interactions between receptors (known as integrins) present on cell surface and ligands (ECM proteins) to provide intracellular connections with the extracellular environment [153]. Integrins and cytoplasmic proteins assemble together to form a complex network called focal adhesions, which regulates interactions between cell and ECM, controls cytoskeletal dynamics and signaling [154-158]. Integrins are trans-membrane heterodimeric (α and β subunits) proteins which bind to ECM proteins, cellular receptors like Vascular Cell Adhesion Molecule-1 (VCAM-1) and the Intercellular Cell Adhesion Molecule (ICAM) family to assemble actin cytoskeleton for signal transduction for different cellular functions [143-145]. As shown in Figure 2.7 and discussed in Table 2.4, there exist 18 different types of α and 8 types of β subunits, associated non-covalently, combining in a heterodimeric fashion to form 24 integrins units that show specificity for different protein recognition and binding [143]. Extra cellular matrix is a three-dimensional scaffold that comprises of various proteins, glycosoaminoglycans and growth factors to provide support for cell adhesion, migration and proliferation into tissue [159-161]. Major ECM proteins such as albumin, laminins, fibronectin and collagens play a central role in integrin binding for cellular communication via intracellular signaling for cell-surface interactions. These ECM proteins are folded and held by disulphide bonds and interact with surface topologies via hydrophobic interactions [162]. Upon interaction with the surrounding environment, various signals are transmitted inside the cell that lead to changes in cellular behavior such as morphology, migrations and differentiation.

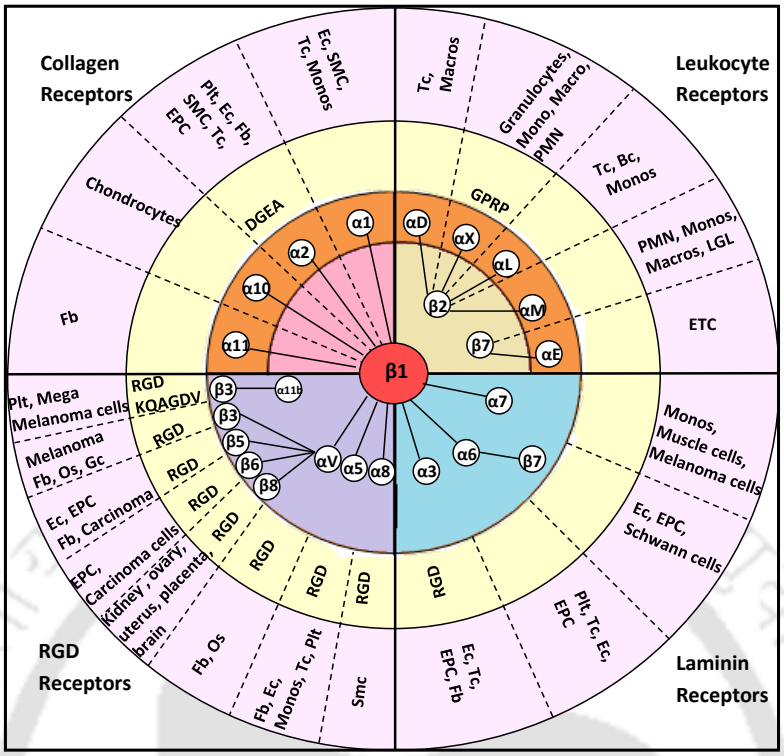

Figure 2.7. Integrin receptors and distribution.

Integrins are the major cell adhesion heterodimeric proteins present on cell membrane to transmit signals from the extracellular environment to cell and vice versa. Except erythrocytes, integrins are found in all metazoan and there number increases with increasing complexity. Extracellular regions of these heterodimeric receptors recognizes and binds to counter-receptors present on cells, bacterial polysaccharides, viral coat protein, or ECM proteins, while its intracellular domain is connected to focal adhesion elements which controls cytoskeletal (actin) arrangement and also regulates signaling pathways by contacting signal transduction machinery [143]. The extracellular domains (~80-150 kDa) are generally larger than transmembrane domain (~25-30 amino acid residues) and cytoplasmic domains (10-70 amino acids, except β4 integrin), studied using X-Ray Crystallography and Nuclear Magnetic Resonance (NMR) techniques [163-167]. It is to be noted that out of 18 α units, 9 α units (α1, α2, α10, α11, αD, αL, αM, αX and αE)

have extra inserted domain (called I or A domain, unknown function) of about 180 residues in transmembrane region, while remaining α subunits have ~25-30 residues due to post translational modifications [168].

Table 2.4. Integrins distribution, connections with cytoplasmic proteins and phenotypes in knockout mice

	Integrin subunit/Gene knockout	Viability	Integrin Distribution	Cytoplasmic proteins	Extracellular ligands	Knockout/defective Phenotype	Ref.
Collagen Receptors	α1	V,F	Smooth muscle, fibroblasts endothelium, hepatocytes, activated T-cells, neural cells	F-actin[169]	Collagen, laminin	Reduced tumor vascularization in adults, hypocellular dermis, increased collagen synthesis, defective cell attachment.	[170-173]
	α2	V,F	Various epithelia, endothelium, platelets, mesenchymal stem cells, leucocytes	F-actin	Collagen, laminin, E-cadherin, tenascin	Mild impaired hemostasis, delayed platelet aggregation, skin infections, defective cell attachment	[174]
	α10	V,F	Chondrocytes, fibroblasts		Collagen, laminin	Mild cartilage phenotype, growth plate defects	[175]
	α11	V,F	Subsets of fibroblasts, cancer associated fibroblasts, odontoblasts, mesenchymal stem cells		Collagen	Defective incisor eruption, dwarfism, increased mortality	[176-178]
RGD Receptors	α5	L,E10	Fibroblasts, endothelium, hepatocytes, platelets, lymphocytes		Fibronectin, osteopontin, fibrillin	Extra and intraembryonic vessel development defects, muscular dystrophy.	[181, 182]
	αv	E10/P,E12-birth	Endometrium, endothelium, osteoblasts, fibroblasts, glial cells, melanoma cells, keratinocytes	RACK1	Fibronectin, vitronectin, tenascin, osteopontin	Placental defects, cerebral vascular defects like cerebral hemorrhage, seizures, axonal degeneration	[183, 184]
	α8	P	Mesenchymal cells, various epithelia, endothelium, brain		Fibronectin, vitronectin, osteopontin	Kidney and inner ear defects	[185, 186]
	αIIb	V,F	Blood platelets, melanoma cells	Talin [179, 180]	Fibronectin, fibrinogen, vWF,ICAM	Glanzmann thrombasthenia, defective platelet aggregation, impaired hemostasis	[187, 188]

Leucocyte Receptors	αD	-	Macrophages and eosinophils		ICAM-3, VCAM-1	No obvious phenotype, mild, T-cell phenotypic changes	[189, 190]
	αE	V,F	Immune cells mostly		E-cadherin	Inflammatory skin lesions, defective gut associated lymphoid tissue	[191]
	αL	V,F	Leucocytes		ICAM-(1-5), JAM-1	[A]Impaired leukocyte recruitment and tumor rejection, reduced lymph node size, reduced neutrophil adhesion,	[192, 193]
	αX	-	Monocytes, macrophages, dendritic cells, NK cells Granulocytes, activated lymphocytes		iC3b, fibrinogen	[B]No obvious phenotype, affects monocyte firm adhesion	[194, 195]
	αM	V,F	Granulocytes, Monocytes, macrophages, NK cells, neutrophils		iC3b, fibrinogen,	[B]Defective development and function of mast cell, Impaired phagocytosis and PMN apoptosis; obesity;	[196-198]
Laminin Receptors	α3	L,Birth	Various epithelia, endothelium	BIN1 [199]	Collagen, laminin, fibronectin	[C]Defects in kidneys, lungs, and cerebral cortex; skin blistering	[200, 201]
	α6	L,Birth	Various epithelia, fibroblasts, neurons		Laminin	[D]Defects in cerebral cortex and retina; skin blistering	[202]
	α7	V,F	Muscle cells, melanoma cells		Laminin	Muscular dystrophy, defective placenta formation	[203]
	α4	L, E11–E14	Tumour cells (some), developing muscle, leucocytes	Paxillin [204]	Fibronectin, VCAM-I, MAdCAM	Defective placentation and cardiac hemorrhage	[205]
	α9	L, perinatal	Activated leucocytes			[E]Defective lymphatic system development	[206]
	β1	L, E5.5	Almost all vertebrate cells (fibroblasts, leucocytes, platelets, myocytes, endothelial cells)	Talin [179, 180], Filamin A, B [207], α-Actinin [208], Skelemin [209]	Collagens, laminins, fibronectin, VCAM-1	ICM deterioration, complete block of peri-implantation development	[215, 216]
	β2	V,F	Leucocytes, keratinocyes, endothelial cells	Filamin A, B [179, 207], α-Actinin [210]	ICAM-1,2, Fibrinogen, iC3b	[F]Defective leukocyte recruitment, T cell proliferation, skin infections	[217, 218]
	β3	V,F	Platelets	Talin [69], Myosin, Skelemin [209]	Most of ECM proteins	[G]Defective platelet aggregation, osteosclerosis,	
	β4	P	Epithelial cells	Plectin/HD1 [211], p27(BBP/eIF6) [212]	Laminin	Defective epithelial tissue, severe blistering of the skin	[219, 220]
	β5	V,F	Keratinocytes, epithelial cells, fibroblasts, osteoclasts, monocytes	Nischarin [213], Talin [214]	Vitronectin, fibronectin	No obvious defects in development, reproduction and healing of cutaneous wounds	[221, 222]
	β6	V,F	Basal airway epithelial cells		Fibronectin, tenascin C, ADAM,	[H]Skin and lung inflammation and impaired lung fibrosis	

					osteopontin Fibronectin,		[206]
	β7	V,F	Lymphocytes	Filamin A, B [207, 208]	VCAM-1,MAdCAM	[I]Impaired GALT formation such as Peyer's patches and mesenteric lymph nodes	[223, 224]
	β8	E10/P	Diffusely expressed on basal cells		Vitronectin, laminin, TGF b-LAP	Placental defects, defective CNS	[225, 226]

V = Viable; F= Fertile; L= Lethal; E#=Embryonic lethal # month
MAdCAM, mucosal addressin cell adhesion molecule; iC3b, inactivated complement component; ICM, Inner cell mass; GALT, Gut associated lymphoid tissue; vWF, von Willebrand factor; TGF b-LAP, transforming growth factor b latency associated peptide; ADAM,a disintegrin-like and metalloproteinase-containing protein
Human associated diseases: A= Psoriasis; B= Systemic lupus erythematosus; C-Interstitial lung disease, nephrotic syndrome, epidermolysis bullosa; D=Epidermolysis bullosa; E= Bilateral chylothorax; F=LAD1, leukocyte adhesion deficiency; G= Glanzmann's disease, excessive bleeding; H=Asthma; I= Inflammatory bowel disease

Arrangement of 18α and 8β subunits in 24 heterodimer integrin pairs have shown to have specificity for different ECM proteins like fibronectin, laminins and collagens as shown in Figure 2.7. In vertebrates, all collagen receptors (α1, α2, α10 and α11); and leucocytes receptors (αD, αE, αL, αM, αX) have inserted domains known as I or A domain [143, 227, 228]. Integrins α3β1 and α6β1 majorly recognizes laminin [229] and other integrin receptors that recognize RGD tripeptide sequence in fibronectin are α5β1, α8β1 and αvβ6, [143, 230]. Fibronectin can be recognized by eight integrins, they are α3β1, α4β1, α5β1, α8β1, αvβ1, αvβ3, αvβ6, and αIIbβ3. Leukocyte specific receptors in vertebrates such as αDβ2, αMβ2 also recognize immunoglobulins receptors and arbitrate cell-cell interaction [143]. Although integrins are known to be specific for ECM proteins recognition and binding but there exists redundancy for some interactions. For example, α1β1 and α2β1 are key receptors for collagen but they bind to laminins as well [168, 231]. Integrins like α4β1 and α9β1 not only recognizes ECM fibronectin but also interacts with membrane proteins of Ig superfamilies such as vascular cell adhesion molecule-1 (VCAM-1) and intercellular cell adhesion molecule (ICAM) for mediating cell-cell adhesion, αvβ1 binds to both fibronectin as well as vitronectin [143, 168]. In each protein, integrin binds to a specific peptide sequence that serves as a binding site for integrins and RGD

was the first sequence to be found acting as binding site in fibrinogen. The tripeptide sequence i.e. RGD (Arg-Gly-Asp) present in fibronectin, vitronectin and other adhesive proteins is the major ligand binding site. But apart from RGD, other peptide sequences have been reported that serve as binding sites for different integrins. For eg. αIIbβ3 recognizes KQAGDV in fibrinogen, α2β1 binds DGEA in collagen, α4β1 binds EILDV sequence in fibronectin and QIDSPL in (VCAM-1) and αXβ2 binds to GPRP of fibrinogen [168, 232].

2.4.2.2. Role of Focal Adhesion Kinase (FAK) in cell adhesion

Cell adhesion, spreading and migration are intracellular signaling derived processes which occur due to interaction of ECM proteins and cell via integrins. Integrin mediated interactions are important for arrangement of actin cytoskeleton at a focal contact which is controlled by tyrosine phosphorylation of various signaling proteins. Integrin clustering due to ECM and cell interaction results in the activation of various non-receptor protein kinases which further regulates the downstream signaling process by activating signaling proteins. FAK is one of the non-receptor and non-membrane linked Protein Tyrosine Kinase-2 (PTK-2), which plays a prominent role in integrin signaling as well as other intracellular signaling pathways. FAK was separately identified and reported as a highly tyrosine-phosphorylated protein by Steve Hanks, Jun-Lin Guan and Michael Schaller during 1991-92 and was for the first time linked as a role in integrin associated signaling [233-236]. Since, this 125 kDa protein is found to be co-localized at focal adhesion points inside the cell; it had been named as focal adhesion kinase [233]. FAK plays a central role in maturation and turnover of focal adhesions (or focal contacts) and acts as signaling kinases as well as scaffold protein, tethering various signaling molecules of different intracellular pathways into complexes [237]. Mesodermal cells from FAK knockout embryos

(FAK-/-) exhibited round topology with ventral surface carrying abnormally large number of focal adhesions resulting in slower migration rates which finally lead to embryonic lethality [238].

2.5. Conclusions

Based on the review of literature, it is well understood that SAMs are highly organized thin films that have been used for various surface modifications applications especifically for bone implants by virtue of their property of cell adhesion and spreading.

SAMs of organosilanes are well studied but their formation mechanism and time constants have still created disparity among researchers, and hence leave the scope to explore the possible mechanism and time constants. Adsorption behavior of various serum proteins such as BSA, FB, IgG have been widely studied on these modified surfaces in terms of adsorbed mass whereas protein conformations and organizations on surfaces after adsorption are less explored. Adsorbed mass of proteins as well as its conformations and packing depend on surface-protein interactions (i.e. hydrophobic interaction, hydrogen bonding and electrostatic interaction etc.) hence, effect of surface modifications on such interactions should be studied. Although cell adhesion behavior, their morphological changes have been studied on different functionalized SAMs surfaces but initial cell adhesion kinetics on such surfaces is not completely studied and well known. The present work endeavors to focus on time constant and SAM formation mechanism. Behavioral differences of proteins and cells on different surfaces have been co-related with the surface properties. This work provides the new insight to a more cyto-compatible, reproducible and long lasting surface modifications for biomedical applications.

Chapter 3
Surface Modification and Characterization

This chapter discusses the modification of silica substrate using silanization method. Surfaces were modified with the aim of generating a wide range of wettability such as hydrophilic (COOH surface), moderately hydrophilic (amine, mixed [amine:octyl], and hybrid) and hydrophobic (octyl) surfaces. Post modification, surfaces were characterized using Fourier-transform infrared spectroscopy (FTIR), contact angle (goniometer) and atomic force microscopy (AFM). Also, the kinetics of SAM formation on silica substrate using triethoxyoctylsilane as a model silane coupling agent is presented in this chapter.

3.1. Introduction

It has been reviewed extensively in Chapter 2 that surfaces can be modified via physical, chemical, physiochemical or biological routes. In the physical method i.e. physisorption- where physically adsorbed surface modifying agents are loosely bound, it was found that they are not stable for a long time, and hence are not appropriate to use for long term applications. Chemical methods such as oxidation and grafting offer a better stability as the modifying agents are covalently attached to the surfaces. Physico-chemical methods involve UV radiation, plasma treatment, and ion implantation. These techniques employ high energy photons (typically UV) to break chemical bonds of surface and desired groups react with the surface. Biological methods involve immobilization of biological molecules such as nucleic acids, proteins for various applications either by physisorption or by chemical methods.

SAMs of organosilanes are highly ordered, robust and are formed by covalent linkage with surfaces. Substrates were cleaned and SAMs were formed using silane-coupling agents, which are available with various functionalities and are relatively very cheap as compared to other modifications methods. Due to a disparity among different researchers about the time constant in SAM formation kinetics, SAM formation of triethoxyoctylsilane (TEOS) on a silica substrate to determine time constant for molecular attachment and re-orientation is studied.

3.2. Materials and Methods

3.2.1. Materials Used

Aminopropyl triethoxysilane (APTES, Cat. no. 440140), triethoxy(octyl)silane (TEOS, Cat. no. 440213), and anhydrous toluene were purchased from Sigma Aldrich, India. Methanol, toluene, circular glass wool, sulfuric acid (H_2SO_4), and potassium bromide (KBr), hydrogen peroxide (H_2O_2) and diiodomethane (MI) were procured from Himedia, India. P-doped silicon wafers ⟨100⟩ were procured from Macwin, India. Double distilled water (Mili-Q, 18 MΩ) was used throughout the work.

3.2.2. Cleaning of Silica/Silicon Wafer Surface

Circular glass coverslips (14 mm, diameter), glass wool, and $1\times1cm^2$ silicon wafer chips were cleaned using a severe cleaning procedure to ensure removal of all contaminants. The procedure is as follows:

Substrates were sonicated for 1 h in a piranha solution prepared freshly by mixing sulfuric acid and 30% hydrogen peroxide (H_2O_2) in 7:3 v/v. In later steps, these chips were sonicated for 30 min each in ammonia solution (Water: H_2O_2:NH_3=5:1:1 v/v) and in HCl

solution (Water: H_2O_2:HCl=3:1:1 v/v). Chips were washed with plenty of water after every step. Finally, washed chips were sonicated in acetone for 5 min before overnight drying in hot air oven at 75°C and were made ready for SAM modification.

3.2.3. Formation of SAMs

Monotype SAMs of amine (-NH_2) and octyl (-CH_3) silanes were formed using APTES and TEOS, respectively, by dipping cleaned surfaces in 1% respective silane solution (in anhydrous toluene) at room temperature (25ºC) under inert N_2 atmosphere. Mixed SAMs, comprising of mixture of NH_2 and CH_3 silanes was prepared by adding 1% of each silane in 1:1 ratio (v/v) under similar environmental conditions. For hybrid SAMs preparation, APTES modified surfaces were immersed in p-Tolyl isocynate solution (1%, v/v in anhydrous toluene) for 4 h in the presence of catalyst dibulyltin dilaurate [140]. Similarly, carboxylic (COOH) SAMs was prepared by oxidizing CH_3 modified surface in 5% acidified (w/w) $KMnO_4$ for 30 min at room temperature [239, 240]. Figure 3.1 shows the schematic representation of surface reaction during modifications.

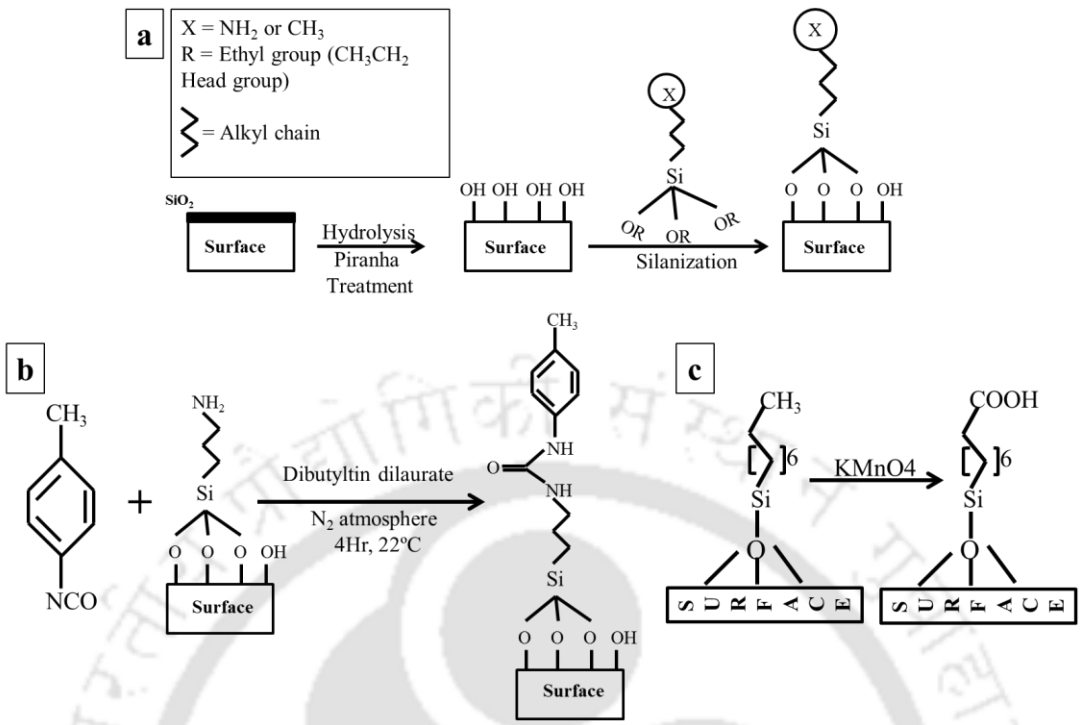

Figure 3.1. (a) Schematic representation of the silanization process on the Si surface, (b) formation of urea linkage on amine SAM during hybrid surface preparation, and (c) acidified oxidation of the CH_3 group of octyl SAM to carboxylic acid during COOH SAM preparation.

Post silanization, the substrates were sonicated consecutively in three different solvents i.e. toluene, mixture of toluene and methanol (v/v=1:1) and methanol for five min each. Finally, wafers were dried overnight at 37ºC.

3.2.4. Surface Characterization

Characterization of the modified surfaces was carried out using the following three methods. (i) The detection of newly formed functional groups on it by Fourier transform infra-red spectroscopy (FTIR), (ii) viewing topography of the modified surfaces using AFM, and (iii) measuring its contact angle against two low molecular weight liquids: water and methylene diiodide (MI).

We performed kinetic studies of the SAM formation by preparing hydrophobic silica surface using TEOS as a model silane coupling agent. FTIR characterization for kinetic studies was carried out on glass wool after certain time intervals, as specified in the following sections. AFM and WCA analysis were recorded soon after treatment with anhydrous TEOS solution after specified time intervals.

3.2.4.1. FTIR

Surfaces were characterized using FTIR (Spectrum TWO, Perkin Elmer) instrument for the conformation of surface silanization. Spectra were recorded at a scanning rate of 15 scans per second with resolution $1cm^{-1}$. Unmodified surface was taken as background every time the sample spectrum was recorded.

For kinetic studies, samples were prepared by making KBr pellet containing 5% cleaned glass wool. 10 µL of 1% TEOS solution (conc. 31.8mM) in anhydrous toluene was dropped on the pellet and left for reaction. The samples were scanned after different time periods (0, 0.5, 1, 2, 4, 8, 16, 32, 60 and 90 min). KBr pellet without glass wool was used as a control. Experiments were triplicated for calculating the standard deviation.

3.2.4.2. Water Contact Angle (WCA)

WCA was measured using well reported sessile drop method. Contact angle was recorded at three different spots on the same sample using Drop Shape Analyzer-DSA25 (Make: Kruss GmbH-Germany). Contact angles at modified surfaces were recorded at least at five different points on same sample and their average values were used [140].

For kinetic studies, surfaces analyzed were modified by forming SAMs of octylsilane by incubating chips in 1% TEOS (v/v) solution in anhydrous toluene for different time periods (0, 1, 2, 4, 8, 16, 32, 60, 90 min, 8.5 h, 17 h and 24 h).

3.2.4.3. Atomic Force Microscopy (AFM)

AFM analysis of modified surfaces (reaction time) were carried out in non-contact mode under clean room conditions at room temperature using Agilent model no. 5500 series with silicon nitride tip of <10 nm radius (Nanosensor, Model: PPPNCH). The roughness parameter ($R_a = \sum_{i=1}^{n}|z_i|$) where z_i is the height of surface features) and wavelength (λ_a) of the peaks and valleys on a surface were determined using the Gwyddion software (covered by GNU General Public License). Pandey and Pattanayek [140, 241] described the method for calculating roughness factor (R_f) and the frequency of texture on the surface was taken into account.

By assuming the spherical texture of surface with average wavelength, λ_a and average height, R_a, the profile perimeter can be calculated by fitting the circle of radius, R, to the profile arc ACB as shown in Figure 3.2.

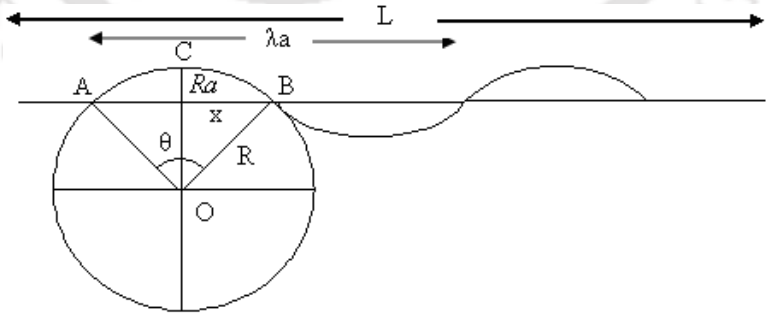

Figure 3.2. Surface profile of AFM image. Reproduced with permission [140]. Copyright 2011 Elsevier.

$The\ arc\ length\ (ABC) = R \times 2\theta \times {}^{\pi}/_{180}$, where $\theta = sin^{-1}({}^{x}/_{R})$ and R can be calculated using following expression:

$$R = \frac{{R_a}^2 + x^2}{2R_a} \quad (3.1)$$

The perimeter of the arc=2×arc ACB, considering the N numbers of waves in the scanned area, the complete profile perimeter will be:

$$P = \frac{4\pi RL}{180\lambda_a} sin^{-1}({}^{x}/_{R}) \quad (3.2)$$

The roughness factor, $R_f = \frac{P^2}{L^2}$, where P^2 is the profile area and L^2 is the scanned area.

3.2.4.4. Ellipsometry

Thickness of octyl monolayer on surface modified for 24 h of reaction time was analyzed from SEMILAB, Spectroscopic Ellipsometry Analyzer-SEA instrument (Model: GES5E). The instrument was equipped with a HeNe laser (632.8 nm) which was focused on sample at an angle of incidence of 70° and the data fitting was carried out using optical constants, n=3.871, k=0.0158 for Si substrate and n=1.521, k=0 for TEOS film [117, 242].

3.3. Results and Discussion

3.3.1. FTIR Spectroscopy

In the present study, we focused on determining the effect of different silanization time intervals on the growth of TEOS SAM on a silica substrate. The functional groups were investigated using FTIR as discussed in the material and method section. Figure 3.3 shows the FTIR spectra in the range from 2850 to 3000 cm^{-1} (stretching modes of CH_x) for different reaction time at room temperature. Although there is an ambiguity among researchers [243]

towards the occurrence of stretching modes of CH_x, as it may be due to the formation of the hydrolyzed product (CH_3CH_2OH) of silanization. But most of the research groups have reported the occurrence of such modes due to the presence of alkyl terminal chain on the surfaces [114, 244, 245]. The presence of symmetric (ν_s-CH_3) and asymmetric (ν_a-CH_3) stretching peaks of CH_3 at 2890 and 2962 cm^{-1} [246, 247] respectively and ν_s-CH_2 and ν_a-CH_2 vibration peaks at 2860 and 2920 cm^{-1} respectively confirm the silanization and the presence of octyl groups (see Figure 3.3). In particular, asymmetric and symmetric stretching peaks of CH_2 were observed at 2932 and 2864 cm^{-1}, which had shifted to 2920 and 2860 cm^{-1}respectively in the present work. This phenomenon is referred to as red shifting [122, 248]. Further, the above peaks had undergone narrowing with time. These red shifting and narrowing of peaks indicate a dense and solid packing of octyl groups due to rearrangement of the attached molecules [122, 248-251]. Increasing peak areas of asymmetric peaks are observed with increase in silanization time. This indicates the presence of more octyl groups on the surfaces with time, which leads to the formation of a complete octyl SAM. It is observed that there was not any significant increase in peak area after 16 min of reaction time, indicating the maximum attainment of silanization within this time.

Figure 3.4 shows the other spectral features of the adsorbed TEOS SAM in FTIR absorbance range of 900-1300 cm^{-1} containing different functional peaks [122]. The most relevant peak of Si-O-Si (siloxane group) is found at 1045 cm^{-1}, which may be attributed to silica substrate, condensation of silane with silica substrate or polymerization of silane molecules [117, 252]. The intensity of peak at 1045 cm^{-1} increases with increase in reaction time indicating a new siloxane bond formation between a silica substrate and silane molecules. This provides confirmative evidence of chemical modification of silica substrate by TEOS SAM.

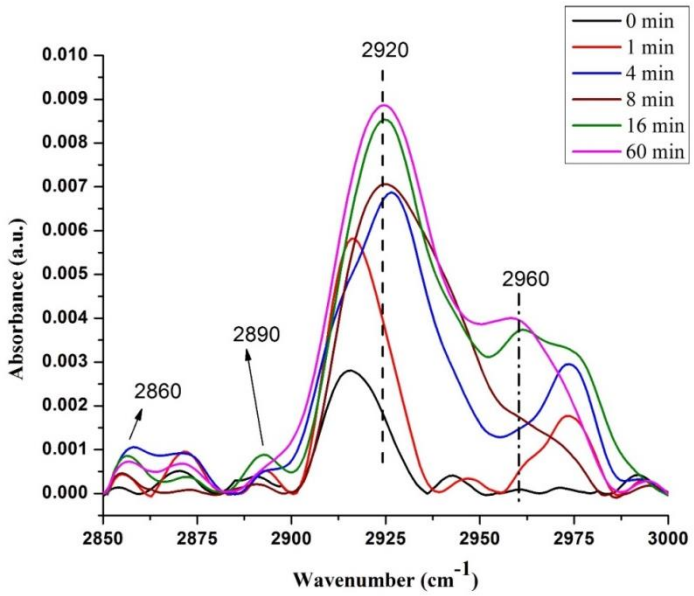

Figure 3.3. FTIR spectra showing CH_x region (range 2850-3000 cm^{-1}) of TEOS SAM prepared under inert atmosphere at room temperature for different reaction time.

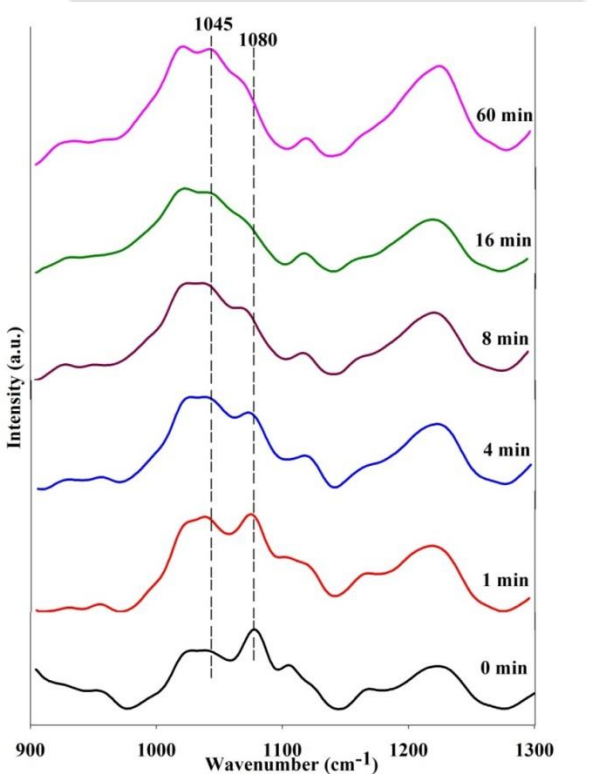

Figure 3.4. FTIR spectra in the range of 900-1300 cm^{-1} showing diminishing peak of Si-O-R at 1080 cm^{-1} indicating hydrolysis of silane molecules and new peak formation takes place at 1045 cm^{-1} indicating siloxane (Si-O-Si) bond formation.

Additionally, the peak intensity of unhydrolyzed ethoxy moieties of silane molecules (asymmetric Si-O-CH_2CH_3) at 1080 cm^{-1} [117, 252, 253] shows a continuous fall due to hydrolysis during condensation step of silanization process (see Figure 3.4). Overlapping of different vibrational modes results in complexity of the absorbance spectra in the range of 900-1300 cm^{-1}. To overcome such complexity issues, the total area under this spectral range was determined for the further investigations considering major peak area due to siloxane bond formation than hydrolysed ethoxy group as shown in Figure 3.5. Increasing peak areas with increase in reaction time clearly indicate the new siloxane bond formation on the surfaces.

3.3.1.1. Kinetic Studies Using FTIR

The peak area in the absorbance range of 900-1300 cm^{-1} for different reaction time intervals were fitted using Exponential Association functions (expression 3.3) [254, 255], which is expressed as:

$$y = A_1\,(1 - e^{-k_1 t_1}) + A_2(1 - e^{-k_2 t_2}) \qquad (3.3)$$

where k_1 and k_2 are the rate constants while A_1 and A_2 are the constants. The rate constants k_1 and k_2 represent covalent attachment and further re-orientation, respectively.

Kinetic fittings of the normalized peak area obtained from FTIR data in the range of 900-1300 cm^{-1} are shown in Figure 3.6. Overall fitted data are shown with black color line while attachment and re-orientation data are shown with blue and green color lines, respectively. Table 3.1 summarizes kinetic fitted parameters. The re-orientation rate was 6.0×10^{-4} s^{-1}. A similar value (4.5×10^{-4} s^{-1}) of re-orientation rate during formation of 11-mercaptoundecanoic acid (MUA) self-assembly on gold surface was obtained by Damos et al. [256].

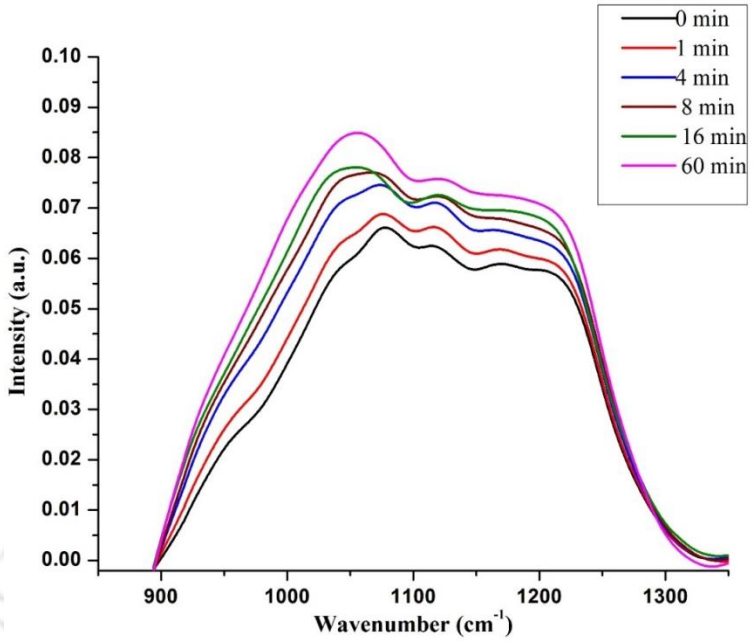

Figure 3.5. FTIR spectral in the region of 900-1300 cm^{-1} for different reaction time intervals.

However, the attachment rate (11.5 M^{-1} s^{-1}) of MUA on gold surface obtained was greater than that obtained in the present work.

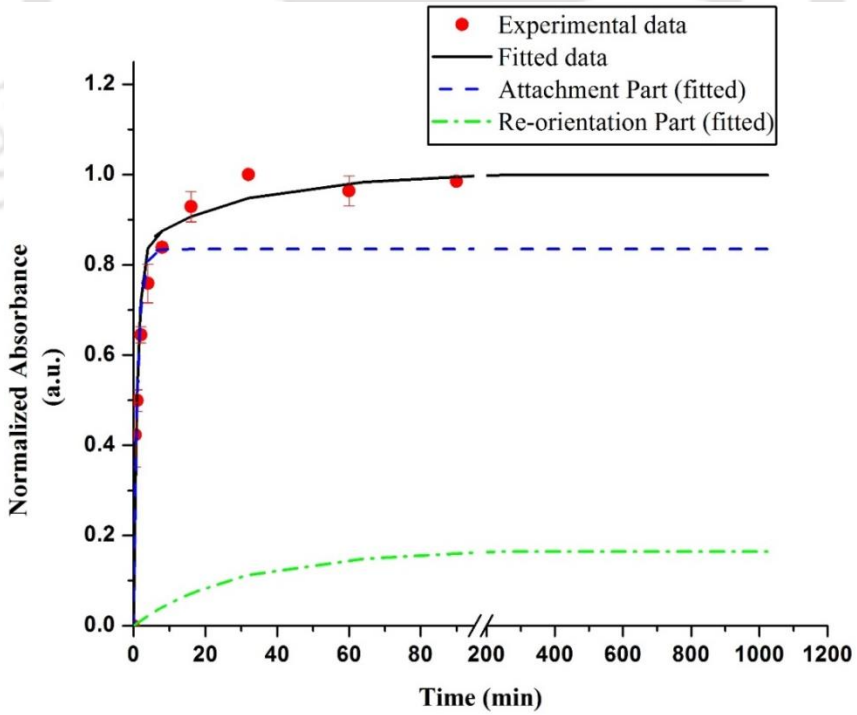

Figure 3.6. Kinetic fitting of IR data in the range of 900-1300 cm^{-1}. (●) represents experimental data while black line, blue line and green line represent fitted data, covalent attachment part and re-orientation part, respectively.

This reflects that attachment rate is dependent on reaction system i.e. substrate, reaction media (solvent), temperature and concentration of modifying agent etc.; while the re-arrangement rate is independent of reaction system. The value of $k_1 >> k_2$ implies that rate of attachment (siloxane bond formation) is much faster than molecular re-orientation. The kinetics of attachment is very fast and reaches to plateau within 16 min of reaction time and corresponds to about 83.5% of the peak area. Re-orientation or re-arrangement of the covalently bonded molecules is slower and continues till 512 min. This clearly suggests that an increase in reaction time results in formation of densely packed TEOS SAM.

Table 3.1. Kinetic parameters obtained after fitting of FTIR data (normalized peak area) in the range 900-1300 cm^{-1} by Exponential Association function.

Parameters	**Values**
A_1	0.835
k_1	$0.49 \pm (0.054)\ M^{-1}\ s^{-1}$
A_2	0.164
k_2	$6.0 \times 10^{-4} \pm (0.093)\ M^{-1}\ s^{-1}$

The above modified surfaces were further investigated using contact angle goniometer and AFM as discussed in the subsequent sections.

3.3.2. Contact Angle Analysis

The wettability of the modified surfaces was measured using contact angle goniometer. Hydrophobicity of the surfaces increases with increasing reaction time as shown in Figure 3.7. Unmodified surface (0 min) was completely hydrophilic surface with θ value of 17.8±0.3 while there was a sharp increase in contact angle within 30 seconds of reaction time which reached maximum (102±1.2º) after 24 h. FTIR data revealed the maximum attachment at around 16 min, however, contact angle at 16 min (θ=83.43±0.85°) is lesser than θ at 24 h. The possible reason for the low contact angle at 16 min is a lack of complete re-orientation of the attached molecules.

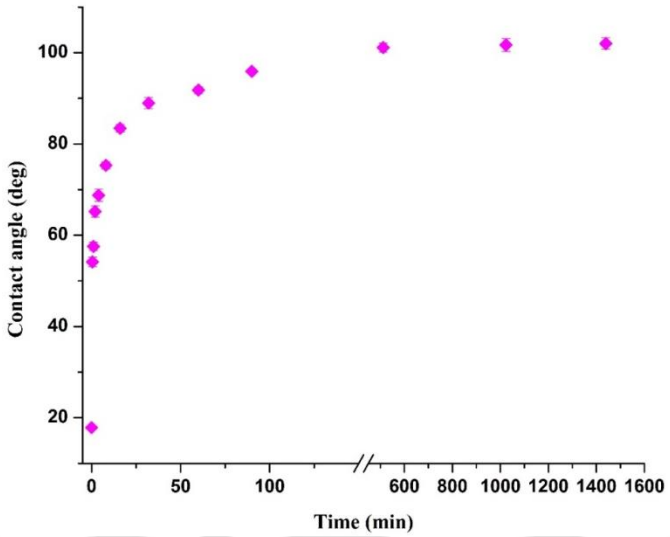

Figure 3.7. Change in water contact angle (°) with respect to reaction time during formation of octyl SAM.

Fraction of octyl groups on surface is calculated using Cassie's equation (expression 3.4). Formation of SAM resulted in a smooth surface (will be described in the next section) and the maximum R_a value reached 1.29±0.36 nm. The R_a value is very small and hence; we have excluded the effect of roughness on wettability. The Cassie's equation is expressed as follows [257]:

$$\cos\theta = f_b \cos\theta_b + f_O \cos\theta_O \qquad (3.4)$$

$$f_b + f_O = 1$$

where f_b is the fraction of blank surface, f_o is the fraction of octyl groups, θ is contact angle, θ_b is contact angle of blank surface (17.8°), θ_o is contact angle of modified surface after 24 h (102°).

Fraction of octyl group coverage with time is plotted in Figure 3.8. These data were fitted using Exponential Association functions (expression 3.3) taking same k_1 value which were obtained from fitting IR data in the range 900-1300 cm^{-1}.

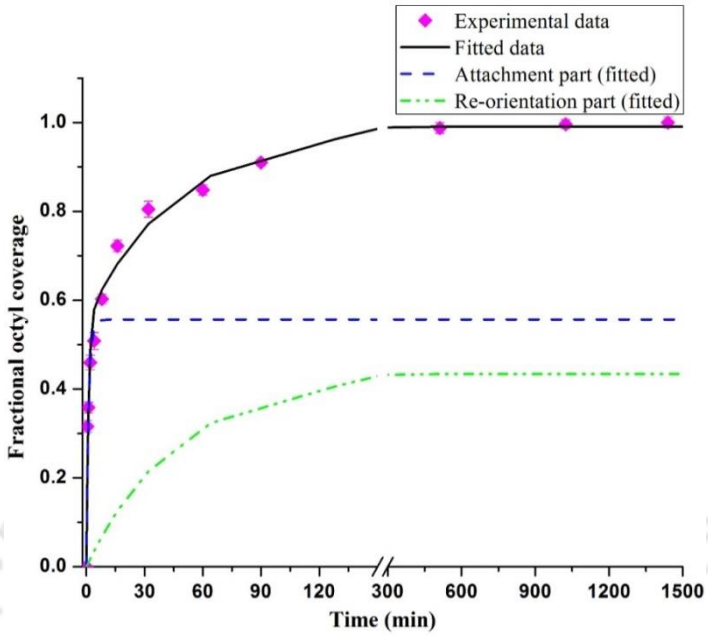

Figure 3.8. Kinetics of fractional surface coverage (f_O) of octyl groups determined from WCA data at different reaction times. (♦) represents experimental data, black line represents fitted curve, blue line represents fitted curve for covalent attachment of silane molecules and green line represents fitted curve for re-orientation of attached molecules.

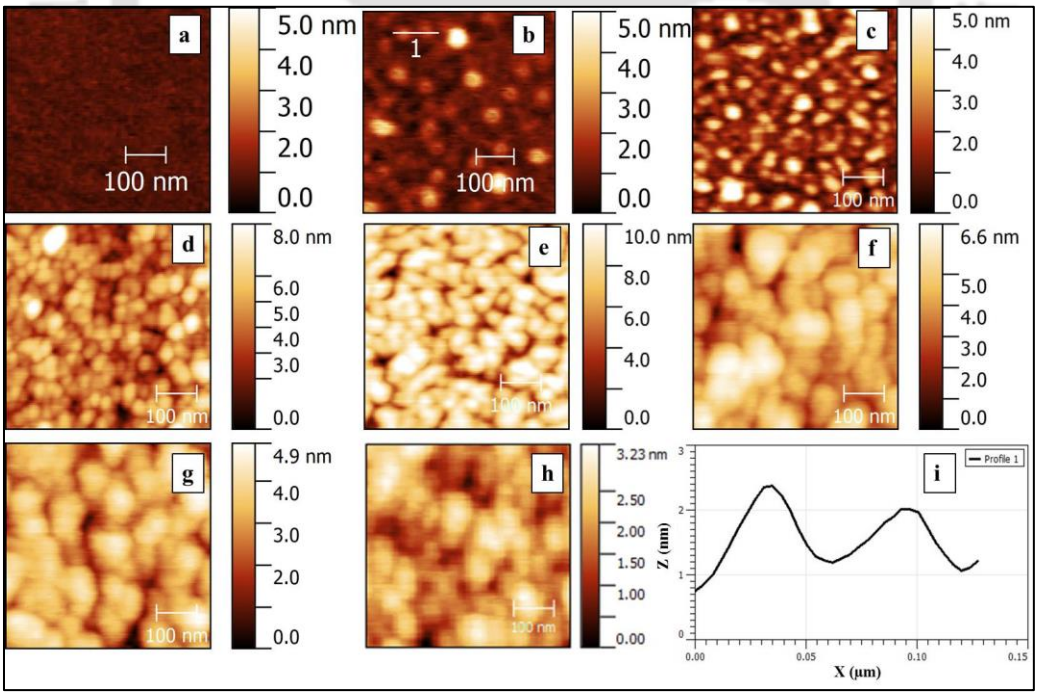

Figure 3.9. AFM images of the silicon wafers modified with TEOS molecules at the following dipping time: (a) 0 min (unmodified), (b) 1 min, (c) 4 min, (d) 8 min, (e) 16 min, (f) 60 min (g) 90 min and (h) 24 h under clean room inert atmosphere. All AFM images shown here are of 500nm×500nm size, (i) Profile graph of line 1 drawn in the image (b).

Re-orientation of the attached molecules completes in 512 min (see Figure 7). The contact angle data measured at 8.5 h and 17 h reaction times were 101.2±1.0° and 101.7±1.5° respectively. These confirm the completion of SAM formation within 8.5 h of reaction time.

3.3.3. AFM Analysis

AFM images of modified surfaces after various reaction time intervals are shown in Figure 3.9. AFM analysis was performed to characterize the growth of octylsilane monolayer and hence to determine the percentage coverage of silica substrate by this monolayer. Experimental images (a-g) infer the formation of islands which increases with the increase in reaction time and then progressively in-fills to form smooth silane monolayer [114, 243, 258, 259]. As soon as the reaction started, circular shaped grains were seen with uniform average size of ~40 nm. This size is overestimated due AFM artifact arising from the tip radius (<10 nm). Small patches of similar size were reported by Banga and Yarwood during initial growth of octadecyltrichlorosilane SAM formation [114]. The number of grains increases with the increase in reaction time and covers surface completely at t=16 min. This indicates the formation of monolayer.

Figure 3.10 shows change in R_a and R_f values with respect to reaction time. The R_a value initially increases from 0.116±0.004 nm (blank surface) to 1.298±0.086 nm after 8 min of reaction time and then decreases. The R_a value after 24 h of reaction was 0.407±0.071 nm indicating SAM formation with nanoscale smoothness. The initial increase in the R_a value states formation of small-small islands which starts covering the entire surface after a span of time, resulting in a smoother surface, hence showing a decrease in R_a value. After 16 min of reaction time, R_a value keeps on decreasing which reconfirms the FTIR observation that the attachment of

silane molecules completes within this time and further re-orientation of the attached molecules continues. The R_f values of modified surfaces were found to be close to 1 for all the samples indicating smooth surface topographies with nanoscale roughness. Moreover, analysis using ellipsometer confirmed uniform thickness of 2.63 nm due to the formation of octyl monolayer after 24 h of reaction time.

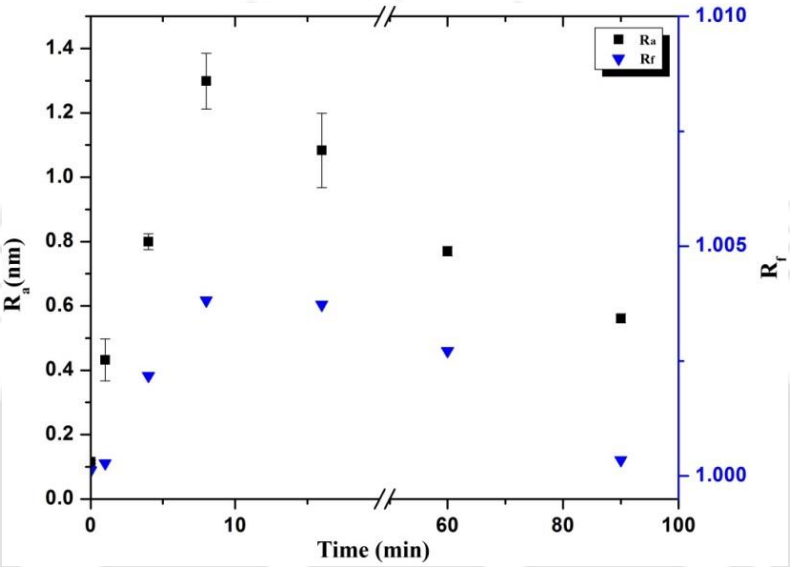

Figure 3.10. Change in R_a and R_f values with respect to reaction time during the formation of octyl SAM.

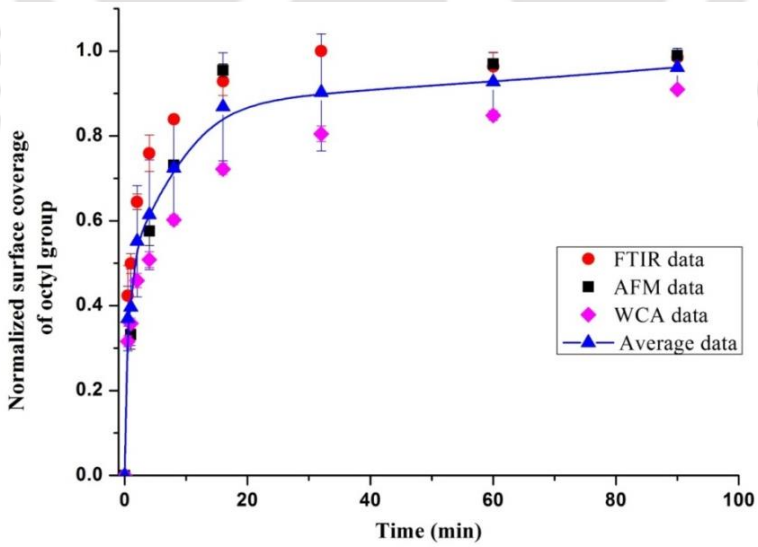

Figure 3.11. Normalized surface coverage calculated by AFM, FTIR and WCA data. Blue line shows average of all three data with standard deviation (~ 10%).

Surface coverage from AFM images were analyzed using ImageJ software [260]. Pixels were adjusted so as to select only the covered region. The particle size was analyzed using particle size analyzer feature, which also provided area of total coverage. Figure 3.10 shows the coverage of surfaces with respect to reaction time. The surface coverage increased rapidly with time and reached to about 96% within 16 min. Figure 3.11 also shows the surface coverage analyzed from contact angle and FTIR data. A best fit line (average data line in blue color) is drawn in Figure 3.11 and surface coverage predicted from FTIR, contact angle and AFM data lie within 10% of the error range.

Hence, it was seen that AFM and FTIR data agree well that at 16 min the maximum coverage takes place reflecting the attachment time of molecules while the re-orientation of the attached molecules continues till about 8.5 h leading to a nanoscale smooth surface. The thickness of the film after 24 h of silanization confirms the formation of TEOS monolayer. The formation of TEOS SAM starts with the formation of uniform size distributed grains and then progressively in-filled. The kinetic fitting data can be explored to design patterned surfaces with varying surface coverage.

3.3.4. FTIR Characterization of Different Modified Surfaces

Figure 3.12 shows the FTIR spectra of amine, octyl, mixed, hybrid and COOH modified surfaces. Peak at 1070 cm^{-1} in all the spectra corresponds to Si–O–Si bending, which indicates siloxane bond formation between silane molecules as well as silanization of surfaces [140, 261]. Presence of peaks at 860 and 1175 cm^{-1} indicate Si-C stretching of Si-CH_2R groups due to silanization.

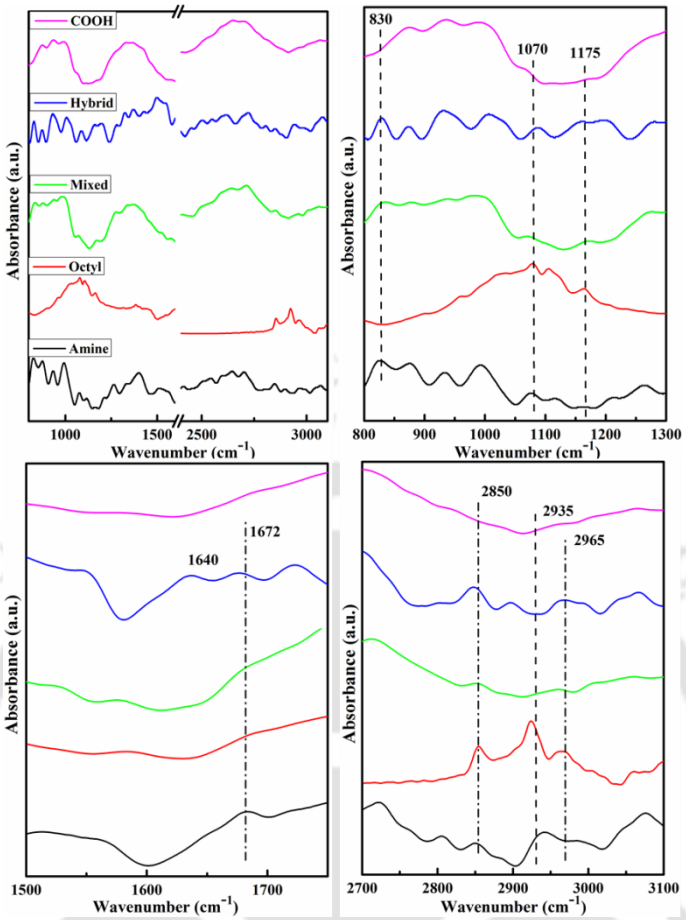

Figure 3.12. FTIR spectra of different modified surfaces.

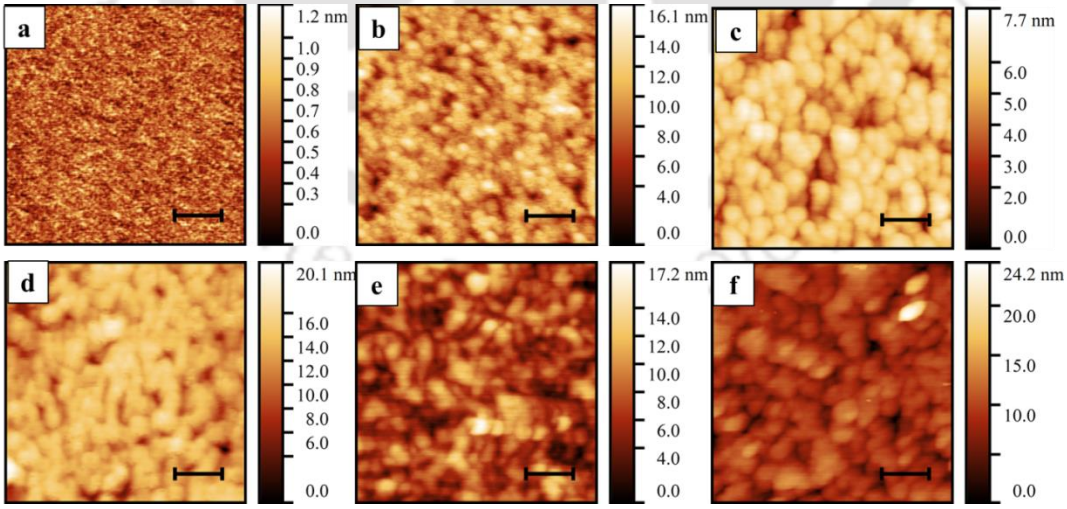

Figure 3.13. AFM images showing surface topologies of (a) unmodified (b) amine, (c) octyl, (d) mixed, (e) hybrid and (f) COOH surfaces. Scale bar is 200 nm.

Furthermore presence of 1672 cm^{-1} peak in the range 1500-1750 cm^{-1} indicates the attachment of N-H group in amine, mixed and hybrid samples specifically. The formation of urea linkage between NH_2 and NCO groups in hybrid samples was confirmed due to the appearance of a peak at 1640 cm^{-1}. Peaks at 2935 and 2850 cm^{-1} correspond to asymmetric and symmetric stretching of CH_2 groups of the corresponding silanes. A broad peak at 2962 cm^{-1} in octylsilane modified surface represents asymmetric (va-CH_3) stretching peak of CH_3 group, and confirmed the attachment of octylsilane [260].

3.3.5. Contact Angle and Surface Energy (SE) of Modified Surfaces

Water and diiodomethane (MI) contact angles were recorded on different modified surfaces at room temperature (22±1ºC). MI is a neutral molecule with little polarity due to the iodine atom. Presence of different chemical functionalities resulted in variable wettability on all the surfaces, as listed in Table 3.2. Maximum wettability was recorded for unmodified and COOH surfaces due to presence of hydrophilic OH and COOH groups on their respective surfaces. Mixed and hybrid surfaces exhibited moderate wettability whereas octyl surface showed a least value due to the presence of hydrophobic/non-polar octyl chain [140-142]. MI and water contact angle data were used to determine surface energies (listed in Table 3.2) of various surfaces by applying expression (3.5) and (3.6) as shown below. Surface energy (SE) defines the intermolecular forces that exist at the interface. Higher surface energy was found for hydrophilic surfaces (unmodified, COOH) whereas hydrophobic octyl surface exhibited the least value. Similar trends of varying SE have been reported elsewhere [141, 262].

Contact angle (θ) primarily depends on interfacial tensions at the air−liquid, solid−liquid, and solid−air interfaces and is related through Young's equation:

$$\gamma_{SV} - \gamma_{SL} = \gamma_{LV} cos\theta \quad (3.5)$$

Where γ_{SV}, γ_{SL}, and γ_{LV} are interfacial tensions between solid−vapor (SV), solid−liquid (SL), and liquid−vapor (LV) phases, respectively.

The surface energy (γ_{SV}) was calculated based on contact angles of both the liquids, using geometric mean expression (shown below) reported previously [142].

$$\gamma_{ij} = \gamma_i + \gamma_j - 2\emptyset[(\gamma_i^d \gamma_j^d)^{\frac{1}{2}} + (\gamma_i^P \gamma_j^P)^{\frac{1}{2}}] \quad (3.6)$$

Where, γ_i^d and γ_i^P are dispersive and polar component of liquid surface energy while γ_j^d and γ_j^P are the dispersive and polar component of solid surface energy, respectively. $\emptyset$ is the interaction parameter, whose value is taken as 1 for most of the similar types of molecules.

Table 3.2. Compilation of the types of silanes used, the surface exposed head group(s) and their effect on surface wettability, energy and roughness.

Silanes Used	**Head group (s)**	**Static Contact Angle**		**Surface energy ($mJ.m^{-2}$)**	**Surface roughness (nm)**	**Roughness factor (R_f)**
		Water	**MI**			
APTES	NH_2 group	61º(±1º)	39º(±1º)	46±1	0.81±0.09	1.00248
TEOS	CH_3 group	102º(±2º)	60º(±1º)	29±1	0.35±0.06	1.00036
Mixed (APTES:TEOS=1:1)	Mixture of NH_2 and CH_3 groups	81º(±1º)	42º(±1º)	39±1	0.84±0.12	1.00182
Hybrid	Hybrid of CH_3 and –NH-CO-NH- groups on same molecule	82º(±1º)	43º(±1º)	38±1	0.69±0.05	1.00125
Acidic carboxylation of CH_3 group	COOH group	41º(±1º)	38º(±1º)	58±1	0.68±0.15	1.00133

3.3.6. AFM Analysis of Modified Surfaces

Effect of silanization on morphology and roughness of SAM surfaces (as shown in Figure 3.13) was determined using AFM analysis. Average height (R_a), root mean square average height (R_q) and wavelength (λ_a) of the peaks and valleys on a surface were used to calculate the

roughness factor (R_f). Increased R_a values and changed topologies of modified surfaces as compared to unmodified surface (R_a<0.1nm) indicated silanization. Surfaces with mono SAMs of COOH and octyl were smoother as compared to surfaces with mixed and hybrid SAMs.

3.4. Conclusions

Kinetics of formation of TEOS SAM at silica/glass substrates has been studied. Characterization was carried out using FTIR spectroscopy, contact angle and the AFM. FTIR data studied in the absorbance range of 2850–3000 cm^{-1} showed an increase in the peak height and area which is correlated with increase in the attached molecules with respect to time. Similarly, the absorbance range of 900–1300 cm^{-1} mainly containing Si-O-Si and Si-O-R peaks was chosen for conferring surface modification. Kinetic fitting of the FTIR data by Exponential Association function revealed that surface modification of substrate was very fast and completed in 16 min while re-orientation of attached molecules was a slow process and continued till 512 min. Contact angle was used to analyze the hydrophobicity of modified surfaces which increased with the increase in reaction time. The surface coverage of octyl groups, calculated using Cassie's equation, were fitted taking same attachment rate constant value obtained from fitting IR data. It also revealed that the re-orientation of the attached molecules completes in 512 min (approximately 8.5 h). This confirms the transition from a lying-down to standing-up phase when surface density of the attached molecules increased. AFM images were used for analyzing surface roughness and coverage with respect to reaction time. Small islands of uniform size of ~20 nm were formed which eventually in-fill indicating a smooth layer formation. It was supported by the fact that the R_a value initially increased until maximum and then decreased indicating a smooth monolayer formation. Smooth monolayer formation was also supported by

the ellipsometry data which stated a uniform thickness of the 2.63 nm throughout the surface. The surface coverage predicted from FTIR, contact angle and AFM data supported each other and fell within 10% of error range.

Other surfaces were also successfully modified via silanization technique and characterized using FTIR, contact angle goniometer and AFM. FTIR analysis of modified surfaces evidenced silanization due to the formation of siloxane (Si-O-Si) bond. Furthermore, change in contact angle and surface roughness (R_a) with the varying surface functional groups confirmed surface modifications. Surfaces with hybrid SAMs have reduced roughness due to uniform distribution of hydrophilic and hydrophobic groups as compared to mixed SAMs. Low roughness may not have an effect in the contact angle. The observed contact angles are due to changes in chemical heterogeneity only. The small physical heterogeneity does not have an effect on surface wettability. Also, it was observed that wettability of a hybrid surface was comparable to that of a mixed surface.

Chapter 4

Adsorption Behaviors of Proteins on Modified Surfaces

Physicochemical interactions of proteins with surfaces mediate the interactions between the implant and biological system. Surface chemistry of the implant is crucial as it regulates such events at interfaces. This chapter focuses on the performances of the modified surfaces for such interactions relevant to various biomedical applications. Due to a wide range of surface wettability, we aimed to study protein behavior (i.e. conformational changes and their packing) during competitive protein adsorption. Three serum proteins (bovine serum albumin, BSA; fibrinogen, FB; and immunoglobulin G, IgG) were tested for their conformational changes and orientation upon adsorption on hydrophilic (COOH and amine), moderately hydrophobic (mixed and hybrid) and hydrophobic (octyl) surfaces. Adsorbed masses of proteins from single and binary protein solutions on different surfaces were quantified along with their secondary structures analysis. Side-on and end-on orientations of adsorbed protein molecules were analyzed using theoretical and AFM analyses. Sodium dodecyl sulfate polyacrylamide gel electrophoresis (SDS-PAGE) was employed to quantify the protein types and their ratio from competitively adsorbed proteins on different surfaces. A theoretical analysis was also used to determine the percent secondary structures of competitively adsorbed proteins from BSA/FB and BSA/IgG binary protein solutions.

4.1. Introduction

Biological fluids comprise of a mixture of small and large molecular weight proteins which compete with each other for adsorption onto surfaces. Smaller weight proteins (such as albumin) found at higher concentrations, undergo fast adsorption during the initial phase and are later displaced by bulky proteins (like fibrinogen); this effect is called as "Vroman effect" and has been confirmed using competitive and sequential adsorption processes [141, 263-266]. Since, larger proteins contain more surface binding domains, larger surface area and are more surface active, they experience stronger interactions with surfaces than smaller globular proteins [267]. In contrary, it was also alternatively proposed that the concentration of the protein is the major driving force that determines the composition of the adsorbed layer [268]. Factors like bulk protein concentration [267], protein-protein interaction [269], change in protein confirmation upon adsorption [270] and the protein's affinity towards the surface [267, 270] play a major role in competitive and sequential adsorptions. Size of the protein and its bulk concentration determines the protein's affinity, transportation and adsorption rate on the surface [241, 271].

Sequential adsorption of bovine serum albumin (BSA), fibronectin (FN), and collagen type I (Col I) on titanium alloy (Ti6Al4V) and Ti6Al4V physisorbed with poly(sodium styrenesulfonate) [poly(NaSS)], Felgueiras et al. [269] using quartz crystal microbalance (QCM), reported displacement of adsorbed BSA (66 kDa) with FN (250 kDa) and adsorbed FN with Col I (360 kDa). Contrary to the Vroman effect, protein adsorption from binary mixture exhibited a different behavior. FN was predominant in case of BSA+FN adsorption; while in case of FN+Col I, both proteins were adsorbed forming multilayers; and whereas in the case of BSA+Col I, adsorbed amount was the highest due to complex formation between BSA and Col I protein molecules. It is important to realize the effect of surface properties in regulating protein

behavior during competitive and single protein adsorption. For example, Lassen et al. reported displacement of BSA with IgG and FB on hydrophilic poly acrylic acid and poly diaminocyclohexane coated surfaces [272], but was not observed on hexamethyldisiloxane coated and methylated surface [272, 273]. Wertz at al. observed no displacement of preadsorbed BSA with FB and vice versa on OH- and C16-SAMs during sequential adsorption. Contrary to the above report, displacement of albumin with FB [273] and gamma-globulin [266] was reported separately on polystyrene and OH and CH_3 SAMs, respectively. These observations clearly highlight that surface chemistry, conformation of the adsorbed proteins and protein-protein interactions govern the competitive adsorption of proteins. Towards this direction, further studies focusing on these factors will give a better insight for the complex phenomenon of competitive protein adsorption.

4.2. Materials and Methods

4.2.1. Materials Used

The proteins BSA (A2153), IgG (I5506), and FB (F8630) were purchased from Sigma Aldrich, India. Proteins were prepared in phosphate buffer (PBS), which was prepared from salts, such as sodium chloride (NaCl), potassium chloride (KCl), monobasic potassium phosphate (KH_2PO_4), dibasic sodium phosphate (Na_2HPO_4) and were purchased from HiMedia, India. Double distilled water (Mili-Q, 18 MΩ) was used throughout the work. PBS (1X) was prepared by dissolving 8 gm of NaCl, 0.2 gm of KCl, 1.44 gm of Na_2HPO_4, and 0.24 gm of K_2HPO_4 in 800 mL of water and pH was adjusted to 7.4 with HCl and finally volume was made to 1000 mL.

4.2.2. Surface Modification and Characterization

Silicon substrates with amine, octyl, mixed (amine:octyl), hybrid, and COOH SAMs were modified using the method described in Chapter 3, Section 3.2. Surface silanization and the chemical groups on the surfaces were identified by using FTIR. Surface wettability and surface energies of the modified surfaces were analyzed using contact angle goniometer, while surface roughness and topological analysis were carried out using AFM instrument.

4.2.3. Protein Adsorption on Modified Surfaces

4.2.3.1. Brief Overview of Proteins Used

BSA is a small but the most abundant globular serum protein (M_W ~66.5 kDa) comprising of 580 amino acid residues, which arrange themselves in α-helix (45-50%), β-sheet (20%) and 20-25% β-turns, giving heart shaped tertiary structure [247, 274] (as shown in Figure 4.1(A)). IgG (Mw, 150 kDa) is the most abundant antibody found in all body fluids, accounting for 10-20% of plasma proteins. It comprises of two identical light and heavy chains, as shown in Figure 4.1(B). These chains assemble together to make three lobes, out of which two lobes contain fragment antigen binding (Fab) region while the other lobe contains a fragment crystallizable (Fc) region. Orientations of these protein molecules upon adsorption are important for various applications like biosensors, biomedical devices etc. and hence require surface engineering to modulate protein behavior [275]. FB is a 340 kDa dimeric protein of 47.5 nm length, consisting of two sets of three non-identical Aα, Bβ, and γ polypeptide chains [276, 277]. Disulfide-linked amino terminals of these chains form central E-region while disulfide-linked carboxyl terminal parts of each chain at the outer opposite end form the D-region. Length of the Aα chain is longer than its counterparts of the other chains, and is termed as αC region [276]. FB

adsorption on hydrophilic surfaces is promoted by αC region whereas D and E regions play the major role in adsorption on hydrophobic surfaces [276].

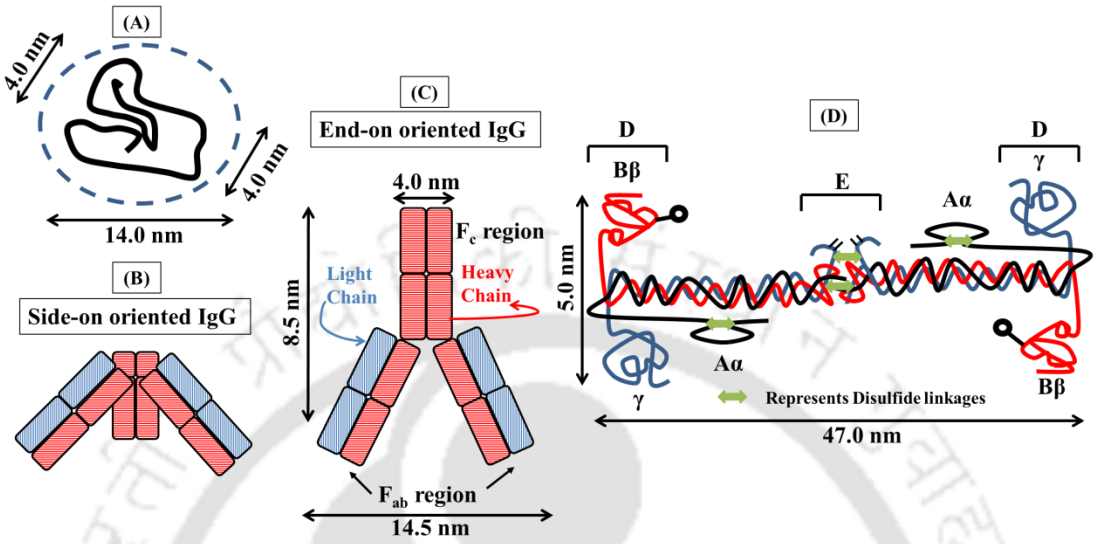

Figure 4.1. Schematic representation of three serum proteins (BSA, IgG and FB) with their dimensions (A) heart shaped BSA molecule, (B) and (C) represent side view of side-on and end-on oriented IgG molecule respectively, and (D) FB molecule.

4.2.3.2. Protein Adsorption and Characterization

Physio-chemical properties of surfaces like roughness, contact angle and surface energies and surface functionalities regulate adsorbed mass and conformation of adhered proteins [140, 141, 247]. Protein adsorption experiments on different modified glass coverslips (14 mm diameter) were carried from single and mixed protein solutions at room temperature for 1 hr, as mentioned in our previous reports [141]. Individual protein solutions of BSA (100 µg/mL), FB (20 µg/mL), and IgG (20 µg/mL) were prepared in a fresh phosphate buffer saline (PBS, pH=7.4) for single protein adsorption experiment. For the competitive protein adsorption experiment, mixed solution of BSA (100 µg/mL)/FB (20 µg/mL) and BSA (100 µg/mL)/IgG (20 µg/mL) were used. Post adsorption, protein adsorbed surfaces were gently washed with fresh PBS to remove any unbound molecules and were desorbed in the presence of 5% SDS under

shaking/agitation (120 rpm) at 37ºC. Estimation of desorbed protein mass was done using QuantiPro^{TM} BCA assay kit (Sigma, India).

Gel electrophoresis technique has been widely used by various research groups for quantification of protein desorbed from surfaces using mechanically assisted SDS elution method [278-280]. Briefly, protein adsorbed on surface modified coverslips were treated with 3 mL of 5% SDS at the above stated conditions and later concentrated to 1 mL using Vivaspin 500 centrifugal concentrators (10 kDa cut off, Sigma India). 100 µL of concentrated protein solution was used for electrophoresis analysis using Mini-PROTEAN System (Bio-Rad Laboratories). Post run, polyacrylamide gels were stained with silver staining due to its better sensitivity up to ng protein per band. SDS-PAGE images were recorded using Gel-doc system (Bio-Rad Laboratories) and analyzed using ImageJ software (developed at the National Institute of Health). Briefly, standard gels of a known protein loading were run and the numbers of pixels were calculated using 'Gels' feature in the analyze toolbar. Calibration curves were plotted (R^2=0.94-0.98) with the increasing mass within the range of interest for individual proteins. Similarly, unknown masses of desorbed proteins from different surfaces were recorded and evaluated by comparing with standard calibrated slope. Protein ladder (10-250 kDa) was used to distinguish the protein band in the case of mixed proteins solutions. For contact angle and AFM analysis, PBS washed protein adsorbed surfaces were dried at 37ºC in a dust free environment and analyzed using a similar method reported above.

4.2.4. Isothermal Titration Calorimetry (ITC)

During competitive protein adsorption, the inter-protein interaction was analyzed so as to determine whether the adsorption process was an enthalpy driven or entropy driven. Protein-

protein interaction was analyzed by isothermal titration calorimetry using MicroCal iTC-200 (MicroCal, Northampton, MA) at 300K. It is widely used to determine thermodynamic parameters such as binding constant (K_b), binding stoichiometry (n), enthalpy (ΔH) and entropy change (ΔS) for the system [281]. All the protein solutions were prepared in PBS (pH 7.4) to minimize the dilution heat contribution and degassed prior experiments. For BSA/FB and BSA/IgG interaction experiments, FB and IgG concentration was fixed at 0.02 mM and were titrated with BSA (0.4 mM) solution. The experiments consisted of 38 successive injections and were continuously stirred at 250 rpm to ensure proper mixing. Initial time delay and reference powers were 60s and 6 µCal/s, respectively for all the experiments. Control experiments were performed under similar conditions to counteract heat changes during mixing.

4.2.5. Statistical analysis

All the experiments were carried out in triplicate and results are expressed as their mean standard deviation. SigmaPlot version 14.0 was used to determine the statistically significant differences ($p<0.005$ (#) and $p<0.001$(##)) between the means of different groups, using one-way analysis of variance (ANOVA) with Benferroni method.

4.3. Results and Discussions

4.3.1. Surface modification and characterization

Detailed characterization of modified surfaces (i.e. amine, octyl, mixed (amine:octyl), hybrid, and COOH SAMs) are described in Chapter 3, Section 3.3. Surface silanization and the chemical groups on the surfaces were investigated by using FTIR (FTIR spectra shown in Fig 3.11). The surface energies of the surfaces were determined from the measured contact angles of

water and MI. These are listed in Table 3.2 and were calculated using geometric mean method as discussed in Chapter 3. AFM analysis revealed the generation of nano-roughness surface features as showed in Figure 3.13 while surface roughness (R_a) and roughness factor (R_f) are tabulated in Table 3.2.

4.3.2. Effect of Pre-adsorbed Protein on Contact Angle and Surface Energy (SE) of Modified Surfaces

Water and diiodomethane (MI) contact angles were recorded on different modified surfaces at room temperature (22±1ºC). Presence of different chemical functionalities resulted in varying wettability and surface energies (SE) of all the modified surfaces, as listed in Table 4.1. Without pre-adsorbed proteins, unmodified and COOH surfaces exhibited maximum wettability due to the presence of hydrophilic OH and COO^- groups on their respective surfaces. Mixed and hybrid surfaces exhibited moderate wettability whereas octyl surface showed a least value due to the presence of hydrophobic/non-polar octyl chain [140-142]. MI and water contact angle data before and after protein adsorption from mono and binary protein solutions were recorded and used to determine surface energies (listed in Table 4.1 and 4.2) of modified surfaces, as described by expressions mentioned in Chapter 3.

Table 4.1. Static contact angles and surface energies of different modified surfaces without and with adsorbed BSA, FB and IgG.

Surfaces	Static contact angle (º)				Surface energy ($mJ.m^{-2}$)			
	Without protein	With BSA	With FB	With IgG	Without protein	With BSA	With FB	With IgG
	Water/MI	Water/MI	Water/MI	Water/MI				
Unmodified	25±1/22±1	43±1/43±1	44±1/42±1	49±1/40±1	68±1	56±1	55±1	53±1
COOH	41±1/38±1	50±1/44±1	63±1/48±1	57±1/43±1	58±1	51±1	43±1	48±1

Amine	61±1/39±1	50±1/45±1	54±1/47±1	60±1/43±1	46±1	51±1	48±1	46±1
Hybrid	82±1/43±1	63±2/50±1	70±1/54±1	71±1/46±1	38±1	42±1	39±1	40±1
Mixed	81±1/42±1	62±1/47±1	73±1/52±1	72±1/45±1	39±1	44±1	37±1	40±1
Octyl	102±1/60±1	73±2/55±1	77±1/63±1	79±2/54±1	29±1	36±1	32±1	34±1

Table 4.2. Static contact angles and surface energies of different modified surfaces with adsorbed BSA/FB and BSA/IgG mixture.

Surfaces	Static contact angle (°)		Surface energy ($mJ.m^{-2}$)	
	With BSA/FB	With BSA/IgG		
	Water / MI	Water / MI	With BSA/FB	With BSA/IgG
Unmodified	44±1 / 42±1	46±1 / 38±1	55±1	55±1
COOH	50±1 / 42±1	52±1 / 42±2	52±1	50±1
Amine	64±2 / 43±1	57±1 / 43±1	44±1	48±1
Hybrid	72±2 / 45±1	67±1 / 46±2	40±1	42±2
Mixed	71±1 / 46±2	71±1 / 46±1	40±1	40±1
Octyl	80±2 / 57±1	75±1 / 54±1	33±1	35±1

SE of modified surfaces varied after protein adsorption (see Table 1 and 2). As compared to SE prior to protein adsorption, surface energy reduced for hydrophilic and moderately hydrophilic surfaces (i.e. unmodified, COOH and amine) while it increased for hybrid, mixed and hydrophobic octyl surfaces, post BSA adsorption. Almost similar trends of varying SE were observed on surfaces after IgG and FB adsorption. Variable SE after protein adsorption is probably due to different orientations of adsorbed protein molecules on different surfaces [282]. The surface energies after protein adsorption (γ_{MP}) were found to be gradually increasing with the increase in the surface energies of the modified surfaces (γ_{MS}), as shown in Figure 4.2. A similar trend was reported by Sharma and Pattanayek [282] for the adsorption of BSA and

lysozyme. We further determined the slope of the γ_{MS} Vs γ_{MP} graphs (Figure 4.2) which can be helpful in determining the role of surfaces chemistry on the behavior of adsorbing protein molecules. The slopes for individually adsorbed BSA, FB and IgG were 0.48, 0.51, and 0.46, respectively; while the slopes for mixed BSA/FB and BSA/IgG adsorbed from their binary solutions increased to 0.56 and 0.50, respectively. Based on the slopes of BSA/FB and BSA/IgG, we can infer that γ_{MP} increases more linearly with γ_{MS} as compared to individually adsorbed monotype proteins.

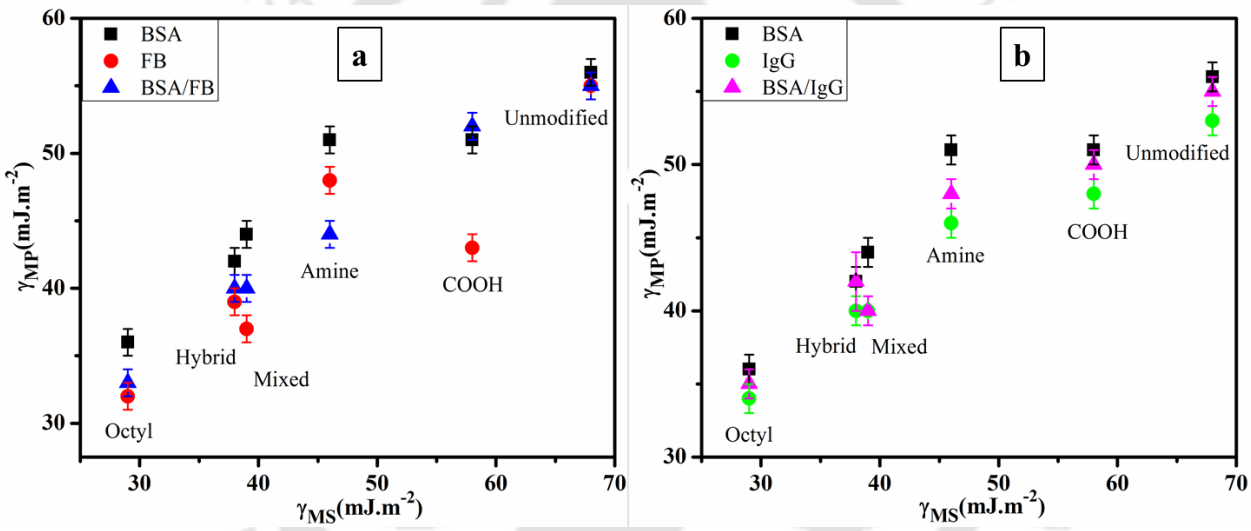

Figure 4.2. Variations in surface energies of adsorbed proteins from (a) BSA, FB and BSA/FB and (b) BSA, IgG and BSA/IgG solutions with different modified surfaces.

4.3.3. AFM Analysis of Modified Surfaces with Pre-adsorbed Proteins

Prior to protein adsorption, surfaces with mono SAMs of amine and octyl were smoother as compared to surfaces with mixed and hybrid SAMs. BSA adsorption on surfaces resulted in a slight increase in surface roughness in all the cases except for COOH surface. Random distribution of end-on and side-on orientations of adsorbed BSA molecules resulted in increased R_a values on all the surfaces. FB adsorption resulted in a reduction of R_a values for all the

surfaces except octyl surface. The FB adsorbed surfaces indicated the major presence of either end-on or side-on orientations, which notably reduced the roughness and resulted in smoother surfaces. Octyl surfaces in both BSA and FB cases exhibited comparatively higher surface roughness due to the presence of randomly distributed end-on and side-on orientations, which resulted in rough surface topologies. BSA/FB adsorption resulted R_a values very close to that resulted after only FB adsorption. This may be possible due to the fact that FB is a bulkier protein molecule than BSA and hence occupies more space on the surface [269].

Table 4.3. Surface roughness with adsorbed proteins.

Surfaces	With BSA		With FB		With BSA/FB	
	R_a (nm)	R_f (nm)	R_a (nm)	R_f (nm)	R_a (nm)	R_f (nm)
Amine	1.07±0.13	1.00389	0.75±0.08	1.00272	0.62±0.08	1.00274
Octyl	1.21±0.16	1.00618	1.56±0.23	1.00672	0.83±0.14	1.00358
Mixed	0.91±0.05	1.00298	0.74±0.17	1.00310	0.79±0.08	1.00590
Hybrid	1.10±0.10	1.00499	0.54±0.08	1.00118	0.32±0.04	1.00052
COOH	0.31±0.07	1.00057	0.27±0.04	1.00045	0.28±0.05	1.00051

4.3.4. Protein Adsorption on Modified Surfaces

Change in surface functionalities alters physio-chemical properties such as wettability, surface potential and energy, and nanoscale surface roughness etc., which in turn regulates protein adsorption behavior and secondary structures at interfaces. Hence, we prepared surfaces with different functional groups and hydrophobicity at the interface to realize their role in protein adsorption and secondary structures. In the present work, we described the effect of surface wettability on the adsorption of serum proteins (BSA, FB and IgG) from single as well as mixed protein solutions (BSA/FB, BSA/IgG) at physiological pH.

4.3.4.1. Adsorbed Proteins from Single Protein Solutions

Figure 4.3 shows the variation in the adsorbed mass of different proteins as a function of surface wettability. Adsorbed amount of BSA, as shown in Figure 4.3(a), increased linearly with the increase in the surface hydrophobicity, except that for COOH surface, it was found to be maximum on octyl surface (408±34 ng/cm^2). Although BSA carries a net negative charge at neutral pH and should adhere less on COOH surface due to electrostatic repulsion, we still observed higher adsorbed mass. Such behavior of BSA molecules on negatively charged COOH surface can be attributed to the presence of positively charged amino acids moieties (lysine, histidine) in BSA molecules [283]. Furthermore, at neutral pH, the pKa values of the carboxylic groups (of BSA molecules) increases and results in protonation [283-286]. This process intensifies the interactions between surface and BSA molecules due to hydrogen bonding, resulting in adsorption of more BSA molecules. Our results agree well with the previously reported behavior of BSA adsorption on negatively charged surfaces [287, 288].

FB and IgG also showed a similar pattern of adsorption i.e. increased amount of adsorbed protein with the increase in the surface hydrophobicity. Maximum adsorbed masses of FB (429±33 ng/cm^2) and IgG (427±46 ng/cm^2) were observed on the octyl surface due to the presence of strong hydrophobic interactions between the protein molecules and surface. Contrarily, the adsorbed amount of FB on mixed and hybrid surface was found less as compared to amine surface. It is due to the fact that the hydrophobic interactions between protein and these two surfaces are moderate [247].

To check if SDS-PAGE analysis results were consistent with the BCA data, we performed both types of analysis with the same desorbed protein solution.

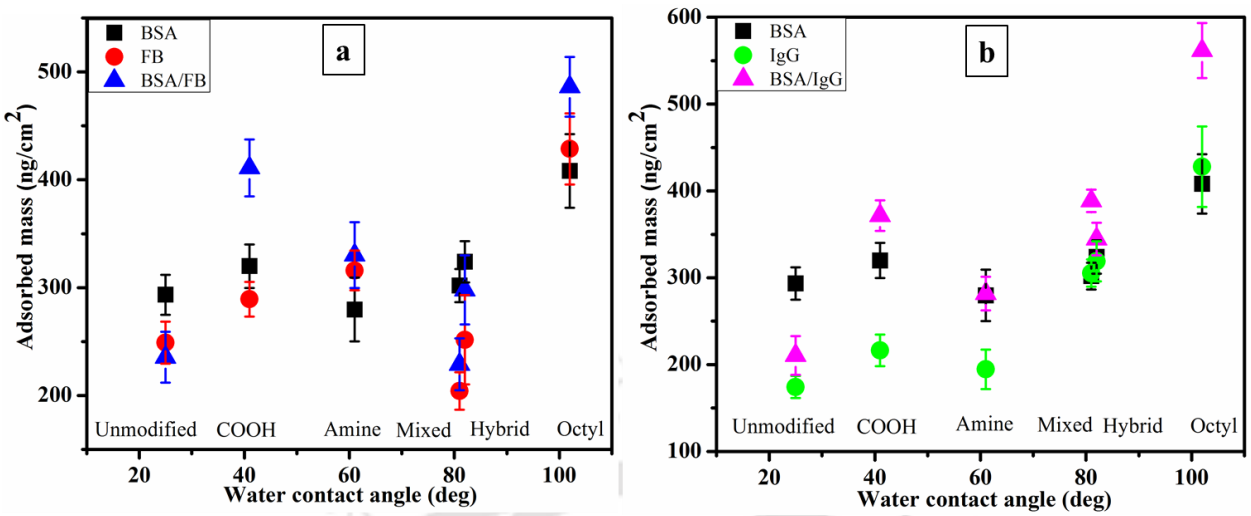

Figure 4.3. Adsorbed amount of protein molecules from (a) mono (BSA, FB, IgG) and (b) mixed (BSA/FB and BSA/IgG) protein solutions on unmodified and modified surfaces.

Figure 4.4 shows the comparative data of the adsorbed masses of proteins (BSA, FB and IgG) from single protein solutions using BCA and SDS-PAGE analyses. Reduced mass of BSA in case of SDS-PAGE analysis as compared to BCA results may be attributed to the loss of molecules due to filtration. BSA is a small protein and may get entrapped in the filter membrane resulting in less recovery post filtration, while FB and IgG are bigger and bulkier and do not encounter such issues. Hence, the standard deviations between the BCA and SDS-PAGE results for BSA were little higher i.e. around 10% whereas for FB and IgG were even less than 5% as shown in Figure 4.4.

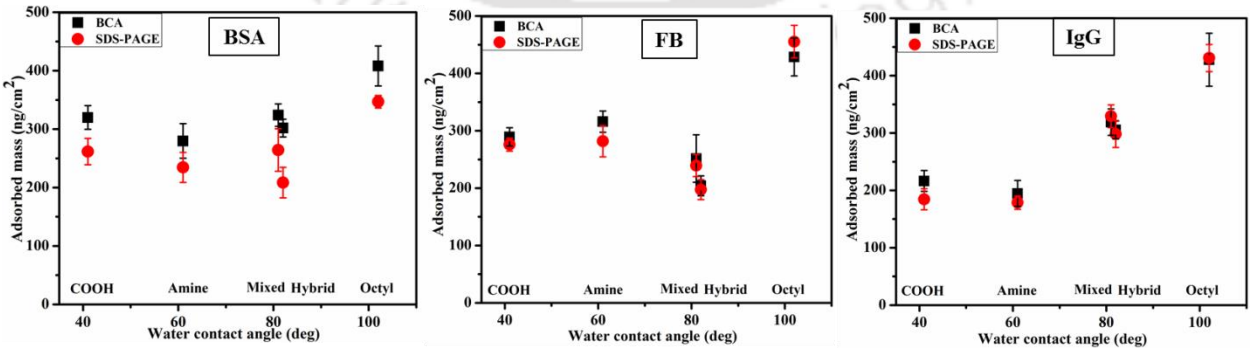

Figure 4.4. Comparison between adsorbed masses of BSA, FB and IgG proteins on different surfaces using BCA and SDS-PAGE analysis.

Based on the molecular weights and dimensions of BSA, FB and IgG molecules, we calculated the possible amount of adsorbed mass of each protein in end-on and side-on orientations theoretically, as shown in Table 4.4. For example, in case of BSA adsorption, if we observe a monolayer of 100% end-on orientation, the maximum adsorbed mass will be 690.06 ng/cm^2, whereas in side-on orientation, it would be 197.16 ng/cm^2. Similarly, we calculated for FB and IgG proteins as well and the data are shown in Table 4.4. The adsorbed amounts (see Figure 4.3) of all three proteins from single protein solutions lie between the theoretical adsorbed masses in end-on and side-on orientations of respective proteins. This indicated that proteins formed monolayer upon adsorption from single protein solutions, comprising of both the orientations on all the modified surfaces.

Table 4.4. Characterization details of BSA, FB and IgG with maximum adsorbed mass in end-on and side-on orientation.

Proteins	Molecular weight (kDa)	Dimensions (nm^3)	Dimensions used for calculating adsorbed mass		Maximum adsorbed mass (ng/cm^2) as monolayer in	
			End-on	Side-on	End-on	Side-on
BSA	66.5	[4 × 4 × 14] [274]	16.0nm^2	56.0nm^2	690.06	197.16
FB	340	[5 × 5 × 47] [247]	25.0nm^2	235.0nm^2	2258.01	240.21
IgG	150	[14.5 × 8.5 × 4] [275]	34.0nm^2	123.25nm^2	732.49	202.07

Further, based on the dimensions of the protein and adsorbed mass, we determined the percentage of side-on and end-on orientation on each surface, using the following expressions:

$$End\ on\ (\%) = \frac{M_{surface} - M_{side-on}}{M_{end-on} - M_{side-on}} \times 100 \quad (4.1)$$

$$Side\ on\ (\%) = 100 - End\ on\ (\%) \quad (4.2)$$

Where $M_{surface}$ is mass adsorbed on surface, $M_{side-on}$ and M_{end-on} are maximum adsorbed mass in side-on and end-on orientations (see Table 4.4 for each protein), respectively.

Initially protein molecules adsorb in end-on orientation to accommodate more and more protein molecules as end-on orientation occupies less space. Later they acquire side-on orientation to achieve stability which results in loss of adsorbed protein molecules [289]. Exceptionally on octyl surfaces, the % of end-on orientation of BSA and IgG were higher as compared to other surfaces (Table 5.5) which imply that hydrophobic-hydrophobic interactions between end-on attached molecules and surfaces did not allow them to change their orientation with the span in a time and hence resulted in more space to accommodate more number of molecules. Furthermore, in case of IgG, charged amine and COOH surfaces resulted in higher % of side-on orientations due to parallel alignment of IgG molecules due to ionic interactions between surfaces and oppositely charged amino acids. Interestingly, the bulky and large size of FB did not physically allow the molecules to remain in the end-on orientation and hence, we observed a majority of side-on oriented molecules irrespective of surface chemistry.

Figure 4.5 shows the AFM images of adsorbed BSA molecules on different surfaces. Due to an interplay between surface and protein molecules, they arrange themselves in different structures and packing [290]. AFM [291] and crystallographic [292] studies revealed compact (triangular, N-form, 8-9 nm each side) and elongated (E-form, ~25 nm) forms of BSA molecules (as shown in Figure 4.5). We also observed N-form predominantly on hydrophilic and moderately hydrophilic surfaces while E-form on hydrophobic (octyl) surface. Formation of N-form on hydrophilic surfaces were in agreement with previously reported results [291]. Formation of elongated, E-form on hydrophobic surface may be due to the presence of

hydrophobic-hydrophobic interactions between surface and amino-acids, and resulting in unfolding of molecules [293].

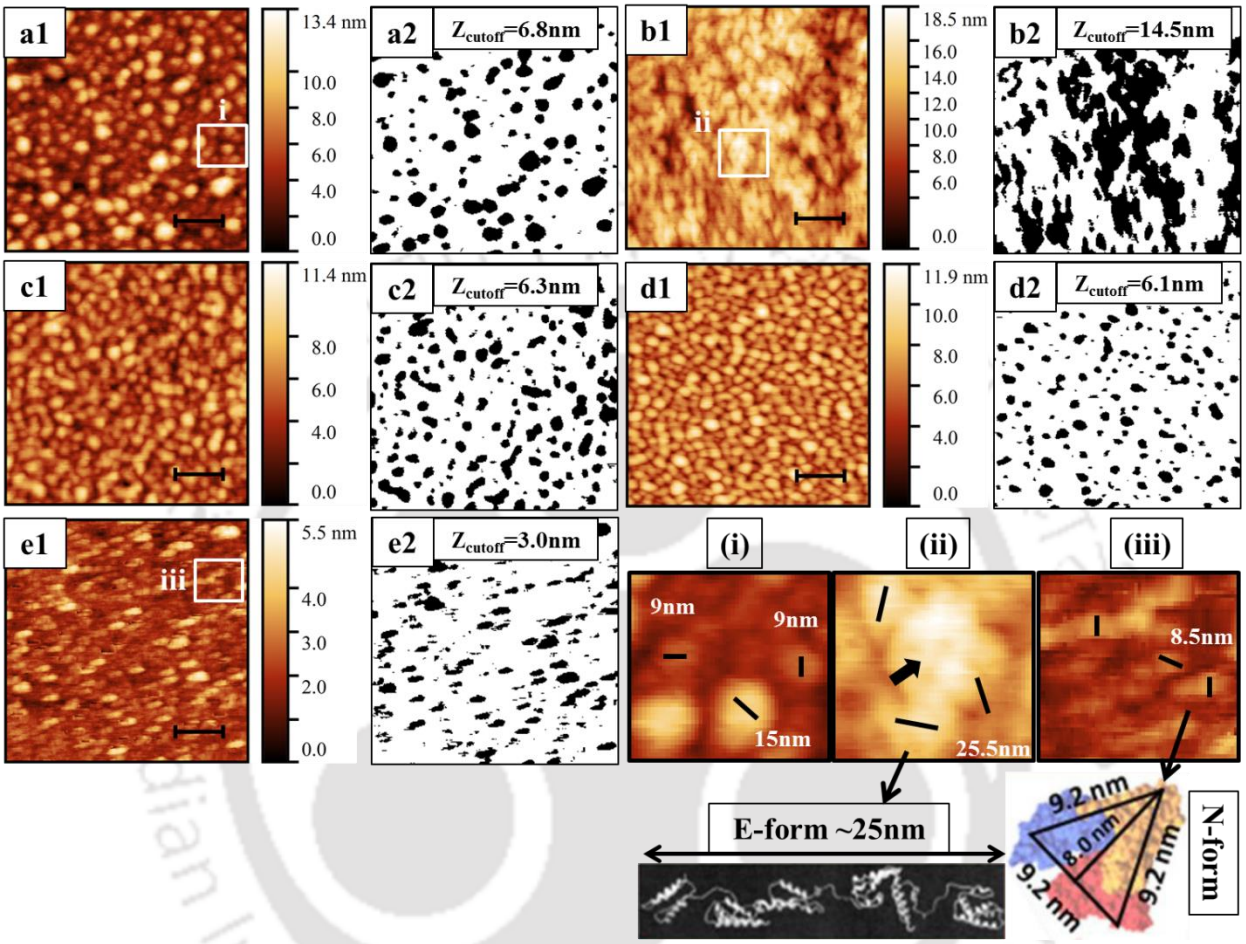

Figure 4.5. AFM images and (2) ImageJ analysis of surface topologies after BSA adsorption on (a) amine, (b) octyl, (c) mixed, (d) hybrid and (e) COOH surfaces. Black shade represents surface coverage by end-on orientation of adsorbed BSA in ImageJ results. Scale bar is 100 nm. (i), (ii) and (iii) are enlarged images of marked areas shown at a1, b1 and e1, respectively. Arrow sign in (ii) points aggregate formation and elongation of BSA (E-form) molecules on octyl surface. Compact N-form appears on hydrophilic surfaces. E-form and N-form images were taken from Ref.[291]

Figure 4.6 presents the different orientations and alignments of adsorbed FB on various chemically and topologically distinct SAMs. Hydrophilic COOH surface exhibited ovoid forms (~34 nm length) of adsorbed FB depicting incomplete unfolding of molecules. Similar behavior of FB was reported by Rafailovich et al. and suggested that the hydrophilic αC region gets

attached to the surface while hydrophobic D and E regions (see Figure 4.1) remains unattached, resulting in a distorted and partly unfolded FB structure [276]. Interactions between the hydrophilic surface and αC region may be due to electrostatic attractions, hydrophilic interactions and hydrogen bonding [294]. Whereas on hydrophobic surfaces (octyl), the strong interactions between surface and hydrophobic D and E regions due to hydrophobic interactions resulted in strong binding while αC region remained free and recruited other FB molecules for fiber formation [276] (as observed in Figure 4.6 (b1 and c1)). Even though hybrid and mixed surfaces exhibited similar water contact angles (θ=82º), we observed fiber formation on mixed surface and not on hybrid surface. Phase change due to a mixture of octyl and amine groups on the mixed surface may be the possible reason for this behavior [140].

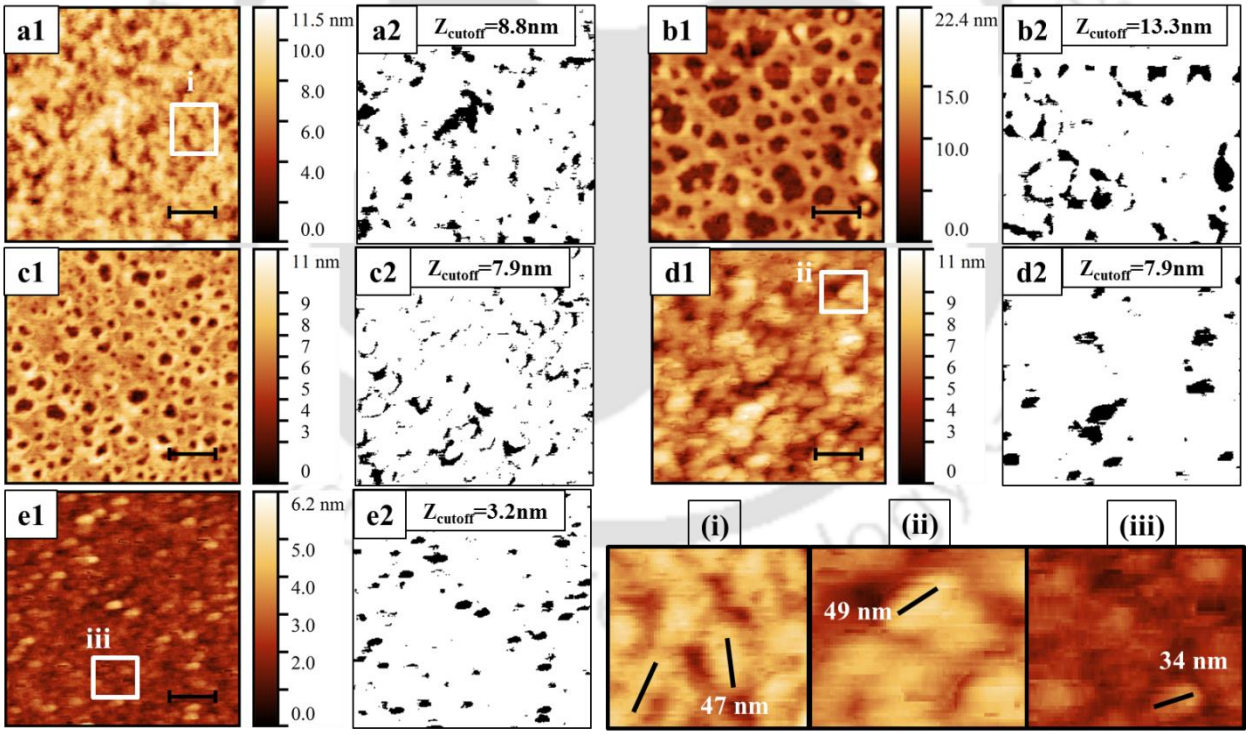

Figure 4.6. AFM images and ImageJ analysis of surface topologies after FB adsorption on (a1 and a2) amine, (b1 and b2) octyl, (c1 and c2) mixed, (d1 and d2) hybrid and (e1 and e2) COOH surfaces, respectively. Black shades represent height and hence surface coverage by end-on orientation of adsorbed FB in ImageJ results. Scale bar is 200 nm. (i), (ii) and (iii) are enlarged images of marked areas shown at a1, d1 and e1, respectively.

Different orientations of the adsorbed proteins were also determined by AFM image analysis. A protein molecule offers different Z values based on its dimensions for side-on and end-on orientations (See Table 4.4). Therefore, we have taken a cutoff Z values during AFM image analysis to distinguish the surface coverage by different orientations (see Figure 4.5 and 4.6). The surface coverages by side-on and end-on orientations are listed in Table 4.5, which competed with theoretically calculated orientations.

The presence of both side-on and end-on orientations on all the surfaces resulted in higher R_a values after BSA adsorption (see Table 4.3). The highest percentage of end-on orientation (~41%, see Table 4.5) on an octyl surface may be responsible for its maximum surface roughness (R_a=1.21 nm). The FB adsorbed surfaces were mainly covered by side-on orientation (90-95%; see AFM data in Table 4.5) which notably reduced R_a values and resulted in smoother surfaces except the octyl surface. The percentage of end-on orientation of FB protein on octyl surface (9-10%) was the highest as compared to other surfaces and hence might be responsible for increased surface roughness.

Table 4.5. Percentage end-on and side-on orientations of adsorbed BSA, FB and IgG molecules from single protein solutions on modified surfaces, calculated theoretically from SDS data and AFM analysis.

Surfaces	BSA				FB				IgG	
	Theoretically		AFM data		Theoretically		AFM data		Theoretically	
	End-on (%)	Side-on (%)	End-on (%)	Side-on (%)	End-on (%)	Side-on (%)	End-on (%)	Side-on (%)	End-on (%)	Side-on (%)
Amine	16.75	83.25	17.45	82.55	3.75	96.25	7.87	92.13	3.7	96.30
Octyl	42.80	57.20	40.60	59.40	9.35	90.65	10.22	89.78	42.55	57.45
Mixed	21.24	78.76	21.93	78.07	0	100	5.29	94.71	19.47	80.53
Hybrid	25.71	74.29	21.63	78.37	0.56	99.44	5.93	94.07	22.04	77.96
COOH	24.90	75.10	31.70	68.30	2.43	97.57	6.61	93.39	2.69	97.31

4.3.4.2. Adsorbed Proteins from a Mixture of Protein Solutions

Competitive adsorption among BSA, FB and IgG proteins on different modified surfaces from mixed protein solutions of BSA/FB and BSA/IgG was also studied and was found to follow a similar adsorption pattern as that of FB and IgG, respectively (Figure 4.3). This indicated higher proportion of FB and IgG in the adsorbed mass as compared to BSA from BSA/FB and BSA/IgG protein solutions, respectively. In the case of BSA/FB mixture, maximum total protein adsorbed mass was observed on octyl followed by COOH and amine surfaces while the least was observed on the mixed surface. Similarly, we observed higher adsorbed mass of BSA/IgG on octyl surface as compared to other surfaces as shown in Figure 4.3(b).

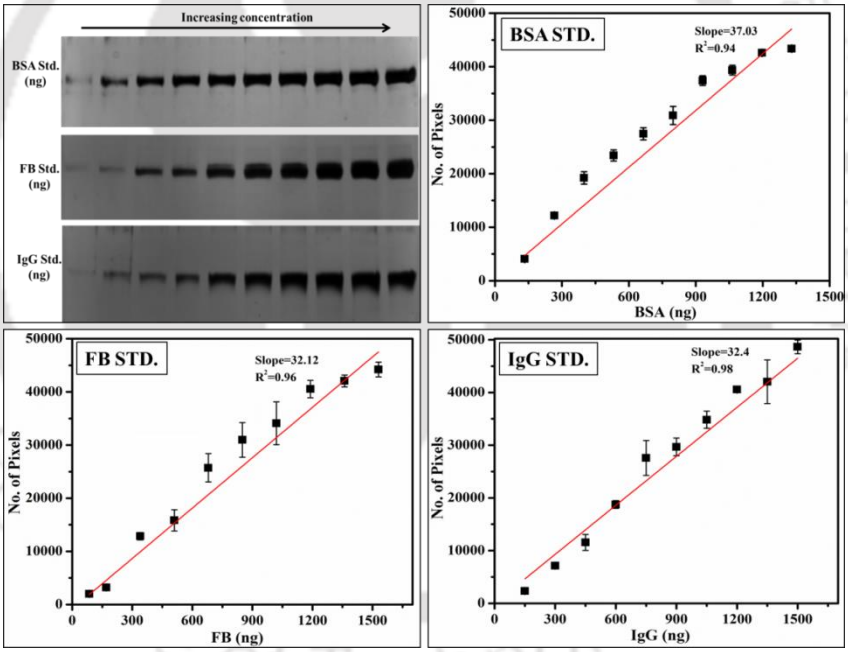

Figure 4.7. Silver stained standard SDS-PAGE gels of BSA, FB and IgG. Linear fitting of data obtained for no. of pixels estimated against known amount of protein.

To confirm the adsorbed mass of individual proteins on surfaces from mixed solutions, we performed SDS-PAGE analysis of the desorbed proteins. SDS-PAGE images of desorbed proteins from mixtures resulted in two distinct bands, indicating the presence of both the proteins

(Figure 4.8). The amount of individual protein was determined using the standard curve of each protein (as shown in Figure 4.7).

The calculated mass ratios of BSA/FB and BSA/IgG on different surfaces are listed in Table 4.6. In case of BSA/FB competitive adsorption, adsorbed amounts of FB on all the surfaces were more as compared to BSA and related to the theory which states that high molecular weight protein molecules displace lower molecular weight adsorbed protein molecules [141]. Likewise, adsorbed amount of IgG was higher than BSA on all the surfaces for BSA/IgG competitive adsorption.

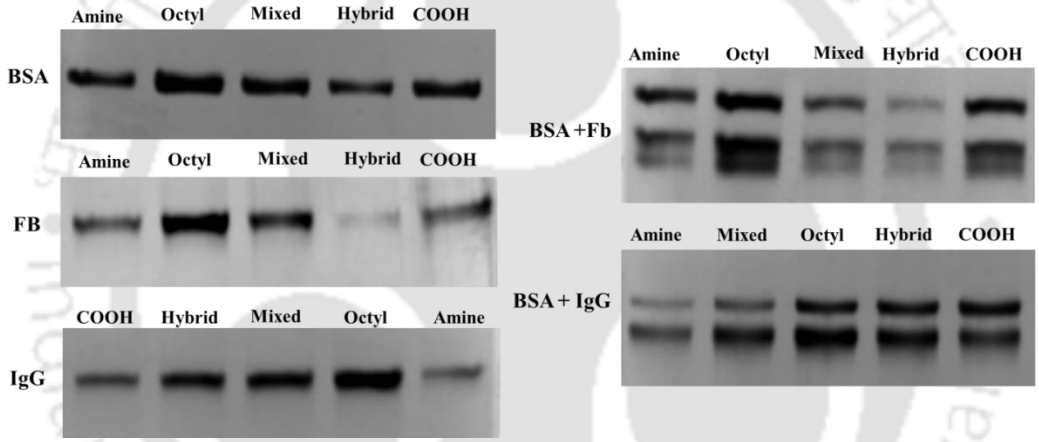

Figure 4.8. SDS-PAGE images of desorbed BSA, FB, and IgG proteins and their mixtures BSA/FB and BSA/IgG from different modified surfaces.

Furthermore, we also calculated the % orientations of adsorbed proteins (BSA, FB and IgG) on the surfaces from their binary mixtures during competitive protein adsorption. Protein molecules adhered via an end-on orientation and experienced lesser interactive force i.e. hydrophobic interaction between protein and the surface. Whereas hydrophobic interactions in case of side-on orientation are higher and hence, results in strong binding of protein molecules to surfaces. The schematic representation of protein adsorption from single and binary solution with different orientation is shown in Figure 4.9. It is expected that the weakly bound (end-on

orientation) molecules of a smaller protein is replaced by a larger one. Further the bigger molecules may partly displace the side-on oriented molecules of the smaller protein and finally dispense themselves in end-on and side-on orientations to reach a minimum energy equilibrium state.

In the case of BSA/FB binary mixture, BSA molecules being smaller in size diffused faster and adhered to the surfaces which were later displaced by adhering FB molecules which are heavier and bulkier in size. We calculated the adsorbed amounts of individual proteins on surfaces from total adsorbed mass (Figure 4.3) and ratio on individual proteins (Table 4.6). The adsorbed amount of smaller protein (BSA) was distributed on surfaces only in side-on orientation (%), which were found to be lesser than that of BSA molecules from single protein adsorption except on the octyl surface (see Tables 4.5 and 4.6). This confirmed our hypothesis of complete displacement of weakly bound (end-on orientation) molecules and partial displacement of strongly bound (side-on orientation) molecules of a smaller protein by a larger one. Strong hydrophobic interactions between octyl group and BSA molecules may be the reason that about 9.85% of end-on oriented BSA molecules remained intact and were not displaced by FB molecules. The adsorbed amount of the larger protein (FB) was distributed on the remaining surface in both end-on and side-on orientations (listed in Table 4.6). These results indicate monolayers of both BSA and FB proteins on surfaces after competitive adsorption from their binary solutions.

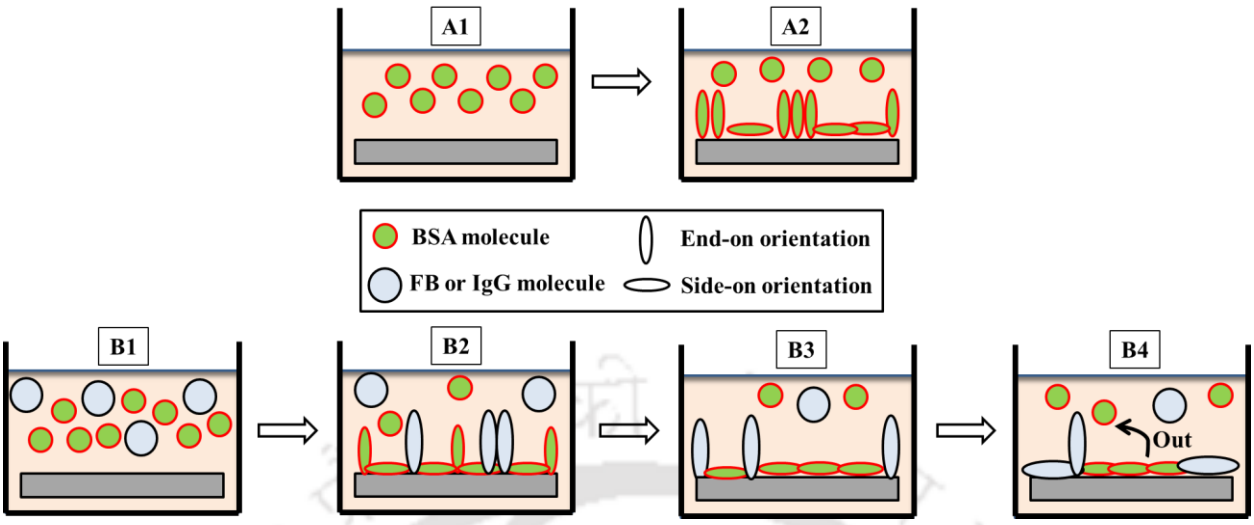

Figure 4.9. Representation of adsorption process from single protein solution (A1 to A2) in end-on and side-on orientations. Similarly, B1 to B2 represents adsorption of smaller size protein molecules (BSA in this case) due to a higher diffusion rate in end-on and side-on orientation. (B3) Displacement of adsorbed smaller protein molecules (which are attached in end-on orientation) from surface by slow diffusing bulkier molecules (BSA or IgG). (B4) Adsorbing bulkier molecules further undergoes change in orientation to attain maximum stability and in due course further displaces few loosely bound side-on oriented BSA molecules.

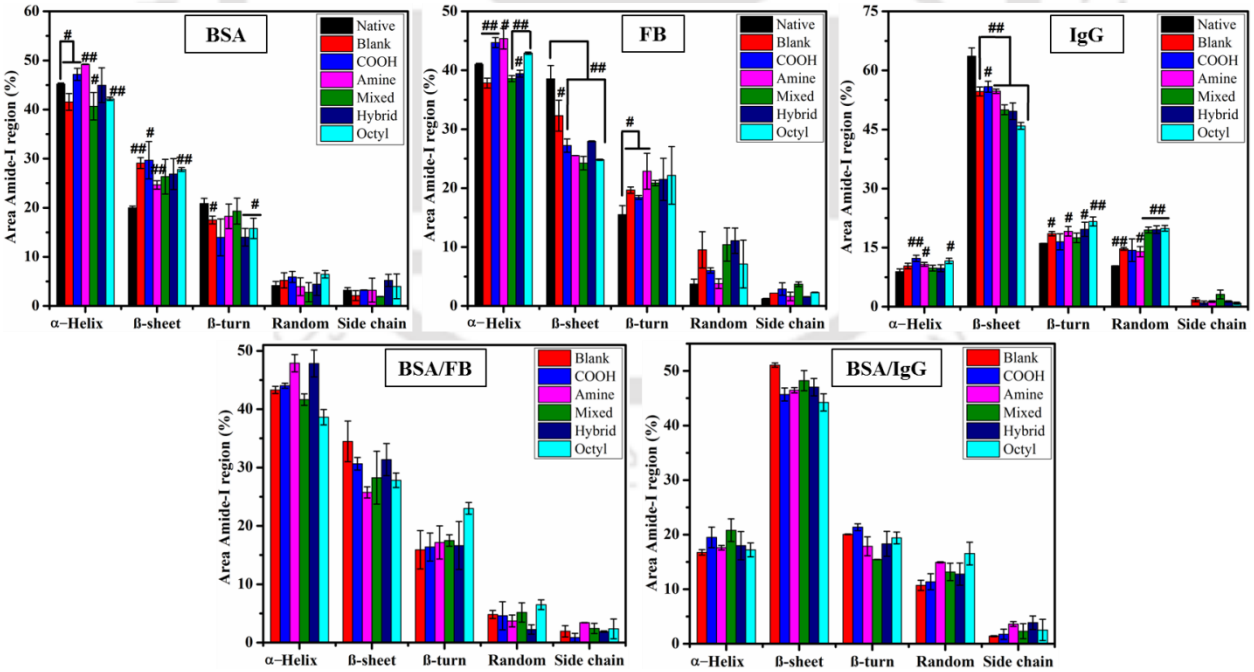

Figure 4.10. Content of secondary structures (α-helix, β-sheet, β-turn, and random and side chain) of adsorbed BSA, FB and IgG from single protein and mixed protein (BSA/FB and BSA/IgG) solution on modified surfaces. Significance comparison was made between native

proteins (BSA, FB and IgG) and after adsorption on different surfaces. Values represent the mean ± SD. # denotes $p<0.05$ and ## denotes $p<0.005$.

Similarly, during competitive adsorption from BSA/IgG binary mixture, end-on attached BSA molecules along with some percent of side-on molecules got displaced by incoming IgG molecules on all the surfaces except for octyl and COOH surfaces. We found 1.63 and 2.75% of end-on oriented BSA molecules un-displaced on octyl and COOH surfaces and can be attributed to strong hydrophobic and electrostatic interactions, respectively. The adsorbed amount of IgG was distributed on remaining surface in both end-on and side-on orientations (listed in Table 4.6) except on octyl and COOH surfaces. We noticed that the remaining surface after BSA coverage was not sufficient enough to place the adsorbed amount of IgG even in end-on orientation on octyl and COOH surfaces. We presumed multilayer adsorption of IgG on these two surfaces and accordingly calculated extra surface coverage (Table 4.6). This may be attributed to strong hydrophobic and moderate ionic/charged interactions between IgG and octyl and COOH surfaces, respectively.

Table 4.6. Percentage end-on and side-on orientations of adsorbed BSA, FB and IgG molecules from a binary mixture of BSA/FB and BSA/IgG protein solutions on modified surfaces.

Surfaces	**BSA/FB**					**BSA/IgG**				
		BSA		**FB**			**BSA**		**IgG**	
	BSA:FB (SDS-PAGE)	**End-on (%)**	**Side-on (%)**	**End-on (%)**	**Side-on (%)**	**BSA:IgG (SDS-PAGE)**	**End-on (%)**	**Side-on (%)**	**End-on (%)**	**Side-on (%)**
Amine	0.38	0	46.50	5.45	48.05	0.36	0	38.24	15.38	46.38
Octyl	0.59	9.85	57.15	11.21	21.74	0.28	1.63	57.20	41.17 +67.29 *	0
Mixed	1.08	0	60.31	0.73	38.96	0.42	0	58.88	35.69	5.43

Hybrid	0.78	0	66.55	4.28	29.17	0.50	0	58.55	27.42	14.03
COOH	0.48	0	68.04	9.92	22.04	0.82	2.75	75.09	22.16+ 20.93*	0

* refers to multilayer adsorption

4.3.5. Secondary Structure of Adsorbed Proteins

The effect of surface modification on secondary structures of adsorbed serum proteins were analyzed using FTIR-ATR. Analysis was performed using Origin 8.5 software and the amide I range (1600-1700 cm^{-1}) of the spectra were fitted with Gaussian curves. Figure 4.10 shows the relative percentage of various secondary structures (α-helix, β-sheet, β-turn, random and side chain) of adsorbed protein molecules on different modified surfaces. Briefly, peaks for α-helix are generally present around 1655 cm^{-1}, peaks for β-sheet are found between 1620 to 1636 cm^{-1}, peaks for side chain are present close to 1600 cm^{-1}, peaks for β-turn are mostly be in the range 1662 to 1688 cm^{-1} while random peak is found close at 1645 cm^{-1} [247].

Data fitting of the amide-I region revealed the significant increase in the α-helix content on amine and COOH surfaces while it reduced for all other surfaces during BSA adsorption. As explained in our previous report, amine and carboxylic groups of BSA amino acid residues establishes and enhances hydrogen bonding with carboxylic and NH_2 group of COOH and amine surfaces, respectively, resulting in a net increase in the α-helix content [247]. Whereas upon adsorption, β-sheet content increased significantly [295] while β-turn content decreased for adsorbed BSA on all the surfaces. Changes in α-helix and β-sheet contents were insignificant on hybrid surfaces, indicating native like structure which implies the formation of a soft layer of adsorbed BSA [247]. β-sheet content of FB significantly reduced upon adsorption on all the surfaces as compared to the native structure [277]. High density of proline and glycine residues in FB induces β-turn formation and hence, we observed an increase in β-turn content on all the

surfaces [141, 247]. Azpiazu and Chapman described that β-sheet contents are mainly localized in two globular D domains, and reduction in content signified unfolding due to adsorption [296]. Significant reduction in % β-sheet content upon adsorption on hydrophobic and hydrophilic surfaces was also seconded by Tunc group [277]. Further, we observed an increase in β-turn upon adsorption on all the surfaces. Similar observation was also reported by Desroches and Omanovic during FB adsorption on 316LLVM surfaces [297]. Increase in β-turn content is probably due to the transformation of α-helix and β-sheet to β-turn content upon adsorption, as explained by Weisel et al. via biomolecular simulations and theoretical modeling [298] and was strongly supported by Desroches and Omanovic [297] and Tunc et al. [277]. IgG mainly contains β-sheet (~50-60%) and β-turn (~10-20%) with a very less amount of α-helix [299, 300]. We observed that β-sheet (%) significantly decreased as compared to native structure on all the surfaces, suggesting that IgG molecules acquire compact conformation upon adsorption [301]. β-turn and random content (%) increased significantly on all the surfaces.

Based on the above observations, we correlated the α-helix content of adsorbed BSA, β-sheet contents of adsorbed FB and IgG with the contents of more stable configuration (side-on) of a particular protein on a surface. Remarkably, α-helix content of adsorbed BSA was found to linearly increase with side-on (%) with R^2=0.60 indicating side-on orientation of BSA leading to the creation of α-helix (Figure 4.11). Similarly, β-sheet contents of adsorbed FB and IgG were found to linearly increase with the respective side-on contents (%) with R^2=0.81 and 0.96, respectively (Figure 4.11). This indicates that side-on orientations of adsorbed FB and IgG lead to formation of the β-sheet.

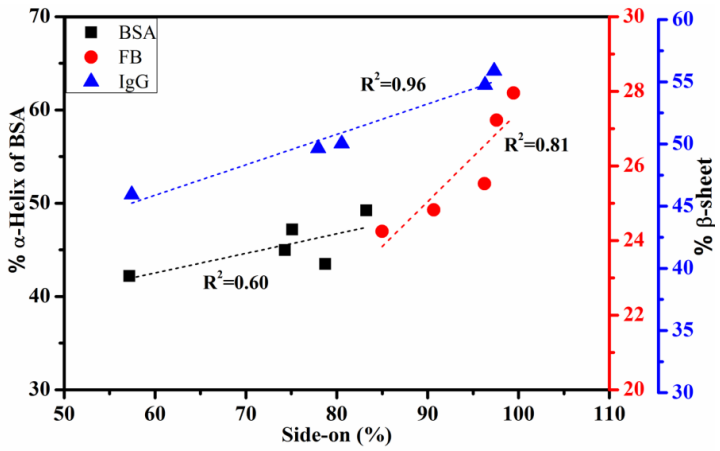

Figure 4.11. Relationship between % of side-on oriented adsorbed BSA, FB and IgG with varying % α-helix content in BSA and %β-sheet of FB and IgG.

In case of competitive adsorption from BSA/FB binary mixture, β-sheet content varied in the range 26 to 34% on all the surfaces and were found to be significant as compared to that of native BSA and FB. This indicated the presence of both the proteins on the surfaces. For BSA/IgG adsorption, we observed a higher percentage of β-sheet in the range of 45 to 51% on all the surfaces which were similar to that observed for adsorbed IgG, indicating higher content of IgG as compared to BSA on all the surfaces.

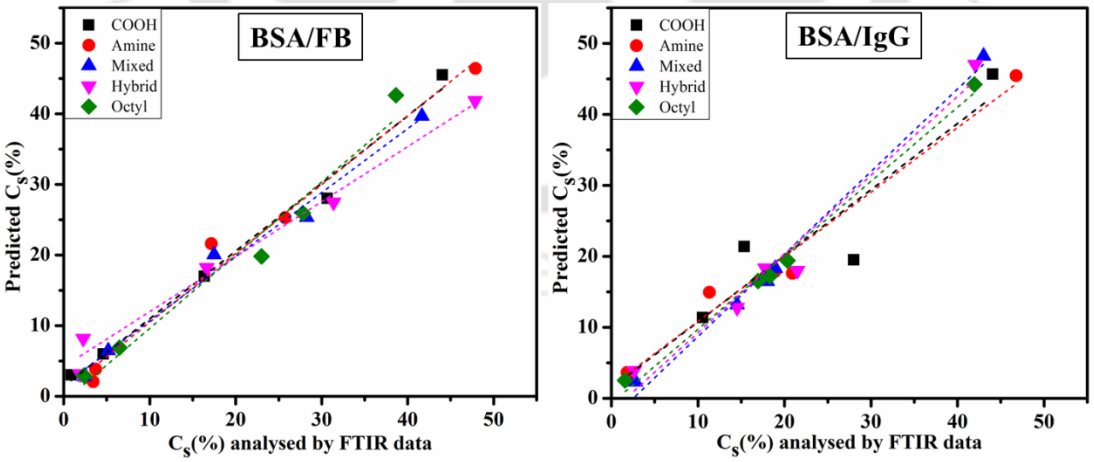

Figure 4.12. Comparison between the theoretically predicted and FTIR data for secondary structures (C_S, %) of adsorbed protein molecules from BSA/FB and BSA/IgG binary solutions on different modified surfaces.

Abundance ratios of individual proteins from BSA/FB and BSA/IgG binary mixtures on different surfaces are listed in Table 4.6. We hypothetically calculated the content of secondary structure of adsorbed mixed proteins on the surfaces by combining the contents of secondary structure of individual adsorbed proteins and their abundance ratios on a given surface.

The expression is as follows:

$$C_S(\%) = \sum_{i=1,2} f_i \times C_S^i \quad (4.3)$$

Where C_S refers to the content of a secondary structure of competitive adsorbed proteins on a surface; C may be α-helix/ β-sheet/ β-turn/ random and S may be unmodified/ carboxylic/ amine/ mixed/ hybrid/ octyl surfaces. f_i refers the fraction of individual proteins (i) present on a surface in case of competitive adsorption. C_S^i refers the content of a secondary structure of i protein adsorbed from a single protein solution on a surface.

Interestingly, predicted C_S values of competitive adsorbed proteins on a surface were linearly related ($y = mx$) with experimentally measured C_S values (Figure 4.12). For the competitive BSA/FB adsorption, m values varied in the range of 0.9-1.0 with R^2 values in the range of 0.95-0.99 on all the surfaces indicting the validity of our hypothesized procedure to predict the secondary structure contents on a surface in case of competitive adsorption from individually adsorbed protein's secondary structure data. Likewise, for the competitive BSA/IgG adsorption, m values varied in the range of 0.94-0.98 with R^2 values in the range of 0.90-0.99 on all the surfaces.

4.3.6. Thermodynamics Analysis Using ITC

The interactions between BSA/FB and BSA/IgG in solution was monitored using ITC (Figure 4.13). It is expected that the thermodynamic properties of a binary solution will regulate

the competitive adosorption. ITC has been exploited to determine the affinity and stoichiometry of BSA binding to FB and IgG to realize the free energy, entahlpy of association and entropy change of the process. The thermodynamic parameters of the interaction between BSA/FB and BSA/IgG have been shown in Table 4.7. We noticed two binding sites (N=1.29 and 1.69) sites during these interactions, this stoichiometry can be explanied due to the dimeric structure of the FB and IgG molecules providing two binding sites for BSA to interact.

In both the cases of BSA/FB and BSA/IgG, change in enthalpy (ΔH) was found to be endothermic. ΔH values for BSA/FB and BSA/IgG were 2.23 ± 0.17 and 8.69 ± 0.41, respectively, indicating weaker intercations between the two protein molecules. These interactions may be due to functional groups, any conformational changes, polarization of the two interacting molecules and electrostatic complementarity [302]. Weaker interactions result in higher possibilities of movement of the interacting molecules due to hydrophobic effect thus increasing the entropy [303]. ΔS values for BSA/FB and BSA/IgG were 25.2 and 52.1, respectively. Entropy compensated sufficiently for the enthalpy loss thus making the Gibbs free energy, ΔG, lesser than zero hence making it an entropy driven process [302]. Therefore, these interactions between BSA/FB and BSA/IgG emphasized that competitve protein adsorption is driven by an increase in entropy.

Table 4.7. Thermodynamic parameters of the interaction of BSA with FB and IgG at 300 K, derived from ITC.

Parameter	BSA/FB (value ±SD)	BSA/IgG (value ±SD)
Stoichiometry (n)	1.29 ± 0.03	1.69 ± 0.06
K (binding constant, M^{-1})	$2.18X10^3$ ± 111	$1.15X10^4$ ± 2170
ΔH (binding enthalpy, kcal per mol)	2.23 ± 0.17	8.69 ± 0.41
ΔS (entropy change, cal per mol·K)	25.2	52.1
ΔG (free energy change, kcal per mol)	-5.3	-6.9

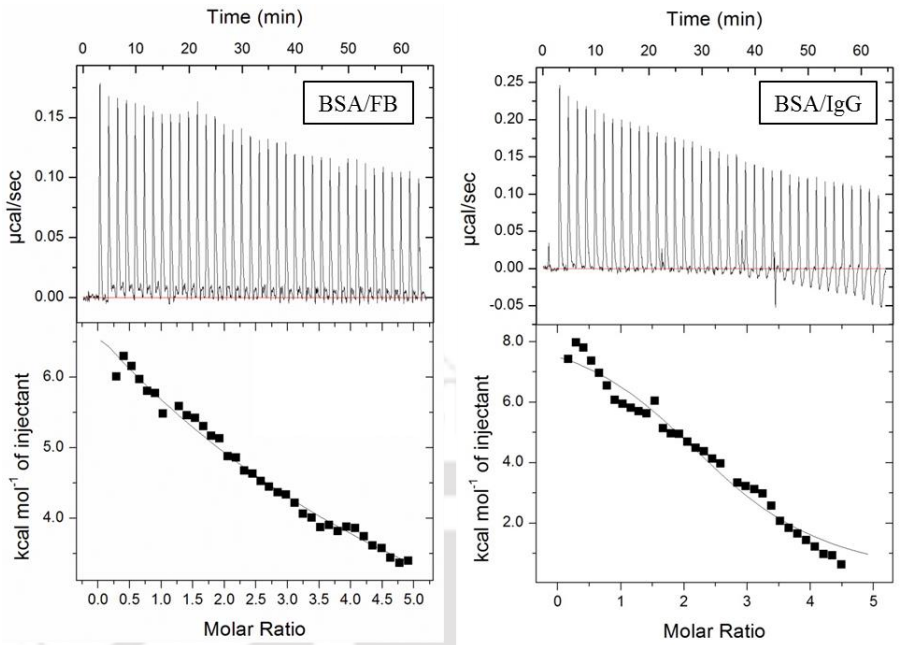

Figure 4.13. ITC thermogram of BSA interaction with FB and IgG at 300K in PBS buffer (pH 7.4).

4.4. Conclusions

We successfully modified the surfaces via silanization and characterized them using various techniques like FTIR, contact angle goniometer and AFM. The purpose of this study was to gain the mechanistic insight of the surface properties and their effect on protein behavior adsorbed from single and binary protein solutions. Surface energy of hydrophilic and moderately hydrophilic surfaces (i.e. unmodified, COOH and amine) decreased after protein adsorption while it increased for hybrid, mixed and hydrophobic octyl surfaces. The surface energies after protein adsorption were found to be gradually increasing with the increase in the surface energies of the modified surfaces with slopes in the range of 0.5 to 0.6. Random distribution of end-on and side-on orientations of adsorbed protein molecules resulted in increased surface roughness. Negatively charged and hydrophobic (octyl) surfaces exhibited the maximum masses of due to electrostatic and hydrophobic interactions between protein molecules and surfaces, respectively. The surface coverages by side-on and end-on orientations, calculated theoretically based on sizes

of proteins, were competed with the experimentally AFM data analysis. Adsorbed proteins were found to be the majority of side-on oriented irrespective of surfaces chemistry. We observed compact (N-form) and elongated (E-form) forms of BSA molecules on hydrophilic and hydrophobic surfaces, respectively. α-helix content of BSA and β-sheet content of FB and IgG proteins were found to increase with an increase in the side-on (%) oriented protein molecules on the surfaces. SDS-PAGE analysis for the competitive adsorbed proteins indicated the presence of both the proteins. However, relative abundances of smaller protein (BSA) on surfaces were lower. Further, complete displacement of weakly bound (end-on orientation) molecules and partial displacement of strongly bound (side-on orientation) molecules of a smaller protein by a larger one was noted. A theoretical analysis was done to determine the % secondary structures of competitively adsorbed proteins from BSA/FB and BSA/IgG binary protein solutions based on secondary structures of individual adsorbed proteins, which agreed well with our experimental results. The protein-protein interactions measured using ITC confirmed the entropy driven competitive adsorption process. These findings will help in designing and tuning the implant surfaces to better understand their responses in various biomedical applications.

Chapter 5

Effect of Surface Modification on Cell Adhesion Behavior

In the present chapter, the effect of previously silanized five different (amine, octyl, mixed, hybrid and COOH) surfaces on protein adsorption behavior and initial cell adhesion has been described. Fetal bovine serum (FBS) was used for the protein adsorption experiment and the effect of FBS was analyzed on initial cell adhesion kinetics (upto 6 h) under three different experimental conditions: (a) with FBS in media, (b) with pre-adsorbed FBS on surfaces and (c) incomplete media, i.e., without FBS. Cell features such as cell morphology/circularity, cell area and nuclei size were also studied for the above stated conditions at different time intervals. Based on the observations, it was concluded that amongst all the modified surfaces and under all three experimental conditions, hybrid surfaces exhibited excellent properties for supporting cell adhesion and growth and hence can be potentially used as surface modifiers in biomedical applications to design biocompatible surfaces.

5.1. Introduction

SAMs of silanes and thiols form highly organized covalently attached organic molecules with nano-thick coatings which in turn provide tunable surface properties [10, 260]. Desirable surface properties can be easily generated by choosing various functionalized molecules from the huge available library. Although SAMs with different functionalities such as $-NH_2$, -COOH, -Cl, -OH, $-CH_3$ and their mixed combinations have been explored for protein adsorption and cell

adhesion [127, 241, 304, 305] but their effect on initial cell adhesion kinetics and spreading is less explored. This inspired us to undertake this challenge to explore the underlying aspects of initial cell adhesion on surfaces exhibiting different surface functionalities (wettability) in the presence and absence of serum proteins.

In the present work, we prepared surfaces with different wettability by varying the surface functionalities using various mono, mixed and hybrid SAMs [140, 247]. The adsorption of serum proteins was examined on these modified surfaces in terms of adsorbed amounts using bicinchoninic acid (BCA) assay and change in secondary structures using FTIR analysis. The kinetics of the initial L929 mouse fibroblast cell adhesion was investigated in the presence of modified surfaces with (a) without fetal bovine serum (FBS) in media, (b) with 10% FBS in media, and (c) FBS pre-adsorbed on surfaces. With the change in protein behavior at differently functionalized surfaces, the behavior of adhering cells also changes. Along with kinetic studies under all the three experimental conditions stated above, we also determined the effect of surface modifications on cell adhesion and spreading, their morphology and nuclei size.

5.2. Materials and methods

5.2.1. Materials Used

Florescent dyes such as phalloidin-fluorescein isothiocyanate (FITC) labeled (Cat. No. P5282) and propidium iodide (PI, Cat. No. P4170), and cell culture plastic consumables were purchased from Sigma Aldrich, India. Fetal bovine serum (10270106), penicillin streptomycin solution (Pen Strep, 15140122), vinculin primary antibody (Cat no. 700062) and secondary antibody-Alexa Fluor 350 (Cat. No. A11046) were purchased from ThermoFisher Scientific,

India. Dulbecco's modified Eagle's medium (DMEM, Cat. No. AL007S) was purchased from HiMedia, India.

5.2.2. Surface Modification and Characterization

Silicon substrates with amine, octyl, mixed (amine:octyl), hybrid, and COOH SAMs were modified using the method described in Chapter 3, Section 3.2. Surface silanization and chemical groups on the surfaces were identified by using FTIR. Surface wettability and surface energies of the modified surfaces were analyzed using contact angle goniometer, while surface roughness and topological analyses were carried out using AFM instrument, as described in materials and methods section (section 3.2) of Chapter 3.

5.2.3 Protein Adsorption and Analysis

Protein adsorption and determination of adsorbed protein mass was carried out using protocol mentioned in sub-section 4.2.3 of Chapter 4. For the protein adsorption experiment, FBS (10%) solution was prepared in PBS (1X, pH 7.4). Preparation of PBS protocol is described in Chapter 4. The secondary structure of adsorbed FBS on different surfaces was analyzed by deconvolution of amide-I spectra, as discussed in Chapter 4.

5.2.4. Cell Adhesion on Modified Surfaces

L929 mouse fibroblast cell line was maintained in CO_2 incubator at 37ºC and 5% CO_2 and cultured in Dulbecco's modified Eagle's medium supplemented with 10% (v/v) FBS and 1% (v/v) antibiotic (Pen Strep). Modified surfaces were sterilized by placing them under UV radiation for 45 min prior to the experiment. Cells were grown in 25 cm^2 cell culture flasks

(Corning) to 80-90% confluency. After trypsin treatment, the cells were washed with excess media, centrifuged and counted using hemocytometer. Cells at a concentration of $1x10^5$ cells per mL were added to each surface and incubated for 6 h under three different conditions: (i) incomplete media i.e. without FBS, (ii) complete media i.e. supplemented with 10% FBS, and (iii) surfaces pre-adsorbed with FBS. Two sets of experiments were established; in one experiment, cells were counted using hemocytometer while in another experiment their images were recorded after 15, 30 45, 60 120, and 360 min of seeding respectively. For cell imaging experiment, cell adhered surfaces were washed thrice with filtered PBS and fixed with 4% (v/v) paraformaldehyde solution overnight at 4ºC.

Cells were further treated with 2% (w/v) BSA and 0.2% (v/v) Triton X-100 for 6 h followed by actin filaments staining with FITC-Phalloidin for 12 h. Vinculin protein was first targeted with anti-vinculin 1º antibody for 6 h, followed by Alexa fluor-350 labelled 2º antibody for another 6 h. Cells nuclei were stained by incubating substrates in 20 μg/ml of PI for 2 h at room temperature under dark conditions. Post staining, substrates were washed thrice with PBS and imaged using Nikon fluorescent microscope (Model: Nikon Eclipse Ti-S). ImageJ software (developed at the National Institutes of Health) was used for analyzing cells and nuclei area and cell circularity of the adhered cells on different modified surfaces.

5.3. Results and Discussion

5.3.1. Characterization of Modified Surfaces

Surface functional groups mainly regulate surface wettability if the surface roughness is significantly low [260], polar groups increase wettability while hydrophobic/non-polar groups decrease it. Figure 5.1 shows the effect of surface modification on change in surface wettability

and its subsequent effect on adsorbed protein mass. Characterization results are described in detail in Chapter 3. Briefly, FTIR analysis confirmed the formation of siloxane bonds (Si-O-Si) as a result of silanization. Varying surface wettability after silanization further confirmed surface modification. Topology analyzed by AFM depicts surfaces with nanoscale roughness.

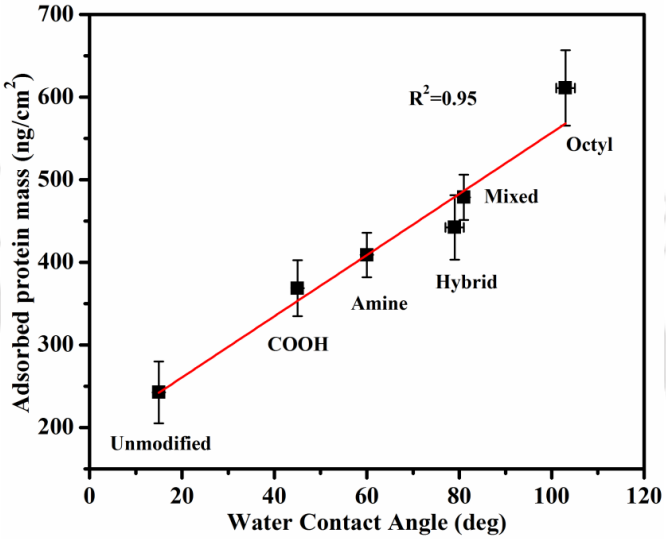

Figure 5.1. Effect of surface modification on surface wettability and adsorbed protein mass from 10% FBS solution (PBS, pH=7.4) on various modified surfaces.

5.3.2. Effect of Surface Modification on Protein Adsorption

Surface roughness and topology, wettability, surface potential and surface energy are physico-chemical properties of a surface that can be regulated by surface modification. We have previously shown that such surface properties do regulate highly complex process of protein (BSA, Fibrinogen) adsorption, adsorbed mass and their secondary structures [141, 247]. In the present work, it was aimed to determine the effect of such modification on serum protein adsorption and subsequently their effect on cell adhesion and spreading. To mimic cell culture conditions, 10% FBS solution for protein adsorption was used and the adsorbed mass using BCA assay was determined [306]. Figure 5.1 shows the adsorbed mass of proteins on different modified surface as a function of surface hydrophobicity. Linearly increasing adsorbed protein

mass with the increasing surface hydrophobicity was noticed. The pattern of protein adsorption observed in this study is similar to the pattern of serum albumin adsorption reported by our group previously [141, 247]. Since, serum contains a very high concentration of albumin (~66 kDa) i.e., 35-50 mg/mL, so it was considered that maximum adsorbed protein molecules were of albumin and this was also evidenced by the observation of the similar protein adsorption pattern as obtained in the case of BSA adsorption [140, 247].

Figure 5.2 shows the distribution of the secondary structure of the adsorbed FBS on different surfaces. Percent secondary structures (α-helix, β-sheet, β-turn, random coil and side chains) were analyzed by deconvolution of the FTIR spectra in the range 1600-1700 cm^{-1}, as reported by our group previously [141, 307]. De-convoluted FTIR spectral images on different surfaces are shown in appendix Figure 5A-1. FBS majorly contains BSA (35-50 mg/mL) followed by IgG (8-22 mg/mL) and fibrinogen (FB) (1.5-4 mg/mL) proteins. Effect of surfaces plays a major role during competitive protein adsorption from mixed protein solution, as reported previously [141]. Hence, the variation in the secondary structures of adsorbed FBS can be attributed to the surface wettability and functionality. Native FBS contains around 45% of α-helix, and approx. 25% of each β-sheet and β-turn, while the remaining 5% comprised of a random coil. α-helix content on amine, COOH and hybrid surfaces was found to be in the range 40-45%, which may either be due to the presence of BSA or FB molecules as IgG (mainly contains β-sheet, ~70%) is a non-helical protein molecule. It was comparable to the unmodified (blank) surface whereas it reduces significantly on other surfaces. β-sheet content significantly increased on COOH surface possibly indicating higher content of IgG comparatively. Percent β-turn on COOH surface also indicated more molar ration of IgG as compared to BSA and FB

whereas turn (%) was higher on other surfaces indicating presence of majority of BSA and FB molecules.

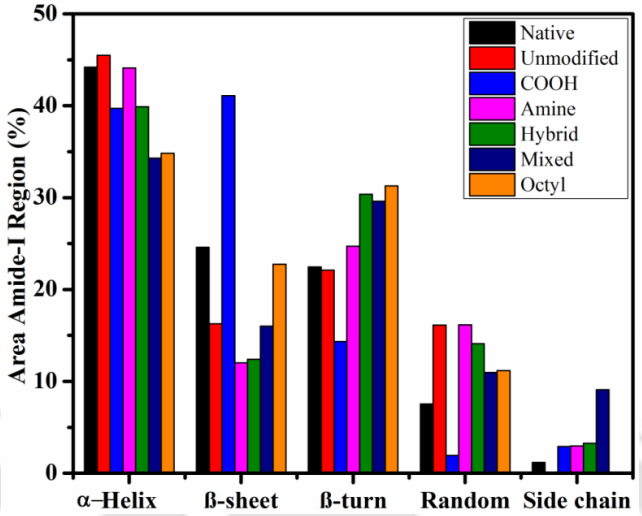

Figure 5.2. Percentage distribution of secondary structures of FBS proteins on different modified surfaces.

5.3.3. Cell Adhesion and Spreading

Surface properties widely regulate cell behavior such as adhesion, spreading, migration, and proliferation at the interface. Various researchers argued that surface wettability directly relates to cell adhesion and that hydrophilic surfaces support better cell adhesion than hydrophobic surfaces [308].

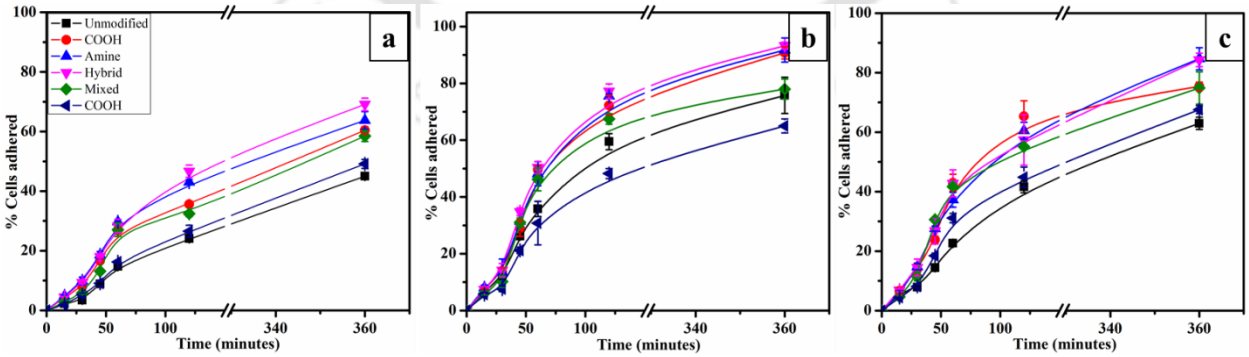

Figure 5.3. Effect of surface modification on % cell adhesion at different time interval under (a) media without FBS, (b) media supplemented with 10% FBS, and (c) surface with pre-adsorbed FBS.

While other researchers contradicted this hypothesis and reported that hydrophobic SAM surfaces offered better cell spreading and proliferation comparatively to lesser hydrophobic surfaces [309]. Arima and Iwata reported several modified surfaces with different chemistry and wettability and showed that surfaces with contact angle range 40-50º exhibit better cell behavior [2, 305]. However, our recent report contradicted to the existing literature and concluded that surface wettability along with surface energy regulates protein adsorption and results in their different secondary structures that in turn regulate cell adhesion [307].

Figure 5.3 shows the % cell adhesion on various modified surfaces under three different conditions: (i) incomplete media i.e. without FBS, (ii) complete media i.e. supplemented with 10% FBS, and (iii) surfaces pre-adsorbed with FBS. It was that the maximum no. of cells adhered (about 90%) on hybrid, amine and COOH surfaces in case of 10% FBS supplemented cell media, around 80% adhesion on amine and hybrid surfaces with pre-adsorbed FBS on surfaces and approx. 60% on hybrid surfaces in the case of incomplete media, after 360 min of cells seeding. Under all the three conditions, we observed better cell adhesion on hybrid and amine surfaces, especially on hybrid surfaces which may be due to the following 3 factors: (i) hybrid surfaces contains both hydrophilic and hydrophobic moieties on the same molecule that might be helping in cell adhesion and spreading. (ii) hybrid surfaces exhibit contact angle (θ=79º) which lies in the range (50-80º) that is shown to be optimal for cell adhesion. (iii) adsorbed protein molecules form a soft layer on hybrid surface [140] and may be helpful for cell adhesion. Amine surfaces exhibited better cell adhesion owing to its positive surface charge which resulted in cell adhesion due to negatively charged cell membranes via ionic interactions. COOH surfaces also exhibited significantly better cell adhesion as compared to unmodified, mixed and octyl surfaces. Surfaces treated with media without FBS exhibited poor cell adhesion.

Protein molecules present in the serum adsorb quickly when they come in contact with surfaces and serves as cushions for adhering cells. Furthermore, serum contains cell adhesive proteins such as FN which contains RGD tripeptide sequences and helps in integrin mediated cell adhesion [310, 311]. Hence, better cell spreading area and morphology on surfaces treated with FBS as compared to surfaces treated with cells in serum free media was observed.

5.3.3.1. Fluorescence Imaging Analysis of Adhered Cells

Phase contrast images of the adhered cells after each time interval under all the three experimental conditions were captured and analyzed using Image J software (refer appendix Figure 5A-2 and 5A-3). We also employed fluorescence microscopy for determining vinculin distribution and actin cytoskeleton of adhered cells. Vinculin is an actin binding focal adhesion protein which not only helps in interactions of integrins with cytoskeleton but also regulates cell spreading and migration [312]. During cell adhesion, vinculin binds to actin and stimulates polymerization and engaging actin remodeling proteins. Hence, fluorescent staining of vinculin protein indicates the formation of focal adhesion sites which further can be used to distinguish between poor and good cell adhesion based on its distribution inside the cells. Charged (i.e. amine and COOH surfaces) and hybrid surfaces exhibited better vinculin distribution as compared to unmodified, mixed and octyl surfaces as showed with arrow marks in Figure 5.4. Whereas actin filament forms the cytoskeleton and helps the cells in mechanosensing and spreading by linking to focal adhesions at cell-substrate sites [313]. By staining the actin filaments, we were able to observe the actual morphology of cells on different modified surfaces. Figure 5.4 shows adhered L929 cells exhibiting spreading and morphological behavior on different modified surfaces with pre-adsorbed FBS after 360 min of incubation. See appendix Figure 5A-4 and 5A-5 for fluorescent cell images for experiments carried out in medium with

and without serum. As shown in Figure 5.4, adhered cells on hybrid and amine surfaces exhibited better cell features such as area and morphology, vinculin distribution (spreading) as compared to other surfaces under pre-adsorbed FBS condition, indicating better integrin expression on these surfaces. Cells adhered on surfaces with FBS in media also exhibited better cell features on hybrid and amine surfaces as compared to other surfaces.

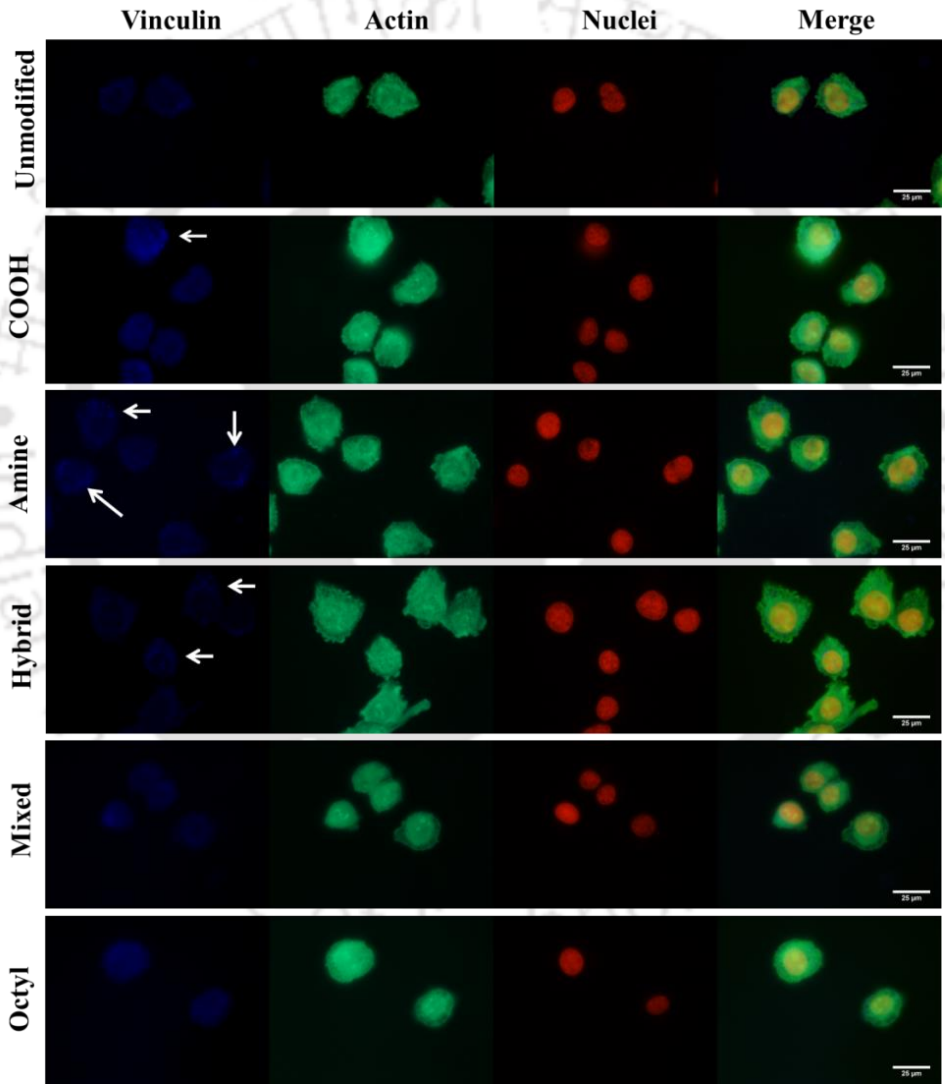

Figure 5.4. Fluorescent images of L929 cells cultured for 6 h on different surfaces pre-adsorbed with FBS and stained for vinculin protein (blue, 1º Ab followed by Alexafluor-350 labelled 2º Ab), actin filaments (green, FITC-Phalloidin) and nuclei (red, PI dye). Arrow marks indicate focal adhesion spots of bright blue color due to vinculin staining by Alexa fluor-350. Scale bar is 25 µm.

Under FBS free media, cells showed poor adhesion (as evidenced by poor vinculin localization inside the cells) and morphology (high cell shape index) even after 360 min of seeding, indicating poor integrins expression. Figure 5.5 presents the analysis of various cell behaviors on different surfaces under all the three stated conditions after 360 min of cell seeding. Interestingly, variation in % cell adhesion (see Figure 5.5(a)) among different surfaces was found to follow a similar pattern in all three cases i.e. maximum on hybrid (θ=79º) surface followed by amine (θ=60º), COOH (θ=45º) and mixed (θ=81º) surfaces while least on extremely hydrophilic (unmodified, θ=15º) and hydrophobic (octyl, θ=102º) surfaces. The data obtained by us agreed well with the previous reports that cell adhesion gets optimum at surfaces exhibiting wettability in the range 50-80º [2, 126, 314]. The maximum cell area was observed on surfaces pre-adsorbed with FBS followed by surfaces treated with cells in media supplemented with 10% FBS and least on surfaces with cells in incomplete media, as shown in Figure 5.5(b). Cell area was found linearly increasing with the increasing contact angle and was observed maximum on hybrid surface and then drastically decreased on mixed and hydrophobic octyl surfaces. Although mixed (θ=81º) and hybrid (θ=79º) surfaces exhibit almost similar contact angle but cell behavior such as number and area of adhered cells on them was entirely different. Hybrid are monomolecular SAMs while mixed SAMs are mixture of amine and octyl silanes and suffers from phase separation issues and hence results in poor cell adhesion and spreading [140, 304]. This confirms that surface wettability is not the only factor that regulates the cell adhesion process.

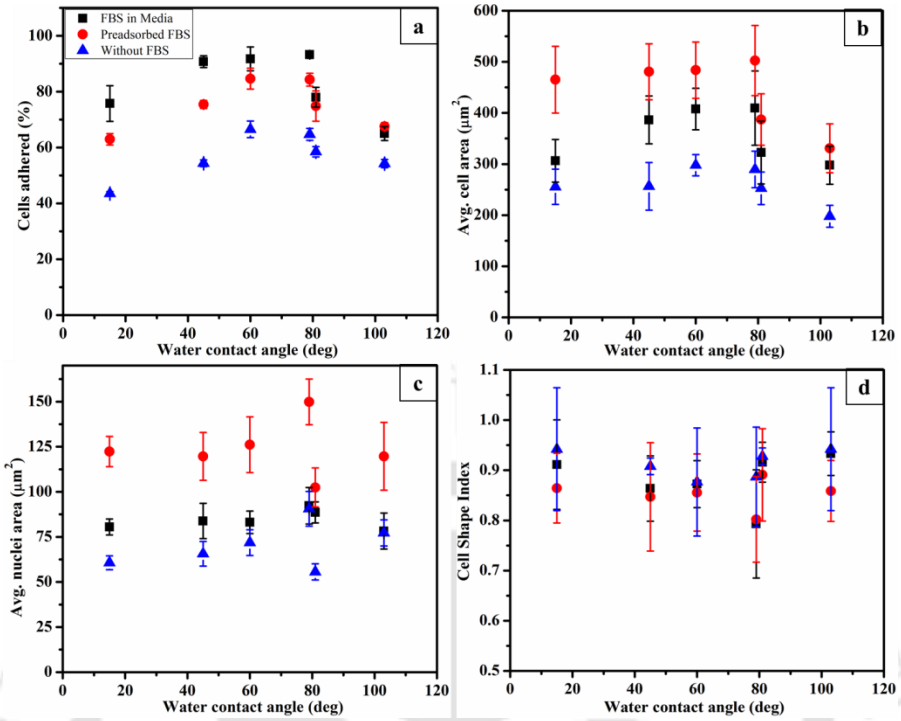

Figure 5.5. Effects of different modified surfaces on (a) % cell adhesion, (b) avg. cell area, (c) avg. nuclei area and (d) circularity after 6 h of incubation from incomplete media, media with FBS and surfaces pre-adsorbed with FBS. Values represent the mean ± SD.

Surfaces with pre-adsorbed FBS exhibited the maximum cell area due to the fact that adsorbed protein molecules undergo re-orientation and expose cell binding sites present in cell adhesive proteins (eg. FN). On pre-adsorbed FBS surfaces, cells adhered on hybrid (502±68 μm^2), amine (484±55 μm^2) and COOH (481±54 μm^2) surfaces exhibited better spreading as compared to blank (465±65 μm^2), mixed (387±50 μm^2) and octyl (330±48 μm^2) surfaces. A similar pattern of cell area variation was observed for cells with FBS in media while cells seeded in incomplete media showed better spreading on amine (297±21 μm^2) surface but was comparable to cell spreading on hybrid surface (289±36 μm^2). Cell area was significantly reduced in the absence of serum proteins indicating that proteins molecules help in cell spreading. Effect of surfaces wettability on nuclei size was also evaluated as nuclei size of the adhered cells indicate the nuclear functional activity occurring during proliferation [315]. Effect

of surface modification on nuclei size is less reported and it is predicted that the increase in nuclei area may result in the higher proliferation rate. Surfaces pre-adsorbed with FBS exhibited the maximum nuclei area and was followed by cell with FBS and least on surfaces treated with media without FBS. Average nuclei area of adhered cells was maximum for the hybrid surfaces, followed by amine and COOH surfaces (shown in Figure 5.5(c)). The least nuclei size was observed on mixed surface due to phase separation issues as mentioned earlier. A similar pattern of nuclei area variation was observed in other two conditions.

Circularity of adhered cells can be explained based on the value of cell shape index (CSI), calculated using the following expression:

$$CSI = {}^{4\pi A}/_{P^2} \tag{5.1}$$

Where; A is area and P is perimeter. It is described on the scale range of 0.0 (line) to 1.0 (circle) and is used to define the shapes of the cell. Lower value of circularity signifies better cell spreading having more focal points due to which cell shape changes. Effect of seeding time on cell circularity (refer appendix Figure 5A-6) was analyzed for all modified surfaces with and without FBS proteins. Hybrid surface showed the least and similar CSI value (0.80±0.08) with pre-adsorbed FBS and FBS in media samples and was significantly lesser, indicating better adhesion and spreading in comparison to other silanized and unmodified surfaces, as presented in Figure 5.5(d).

Figure 5.6 shows the relationship between average cell spreaded area with no. of adhered cells on different surfaces in the presence and absence of FBS. The average area of adhered cells, however, significantly increased on surfaces with pre-adsorbed FBS and media with FBS but did not significantly enhance the number of adhering cells after 6 h of cell seeding.

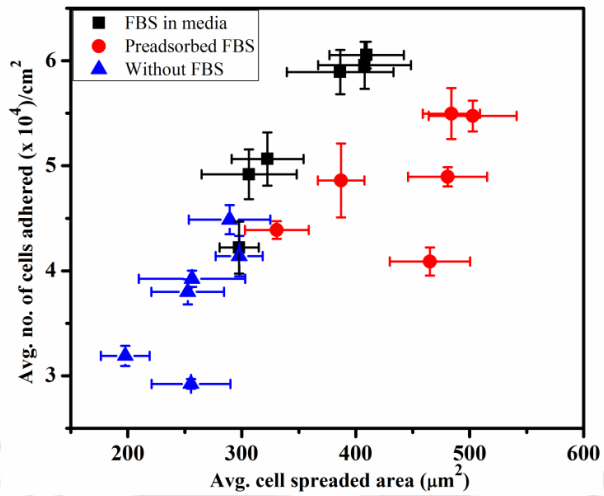

Figure 5.6. Average no. of cells adhered vs average cell area during cell adhesion studied under three different conditions.

A relation between FBS proteins and cell adhesion and spreading was established. We found cell area and % surface coverage linearly related to each other with R^2 ranging between 0.80 to 0.99, as shown in Figure 5.7. Percentage coverage data are shown in appendix Figure 5A-7. Percent coverage depends on the number of adhered cells and average cell area in totality. Surfaces treated with media supplemented with FBS exhibited better correlation (R^2=0.99) as compared to pre-adsorbed (R^2=0.80) and media without FBS (R^2=0.82).

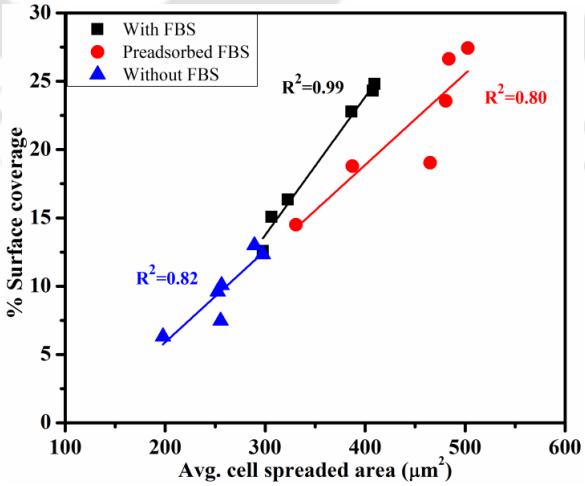

Figure 5.7. Correlation between % surface coverage and average cell area on surfaces studied under the effect of FBS proteins.

5.3.4. Cell Adhesion Kinetics

The adhesion of cells on surfaces was modeled theoretically as shown in Figure 5.8. The simplest kinetics of cell adhesion is explained as follows:

$$N_B \xrightarrow{k_f} N_I + S \underset{k_d}{\overset{k_a}{\leftrightarrow}} N_S \tag{5.2}$$

Where N is the number of cells and *B*, *I* and *S* refer bulk suspension, interface and surface, respectively. k_f is film mass transfer coefficient, k_a is rate constant for cell adhesion and k_d is rate constant for cell detachment.

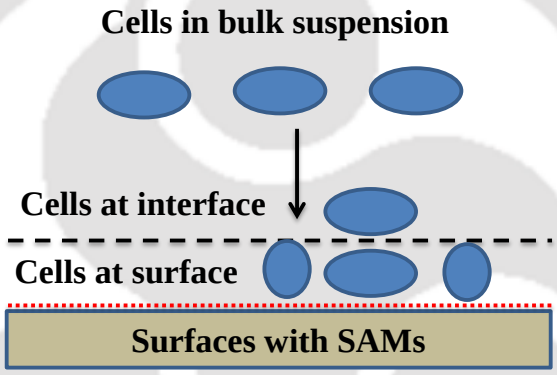

Figure 5.8. Representation of cell adhesion phenomenon from bulk suspension onto the surface.

We assumed the absence of film mass transfer resistance due to higher concentration of cells in bulk and k_d was considered as negligible under present experimental time duration. Thus, the simple kinetic equation describing the cell adhesion is as follows:

$$\frac{dN_S}{dt} = k_a[N_I][S] = k_a[N_B - N_S][S] \quad \{N_I + N_S = N_B\} \tag{5.3}$$

The above equation can be written in term of surface coverage, $\theta(N_S \times A_C/A_S)$ as follows:

$$\frac{d\theta}{dt} = k_a[(N_B \times A_C/A_S) - \theta][S_f] \tag{5.4}$$

Where A_S refers to the total surface area, A_C denotes the average area of adhered cells and $[S_f]$ refers the surface fraction available for cell adhesion. The solution of the above

equation, $\theta(\%) = 100(1 - \exp(-[S_f] \times k_a \times t))$, was used to fit the experimental data and the k_a values for different surfaces were determined as listed in Table 5.1. The highest rate of cell adhesion was found to be 0.0725 h^{-1} on hybrid surface with pre-adsrobed FBS. The theoretical model proposed above was verified by fitting the experimental data of the % surface coverage. The fitted data agreed well with the experimental data (as shown in appendix Figure 5A-7) and hence justifies the validity of the model. A better/faster cell adhesion on surfaces with pre-adsorbed FBS was observed due to adhered proteins molecules undergoes reorientation resulting in exposure of cell binding sites, which in turn promotes cell adhesion.

Table 5.1. Rate of surface coverage on different modified surfaces by adhering cells in three different conditions.

Surface	Without FBS (h^{-1})	With FBS (h^{-1})	Pre-adsorbed FBS (h^{-1})
Unmodified	0.0140	0.0366	0.0423
COOH	0.0208	0.0602	0.0623
Amine	0.0263	0.0639	0.0716
Hybrid	0.0277	0.0647	0.0725
Mixed	0.0192	0.0402	0.0466
Octyl	0.0121	0.0278	0.0330

5.3.5. Relation between Secondary Structure of Protein and Cell Adhesion

Rearrangement or re-orientation of secondary structures of protein post adsorption influences cell adhesion. Grohmann et al. reported that β-sheet secondary structure of biomimetic polypeptide enhanced cell adhesion and proliferation over random coil structures [316]. β-sheet provide more rigidity and space for cells to spread and hence, proliferation rates are higher on them as compared to random coils. Apart from structural rigidity, exposure of cell binding motifs (e.g. RGD tripeptide) upon adsorption of cell binding proteins (e.g. FN) mainly regulates the cell adhesion and spreading process [307].

For better realizing the role of the secondary structure of adsorbed FBS proteins on surfaces, we analyzed the effect of all secondary structures on cell adhesion rate, individually. We found that the change in the α-helix content of adsorbed FBS with respect to unmodified surface exhibited a linear relationship with change in % adhered cells (Figure 5.9(a)) as well as with the initial surface coverage rate (Figure 5.9(b)) of L929 cells. The cell adhesion data in presence of FBS in media (R^2=0.65) and pre-adsorbed FBS (R^2=0.65) showed better correlation with change in α-helix content as compared to cells adhered on surface in absence of FBS (R^2=0.45). Moreover, the correlation between the change in α-helix content and initial surface coverage rate was better on pre-adsorbed FBS (R^2=0.76) and FBS in media (R^2=0.72) as compared to control i.e. without FBS in media (R^2=0.61).

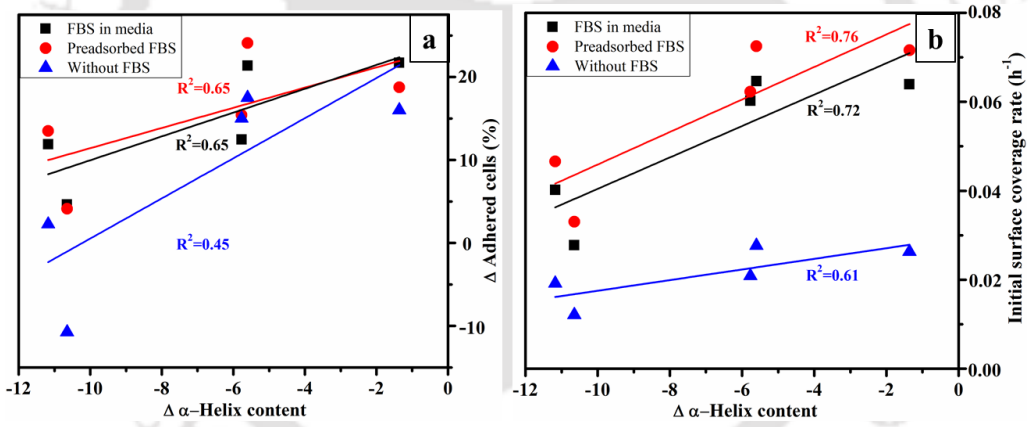

Figure 5.9. Relationship between change in α-helix content with (a) change in % adhered cells and (b) initial surface coverage rate by L929 cells on modified surfaces under different experimental conditions.

Hence, this clearly indicates that α-helix content of the adsorbed protein molecules in case of FBS plays a key role in regulating cell adhesion. These findings will enable researcher's working in this domain to predict cell adhesion behavior based on surface properties and secondary structure of the adsorbed protein. This study will ultimately facilitate in designing biocompatible surfaces.

5.4. Conclusions

Nanoscaled modified surfaces were successfully prepared via silanization as evidenced by FTIR, WCA and AFM results. We created surfaces with varying wettability to demonstrate their effect on protein adsorption and subsequently on cell adhesion for tissue engineering applications. We employed three different experimental conditions i.e. (a) complete media supplemented with 10% FBS, (b) surfaces with pre-adsorbed FBS, and (c) incomplete media i.e. without FBS, to determine the effect of FBS proteins and surfaces on cell adhesion and behavior. Surfaces treated with incomplete media exhibited the least cell adhesion rate, poor morphology and smaller adhered cell and nuclei area irrespective of surfaces. Whereas, surfaces in the presence of FBS in media and pre-adsorbed FBS exhibited excellent cell features on amine, hybrid and COOH surfaces. Surface coverage rate of adhering cells was the highest on hybrid surfaces under all three conditions. It is noteworthy that orientation and secondary structure of adsorbed FBS protein molecules helped in cell adhesion and spreading in case of pre-adsorbed FBS. Especially, hybrid surface showed better cell and nuclei area amongst all the surfaces indicating better surface properties for cell adhesion and proliferation. Furthermore, we found that the initial surface coverage rate and Δ adhered cells (%) linearly increased with the change in α-helix content of adsorbed FBS proteins. Based on the results obtained, we can conclude that protein adsorption and its orientation regulates cell adhesion and spreading and hybrid surface can be potentially used for biomedical application especifically for tissue engineering owing to its excellent cell supporting properties.

Chapter 6

Effect of Surface Modification of Biomedically Relevant Titanium Alloy Surface on Protein and Cell Behavior

A great challenge since decades for metallic biomaterials to find biomedical applications has been mainly due to their inherent low bioactivity and poor osteointegration property. Surface modification via silanization can serve as an attractive method for improving the aforementioned properties of such substrates. This chapter discusses about the surface modification of biomedically relevant titanium alloy (Ti6Al4V) and their potential scope in tissue engineering applications.

6.1. Introduction

SAMs modified Ti surfaces have been reported for various applications such as drug delivery, formation of antibacterial layers, mineral deposition for improving osteoconductivity, regulating non-specific protein adsorption and cell adhesion, and immobilization of biological molecules [317-322] etc. A recent report stated the surface modification of magnesium alloy using silanization for improved bio-functionality and biocompatibility [323]. Though very few reports exist in which silane and phosphate based SAMs have been investigated on sputtered TiO_2 substrates rather than commercially available Ti sheets [240, 261]. Liu et al. demonstrated the formation of different functionalities (such as –OH, –COOH, $–NH_2$, $–PO_4H_2$, $–CHCH_2$, $–CH_3$) on Ti substrates and their role in hydroxyapatite deposition and calcium phosphate nucleation

[240, 324]. Marin-Pareja et al. recently demonstrated the effect of silanized Ti surfaces on the organization of type-1 collagen which regulated fibroblast adhesion, spreading and fibronectin secretion [325]. Collagen organized into globular clusters on a hydrophilic surface enhanced fibroblast adhesion and spreading. Authors also stressed on the concentration of collagen used, as on increasing its value above the threshold, resulted in masking of collagen conformation, hence, similar behavior of fibroblast was observed on all the surfaces [325].

Although some efforts have been made to determine the effect of physio-chemical properties at the interface on the behavior of adsorbed FN and initial cell response [127, 326], the effect of silanized Ti/Ti-alloy on FN secondary structure and subsequent fibroblast adhesion has not been reported yet to our best knowledge. This knowledge lacuna inspired us to analyze the behavior of FN adsorption and the effect of surface modification on secondary structure. We were also interested to know whether or not the secondary structures of adsorbed FN on different surfaces play any role in cell adhesion.

6.2. Materials and Methods

6.2.1. Materials Used

The materials used for this study and their sources are mentioned in previous chapters. The remaining materials that were procured are FN (F1141), propidium iodide (PI, P4170), 4′,6-diamidino-2-phenylindole dihydrochloride (DAPI, D9542), 3-(4,5-dimethylthiazol-2-yl)-2,5-diphenyltetrazolium bromide (MTT, M2128) and were purchased from Sigma Aldrich, India. Ti6Al4V alloy sheets with 1 mm thickness were a kind gift from Dr. Ravi M. Sankar, Assistant Professor, Department of Mechanical Engineering, IIT Guwahati.

6.2.2. Surface Modification and Characterization

Ti6Al4V substrates with amine, octyl, mixed (amine:octyl), hybrid, and COOH SAMs were modified using the silanization method described in Chapter 3. Surface silanization and the chemical groups on the surfaces were identified by using FTIR (FTIR spectra shown in Figure 3.11). The surface energies of the surfaces were determined from the measured contact angles of water and MI as described in Chapter 3.

Roughness of the SAM modified Ti surfaces was analyzed using high precision non-contact computerized surface profilometer (Taylor Hobson, UK). The instrument was fitted with 20X lens that scanned an area of 850×850 μm^2 at a focal length of 4.7 mm. Profilometer is based on optical light interference principle that provides surface information such as topography and roughness. Due to its non-contact mode of operation, it does not damage actual surface features.

Surface morphologies of unmodified and modified Ti6Al4V substrates were distinguished using FESEM (Zeiss, Model: Sigma) instrument which was operated at an accelerating voltage of 2-4 kV and at a magnification of 150 KX. Energy-dispersive X-ray spectroscopy (EDX) equipped with the instrument was used to determine the distribution of elements on the modified surfaces.

6.2.3. Protein Adsorption and Secondary Structure Analysis

Protein adsorption and quantification of adsorbed mass was carried out using the methods mentioned in Chapter 4 in detail. Protein samples of BSA (100 µg/ml) and FN (10 µg/ml) were prepared in phosphate buffer saline (PBS, pH 7.4) and used for analysis. Change in secondary structures of the adsorbed proteins (BSA and FN) was also investigated using ATR-FTIR

particularly in the amide I range 1600-1700 cm^{-1}. Please refer to Chapter 4, Section 4.3.5 for secondary structure analysis.

Surface wettability and energies were calculated after FN adsorption in a similar way as described in chapter 3. Their effects on cell adhesion and spreading were studied and are shown in later sections.

6.2.4. Cell culture studies

Mouse fibroblast cell line, L929 was maintained under conditions mentioned in Chapter 5. Cells were grown to 90% confluency, trypsinised, centrifuged and counted using a hemocytometer before performing cell culture experiments.

6.2.4.1. Cytotoxicity assay

Biocompatibility of modified surfaces was assessed by performing cytotoxicity analysis based on MTT assay. Cells were seeded onto samples (UV sterilized, 30 W, 30 min) at a density of 5×10^4cells/cm^2 and incubated for 2, 4 and 6 days. After each specified time interval, media was replaced with fresh media containing 20 µl of MTT solution (5mg/ml, sterilized PBS, pH 7.4) and incubated at 37 ºC for 4 h. Post incubation, media was replaced with 500 µl of DMSO and incubated for another 10 min to dissolve formazan crystals formed due to metabolic activity of live cells. Optical density of the dissolved formazan was recorded at 570 nm (Infinite 200 Pro, Tecan). The absorbance result was used to determine the cells proliferation rate as a function of different functional groups present on modified surfaces. Assay was performed in triplicates to calculate the standard deviation.

6.2.4.2. Cell morphology using FESEM

Effect of surface functionalities and wettability were also analyzed for understanding their role in promoting cell adhesion. Cell spreading or cell morphology of the adhered L929 cells was studied using FESEM after 6 h of incubation on modified surfaces. Post incubation, surfaces were washed thrice with PBS (pH 7.4) to remove non-adhered cells whereas adhered cells were fixed using 2.5% (v/v) glutaraldehyde solution for 2 h at room temperature. Surfaces were later washed with PBS followed by graded dehydration with 40%, 60%, 80%, 90% ethanol for 10 min, respectively and with 95% and 100% ethanol for 30 min each. Surfaces were then critical point dried using hexamethyldisilazane (Sigma, India) for 10 min, gold sputtered, and examined using FESEM.

6.2.4.3. Fluorescent Imaging

Fibroblast cells were seeded at a density of $5x10^4$ cells/cm^2 on modified surfaces and incubated for 6 h under two different conditions: (a) surfaces without pre-adsorbed protein, in the presence of FBS, (b) surfaces pre-adsorbed with FN. Samples with pre-adsorbed FN were incubated with cells which were dispersed in FBS free DMEM media for 6 h at 37ºC in a CO_2 incubator. Post incubation, surfaces were washed thrice by filter sterilized PBS (pH 7.4) to remove non-adhered cells. Adherent cells were fixed with 4% (v/v) paraformaldehyde solution (HiMedia, India) overnight at 4ºC. Cells were later washed and treated with 2% (w/v) BSA and 0.2% (v/v) triton X100 for 6 h followed by fluorescent staining of actin filaments with FITC-Phalloidin for 12 h. Cells nuclei were stained by incubating substrates in 20 µg/ml of DAPI (Sigma, India) for 10 min at room temperature. Post staining, substrates were washed thrice with PBS and imaging was carried out by Nikon (Nikon Eclipse Ti-S) fluorescent microscope. Using

image processing software (ImageJ), we calculated the % cell adhered, cell spreading area, nuclei area and circularity of the adhered cells on different modified surfaces.

6.2.5. Bacterial Adhesion Studies

Effect of surface functional groups against bacterial cells adhesion was also investigated to determine their antimicrobial properties. We investigated the adhesion of both Gram positive (*Staphylococcus aureus*, ATCC 6538) and Gram negative (*Escherichia coli*, MTCC 1610) bacteria on modified surfaces for 2 h at 37ºC. Functionalized surfaces were UV sterilized (30W) for 30 min and were seeded with $1x10^7$ CFU/mL in sterilized phosphate buffer saline (PBS). Post incubation, non-adhered bacterial cells were removed and surfaces were washed thrice with PBS. Cells were later fixed with 4% (v/v) paraformaldehyde solution (Himedia, India) for 2 h followed by washing with PBS thrice. Fixed cells were permeabilized with 0.2% (v/v) triton X-100 (Himedia, India) for 30 min and fluorescent stained overnight with PI at room temperature. Cells were visualized under an inverted fluorescent microscope with 100X lens and at least 10 images were captured at different places on the same surface to determine the average number of adhered cells. ImageJ software was utilized for counting cells on different surfaces.

6.2.6. Statistical Analysis

All the experiments were carried out in triplicate and results are expressed a as mean standard deviation for at least n=3. Software SigmaPlot version 14.0 was used to determine the statistically significant differences ($p<0.05$ (#) and $p<0.005$(##)) between the means of different groups, using a one-way analysis of variance (ANOVA) with Tukey test.

6.3. Results and Discussion

6.3.1. Characterization of modified surfaces

Figure 6.1 shows the FTIR-ATR spectra of amine, octyl, mixed, hybrid and COOH modified Ti6Al4V surfaces. Presence of peaks at 720 and 1090 cm^{-1} in all the spectra correspond to bending and stretching of Si-O-Ti bonds similar to Si–O–Si bonds on silica substrates [260], respectively. These indicate the presence of a siloxane bond formation between the silane molecules along with silanization of surfaces [140, 261]. Peaks at 860 and 1175 cm^{-1} indicate Si-C stretching of Si-CH_2R groups further confirming silanization as shown in Figure 6.1(b). Spectra in the range 1500-1750 cm^{-1} as presented in Figure 6.1(c) showing peaks at 1672 cm^{-1} indicate the attachment of N-H group in amine, mixed and hybrid Ti6Al4V samples and are not seen in octyl and COOH samples. Hybrid surface was prepared from previously modified fresh amine surface by attaching the toluene group via urea linkage. Attachment of the toluene group can be clearly observed due to the appearance of a peak at 1642 cm^{-1} in hybrid sample which signifies the formation of urea linkage formed due to reaction between NH_2 and NCO groups [140]. Although the reaction between primary amine and p-Tolyl isocyanate groups is very fast (completes within10 min) in the presence of dibutyl dilaurate, we kept for incubation for 4 h to ensure total conversion of free amine. We previously optimized this conversion process by measuring the diminishing peak at 2270 cm^{-1} which corresponds to NCO (not shown) and enhancing peak at 1642 cm^{-1} which corresponds to urea linkage [140]. Detailed characterization of mixed [306] and hybrid [140] surfaces were reported previously by our group.

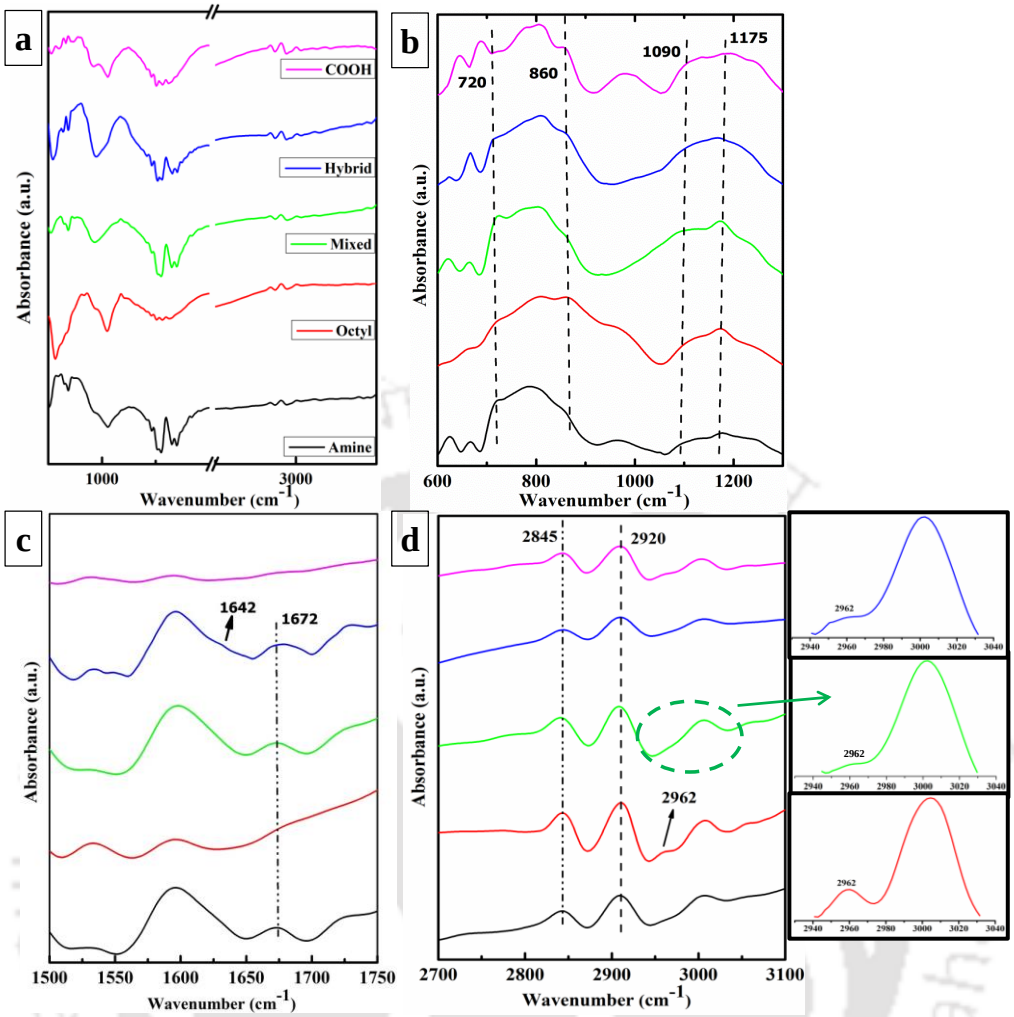

Figure 6.1. FTIR-ATR spectra of modified surfaces.

Generally, peaks at 2932 and 2864 cm^{-1} correspond to asymmetric and symmetric stretching of CH_2, which shifted to 2920 and 2845 cm^{-1} respectively, as shown in Figure 6.1(d). This phenomenon is referred as red shifting and indicates a dense and solid packing of silane groups due to rearrangement of the attached molecules [260]. A broad peak at 2962 cm^{-1} in the octylsilane modified surface represents asymmetric (ν_a-CH_3) stretching peak of the CH_3 group and confirmed the attachment of octylsilane. The intensity of peak at 2962 cm^{-1} reduced significantly (see Figure 6.1(d)) in mixed surface, indicating lesser concentration of octyl groups

due to the presence of amine groups on surface. We used this peak area to determine the surface fraction, C_{amine} (%) of NH_2- groups in mixed SAMs using a reported procedure [2] as follows:

$$C_{amine}(\%) = \left(1 - \frac{A_{mixed} - A_{Octyl}}{A_{amine} - A_{Octyl}}\right) \times 100 \quad (6.1)$$

The C_{amine} was found to be ~ 46% i.e. the mixed surface contained ~46% amine and ~54% octyl groups. This confirms that silanes are immobilized on the surface in proportion to the mixing ratios (1:1) of coupling agents in solution. Moreover, using AFM surface characterization, we previously described the effect of different fractions of amine and octyl silane on average surface roughness and roughness factor [306]. We found that 1:1 ratio resulted in the maximum surface roughness indicating non-uniform but equal distribution of mixed groups hence referred them as mixed surfaces.

Contact angle goniometer was used to determine the wettability of the modified surfaces against water and diiodomethane at room temperature (22±1ºC). Piranha treated unmodified surface exhibited hydrophilic nature (θ=30±2°) due to formation of hydroxide layer (TiOH) on the surface. Similar values of contact angle and surface energies on piranha cleaned surfaces has been reported previously [239, 327]. Different wettability were observed on modified surfaces as shown in Table 6.1 due to the presence of different chemical functionalities. Surface fractions of amine and octyl groups in mixed surface were calculated using the Cassie equation, $cos\theta_{mixed} = f_A cos\theta_A + f_O cos\theta_O$, [306] where, f is the fraction of each constituent and subscript A refers to amine and O to octyl. The f_A was found to be 46±1.8 %, which agreed to C_{amine} value determined from FTIR data analysis.

We noticed the wettability difference between unmodified glass (θ=17.8±0.3º) and Ti (θ=30±2º) surfaces. Also, roughness of Ti surfaces was higher as compared to glass/silicon (<1nm scale) surfaces. However, post modification, the surfaces of both glass/silicon and Ti

systems possess comparable wettability [140, 142, 247]. Contact angle data of water and diiodomethane were used to determine their surface energies and are shown in Table 6.1. Surface energy defines the intermolecular forces that exist at the interface. We found higher surface energy for polar surfaces like amine and COOH, whereas the minimum for hydrophobic octyl surface and was found to be in agreement with the previous reports [247, 262]. The surface energy of hybrid and mixed surfaces lies in between amine and octyl surfaces as shown in Table 6.1.

Table 6.1. Characteristics of modified surfaces having various SAMs.

Surfaces	Static contact angle (°)				Surface energy ($mJ.m^{-2}$)		Surface roughness (µm)
	Without FN		With preadsorbed FN		Without FN	With preadsorbed FN	Without FN
	Water	MI	Water	MI			
Blank	30 ± 2	21 ± 1	36 ± 1	33 ± 1	66 ± 1	61 ± 1	0.71 ± 0.1
Amine	63 ± 1	39 ± 2	47 ± 2	38 ± 1	46 ± 1	54 ± 2	0.72 ± 0.1
Octyl	105 ± 2	74 ± 2	61 ± 2	53 ± 2	20 ± 1	42 ± 2	0.74 ± 0.1
Mixed	86 ± 2	53 ± 1	52 ± 2	45 ± 1	33 ± 1	49 ± 2	0.83 ± 0.1
Hybrid	82 ± 2	50 ± 2	54 ± 2	43 ± 1	35 ± 2	49 ± 1	0.75 ± 0.1
COOH	42 ± 2	29 ± 2	39 ± 1	40 ± 1	59 ± 2	58 ± 1	0.71 ± 0.1

We determined surface roughness of different modified surfaces using profilometer and found its value below 1 µm for all the surfaces, as presented in Table 6.1. FESEM analysis exhibited changes in surface morphology due to modifications and are shown in appendix Figure 6A-1. EDX analysis of amine modified surface further confirmed modification due to uniform distribution of Si, C, O, and N elements throughout the surface indicating proper SAM coverage on Ti6Al4V surfaces (shown in appendix Figure 6A-2).

6.3.2. Protein Adsorption on Modified Surfaces

Protein adsorption is a complex process which is regulated by physical and chemical properties of surfaces such as wettability, roughness, surface energy and chemical functionalities. We explored modified surfaces with different functionalities and wettability to understand their role in protein adsorption. Previously, we have reported the effect of functionalized-silane modified silicon surfaces on BSA and fibrinogen (FB) adsorption and the change in their secondary structure upon adsorption [140, 247]. Figure 6.2 shows the adsorbed mass of BSA and FN on modified surfaces, evaluated using BCA assay. Adsorbed amount of BSA was found to increase with decrease in surface wettability; while the same for FN was found to decrease with decrease in surface wettability. A similar pattern of BSA adsorption on SAM functionalized silicon surfaces were also previously reported by our group [140, 142, 247]. Bardeau and coworkers recently demonstrated similar amount of adsorbed BSA mass on bare Ti surface with nanoscale roughness [328].

Hydrophobic octyl surfaces (1035±38 ng/cm^2) showed the maximum adsorption of BSA which reduced on mixed (609±69 ng/cm^2) and hybrid (584±28 ng/cm^2) surfaces and further decreased on blank (Ti) surface (395±17 ng/cm^2) due to decrease in hydrophobicity. Higher amount of adsorbed BSA on octyl surface is attributed to the hydrophobic interactions between methyl groups and hydrophobic BSA moieties. Moreover, hydrophobic surfaces repel water molecules and thus reduces steric hindrance for BSA molecules to adhere via hydrophobic-hydrophobic interactions [140]. BSA molecules possess negative charge at neutral pH and are expected to adhere less on negatively charged COOH surface due to electrostatic repulsion. However, at neutral pH, we observed higher adsorbed mass at COOH surface and is attributed to the presence of positively charged moieties (lysine, histidine) on BSA molecules [283].

Moreover, increased pKa value of the carboxylic groups (of BSA molecules) upon adsorption at neutral pH results in their protonation, which causes strong hydrogen bonding interactions between surface and BSA molecules, promoting protein adsorption [283-286]. Similar behavior of BSA adsorption on negatively charged surfaces have also been reported [287, 288].

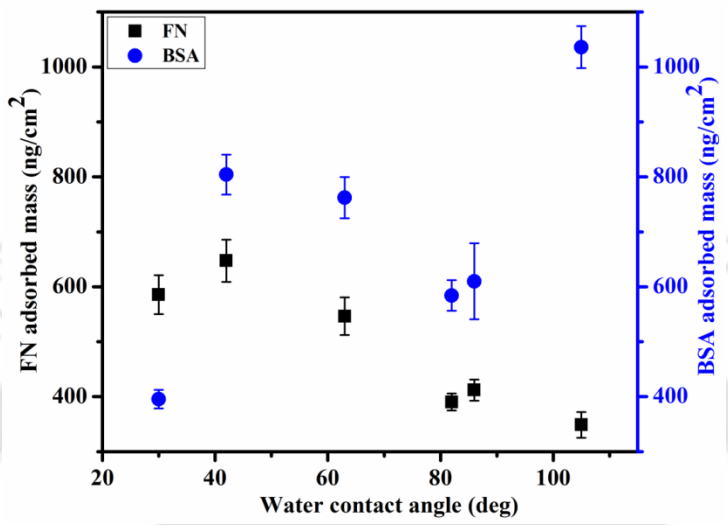

Figure 6.2. Adsorbed mass of BSA and FN on different modified surfaces.

In case of FN adsorption, amine and COOH surfaces showed the maximum adsorption with 546±34 and 647±38 ng/cm^2, respectively in comparison to octyl, mixed and hybrid surfaces which showed adsorption in the range 350 to 400 ng/cm^2.

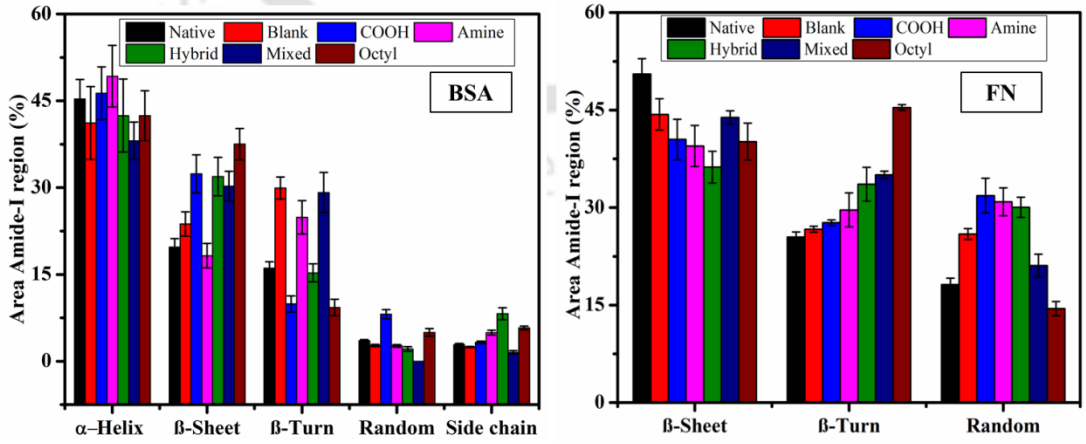

Figure 6.3. Comparison of amount of secondary structures (α-helix, β-sheet, β-turn, and random) of BSA and FN in solution and on various substrates.

FN contains more hydrophobic domains which impart hydrophobicity to the molecule and therefore adsorbs more on hydrophilic surfaces as compared to hydrophobic surfaces. Kushiro et al. investigated the adsorbed mass of FN on silica surfaces using quartz crystal microbalance with dissipation (QCM-D) and reported the maximum FN density on hydrophilic COOH surface which significantly reduced on hydrophobic CH_3 surface, under similar conditions to those used in the present investigation [326]. Similarly, Rodriguez et al. also reported higher mass of adsorbed FN on hydrophilic surface in comparison to hydrophobic surfaces at varied FN concentrations [329].

6.3.3. Secondary Structure of Adsorbed BSA and FN

ATR-FTIR spectra of BSA and FN proteins were analyzed in solution and after adsorption. The effect of five different modified substrates on secondary structure of adsorbed proteins was observed. The amide I range (1600-1700 cm^{-1}) of the spectra were fitted with Gaussian curves using Origin 8.5 software. Relative content of various secondary structures (α-helix, β-sheet, β-turn, random and side chain) were determined and are shown in Figure 6.3 (also see appendix Figure 6A-4). Briefly, peak for α-helix is present at around 1655 cm^{-1}, peaks for β-sheet are found to lie between 1620 to 1636 cm^{-1}, peaks for β-turn are mostly found to be in the range 1662 to 1688 cm^{-1} while random peak is found close at 1645 cm^{-1} (see appendix Table 6A-1) [247]. Crystal structure revealed that BSA is predominantly alpha-helical (more than 50%) and remaining part comprising of β-turn and few percent of sheets [330, 331]. We observed slight increase in α-helix content of BSA on amine as well as on COOH modified surfaces, which is attributed to the increased hydrogen bonding between amine and carboxylic groups of surfaces and proteins [247]. While on all other surfaces, we noticed reduction in α-helix content

of the adsorbed BSA. β-sheet content of the adsorbed BSA was found to be the maximum on the hydrophobic octyl surface.

We also investigated the impact of different modified surfaces on FN adsorption using ATR-FTIR, as unfolding of FN may expose type III domain, which is mainly responsible for cell adhesion and spreading [326, 332]. Secondary structure of FN in solution is found to have 47% β-sheet, 28% β-turn and 25% random/unordered structures [333] while the literature on peak positions can be found in various reports [334, 335]. We also report similar observation on FN structure (Figure 6.3) in solution. As compared to native structure, we observed reduction in the β-sheet content while % β-turn increased on all the surfaces indicating unfolding of FN. β-turn content of the adsorbed FN was found to be the maximum on the hydrophobic octyl surface. Random structures were also increased upon adsorption except for octyl surface.

6.3.4. Cells Adhesion, Spreading and Morphology Studies

6.3.4.1. Surfaces without Pre-adsorbed FN

Figure 6.4 (a1-a6) shows morphology of fibroblasts cells cultured on different surfaces without pre-adsorbed FN for 6 h in complete DMEM media. FESEM images of adhered cells on unmodified and modified surfaces post 6 h of seeding as also showed in appendix Figure 6A-3. The morphology of the adhered cells varies with properties like surface wettability, charge, roughness and cell type [2].

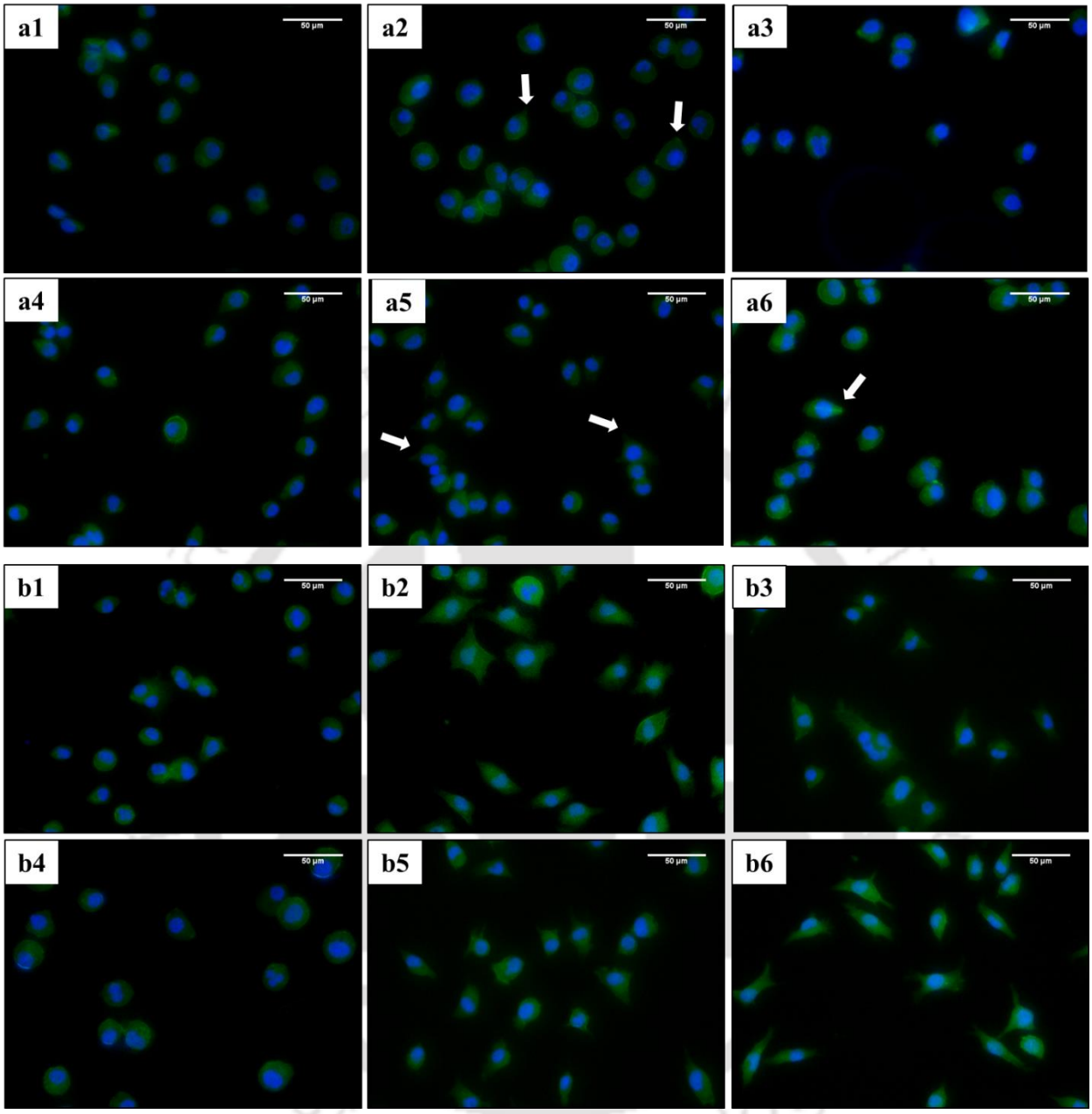

Figure 6.4. Cell spreading and morphology of fibroblast cells on surfaces (a) without pre-adsorbed FN and (b) with pre-adsorbed FN on (1) blank, (2) amine, (3) octyl, (4) mixed, (5) hybrid and (6) COOH surfaces after 6 h of culture. Actin fibers were stained with FITC-phalloidin and the nucleus with DAPI. White arrow marks points out the cytoplasmic protrusions on amine, hybrid and COOH surfaces. Scale bar in all the images is 50 µm.

The maximum cell adhesion was observed on hybrid (73±10%) followed by amine (58±13%) surface. COOH (47±5%) and mixed (46±7%) surfaces showed similar percentage of adhered cells while hydrophobic octyl surface exhibited the least. Various reports have stated

that cell adhesion is favorable on surfaces with the moderate hydrophobicity i.e. in the range 60-70º (WCA). However, there is a lot of ambiguity as there exists no direct relationship between contact angle and cell adhesion. Arima and Iwata reported the maximum attachment of HUVECs and HeLa cells on CH_3/OH and CH_3/COOH mixed SAMs, respectively, having water contact angle in the range 40-50º [2]. Similarly, Groth and Altankov reported better fibroblasts adhesion and spreading on hydrophilic surfaces as compared to hydrophobic surfaces [308]. Contradictorily, Kennedy et al. studied osteoblast attachment and spreading on SAM surfaces and reported increase in cell spreading and proliferation with the increase in hydrophobicity of the surfaces [309]. Hence, it is clear that along with wettabilities, there are other crucial factors such as nanotopologies, surface energy, surface potential, amount and conformation of adsorbed proteins and cell types etc. that also regulate cell adhesion.

Initial adhesion on blank/unmodified surface showed cytoplasmic protrusions which indicated incomplete cell spreading (cell area, 339±14 μm^2) (or slow spreading) and poor focal adhesion. Fluorescent staining of adhered cells on surfaces showed bundling of actin filaments without much spreading which indicated limited focal adhesions. Cells adhered on amine (459±10 μm^2) and COOH (450±65 μm^2) surfaces exhibited better spreading as compared to blank and octyl (406±21 μm^2) surfaces. Mixed (441±15 μm^2) and hybrid (433±19 μm^2) surfaces also showed significantly better cell spreading. Similar to % cell adhesion, surfaces with the moderate hydrophobicity promoted cell spreading. Extreme surface conditions such as hydrophobic octyl surface and hydrophilic unmodified Ti6Al4V surfaces showed lesser cell spreading as shown in Figure 6.4 (b). The results obtained were in agreement with the previously reported data on cell adhesion and spreading [308, 314, 336].

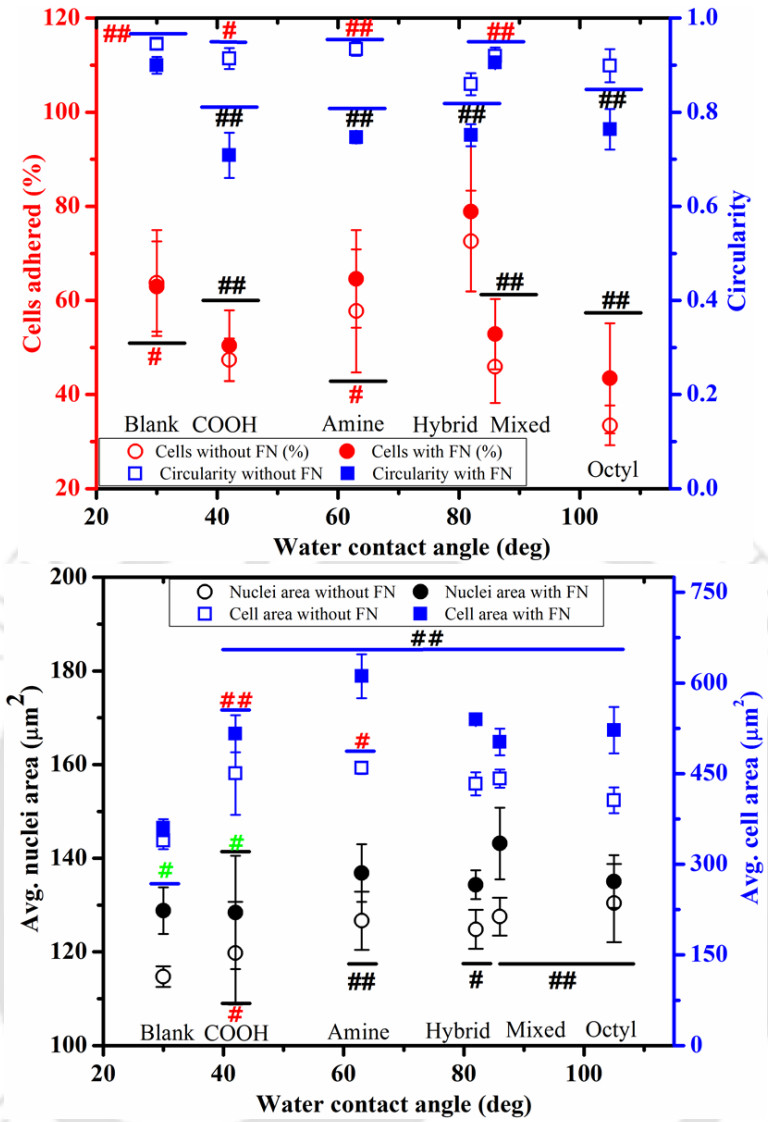

Figure 6.5. Effect of different modified surfaces with and without pre-adsorbed FN on (a) % cells adhesion and cell circularity and (b) average nuclei and cell area (μm^2) after 6 h of cell seeding. Values represent the mean ± SD. # denotes $p<0.05$ and ## denotes $p<0.005$. Statistically significant difference between hybrid and other surfaces were noted for both with and without pre-adsorbed FN in % cell adhered study. Additionally, % cell adhered on octyl surface without FN showed significant difference (#, $p<0.05$) with blank and amine surfaces. Similarly for circularity with pre-adsorbed FN, ## represents significant differences between blank and mixed surfaces with other surfaces. COOH too showed significant difference ($p<0.05$) with hybrid and octyl surfaces but not shown in image to avoid complexity and confusion. For Circularity data without pre-adsorbed FN, ## represents significant differences between hybrid and other surfaces. Octyl surface too showed significant difference ($p<0.05$) with amine and blank surfaces. For avg. nuclei area, # represents significant difference ($p<0.05$) between mixed, and COOH and blank surfaces with pre-adsorbed FN. Whereas for surfaces without FN, we observed significant difference (##, $p<0.005$) between blank and other surfaces. # represents significant difference between COOH and octyl surfaces. For cell area studies, blank surface showed

significant differences with all other surfaces with and without FN. # represents significant difference between octyl and COOH and amine surfaces.

Circularity of adhered cells defines the degree of polarization [326] on the scale range of 0.2 to 1 and is used to define the shapes of the cell. Lower value of circularity signifies better cell spreading having more focal points due to which cell shape changes. Cell circularity on hybrid (0.86±0.02) surface showed the least values and was significantly lesser, indicating better adhesion and spreading in comparison to other silanized (0.91-0.94) and blank/unmodified Ti (0.95±0.01) surfaces, as presented in Figure 6.5 (a). The maximum cell adhesion (73%) and the least circularity (0.86) on hybrid surface confer it as a potential surface modifier in bone tissue engineering.

Many researchers have reported the effect of surface properties like roughness, surface potential and wettability on cell adhesion and proliferation but very few have reported their effect on the morphology of the cytoplasm and the nucleus [337-340]. Here, we report the effect of wettability arising due to various functional groups on the nuclei size during initial the cell adhesion phase (i.e. after 6 h of cells seeding). Nuclei size of the adhered cells signify the nuclear functional activity occurring during cell differentiation and proliferation [315]. It is predicted that the increase in nuclei area may result in the higher division rate. Nuclei area of cells adhered on amine, hybrid, mixed and octyl surfaces were significantly higher as compared to blank surface (shown in Figure 6.5 (b)). We observed almost increasing trend in nuclei size with the increase in hydrophobicity (Figure 6.5 (b)) on modified surfaces prior to FN adsorption. The minimum nuclei size was observed on hydrophilic blank (114.7±2.2 μm^2) and the maximum was observed on hydrophobic octyl surfaces (130.4±8.3 μm^2).

6.3.4.2. Surfaces with Pre-adsorbed FN

Surfaces with pre-adsorbed FN witnessed significant increase in % cell adhered as shown in Figure 6.5 (a). Cell adhesion (%) increased to 79±17% for hybrid, 65±10% for amine, 53±7% for mixed, 50±7% for COOH and 43±11% for octyl surfaces. Also cell spreading on surfaces with pre-adsorbed FN, increased considerably, with maximum on amine (611±36 μm^2) followed by hybrid (540±9 μm^2), octyl (522±38 μm^2), COOH (516±30 μm^2) and mixed (502±22 μm^2) surfaces (see Figure 6.5 (b)).

Increased cell adhesion and spreading on surfaces with pre-adsorbed FN may be attributed to the exposure of arginine-glycine-aspartic acid (RGD) motifs of FN that serves as adhesives for integrin mediated cell adhesion [326]. The difference between such cellular behaviors can be explained by the specificity of the proteins towards cell adhesion. Serum proteins are generally non-adhesive in nature due to a lack of cell binding motifs (like RGD) and hence do not strongly/necessarily promote cell adhesion but still they serve as cushions for adhering cells. On the contrary, FN is an adhesive ECM glycoprotein that mediates cell attachment, cell migration, growth and differentiation via signaling pathways [341]. Type III_{10} and III_9 domains of FN-III region play crucial role in regulating aforementioned cellular process. Type III_{10} domain contains RGD sequence, which is recognized by α5β1 integrin, while type III_9 domain contains PHSRN (Pro−His−Ser−Arg−Asp) sequence, and is located 32Å away from RGD sequence. Type III_9 domain acts as a 'synergy site' and together with the FN-III_{10}, enhances interaction and affinity of RGD sequences towards α5β1 and αVβ3 integrins [332, 342, 343]. FN-III domain which contains these cell attachment sites (CAS), is located in the β-turn of FN molecule, embedded inside, and unfolds upon FN adsorption on surfaces [344]. This persuaded us to determine the effect of surface wettability on change in the % β-turn.

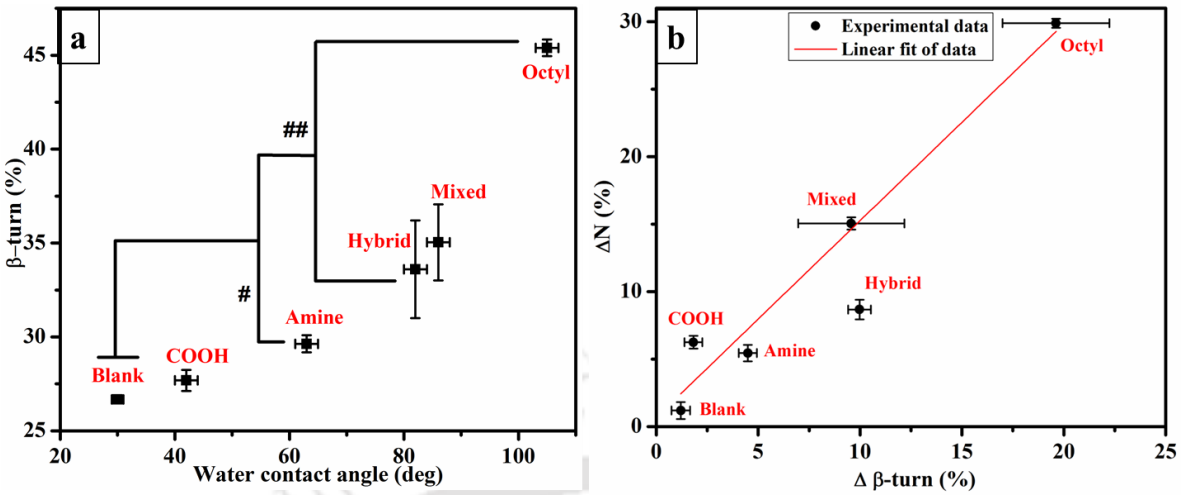

Figure 6.6. (a) Change in %β-turn of adsorbed FN on modified surfaces with increasing hydrophobicity, (b) Correlation between the change in % adhered cells (ΔN) with change (Δ) in % β-turn on different modified surfaces. Red line shows the linear fit of the experimental data. Values represent the mean ± SD. # denotes $p<0.05$ and ## denotes $p<0.005$, compared with blank surface.

Interestingly, we noticed linear increase in the % β-turn with the increase in the surface hydrophobicity with the minimum at hydrophilic (blank, COOH and amine) and maximum at hydrophobic octyl surface, as shown in Figure 6.6 (a).

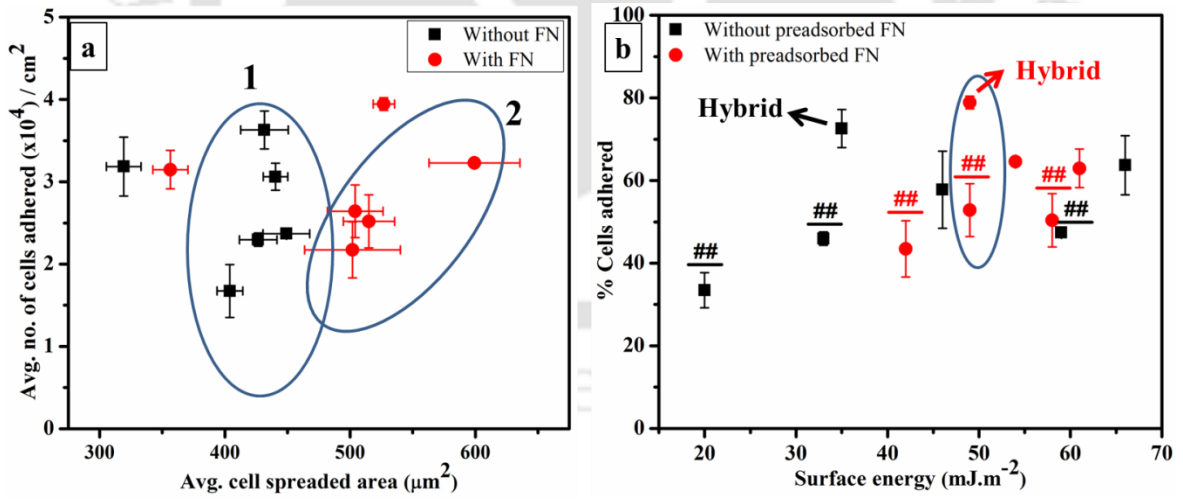

Figure 6.7. (a) Average number of adhered cells Vs cell spreaded area (μm^2) on modified surfaces and (b) effect of surface energy on % cell adhesion on surfaces with and without pre-adsorbed FN. ## represents $p<0.005$, compared with hybrid surface for both without and with pre-adsorbed FN.

Recently, Kushiro et al. also reported the similar pattern of relative exposure of RGD sequences on CH3>NH2>COOH-SiO2 surfaces using sophisticated immunosorbent enzyme-linked immunosorbent assay (ELISA) [11]. We also observed an interesting correlation between the change in % adhered cells (ΔN) with change (Δ) in % β-turn on different modified surfaces. Δβ-turn (%) represents the increase in the β-turn content of adsorbed FN on surfaces with respect that of the native FN. Likewise, ΔN represents the % increment in the cells adhered on surfaces with and without pre-adsorbed FN. Δβ-turn is found to be linearly related with ΔN (R^2=0.85) as shown in Figure 6.6 (b). We hypothesize that an increase in Δβ-turn exhibits increase in the type-III domain, which in turn enhances the cells attachment.

Prior to FN adsorption, cells showed moderate polarization while its value changed immensely on all the surfaces with pre-adsorbed FN. As shown in Figure 6.5 (a), the least circularity was observed on COOH (0.71±0.05) followed by amine (0.75±0.01), hybrid (0.75±0.02), and octyl (0.76±0.04) surfaces indicating the least polarization with rectangular shaped morphology. While blank (0.90±0.02) and mixed (0.90±0.01) surfaces exhibited the maximum degree of polarization with circular morphologies. This implies that cells on the blank and mixed surfaces did not adhere well. Mixed SAMs suffers from phase separation problems and hence may be responsible for poor adhesion and circularity. Kushiro et al. also reported the similar trend of varying circularity on NH_2-, COOH-, OH, and CH_3-SAMs on SiO_2 surfaces [326].

For a better understanding about the effect of pre-adsorbed FN on cell adhesion and spreading, we plotted the average cell area (μm^2) against the average number of adhered cells as shown in Figure 6.7 (a). Average spread area of adhered cells significantly increased on surfaces

with pre-adsorbed FN but did not enhance the number of adhering cells, as represented by circles 1 and 2 in Figure 6.7 (a).

In-spite of the fact that many researchers have reported that surfaces with low wettability or high surface energies promote cell attachment and spreading [345, 346]. However, no strong relationship can be drawn as contact angles and surface energies are not necessarily directly related to cell adhesion. To address such issues, we tried to verify the effect of surface properties such as contact angle, surface functionalities and surface energies on protein adsorption and conformation which further regulates cell adhesion, spreading and proliferation. As shown in Figure 6.7 (b), increase in surface energy promoted cell adhesion in both the cases i.e. with and without pre-adsorbed FN.

Interestingly, among surfaces without pre-adsorbed FN, we observed higher cell adhesion (72.6±4.6%) on hybrid surface (35±2 $mJ.m^{-2}$) as compared to mixed surface (45.9±7.7%) whose surface energies (33±1 $mJ.m^{-2}$) are close to each other. We saw intermittent values of % cell adhesion on mixed surface which lied in between amine (57.7±4.6%) and octyl (33.5±4.2%) surfaces and were in accordance with the surface energy data. Moreover, hybrid and mixed surfaces with pre-adsorbed FN, exhibit same surface energy (49±1 $mJ.m^{-2}$) but we still observed better cell adhesion on hybrid surface (79±1.5%) as compared to mixed surface (53±6.3%). Hence, we conclude that although increasing surface energies promote cell adhesion but the effect of surface morphology/ nanostructure further regulate this phenomenon. While hybrid surface showed better cell adhesion results due to the difference in surface morphology of mixed and hybrid SAMs. Hybrid surfaces are SAMs of monomolecules while mixed surfaces suffers from phase separation due to distribution of amino and octyl silanes molecules [140].

6.3.5. Cell Viability Analysis on Modified Surfaces

Figure 6.8 shows the absorbance (at 570 nm due to formazan) versus incubation time (days) graph of fibroblast cells grown on different silanized Ti6Al4Vsurfaces.

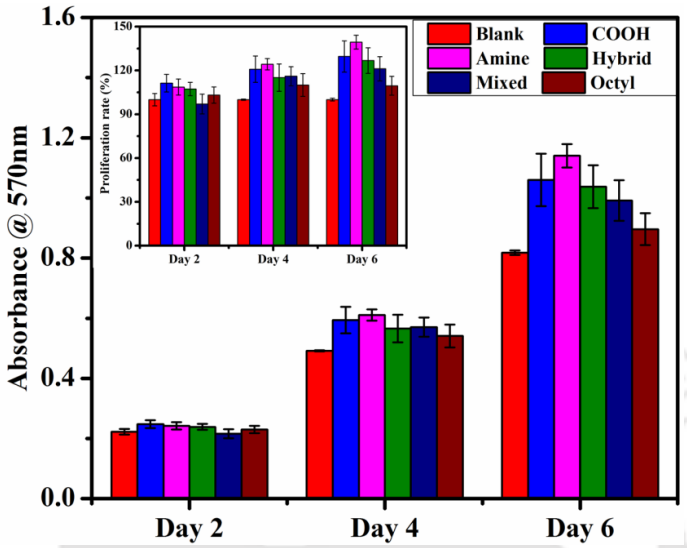

Figure 6.8. Cell viability assay of fibroblast cells incubated with different modified surfaces for different time interval. Inset shows cell viability in terms of proliferation rate (%).

Cells exhibited higher proliferation rate on all the modified surfaces as compared to unmodified Ti6Al4V, suggesting good cyto-compatibility of the surfaces for tissue engineering applications.

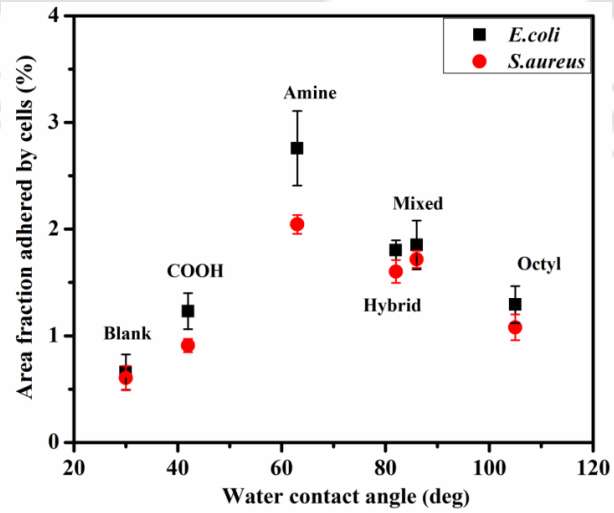

Figure 6.9. Area fraction (%) adhered by *S.aureus* and *E.coli* on modified surfaces exhibiting different contact angels.

Among all the surfaces, amine, hybrid and COOH surfaces showed the better cell viability as compared to octyl and mixed surfaces. Amine and COOH surfaces contain NH4+ and COO- groups, respectively, which attract protein molecules, serve as cushions and in turn promote cell adhesion. Although adsorbed mass of BSA on octyl surfaces were found to be the maximum but its highly hydrophobic nature did not support cell adhesion. Moreover, surface wettability also plays an important role in cell adhesion and is promoted by moderate hydrophobicity in the range 40-70º [16, 38]. Hence, better cell viability was observed for amine and COOH samples.

6.3.6. Bacterial Adhesion Studies

Titanium and stainless steel alloys are widely used in orthopaedic implants and are susceptible to bacterial infections. A prosthetic implant infection is a severe biomedical problem and is highly responsible for implant failure [322] and contributed to 40-70% of hospital-acquired infections (HAI). Millions of such devices are used annually and the healthcare burden of infection-related device failure is great. Hence, a desirable biomaterial surface should exhibit reversible protein adsorption, better cell adhesion and minimal microbial adhesion, for a better interaction with biological system. *S.aureus* is a well-known pathogen associated with infections related to medical devices and implants. Their ability to adhere on surfaces and form biofilm resulted in a huge loss due to a deleterious effect and hence, it is desirable to prevent their adhesion in order to control infection. Effect of physico-chemical properties of chemically modified surfaces were analyzed for determining the adhesion of both Gram positive (*S.aureus*) and negative (*E.coli*) bacteria.

Bacterial cell wall of both Gram positive and negative bacteria carries overall negative charge. Cell wall of Gram positive bacteria contains teichoic acid that imparts negative charge

due to the presence of phosphodiester bonds. Where as in Gram negative bacteria, highly charged phospholipids and lipopolysaccharides are widely distributed throughout the outer membrane and imparts negative charge to cell wall. Figure 6.9 shows the change in the % area fraction adhered by the cells with respect to WCA. Initially, bacterial adhesion increased with the increase in the WCA and was found maximum for amine surface (63±2º). High wettability due to the presence of OH groups on unmodified Ti surfaces (30±2º) also exhibited lesser adhesion of both *E.coli* (0.7±0.1%) and *S.aureus* (0.6±0.1%). Amine surface exhibits positive charge (due to NH^{4+}) which attracts bacterial cells due to their negatively charged cell wall, resulting in the maximum adhesion of *E.coli* (2.8±0.3 % area covered) and *S.aureus* (2.0±0.1%). It subsequently dropped down upon further increasing the hydrophobicity, with the least observed at highly hydrophobic octyl surface (*E.coli*, 1.3±0.2%; *S.aureus*, 1.0±0.1%). Self-cleaning and hydrophobic properties act as barriers in bacterial adherence and may be responsible for lesser density at octyl surface. A similar trend of changing bacterial adhesion with the change in hydrophobicity has been recently reported by Yuan et al. [347]. Likewise in other reports [348-350] as well, researchers emphasized that the surfaces with a moderate hydrophobicity resulted in higher bacterial density due to enhanced hydrophobic interactions between bacterial membrane and surfaces.

6.4. Conclusions

Although numbers of studies have described the effect of physio-chemical properties at the interface on the behavior of protein adsorption and subsequent cell adhesion and spreading, the underlying mechanisms that regulate these processes remain uncertain. Moreover, very few reports exist on the behavior of adsorbed FN, the effect of silanized Ti/Ti-alloy on FN secondary

structure and subsequent fibroblast adhesion has not been reported yet. We successfully modified Ti6Al4V surfaces with SAMs of amine, octyl, mixed, hybrid and COOH functional groups. The modified surfaces were confirmed by FTIR-ATR analysis due to the appearance of characteristic peaks for various functional groups in the spectra. Furthermore, change in the wettability of the surfaces confirmed SAM formation that regulated water and diiodomethane contact angles at the interface. The maximum BSA adsorption was observed on hydrophobic octyl surface (1035±38 ng/cm^2) due to hydrophobic interactions between methyl group and hydrophobic moieties of BSA molecules. A reverse pattern was detected in the case of FN adsorption and was found to be the maximum on hydrophilic COOH surface (647±38 ng/cm^2). Change in secondary structures of adsorbed BSA and FN was determined using FTIR-ATR analysis. Amine and COOH surfaces exhibited increase in α-helix content while it was found decreasing on other surfaces, for BSA molecules. In the case of FN protein, β-turn content was found increasing linearly with the increase in surface hydrophobicity. Cell adhesion and spreading was analyzed on surfaces with and without pre-adsorbed FN. FN being an ECM protein serves as an adhesive for cell adhesion and interacts via α5β1 integrin signaling pathway to promote cell spreading. In FN, RGD loops are located in β-turn and Δ adhered cells (%) were linearly increased with increase in Δ β-turn content (%). Hybrid surface resulted in moderate adsorption of BSA and FN as compared to other surfaces and was found to be the most promising surface modifier due to the maximum cell adhesion (%) and proliferation, larger nuclei area and the least cell circularity. Bacterial density was found to increase with the increase in hydrophobicity and was maximum on amine surface (θ=63±1°) which further decreased with the increasing hydrophobicity.

Chapter 7

Antimicrobial Peptoids Synthesis for Biomedical Applications

Biocompatible and antimicrobial surfaces had been the demand since decades for various biomedical applications. For antimicrobial surfaces, stability, efficiency and wide spectrum of activity are the few challenges those are still unmet. In this chapter, we showed the synthesis of antimicrobial peptoid sequences and their possible application in designing antimicrobial surfaces. Peptoids are stable against enzymatic degradation and are highly efficient with very low MIC values

7.1. Introduction

Antimicrobial peptides (AMPs) are found in most living organisms, also known as 'host defense peptides' and are intrinsic component of an innate defense mechanism against invading pathogens [351]. They have attracted significant attention as lead compounds for various clinical uses and have exhibited broad spectrum antimicrobial activity [352-354]. AMPs target bacterial membranes via non-specific interactions, causing membrane rupture, hence there are lesser chances of inducing bacterial resistance against them. Antibiotics work against specific target substrates which are involved in the bacterial growth mechanism, and gradually lose their efficacy and make them highly prone to the development of resistance [351, 355]. Moreover, the development and approval of new antibiotics is very slow and also steadily decreasing year by year [356]. Short chain amphiphilic AMPs sequences which are cationic in nature interact with

negatively charged phospholipids. Eukaryotic cells exhibit more zwitterionic membrane nature as compared to bacterial membrane which results in the selectivity of bacteria against mammalian cells [357]. Apart from their direct interaction with bacterial surfaces, indirect mechanism (non-membrane disruptive) of their activity also includes interactions with bacterial nucleic acid (DNA, RNA) and protein synthesis machinery [358]. Some AMPs exhibit dual effects by disrupting cell membrane as well as inhibiting intracellular bacterial processes. Hence these salient features of AMPs such as high selectivity, low tendency of inducing resistance and activity against a broad spectrum makes them potential antimicrobial candidates [351, 355]. Despite of these advantages, AMPs suffer from enzymatic degradation resulting in the poor bioavailability [357, 359]. Hence, peptidomimetics were designed to overcome these drawbacks by using non-natural amino acids. Recently, various peptidomimetics of AMPs have been reported such as β-peptides [360], arylamides [361], β-peptoids [362], oligoureas [363], and oligo(phenylene ethynylene)s [364], and peptoids [365].

Peptoids are poly-N substituted glycines and exhibit a structural difference with peptides i.e. shifting of side chains from α-carbon to the adjacent amide nitrogen [365, 366], as shown in Figure 7.1 (A). This shifting of side chains turn them resistant against bacterial proteases [367]. Although peptoids lack backbone chirality and intra-chain hydrogen bonding due to which they may be supposed to loose helical secondary structures, a periodic incorporation of bulky, α-chiral side chains have helped them to form helical structures [368], which may facilitate the formation of amphipathic designs similar to AMPs i.e. accommodating three monomers per turn [369, 370]. Peptoids are known to be 'foldamers' since they exhibit discrete folding properties which mimic biopolymers [371].

Peptoids have been used for various applications such as drug delivery, as ligands for GPCRs, and for blocking calcium channels. Their nanosheets have been used for bio-sensing applications, and for hydrogel synthesis for stem cell differentiation [372-376]. Recent years have witnessed significant increase in the designs of peptoids for antimicrobial applications. They have also been referred as 'ampetoids' exhibiting a helical secondary structure and biomimetic sequences similar to cationic AMPs with a wide spectrum against antimicrobial activity and low mammalian cytotoxicity [357].

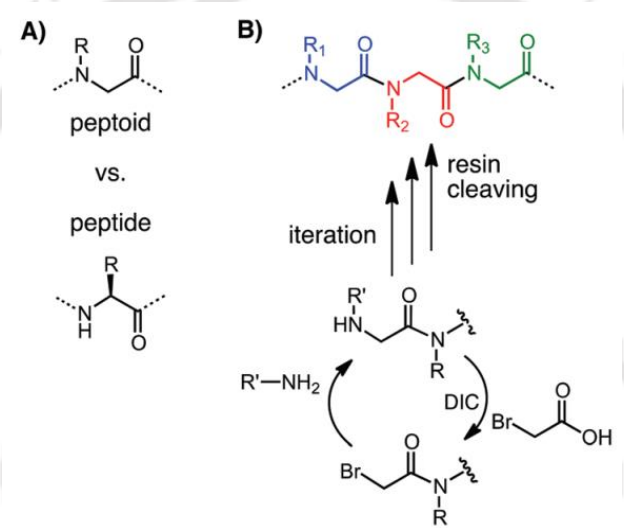

Figure 7.1. (A) Structural difference between peptide and peptoid and (B) synthesis route of peptoid using submonomer solid phase synthesis. Adapted from ref. [12] with permission from The Royal Society of Chemistry.

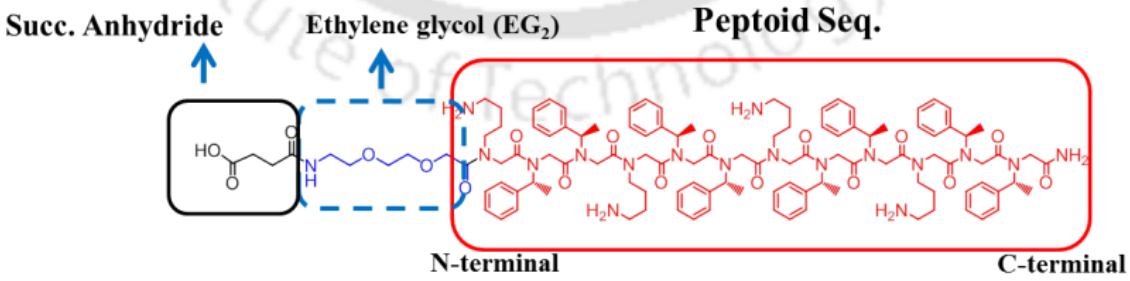

Figure 7.2. Synthesis of antimicrobial peptoid sequence, N terminal modified with linker ethylene glycol $(EG)_2$ and succinic anhydride to obtain acid moiety.

7.2. Materials and Methods

7.2.1. Materials Used

The two submonomers used were: (1S)-(-)-1-Phenylethylamine (Nspe) and tert-butyl N-(4-aminobutyl) carbamate (NLys) and purchased from Apollo Scientific, UK. Rink amide-MBHA resin, H-Gly-2-ClTrt resin and N,N,N′,N′-Tetramethyl-O-(1H-benzotriazol-1-yl)uronium hexafluorophosphate (HBTU) were procured from Novabiochem/EMD Merck, UK. Bromoacetic acid (BAA; 98+%), diisopropyl-carbodiimide (DIC; 99%), piperidine (99%), trifluoroacetic acid (TFA; 99%), N-Ethyldiisopropylamine (DIPEA; 99%) were Alfa-Aesar products purchased from VWR, UK. Triisopropylsilane (Acros brand, 99%) and HPLC grade acetonitrile were purchased from Fisher Scientific UK. Mueller Hinton (MH) Broth was purchased from Sigma, UK.

7.2.2. Peptoids Synthesis and Reverse-Phase High-Pressure Liquid Chromatography (RP-HPLC) analysis

We manually synthesized the peptoid sequences at room temperature using the established submonomer peptoid synthesis protocol [13, 365]. Briefly, the rink amide resin was first deprotected using 20% piperidine (v/v) in DMF, under continuous shaking for 20 min and repeated twice. Bromoacetylation was carried out using BAA (1.5 M) in DMF at 20x excess of the resin loading. DIC was used at 18.5x excess and allowed to proceed for 15 min. 1.5 M of submonomers at 20x excess of resin was prepared in NMP and was allowed to proceed for 30 min. For EG_2 coupling at the C terminal, the H-Gly-2-ClTrt resin was used. The DCM swollen resin was first coupled with NH_2-EG_2-COOH using HBTU/DIPEA coupling for 2 h at room temperature. Post coupling, the synthesis of sequences was carried out using similar protocol mentioned above. Whereas for coupling EG_2 at N terminal, the complete peptoid sequence was

first synthesized on rink amide resin and later capped with EG_2 using same coupling conditions as stated above. Succinic anhydride (1M in DMF, 10x excess) was used for creating acidic moiety at the N terminal post EG_2 capping (as shown in Figure 7.2). After synthesis, sequence cleavage from resin and sidechain deprotection were performed by treating with deprotection recipe, i.e. 95% TFA (v/v), 2.5% UP water, and 2.5% TIPS for 15 min.

The cleaved peptoid was then filtered, dried and purified by preparative gradient RP-HPLC (Dionex Ultimate 3000) using C18 column. HPLC fractions were further analyzed using LC-MS (Agilent) for pure product. The fractions containing pure product were collected, lyophilized and stored at -20ºC for further use.

7.2.3. Potentiometric Titration Analysis

Titration was performed manually using the protocol reported previously [13]. Briefly, 10 mg of peptoid was dissolved in 1.5 mL of KCl (100mM) and titrated step by step with 5 µL of 100 mM KOH base. pH was recorded after each step of KOH addition.

7.2.4. Antimicrobial Analysis

The purified peptoid sequences were tested for minimal inhibition concentration (MIC)against *E.coli* (ATCC 25922) and *P.aeroginosa* (PA 01) according to the broth microdilution method mentioned in CLSI M7-A10 protocol [377]. MIC is defined as the minimal concentration at which no bacterial growth is observed when incubated for 16 h at 37°C. Briefly, 90 µL of each peptoid samples prepared in MH broth at different concentrations were added to 96 well plates. 10 µL of bacterial inoculum (5×10^6 CFU/mL) was added to all peptoid samples.

Positive control contained 10 µL of bacterial inoculum and 90 µL of MB broth without peptoids. Experiments were repeated thrice giving reproducible MIC values.

7.3. Results and Discussion

7.3.1. Peptoid Characterization

The peptoids were successfully synthesized and confirmed using RP-HPLC and LC-MS. Figure 7.3 shows the HPLC chromatograph of various synthesized peptoid sequences.

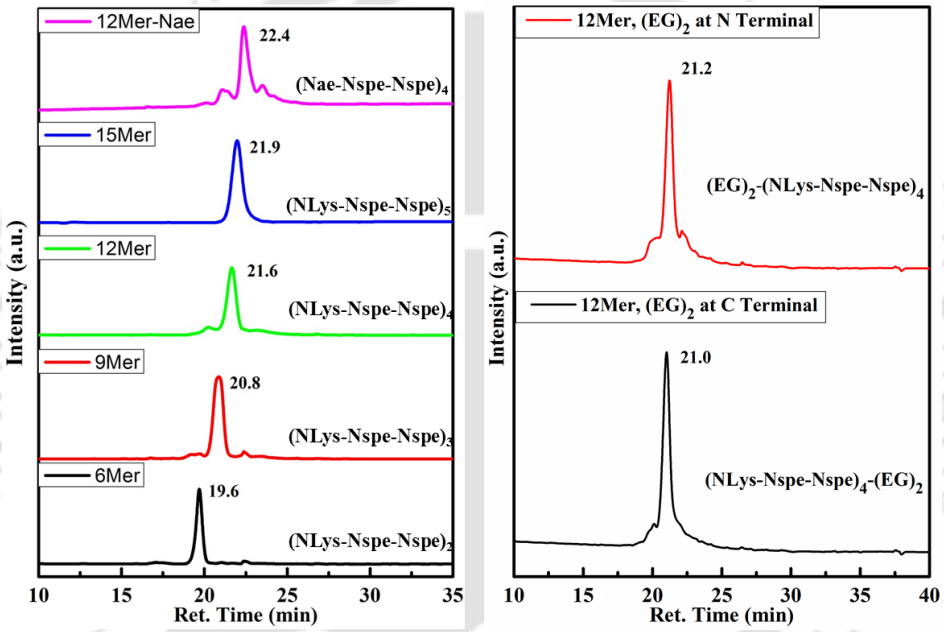

Figure 7.3. RP-HPLC chromatographs of the synthesized peptoid sequences before purification.

Figure 7.4 shows the representative mass spectra of 12Mer with EG_2 capping at the C terminal. Similarly, all of the peptoid sequences were tested after purification using LC-MS. For 12Mer, with EG2 at C terminal, the exact mass (M) is 2021.2 g/mol, hence we observed mass/charge (m/z) due to $[M+2H]^+$ at 1012, $[M+3H]^+$ at 674.8, and $[M+4H]^+$ at 506.5. The spectra confirmed the purity of the collected fractions.

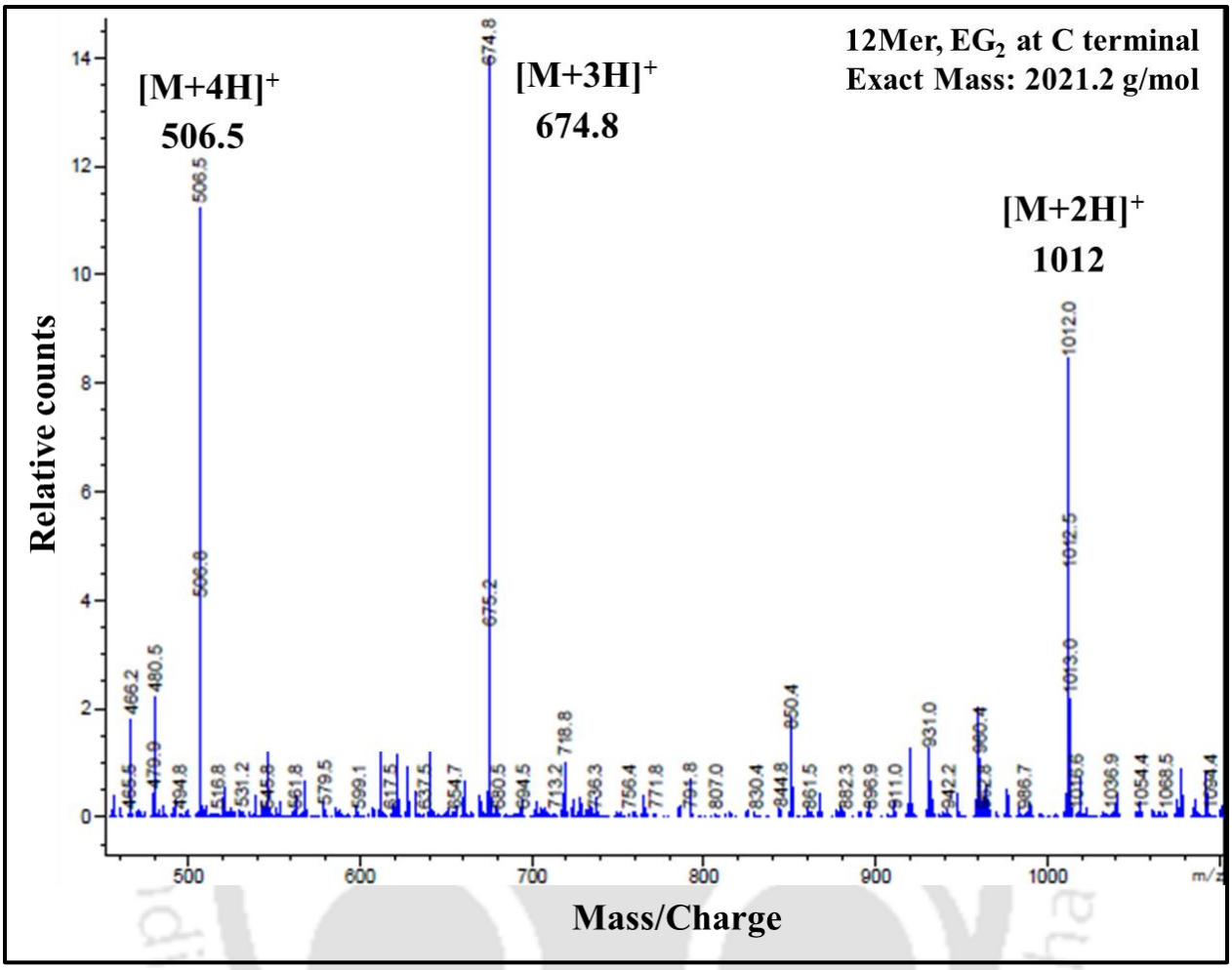

Figure 7.4. Mass spectra (relative counts vs. mass/charge) of the purified fractions of 12Mer with EG_2 at C terminal.

Figure 7.5 shows the pKa estimation of the peptoid sequence 12Mer with EG2 at N terminal whose structure is shown in Figure 7.2. The equivalence point was determined based on derivative equivalence point method. The pKa was calculated using Henderson–Hasselbalch equation as shown below by expression 7.1.

$$pH = pKa + log\frac{[A^-]}{[HA]} \quad (7.1)$$

Where, K_a is the acid dissociation constant and pK_a represents $-\log 10\ K_a$. [HA] is the molarity (M) of the undissociated weak acid and $[A^-]$ is the molarity of this acid's conjugate base.

Equivalence point represents the volume of base required to produce the largest first derivative, which is 200 µL in this case. Half of the volume of the equivalence point signifies that the concentration equivalents of acid are equal to base. Hence, at [HA]=[A^-] the expression 7.1 becomes $pH = pKa$ as shown in Figure 7.5.

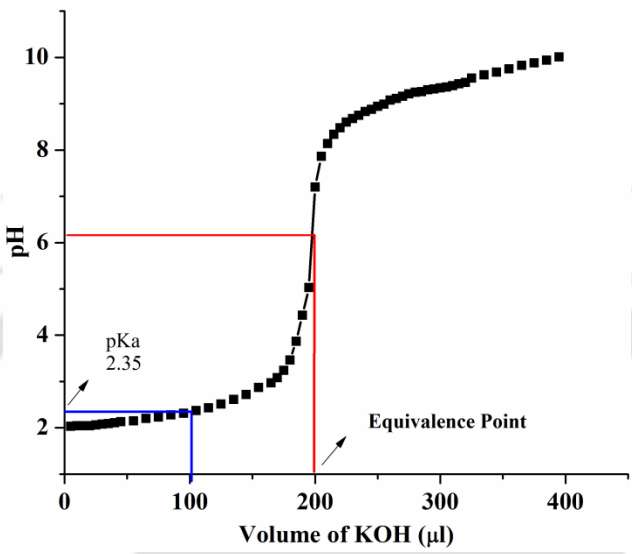

Figure 7.5. pKa estimation of 12Mer with EG_2 at N terminal using titration curve.

7.3.2. Antimicrobial Analysis

Antimicrobial activity of the synthesized peptoids was analyzed using the broth microdilution method. Cationic peptoids exhibit better interactions with Gram negative bacterial membrane due to the presence of lipopolysaccharides (LPS). LPS are anionic glycolipids containing cation binding sites for Ca^{2+} and Mg^{2+} and are hence also serves as sites for interaction with cationic peptoids [378]. Using LPS binding dye, i.e. fluorescently labeled lipopeptide dansyl polymyxin B (DPX) dye, it was demonstrated that highly charged cationic peptide (MSI-78, +10 charge) displaced 100% dye molecules bound to LPS [379, 380]. This indicated that cationic species can effectively interact with LPS and may help in antimicrobials penetration and cell death. The peptoid sequences used in this study, too are cationic species with

varying charge density based on number of NLys side chain. For example, 6Mer contains two NLys and hence have +2 charge. There was huge dip in MIC value as we increased the sequence length from 6 Mer (>200 μM) to 9 Mer (10 μM) that also resulted in the increase in charge from +2 to +3. There was no observable difference between MICs of 9, 12 and 15Mer, indicating that charge density doesn't play a significant role after +3 in our peptoid sequences. We were further interested in determining which end of the 12Mer peptoid sequence plays major role during activity. With this aim, we modified the 12 Mer sequence by capping both C and N terminals with two molecules of ethylene glycol (EG_2). To our surprise, we noticed reduction in MIC value against *E.coli* for both termini modifications. We observed an increase in the MIC against *P.aeroginosa* for 12Mer with EG_2 at C terminal whereas 12Mer with EG_2 at N terminal seems to be more effective against both *E.coli* and *P.aeroginosa*. We also determined the effect of chain length of NLys (4 carbon) side chain by replacing it with aminoethane (using submonomer Nae, with 2 carbon) side chain. We noticed no difference between the activity of 12Mer with NLys and 12Mer with Nae against both the strains, ruling out the effect of length of side chain.

Table 7.1. Molecular weight and antimicrobial activity of synthesized ampetoids sequences against *E.coli* and *P.aeroginosa.*

Ampetoids Sequence	**Molecular weight (Mw)**	**MIC (μM) against *E.coli* (ATCC 25922)**	**MIC (μM) against *P.aeroginosa* (PA 01)**
6Mer-(NLys-Nspe-Nspe)$_2$	918.2	>200	>50
9Mer-(NLys-Nspe-Nspe)$_3$	1368.8	10	10
12Mer-(NLys-Nspe-Nspe)$_4$	1819.0	10	10
15Mer-(NLys-Nspe-Nspe)$_5$	2268.3	10	10
12Mer; (EG)$_2$ at C terminal	2021.2	5	20
12Mer; (EG)$_2$ at N terminal	2063.2	5	10
12Mer-(Nae-Nspe-Nspe)$_4$	1732.5	10	10

7.4. Conclusions

Antimicrobial sequences were successfully synthesized and modified on C and N terminals by capping with EG_2. Purification of the synthesized sequences was confirmed by RP-HPLC and LC-MS results. The synthesized sequences were tested against *E.coli* (ATCC 25922) and *P.aeroginosa* (PA 01). 12Mer with EG_2 at the N terminal was found to be the most effective against both strains. The pKa was estimated using a titration curve for the same peptoid sequence was found to be 2.35.

Chapter 8

Conclusions and Suggestions for Future Works

8.1 Conclusions of the Present Work

Silanization technique was used for modifying surfaces with mono, mixed and hybrid SAMs. A wide range of wettability exhibiting hydrophilic (COOH and amine), moderately hydrophobic (mixed and hybrid) and hydrophobic (octyl) surfaces properties were created using amine and octyl silanes. The physical and chemical characteristics of surfaces were characterized in terms of functional groups, surface morphology and roughness. The kinetic studies of the formation of octyl SAM at silica/glass substrates was carried out and revealed that silane attachment was very fast and completed in 16 min while re-orientation of the attached molecules was a slow process and continued till 512 min. Confirming the transition from lying-down to standing-up phase when surface density of the attached molecules increased. Further, it was desired to gain the mechanistic insight of the above modified surfaces and their effect on serum proteins (BSA, FB and IgG) adsorbed from single and binary protein solutions. Negatively charged and hydrophobic (octyl) surfaces exhibited the maximum mass due to electrostatic and hydrophobic interactions between protein molecules and surfaces, respectively. The surface coverages by side-on and end-on orientations, calculated theoretically based on sizes of proteins, were competed with the experimentally AFM data analysis. Adsorbed proteins were found to be majority of side-on oriented irrespective of surfaces chemistry. We observed compact (N-form) and elongated (E-form) forms of BSA molecules on hydrophilic and hydrophobic surfaces,

respectively. α-helix content of BSA and β-sheet content of FB and IgG proteins were found to increase with the increase in side-on (%) oriented protein molecules on surfaces. The protein-protein interactions measured using ITC confirmed the entropy driven competitive adsorption process.

We observed that adsorbed protein on different modified surfaces exhibited different behaviors and motivated us to study cell adhesion on the above modified surfaces with and without proteins. We employed three different experimental conditions i.e. (a) complete media supplemented with 10% FBS, (b) surfaces with pre-adsorbed FBS, and (c) incomplete media i.e. without FBS, to determine the effect of FBS proteins and surfaces on cell adhesion and spreading. Surfaces treated with incomplete media exhibited the least cell adhesion rate, poor morphology and smaller adhered cell and nuclei area irrespective of surfaces. Whereas surfaces in the presence of FBS in media and pre-adsorbed FBS exhibited excellent cell features on amine, hybrid and COOH surfaces. Surface coverage rate of adhering cells was the highest on hybrid surfaces under all the three conditions. It is noteworthy that orientation and secondary structure of adsorbed FBS protein molecules helped in cell adhesion and spreading in case of pre-adsorbed FBS. Especially, hybrid surface showed better cell and nuclei area amongst all the surfaces indicating better surface properties for cell adhesion and proliferation. Furthermore, we found the initial surface coverage rate and Δ adhered cells (%) linearly increased with the change in α-helix content of adsorbed FBS proteins.

With the aim of improving surface properties for better biomolecules and cellular response, we modified Ti surface using silanization. Effects of modified Ti surfaces were tested for the adsorption behavior of serum (BSA) and cell adhesive (for eg. FN) proteins. Adsorbed BSA exhibited similar behavior as that on modified silica surfaces (chapter-4) i.e. amine and

COOH modified Ti surfaces exhibited increase in α-helix content while it was found decreasing on other surfaces. While in the case of FN protein, β-turn content was found increasing linearly with the increase in surface hydrophobicity. Cell adhesion and spreading was analyzed on surfaces with and without pre-adsorbed FN. In FN, RGD loops are located in β-turn and Δ adhered cells (%) were linearly increased with an increase in Δβ-turn content (%). Hybrid surface has resulted moderate adsorption of BSA and FN as compared to other surfaces and was found to be the most promising surface modifier due to maximum cell adhesion (%) and proliferation, larger nuclei area and the least cell circularity.

We also synthesized antimicrobial peptoid sequences which could possibly be used for developing antimicrobial surfaces for biomedical applications. The antimicrobial peptoid sequences were synthesized and 12 Mer sequence was modified on C and N terminal by capping with EG_2. Purification of synthesized sequences was confirmed by RP-HPLC and LC-MS. Synthesized sequences were tested against *E.coli* (ATCC 25922) and *P.aeroginosa* (PA 01) and 12Mer with EG_2 at N terminal was found to be the most effective against both the strains.

8.2. Suggestions for Future Works

Hybrid surfaces have shown a promising role during *in vitro* studies (i.e. protein adsorption and cell adhesion). Biomedically relevant substrates such as Ti and stainless steel exhibit superior physical properties but suffer from inherently poor osteointegration. Moreover, such surfaces get oxidized in atmospheric conditions and may exhibit deleterious effects during implantation. These surfaces can be cleaned either by Piranha solution or O_2 plasma to get rid of oxide layer and can be further modified by hybrid SAMs and tested *in vivo* for bone plates and screws etc., as shown in Figure 8.1.

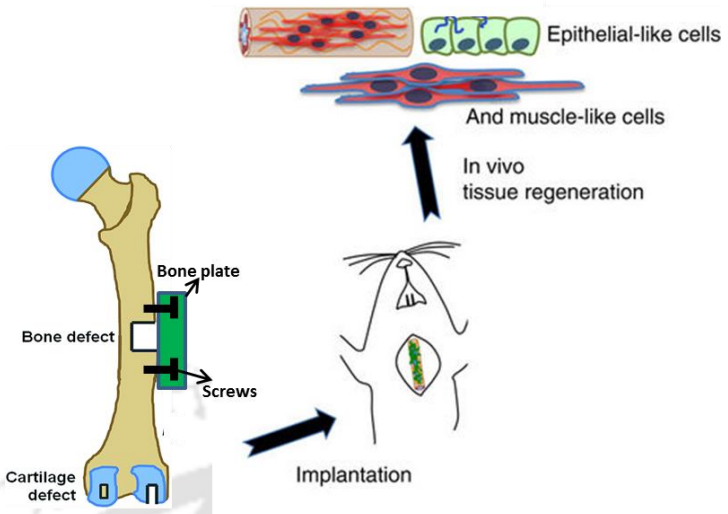

Figure 8.1. Representation of i*n vivo* testing of hybrid SAMs modified bone plates and screws.

Cell adhesion is an integrin mediated process and therefore, it is desirable to determine the integrin expression of different cell lines especially osteoblast cells on such modified surfaces in the presence and absence of cell adhesive proteins. α/β integrin kits are available in the market, supplied from Merck-USA, and can be useful for determining integrin expressions on different surfaces. Reverse transcription-polymerase chain reaction (RT-PCR) is also an important technique to quantify the expression of integrin related genes expressed during cell adhesion on different surfaces.

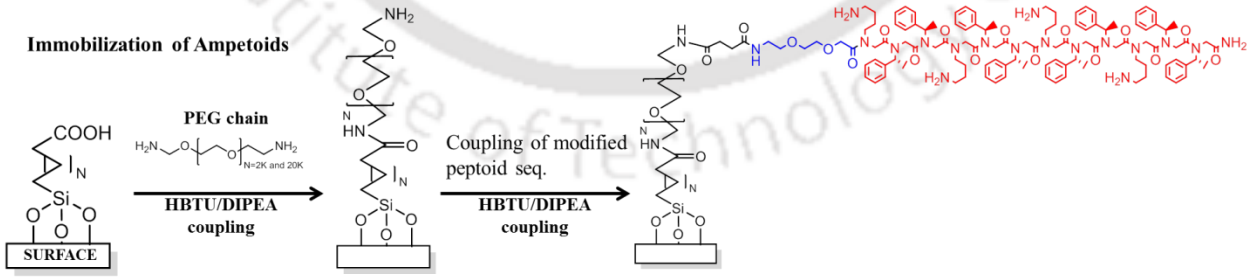

Figure 8.2. Schematic representation of immobilization of antimicrobial peptoids on biomedically relevant surfaces.

We have studied the adsorption behavior of BSA, FB, and IgG and their mixtures on different surfaces under static conditions. To mimic with physiological conditions, it is necessary to study adsorption behavior under dynamic conditions. High end techniques such as quartz crystal microbalance with dissipation monitoring (QCM-D) and surface plasmon resonance (SPR) will be highly beneficial for performing protein adsorption and cell adhesion studies on different modified surfaces under dynamic conditions.

Synthesized antimicrobial peptoids (ampetoids) have shown excellent antimicrobial activities and they can be immobilized on surfaces for generating antimicrobial properties for biomedical applications. For immobilization of ampetoids, grafting density and chain length play crucial roles in regulating their activities. Grafting density is important as closely packed ampetoid molecules may not be efficient enough due to improper interactions with the bacterial membrane. Moreover, distantly placed ampetoid molecules will too render less activity. Hence, optimization of grafting density is crucial and can be regulated by using different concentrations of ampetoids as well as types of surface linkers such as silanes (for dense packing, as shown in Figure 8.2) or biotin (for sparse packing). Ampetoids chain length i.e. sequence distance from surface also regulates interactions with the bacterial membrane. Using PEG chains, we can easily tailor the sequence length and optimize the antimicrobial activity of such modified surfaces. A schematic representation of ampetoids immobilization is shown in Figure 8.2.

Appendices

Appendix 5A

Effect of Surface Modification on Cell Adhesion Behavior

The region 1600-1700 cm^{-1}, which corresponds to Amide-I band was analysed to determine the various secondary structures such as α-helix, β-sheet, β-turn, random coil and side chain of adsorbed FBS on different modified surfaces, as shown in Fig. 5A-1. Peaks were fitted with Gaussian shape curves using OriginPro 8.5 and corresponds to the secondary structures.

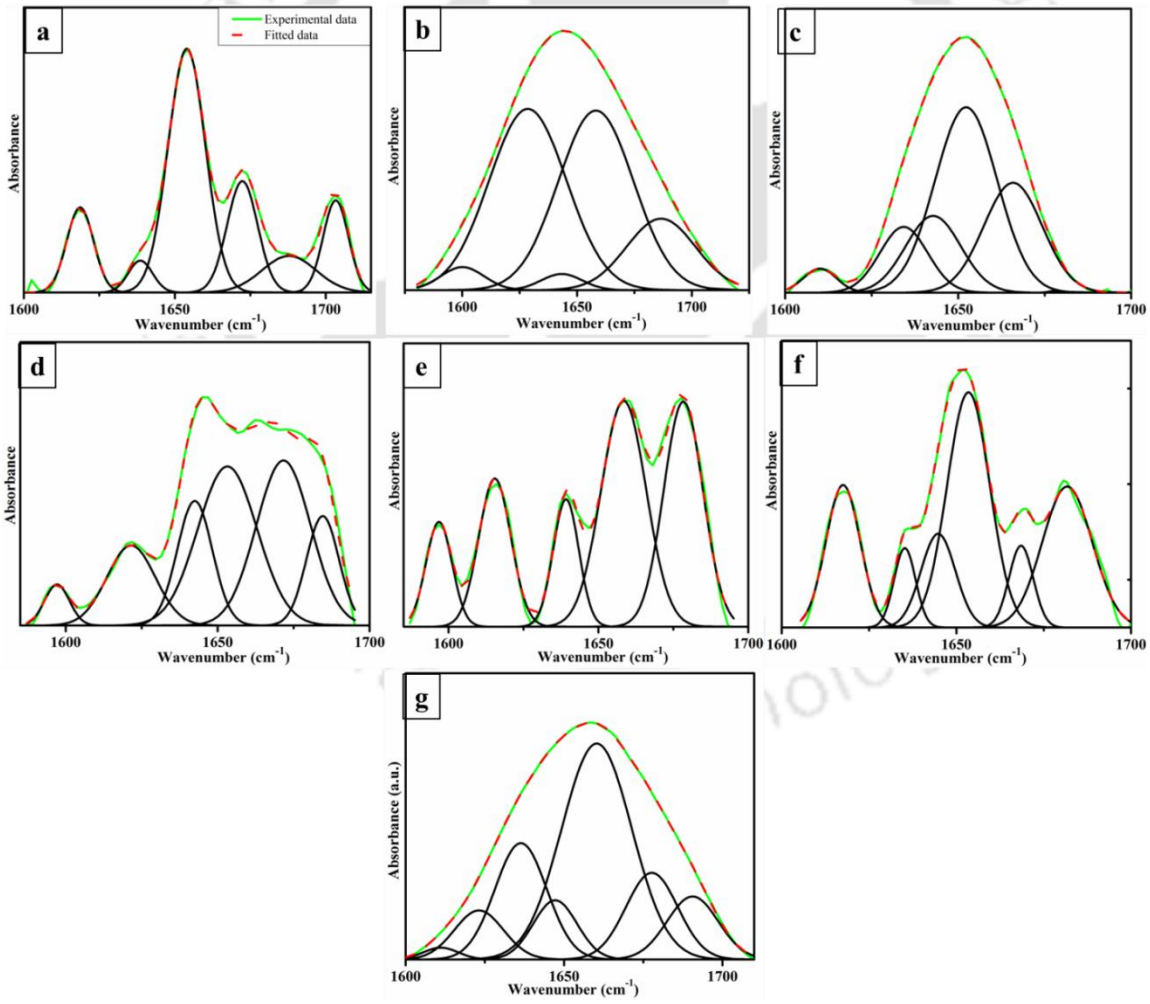

Figure 5A-1. Fitted amide-I FTIR spectra of FBS adsorbed on (a) unmodified, (b) COOH, (c) amine, (d) hybrid, (e) mixed, (f) octyl surfaces, and (g) native FBS.

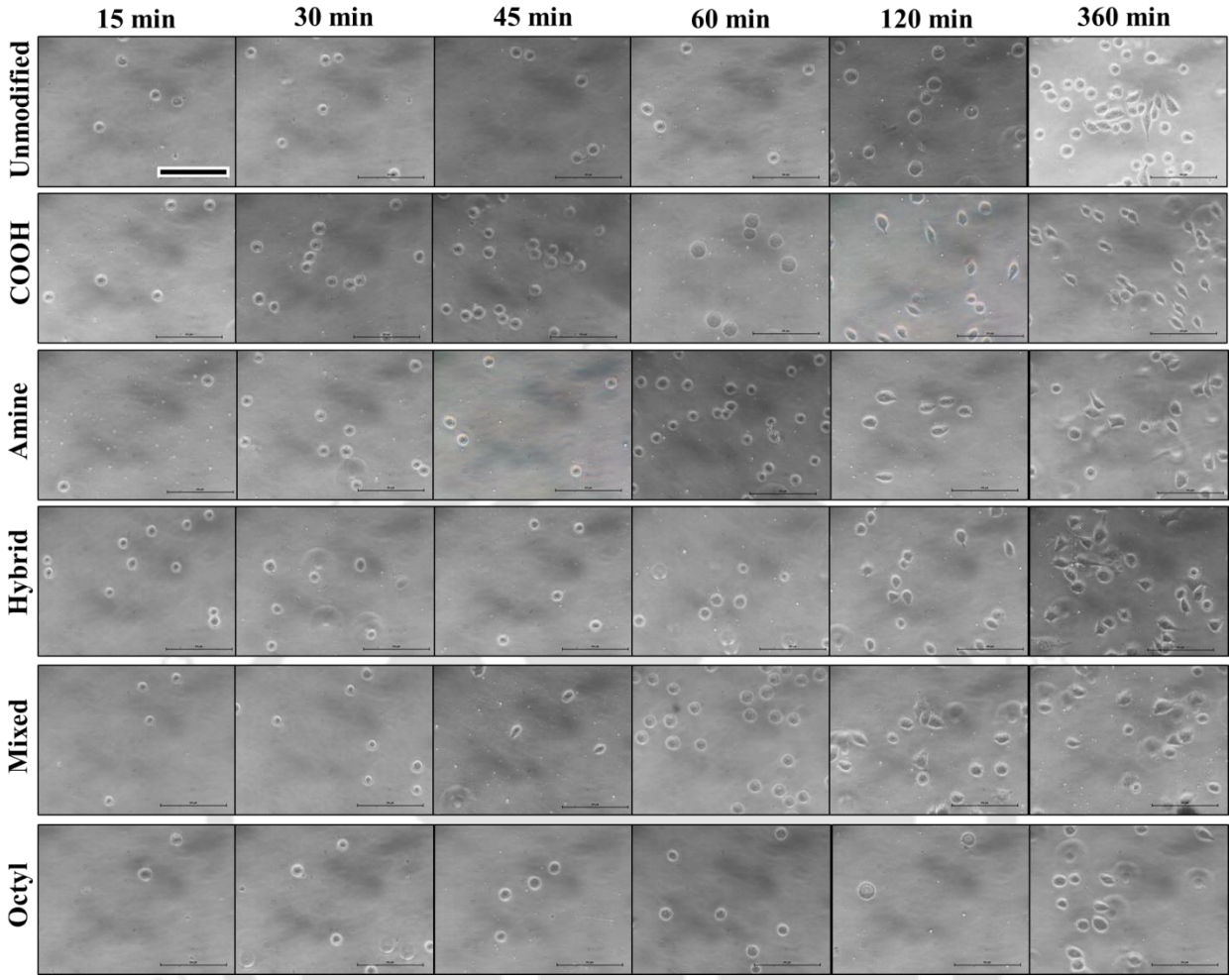

Figure 5A-2. Bright field images of the adhered cells after different time interval on different modified surfaces pre-adsorbed with FBS.

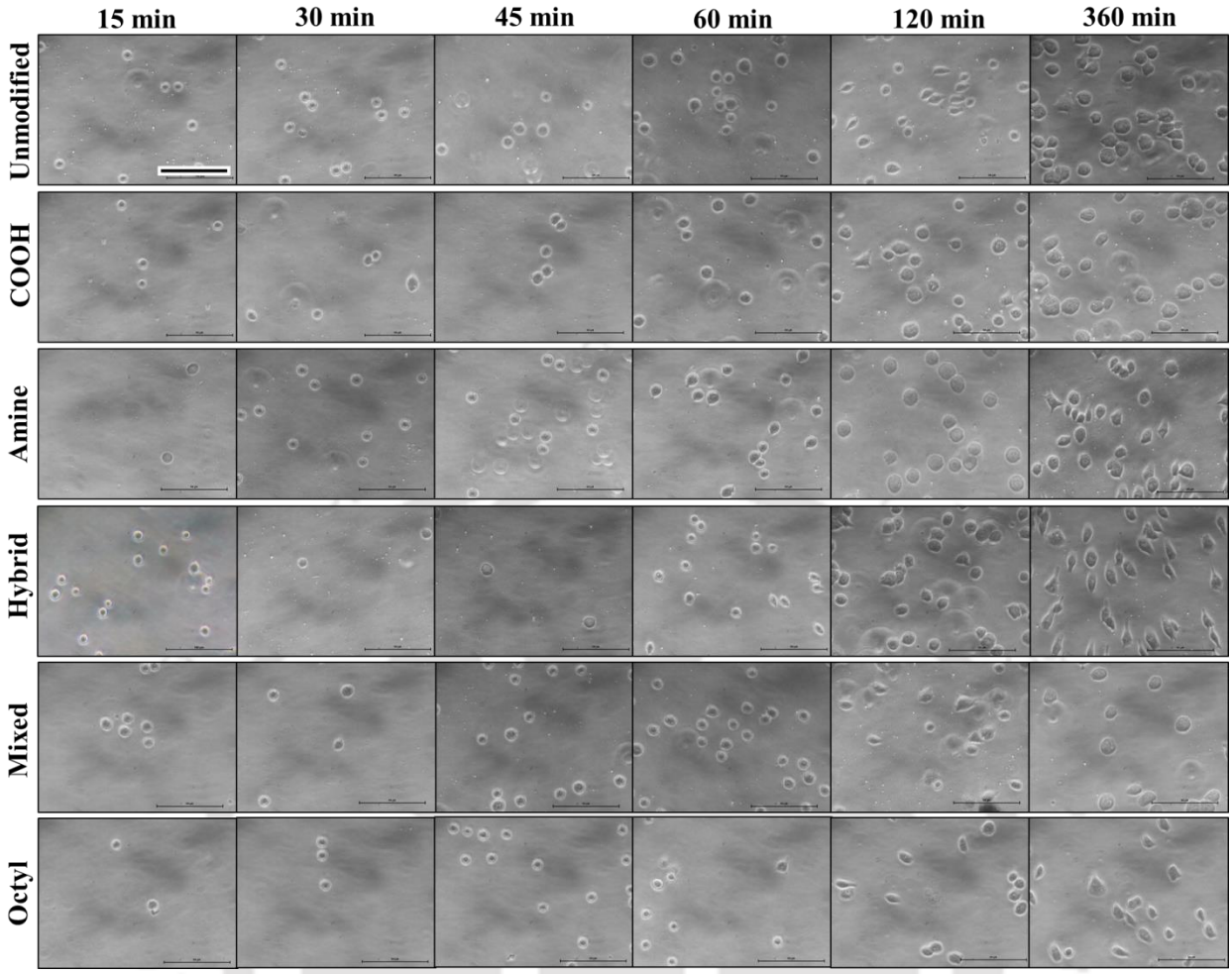

Figure 5A-3. Bright field images of the adhered cells after different time interval on different modified surfaces with FBS in media.

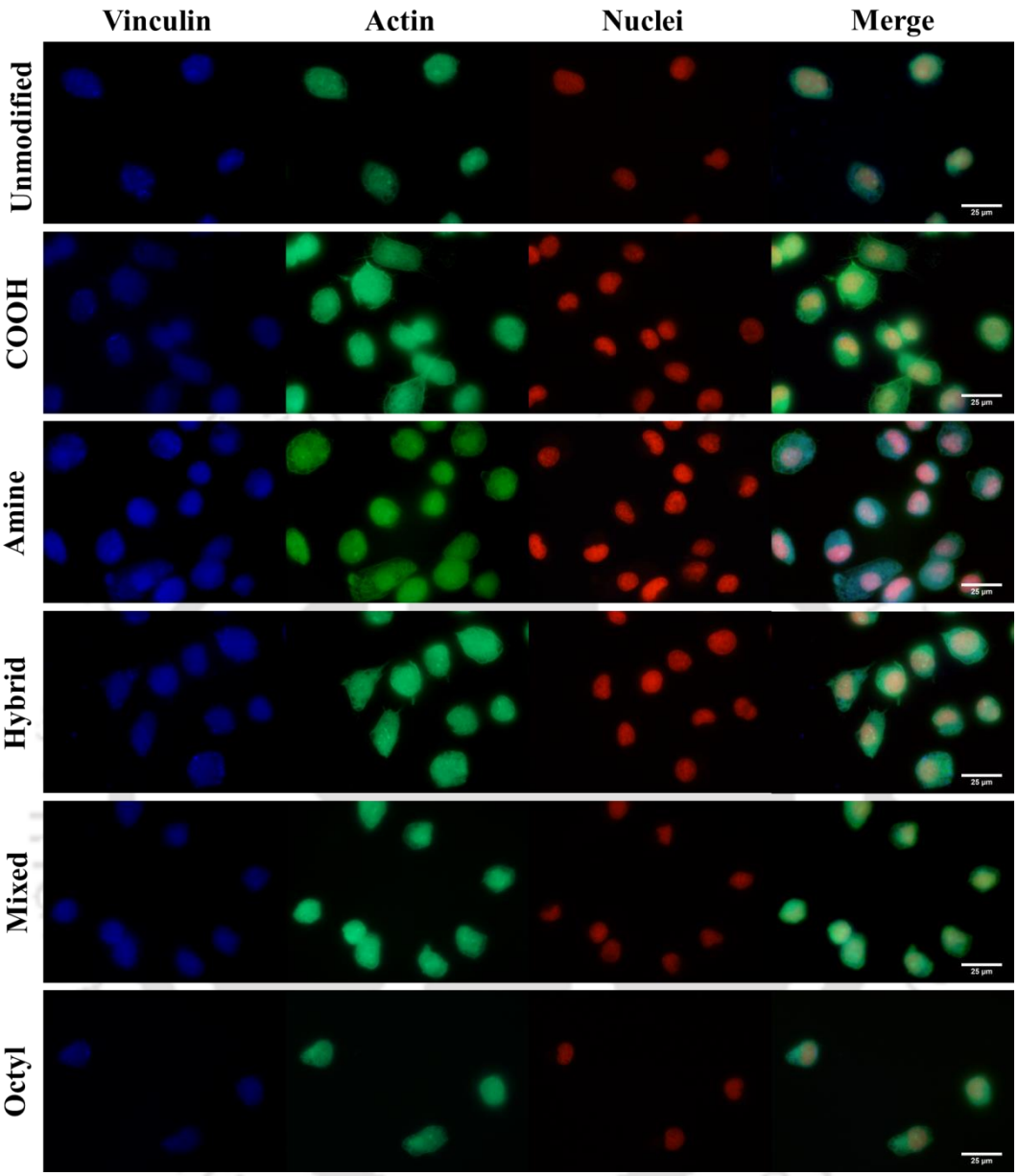

Figure 5A-4. Fluorescent images of L929 cells cultured for 6 h on different surfaces in presence of FBS in media and stained for vinculin protein (blue, 1º Ab followed by Alexafluor-350 labelled 2º Ab), actin filaments (green, FITC-Phalloidin) and nuclei (red, PI dye). Arrow marks indicate focal adhesion spots of bright blue color due to vinculin staining by Alexa fluor-350. Scale bar is 25 μm.

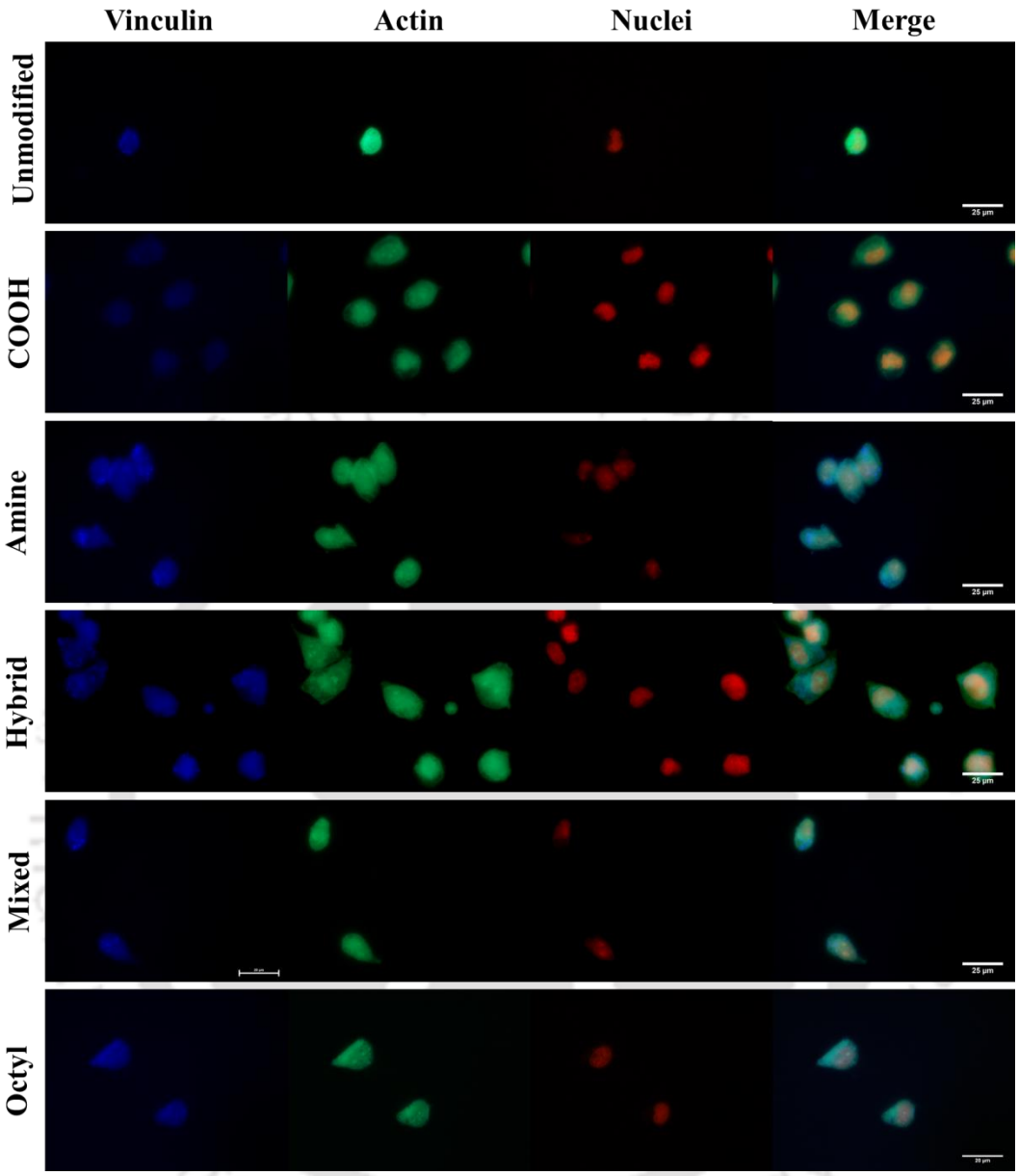

Figure 5A-5. Fluorescent images of L929 cells cultured for 6 h on different surfaces in incomplete media (i.e. without FBS) and stained for vinculin protein (blue, 1º Ab followed by Alexafluor-350 labelled 2º Ab), actin filaments (green, FITC-Phalloidin) and nuclei (red, PI dye). Arrow marks indicate focal adhesion spots of bright blue color due to vinculin staining by Alexa fluor-350. Scale bar is 25 µm.

Cell circularity or also referred as cell shape index (CSI) are used to demonstrate the cell morphology with the CSI=1 indicates circular while CSI=0.4 indicated rectangular shaped cells.

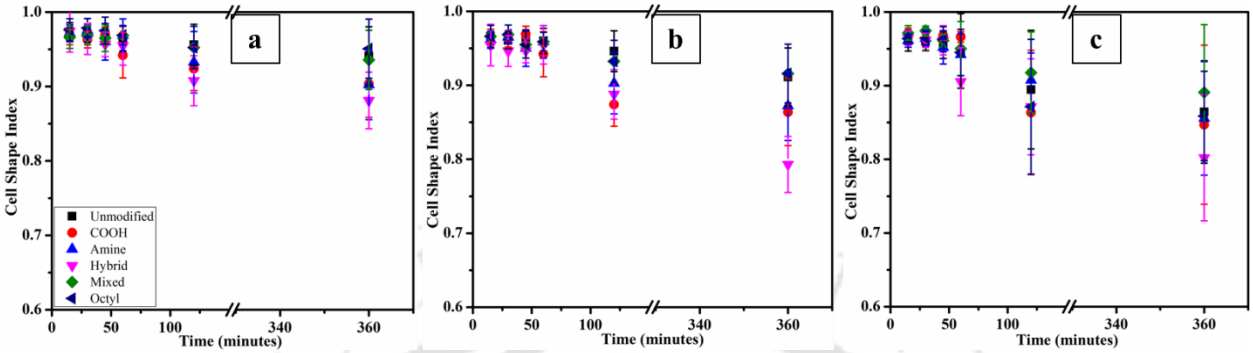

Figure 5A-6. CSI values of adhered cells at different time interval on different modified surfaces when treated with (a) incomplete media i.e. without FBS, (b) with FBS in media and (c) pre-adsorbed FBS on surfaces.

Percentage coverage of the adhered cells were calculated using formula:

$$\%\, Surface\ Coverage = \frac{No.of\ adhered\ cells \times Avg.cell\ area}{Total\ surface\ area\ of\ the\ substrate} \times 100$$

It was evaluated for different surfaces at different time interval under all three experimental conditions.

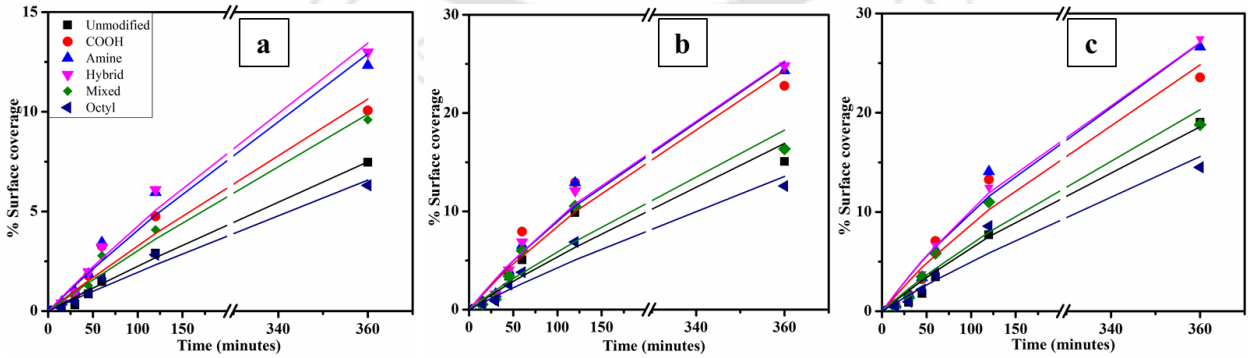

Figure 5A-7. Surface coverage (%) by adhering L929 cells on different surfaces at different time interval under three experimental conditions (a) media without FBS, (b) media with FBS and (d) with pre-adsorbed FBS. Lines represent the fitted data obtained using theoretical model used.

Appendix 6A

Effect of Surface Modification of Biomedically Relevant Titanium Alloy Surface on Protein and Cell Behavior

FESEM analysis was carried out to determine the surface morphology of the oxidized and silanized surfaces at higher maginifications (150 KX). There were no microcracks observed after oxidation as reported by Dunn et al. [381] reported microcracks formation on surfaces after oxidation which was overcome using Pirhana solution. The surface topology both before and after silanization at higher magnification was similar to that reported by Nanci et al. [317]. We noticed different textures for silanized surfaces having different functionalities in comparision to oxidised surface, as reported in other previous studies [382, 383]. Amine modified surface was more rough may be due to multilayer deposition of SAMs (shown in Fig. 6A-1).

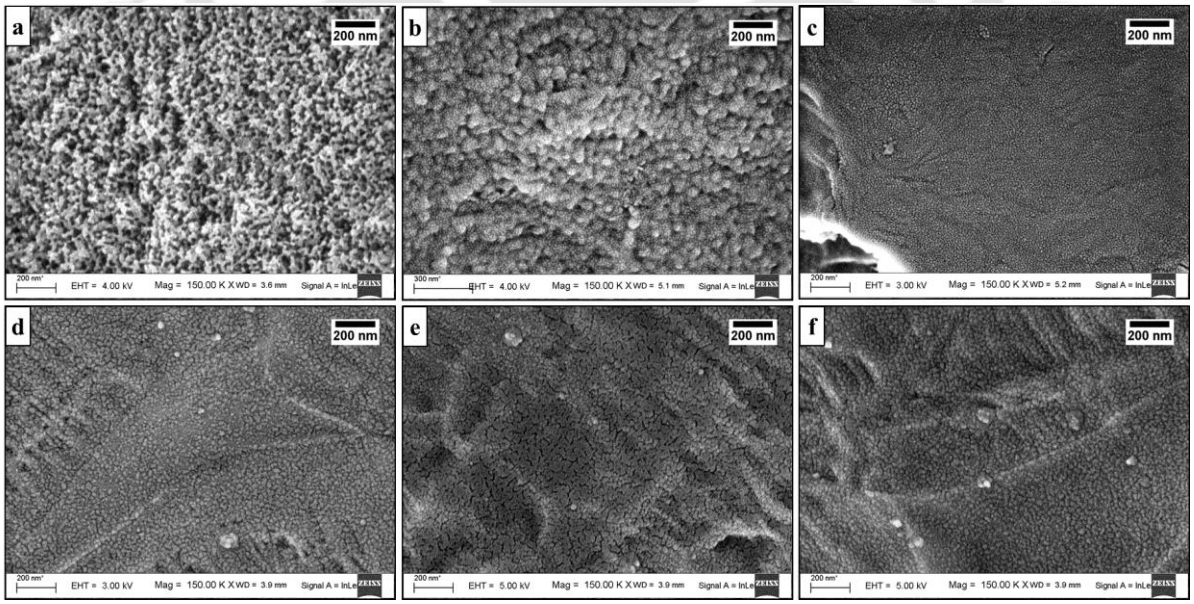

Figure 6A-1. FESEM images of surface topologies of silanized Ti6Al4V surfaces. (a) unmodified, (b) amine, (c) octyl, (d) mixed, (e) hybrid, and (f) COOH surfaces. Images were recorded at 150KX magnification showing 200 nm scale bar.

Elemental analysis using EDS mapping scanning confirmed the silanization of surfaces. Uniform distribution of Si, C, O, and N throughout the surface indicates proper SAM coverage on Ti6Al4V surfaces. We have shown representative mapping image for only amine modified surface in Fig. 6A-2. Ti, Al, and V being the underlying substrate elements were densely located in the mapping images of surfaces whereas C, N, O, and Si were although evenly distributed but mapping concentration was lesser than the elements of the base material. Presence of C, N, O, and Si elements confirmed modification of Ti6Al4V surface with amine SAMs.

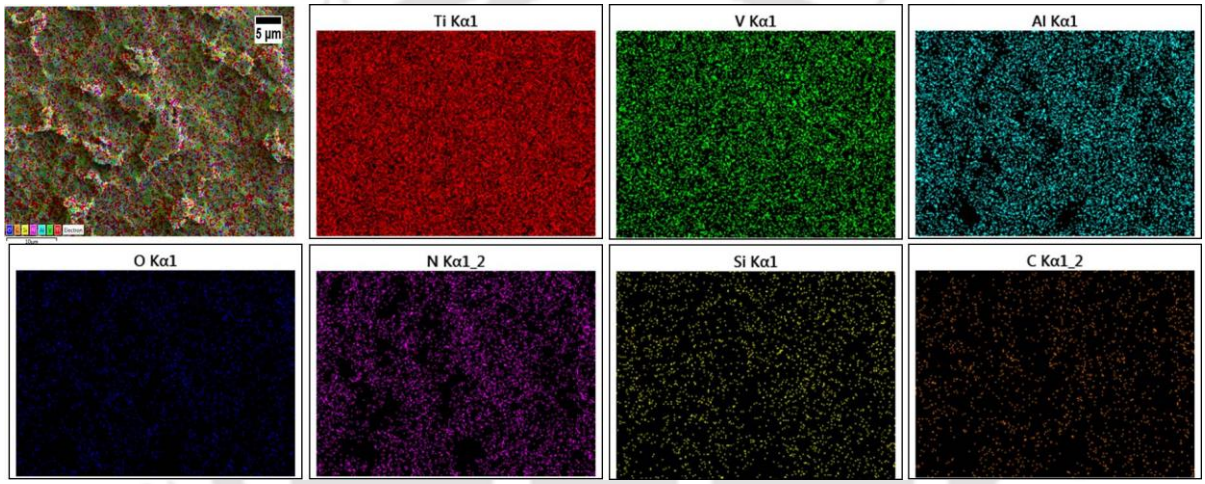

Figure 6A-2. EDS mapping images of elements (Ti, Al, V, Si, N, O, C) present on the surface of amine modified Ti6Al4V sample.

Apart from fluorescent analysis, we also performed FESEM imaging of adhered cells on unmodified and modified surfaces to determine cell morphology/spreading post 6 h of seeding as shown in Fig. 6A-3. Unmodified surface showed irregular morphology and small cell size with less filopodia and cytoplasmic extensions as compared to surfaces having amine, hybrid and COOH functionalities. Whereas, it was also found for modified surfaces that several multiple microvilli, cytoplasmic extensions and lamellipodia formation in multiple directions were formed that signifies proper cell adhesion and active cell migration. The enhanced cell adhesion on amine surface may be attributed to the surface positive charge which induces protein adsorption, causing surface to interact more firmly with negative charge of cell membrane.

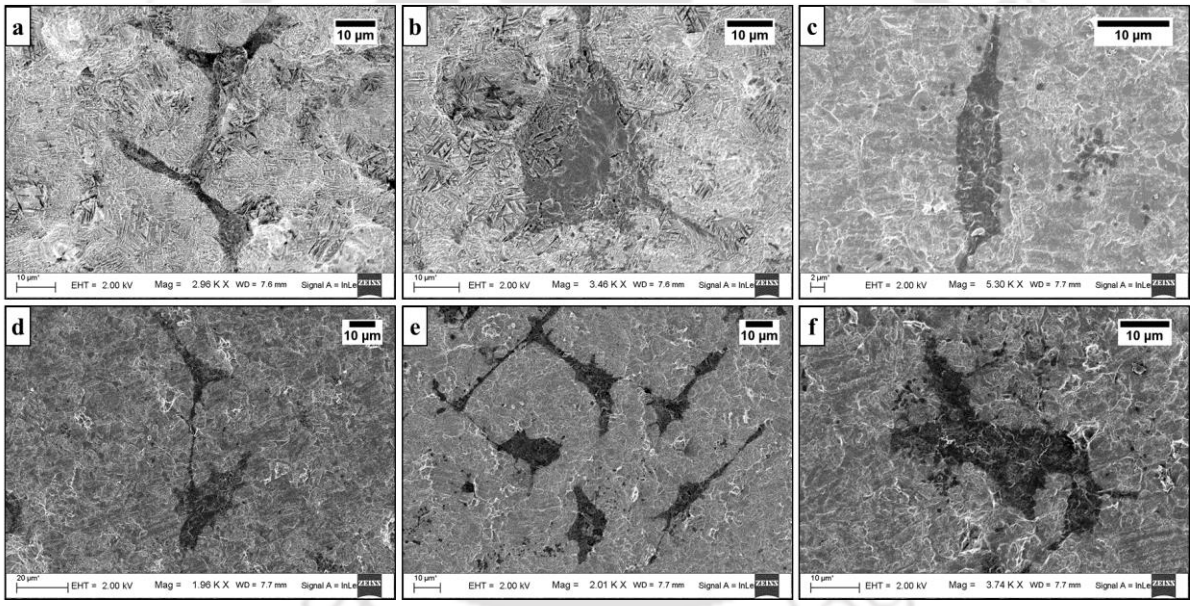

Figure 6A-3. Cell morphology and spreading after 6 h of incubation on (a) unmodified, (b) amine, (c) octyl, (d) mixed, (e) hybrid, and (f) COOH Ti6Al4V surfaces. Scale bar 10 µm.

The region 1600-1700 cm^{-1}, which corresponds to aminde-I band was analysed to determine the various secondary structures such as β-sheet, β-turn, random and side chain of FN after adsorption on different modified surfaces. Fig. 6A-4 shows various graphs obtained for adsorbed FN on different surfaces. Peaks were fitted with Gaussian shape curves and corresponds to the secondary structures. Table A6-1 lists the various secondary structures of FN with their spectral peak positions. The change in the peaks area post adsorption reflect the change in the secondary structure due to physico-chemical properties of surface.

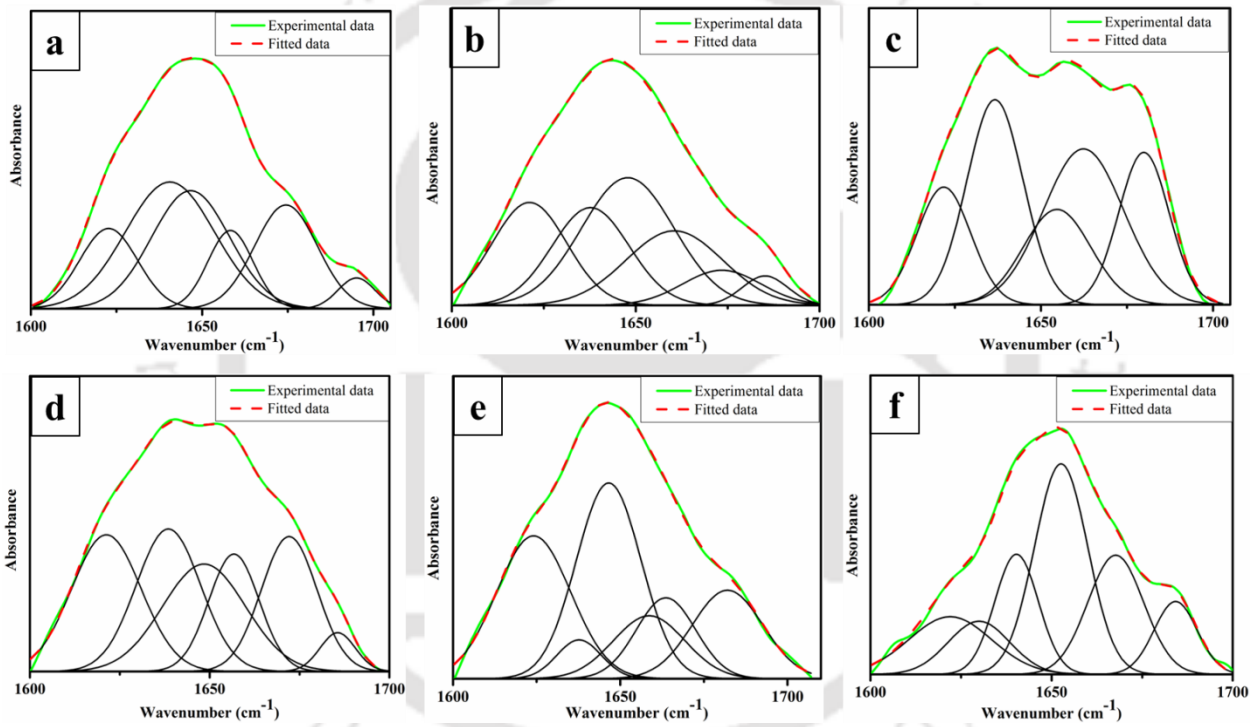

Figure A6-4. Fitted amide-I FTIR spectra of FN adsorbed on (a) blank, (b) amine, (c) octyl, (d) mixed, (e) Hybrid and (f) COOH surfaces.

Table A6-1. Spectral peak position (cm^{-1}) of FN on different modified surfaces in the amide-I region.

Surfaces	**β-sheet**	**Random**	**β-turn**
Blank	1622±1, 1637±1	1646±1	1674±1, 1695±1
Amine	1621±1, 1637±1	1647±1	1660±1, 1673±1, 1685±1
Octyl	1621±1, 1636±1	1645±1	1662±1, 1679±1
Mixed	1621±1, 1638±1	1648±1	1666±1, 1672±1, 1685±1
Hybrid	1624±1, 1637±1	1646±1	1662±1, 1671±1, 1682±1
COOH	1622±1, 1629±1, 1638±1	1650±1	1667±1, 1684±1

References

[1] J. Sibarani, M. Takai, K. Ishihara, Surface modification on microfluidic devices with 2-methacryloyloxyethyl phosphorylcholine polymers for reducing unfavorable protein adsorption, Colloids and Surfaces B: Biointerfaces, 54 (2007) 88-93.
[2] Y. Arima, H. Iwata, Effect of wettability and surface functional groups on protein adsorption and cell adhesion using well-defined mixed self-assembled monolayers, Biomaterials, 28 (2007) 3074-3082.
[3] C. Freij-Larsson, P. Jannasch, B. Wesslén, Polyurethane surfaces modified by amphiphilic polymers: effects on protein adsorption, Biomaterials, 21 (2000) 307-315.
[4] S.A. Skoog, G. Kumar, R.J. Narayan, P.L. Goering, Biological responses to immobilized microscale and nanoscale surface topographies, Pharmacology & therapeutics, (2017).
[5] S.A. Skoog, G. Kumar, P.L. Goering, B. Williams, J. Stiglich, R.J. Narayan, Biological response of human bone marrow-derived mesenchymal stem cells to commercial tantalum coatings with microscale and nanoscale surface topographies, JOM, 68 (2016) 1672-1678.
[6] T. Tsukagoshi, Y. Kondo, N. Yoshino, Preparation of thin polymer films with drug release and protein adsorption resistance, Colloids and Surfaces B: Biointerfaces, 55 (2007) 19-25.
[7] B.D. Ratner, S.J. Bryant, Biomaterials: where we have been and where we are going, Annu. Rev. Biomed. Eng., 6 (2004) 41-75.
[8] D. Bhatia, Bone-Cement: The new medical quick fix, Chronicles of Young Scientists, 1 (2010) 6.
[9] S.N. Rodrigues, I.C. Gonçalves, M. Martins, M.A. Barbosa, B.D. Ratner, Fibrinogen adsorption, platelet adhesion and activation on mixed hydroxyl-/methyl-terminated self-assembled monolayers, Biomaterials, 27 (2006) 5357-5367.
[10] N.K. Chaki, K. Vijayamohanan, Self-assembled monolayers as a tunable platform for biosensor applications, Biosensors and Bioelectronics, 17 (2002) 1-12.
[11] T. Manifar, A. Rezaee, M. Sheikhzadeh, S. Mittler, Formation of uniform self-assembly monolayers by choosing the right solvent: OTS on silicon wafer, a case study, Applied Surface Science, 254 (2008) 4611-4619.
[12] K.H. AaronáLau, Peptoids for biomaterials science, Biomaterials Science, 2 (2014) 627-633.
[13] K.H.A. Lau, T.S. Sileika, S.H. Park, A.M. Sousa, P. Burch, I. Szleifer, P.B. Messersmith, Molecular Design of Antifouling Polymer Brushes Using Sequence-Specific Peptoids, Advanced materials interfaces, 2 (2015).
[14] G. Wu, P. Li, H. Feng, X. Zhang, P.K. Chu, Engineering and functionalization of biomaterials via surface modification, Journal of Materials Chemistry B, 3 (2015) 2024-2042.
[15] B.M. Holzapfel, J.C. Reichert, J.-T. Schantz, U. Gbureck, L. Rackwitz, U. Nöth, F. Jakob, M. Rudert, J. Groll, D.W. Hutmacher, How smart do biomaterials need to be? A translational science and clinical point of view, Advanced drug delivery reviews, 65 (2013) 581-603.
[16] D. Bhatia, T. Bejarano, M. Novo, Current interventions in the management of knee osteoarthritis, Journal of pharmacy & bioallied sciences, 5 (2013) 30.
[17] A. Hasan, L.M. Pandey, Review: polymers, surface-modified polymers, and self assembled monolayers as surface-modifying agents for biomaterials, Polymer-Plastics Technology and Engineering, 54 (2015) 1358-1378.

[18] J.C. Love, L.A. Estroff, J.K. Kriebel, R.G. Nuzzo, G.M. Whitesides, Self-assembled monolayers of thiolates on metals as a form of nanotechnology, Chemical reviews, 105 (2005) 1103-1170.
[19] M. Sun, J. Deng, Z. Tang, J. Wu, D. Li, H. Chen, C. Gao, A correlation study of protein adsorption and cell behaviors on substrates with different densities of PEG chains, Colloids and Surfaces B: Biointerfaces, 122 (2014) 134-142.
[20] Y. Inoue, K. Ishihara, Reduction of protein adsorption on well-characterized polymer brush layers with varying chemical structures, Colloids and Surfaces B: Biointerfaces, 81 (2010) 350-357.
[21] F. Zhang, E. Kang, K. Neoh, P. Wang, K. Tan, Reactive coupling of poly (ethylene glycol) on electroactive polyaniline films for reduction in protein adsorption and platelet adhesion, Biomaterials, 23 (2002) 787-795.
[22] P.-S. Liu, Q. Chen, S.-S. Wu, J. Shen, S.-C. Lin, Surface modification of cellulose membranes with zwitterionic polymers for resistance to protein adsorption and platelet adhesion, Journal of Membrane Science, 350 (2010) 387-394.
[23] A.K. Sen, S. Roy, V.A. Juvekar, Effect of structure on solution and interfacial properties of sodium polystyrene sulfonate (NaPSS), Polymer international, 56 (2007) 167-174.
[24] R.K. Sharma, A. Nisar, K. Balani, Mechanics of ZnO morphological dependence on wear resistance of ultra high molecular weigh polyethylene, European Journal of Mechanics-A/Solids, 65 (2017) 149-158.
[25] K. Reimer, P. Vogt, B. Broegmann, J. Hauser, O. Rossbach, A. Kramer, P. Rudolph, B. Bosse, H. Schreier, W. Fleischer, An innovative topical drug formulation for wound healing and infection treatment: in vitro and in vivo investigations of a povidone-iodine liposome hydrogel, Dermatology, 201 (2000) 235-241.
[26] Z. Liu, S. Rimmer, Synthesis and release of 5-fluorouracil from poly (N-vinylpyrrolidinone) bearing 5-fluorouracil derivatives, Journal of controlled release, 81 (2002) 91-99.
[27] L.-S. Wan, Z.-K. Xu, X.-J. Huang, Z.-G. Wang, J.-L. Wang, Copolymerization of acrylonitrile with N-vinyl-2-pyrrolidone to improve the hemocompatibility of polyacrylonitrile, Polymer, 46 (2005) 7715-7723.
[28] A.M. Telford, M. James, L. Meagher, C. Neto, Thermally cross-linked PNVP films as antifouling coatings for biomedical applications, ACS applied materials & interfaces, 2 (2010) 2399-2408.
[29] Z. Wu, H. Chen, X. Liu, Y. Zhang, D. Li, H. Huang, Protein adsorption on poly (N-vinylpyrrolidone)-modified silicon surfaces prepared by surface-initiated atom transfer radical polymerization, Langmuir, 25 (2009) 2900-2906.
[30] M.S. Tijink, M. Wester, J. Sun, A. Saris, L.A. Bolhuis-Versteeg, S. Saiful, J.A. Joles, Z. Borneman, M. Wessling, D.F. Stamatialis, A novel approach for blood purification: mixed-matrix membranes combining diffusion and adsorption in one step, Acta biomaterialia, 8 (2012) 2279-2287.
[31] M. Hayama, K.-i. Yamamoto, F. Kohori, K. Sakai, How polysulfone dialysis membranes containing polyvinylpyrrolidone achieve excellent biocompatibility?, Journal of membrane science, 234 (2004) 41-49.
[32] X. Liu, K. Sun, Z. Wu, J. Lu, B. Song, W. Tong, X. Shi, H. Chen, Facile synthesis of thermally stable poly (N-vinylpyrrolidone)-modified gold surfaces by surface-initiated atom transfer radical polymerization, Langmuir, 28 (2012) 9451-9459.

[33] H. Wang, Y. Wang, L. Yuan, L. Wang, W. Yang, Z. Wu, D. Li, H. Chen, Thermally responsive silicon nanowire arrays for native/denatured-protein separation, Nanotechnology, 24 (2013) 105101.
[34] B.R. Coad, Y. Lu, L. Meagher, A substrate-independent method for surface grafting polymer layers by atom transfer radical polymerization: Reduction of protein adsorption, Acta biomaterialia, 8 (2012) 608-618.
[35] P. Liu, Q. Chen, B. Yuan, M. Chen, S. Wu, S. Lin, J. Shen, Facile surface modification of silicone rubber with zwitterionic polymers for improving blood compatibility, Materials Science and Engineering: C, 33 (2013) 3865-3874.
[36] B. Nisol, G. Oldenhove, N. Preyat, D. Monteyne, M. Moser, D. Perez-Morga, F. Reniers, Atmospheric plasma synthesized PEG coatings: non-fouling biomaterials showing protein and cell repulsion, Surface and Coatings Technology, 252 (2014) 126-133.
[37] Z. Zhang, J. Wang, Q. Tu, N. Nie, J. Sha, W. Liu, R. Liu, Y. Zhang, J. Wang, Surface modification of PDMS by surface-initiated atom transfer radical polymerization of water-soluble dendronized PEG methacrylate, Colloids and Surfaces B: Biointerfaces, 88 (2011) 85-92.
[38] D.J. Menzies, M. Jasieniak, H.J. Griesser, J.S. Forsythe, G. Johnson, G.A. McFarland, B.W. Muir, A ToF-SIMS and XPS study of protein adsorption and cell attachment across PEG-like plasma polymer films with lateral compositional gradients, Surface science, 606 (2012) 1798-1807.
[39] Z. Li, E. Ruckenstein, Grafting of poly (ethylene oxide) to the surface of polyaniline films through a chlorosulfonation method and the biocompatibility of the modified films, Journal of colloid and interface science, 269 (2004) 62-71.
[40] R. Li, J. Jin, Y. Sun, Surface modification of poly (styrene-b-(ethylene-co-butylene)-b-styrene) elastomer and its plasma protein adsorption by QCM-D, Applied Surface Science, 301 (2014) 300-306.
[41] Y. Zhou, B. Liedberg, N. Gorochovceva, R. Makuska, A. Dedinaite, P.M. Claesson, Chitosan-N-poly (ethylene oxide) brush polymers for reduced nonspecific protein adsorption, Journal of colloid and interface science, 305 (2007) 62-71.
[42] T. Tsukagoshi, Y. Kondo, N. Yoshino, Surface modification of poly (oligoethylene oxide methacrylate) for resisting protein adsorption, Colloids and Surfaces B: Biointerfaces, 54 (2007) 94-100.
[43] Y. Sui, X. Gao, Z. Wang, C. Gao, Antifouling and antibacterial improvement of surface-functionalized poly (vinylidene fluoride) membrane prepared via dihydroxyphenylalanine-initiated atom transfer radical graft polymerizations, Journal of membrane science, 394 (2012) 107-119.
[44] M. Casiano-Maldonado, G.T. Lim, X. Li, D.H. Reneker, J.E. Puskas, C. Wesdemiotis, Protein adsorption on thermoplastic elastomeric surfaces: A quantitative mass spectrometry study, International Journal of Mass Spectrometry, 354 (2013) 391-397.
[45] X. Hu, C.B. Gorman, Resisting protein adsorption on biodegradable polyester brushes, Acta biomaterialia, 10 (2014) 3497-3504.
[46] Y. Inoue, T. Nakanishi, K. Ishihara, Elastic repulsion from polymer brush layers exhibiting high protein repellency, Langmuir, 29 (2013) 10752-10758.
[47] W. Feng, J.L. Brash, S. Zhu, Non-biofouling materials prepared by atom transfer radical polymerization grafting of 2-methacryloloxyethyl phosphorylcholine: separate effects of graft density and chain length on protein repulsion, Biomaterials, 27 (2006) 847-855.

[48] T. Xiang, L.-S. Zhang, R. Wang, Y. Xia, B.-H. Su, C.-S. Zhao, Blood compatibility comparison for polysulfone membranes modified by grafting block and random zwitterionic copolymers via surface-initiated ATRP, Journal of colloid and interface science, 432 (2014) 47-56.
[49] W.-W. Yue, H.-J. Li, T. Xiang, H. Qin, S.-D. Sun, C.-S. Zhao, Grafting of zwitterion from polysulfone membrane via surface-initiated ATRP with enhanced antifouling property and biocompatibility, Journal of membrane science, 446 (2013) 79-91.
[50] H.-W. Chien, C.-C. Tsai, W.-B. Tsai, M.-J. Wang, W.-H. Kuo, T.-C. Wei, S.-T. Huang, Surface conjugation of zwitterionic polymers to inhibit cell adhesion and protein adsorption, Colloids and Surfaces B: Biointerfaces, 107 (2013) 152-159.
[51] T. Xiang, W.-W. Yue, R. Wang, S. Liang, S.-D. Sun, C.-S. Zhao, Surface hydrophilic modification of polyethersulfone membranes by surface-initiated ATRP with enhanced blood compatibility, Colloids and Surfaces B: Biointerfaces, 110 (2013) 15-21.
[52] F. Ran, S. Nie, W. Zhao, J. Li, B. Su, S. Sun, C. Zhao, Biocompatibility of modified polyethersulfone membranes by blending an amphiphilic triblock co-polymer of poly (vinyl pyrrolidone)–b-poly (methyl methacrylate)–b-poly (vinyl pyrrolidone), Acta biomaterialia, 7 (2011) 3370-3381.
[53] J.H. Jeong, D.W. Lim, D.K. Han, T.G. Park, Synthesis, characterization and protein adsorption behaviors of PLGA/PEG di-block co-polymer blend films, Colloids and Surfaces B: Biointerfaces, 18 (2000) 371-379.
[54] P. Kingshott, H. Thissen, H.J. Griesser, Effects of cloud-point grafting, chain length, and density of PEG layers on competitive adsorption of ocular proteins, Biomaterials, 23 (2002) 2043-2056.
[55] B. Zhu, T. Eurell, R. Gunawan, D. Leckband, Chain-length dependence of the protein and cell resistance of oligo (ethylene glycol)-terminated self-assembled monolayers on gold, Journal of Biomedical Materials Research Part A, 56 (2001) 406-416.
[56] L.V. Mohite, V.A. Juvekar, Quantification of thermodynamics of aqueous solutions of poly (ethylene glycols): Role of calorimetry, Fluid Phase Equilibria, 278 (2009) 41-53.
[57] P. De Gennes, Polymers at an interface; a simplified view, Advances in colloid and interface science, 27 (1987) 189-209.
[58] M. Malmsten, K. Emoto, J.M. Van Alstine, Effect of chain density on inhibition of protein adsorption by poly (ethylene glycol) based coatings, Journal of colloid and interface science, 202 (1998) 507-517.
[59] P. Harder, M. Grunze, R. Dahint, G. Whitesides, P. Laibinis, Molecular conformation in oligo (ethylene glycol)-terminated self-assembled monolayers on gold and silver surfaces determines their ability to resist protein adsorption, The Journal of Physical Chemistry B, 102 (1998) 426-436.
[60] S.-W. Lee, P.E. Laibinis, Protein-resistant coatings for glass and metal oxide surfaces derived from oligo (ethylene glycol)-terminated alkyltrichlorosilanes, Biomaterials, 19 (1998) 1669-1675.
[61] H. Lee, S.M. Dellatore, W.M. Miller, P.B. Messersmith, Mussel-inspired surface chemistry for multifunctional coatings, science, 318 (2007) 426-430.
[62] X. Ding, C. Yang, T.P. Lim, L.Y. Hsu, A.C. Engler, J.L. Hedrick, Y.-Y. Yang, Antibacterial and antifouling catheter coatings using surface grafted PEG-b-cationic polycarbonate diblock copolymers, Biomaterials, 33 (2012) 6593-6603.

[63] T. Kuhl, D. Leckband, D. Lasic, J. Israelachvili, Modulation of interaction forces between bilayers exposing short-chained ethylene oxide headgroups, Biophysical journal, 66 (1994) 1479-1488.
[64] N. Huebsch, D.J. Mooney, Inspiration and application in the evolution of biomaterials, Nature, 462 (2009) 426.
[65] K.B. Blodgett, Films built by depositing successive monomolecular layers on a solid surface, Journal of the American Chemical Society, 57 (1935) 1007-1022.
[66] K.B. Blodgett, I. Langmuir, Built-up films of barium stearate and their optical properties, Physical Review, 51 (1937) 964.
[67] W. Bigelow, D. Pickett, W. Zisman, Oleophobic monolayers: I. Films adsorbed from solution in non-polar liquids, Journal of Colloid Science, 1 (1946) 513-538.
[68] E. Polymeropoulos, J. Sagiv, Electrical conduction through adsorbed monolayers, The Journal of Chemical Physics, 69 (1978) 1836-1847.
[69] J. Sagiv, Organized monolayers by adsorption. 1. Formation and structure of oleophobic mixed monolayers on solid surfaces, Journal of the American Chemical Society, 102 (1980) 92-98.
[70] L. Netzer, J. Sagiv, A new approach to construction of artificial monolayer assemblies, Journal of the American Chemical Society, 105 (1983) 674-676.
[71] R.G. Nuzzo, D.L. Allara, Adsorption of bifunctional organic disulfides on gold surfaces, Journal of the American Chemical Society, 105 (1983) 4481-4483.
[72] F. Schreiber, Structure and growth of self-assembling monolayers, Progress in surface science, 65 (2000) 151-257.
[73] J.-W. Park, H. Kim, M. Han, Polymeric self-assembled monolayers derived from surface-active copolymers: a modular approach to functionalized surfaces, Chemical Society Reviews, 39 (2010) 2935-2947.
[74] S. Asiaei, P. Nieva, M.M. Vijayan, Fast kinetics of thiolic self-assembled monolayer adsorption on gold: Modeling and confirmation by protein binding, The Journal of Physical Chemistry B, 118 (2014) 13697-13703.
[75] R. Urcuyo, E. Cortés, A. Rubert, G. Benitez, M. Montero, N. Tognalli, A. Fainstein, M. Vela, R. Salvarezza, Aromatic and aliphatic thiol self-assembled monolayers on Au: Anchoring and delivering copper species, The Journal of Physical Chemistry C, 115 (2011) 24707-24717.
[76] S.A. DiBenedetto, A. Facchetti, M.A. Ratner, T.J. Marks, Molecular Self-Assembled Monolayers and Multilayers for Organic and Unconventional Inorganic Thin-Film Transistor Applications, Advanced materials, 21 (2009) 1407-1433.
[77] A. Ulman, Formation and structure of self-assembled monolayers, Chemical reviews, 96 (1996) 1533-1554.
[78] M. Mrksich, Tailored substrates for studies of attached cell culture, Cellular and Molecular Life Sciences CMLS, 54 (1998) 653-662.
[79] R.G. Nuzzo, B.R. Zegarski, L.H. Dubois, Fundamental studies of the chemisorption of organosulfur compounds on gold (111). Implications for molecular self-assembly on gold surfaces, Journal of the American Chemical Society, 109 (1987) 733-740.
[80] T. Ishida, S.i. Yamamoto, W. Mizutani, M. Motomatsu, H. Tokumoto, H. Hokari, H. Azehara, M. Fujihira, Evidence for cleavage of disulfides in the self-assembled monolayer on Au (111), Langmuir, 13 (1997) 3261-3265.
[81] J. Noh, M. Hara, Nanoscopic evidence for dissociative adsorption of asymmetric disulfide self-assembled monolayers on Au (111), Langmuir, 16 (2000) 2045-2048.

[82] A. Hasan, L. Pandey, Self-assembled monolayers in biomaterials, in: Nanobiomaterials, Elsevier, 2017, pp. 137-178.
[83] P. Fenter, A. Eberhardt, P. Eisenberger, Self-assembly of n-alkyl thiols as disulfides on Au (111), Science, 266 (1994) 1216.
[84] C.D. Bain, E.B. Troughton, Y.T. Tao, J. Evall, G.M. Whitesides, R.G. Nuzzo, Formation of monolayer films by the spontaneous assembly of organic thiols from solution onto gold, Journal of the American Chemical Society, 111 (1989) 321-335.
[85] C.D. Bain, G.M. Whitesides, Formation of two-component surfaces by the spontaneous assembly of monolayers on gold from solutions containing mixtures of organic thiols, Journal of the american chemical society, 110 (1988) 6560-6561.
[86] P.E. Laibinis, M.A. Fox, J.P. Folkers, G.M. Whitesides, Comparisons of self-assembled monolayers on silver and gold: mixed monolayers derived from HS (CH2) 21X and HS (CH2) 10Y (X, Y= CH3, CH2OH) have similar properties, Langmuir, 7 (1991) 3167-3173.
[87] J. Venables, Introduction to surface and thin film processes, Cambridge University Press, 2000.
[88] M. Electroplating, ; Schlesinger, M., Paunovic, M., Eds, in, John Wiley & Sons: New York, 2000.
[89] J.C. Love, D.B. Wolfe, R. Haasch, M.L. Chabinyc, K.E. Paul, G.M. Whitesides, R.G. Nuzzo, Formation and structure of self-assembled monolayers of alkanethiolates on palladium, Journal of the American Chemical Society, 125 (2003) 2597-2609.
[90] M.D. Porter, T.B. Bright, D.L. Allara, C.E. Chidsey, Spontaneously organized molecular assemblies. 4. Structural characterization of n-alkyl thiol monolayers on gold by optical ellipsometry, infrared spectroscopy, and electrochemistry, Journal of the American Chemical Society, 109 (1987) 3559-3568.
[91] C. Tripp, M. Hair, An infrared study of the reaction of octadecyltrichlorosilane with silica, Langmuir, 8 (1992) 1120-1126.
[92] R. Wang, S.L. Wunder, Effects of silanol density, distribution, and hydration state of fumed silica on the formation of self-assembled monolayers of n-octadecyltrichlorosilane, Langmuir, 16 (2000) 5008-5016.
[93] C. Tripp, M. Hair, Reaction of methylsilanols with hydrated silica surfaces: the hydrolysis of trichloro-, dichloro-, and monochloromethylsilanes and the effects of curing, Langmuir, 11 (1995) 149-155.
[94] H. Finklea, L. Robinson, A. Blackburn, B. Richter, D. Allara, T. Bright, Formation of an organized monolayer by solution adsorption of octadecyltrichlorosilane on gold: electrochemical properties and structural characterization, Langmuir, 2 (1986) 239-244.
[95] P. Silberzan, L. Leger, D. Ausserre, J. Benattar, Silanation of silica surfaces. A new method of constructing pure or mixed monolayers, Langmuir, 7 (1991) 1647-1651.
[96] M. Hair, C. Tripp, Alkylchlorosilane reactions at the silica surface, Colloids and Surfaces A: Physicochemical and Engineering Aspects, 105 (1995) 95-103.
[97] Y. Wang, M. Lieberman, Growth of ultrasmooth octadecyltrichlorosilane self-assembled monolayers on SiO2, Langmuir, 19 (2003) 1159-1167.
[98] U. Jönsson, G. Olofsson, M. Malmqvist, I. Rönnberg, Chemical vapour deposition of silanes, Thin Solid Films, 124 (1985) 117-123.
[99] H. Handa, S. Gurczynski, M.P. Jackson, G. Auner, J. Walker, G. Mao, Recognition of Salmonella typhimurium by immobilized phage P22 monolayers, Surface science, 602 (2008) 1392-1400.

[100] N. Semaltianos, J.-L. Pastol, P. Doppelt, Copper chemical vapour deposition on organosilane-treated SiO 2 surfaces, Applied surface science, 222 (2004) 102-109.
[101] A.K. Mahapatro, A. Scott, A. Manning, D.B. Janes, Gold surface with sub-nm roughness realized by evaporation on a molecular adhesion monolayer, Applied physics letters, 88 (2006) 151917.
[102] B. Pattier, J.-F. Bardeau, M. Edely, A. Gibaud, N. Delorme, Cheap and robust ultraflat gold surfaces suitable for high-resolution surface modification, Langmuir, 24 (2008) 821-825.
[103] H. Sugimura, A. Hozumi, T. Kameyama, O. Takai, Organosilane self-assembled monolayers formed at the vapour/solid interface, Surface and interface analysis, 34 (2002) 550-554.
[104] G.J. Zhang, T. Tanii, T. Zako, T. Hosaka, T. Miyake, Y. Kanari, T. Funatsu, I. Ohdomari, Nanoscale Patterning of Protein Using Electron Beam Lithography of Organosilane Self-Assembled Monolayers, Small, 1 (2005) 833-837.
[105] K.M. Kallury, M. Thompson, C.P. Tripp, M.L. Hair, Interaction of silicon surfaces silanized with octadecylchlorosilanes with octadecanoic acid and octadecanamine studied by ellipsometry, X-ray photoelectron spectroscopy and reflectance Fourier transform infrared spectroscopy, Langmuir, 8 (1992) 947-954.
[106] R. Yamada, H. Sakai, K. Uosaki, Solvent Effect on the Structure of the Self-Assembled Monolayer of Alkanethiol, Chemistry Letters, (1999) 667-668.
[107] M. Kawasaki, T. Sato, T. Tanaka, K. Takao, Rapid self-assembly of alkanethiol monolayers on sputter-grown Au (111), Langmuir, 16 (2000) 1719-1728.
[108] J. Woodward, D. Schwartz, In situ observation of self-assembled monolayer growth, Journal of the American Chemical Society, 118 (1996) 7861-7862.
[109] R. Maoz, J. Sagiv, On the formation and structure of self-assembling monolayers. I. A comparative atr-wettability study of Langmuir—Blodgett and adsorbed films on flat substrates and glass microbeads, Journal of Colloid and Interface Science, 100 (1984) 465-496.
[110] S.R. Cohen, R. Naaman, J. Sagiv, Thermally induced disorder in organized organic monolayers on solid substrates, The Journal of Physical Chemistry, 90 (1986) 3054-3056.
[111] T. Ohtake, N. Mino, K. Ogawa, Effect of hydrocarbon chain length on arrangement of chemically adsorbed monolayers, Langmuir, 8 (1992) 2081-2083.
[112] K. Mathauer, C.W. Frank, Naphthalene chromophore tethered in the constrained environment of a self-assembled monolayer, Langmuir, 9 (1993) 3002-3008.
[113] D. Schwartz, S. Steinberg, J. Israelachvili, J. Zasadzinski, Growth of a self-assembled monolayer by fractal aggregation, Physical review letters, 69 (1992) 3354.
[114] R. Banga, J. Yarwood, A.M. Morgan, B. Evans, J. Kells, FTIR and AFM studies of the kinetics and self-assembly of alkyltrichlorosilanes and (perfluoroalkyl) trichlorosilanes onto glass and silicon, Langmuir, 11 (1995) 4393-4399.
[115] S. Brandriss, S. Margel, Synthesis and characterization of self-assembled hydrophobic monolayer coatings on silica colloids, Langmuir, 9 (1993) 1232-1240.
[116] M.E. McGovern, K.M. Kallury, M. Thompson, Role of solvent on the silanization of glass with octadecyltrichlorosilane, Langmuir, 10 (1994) 3607-3614.
[117] J. Kim, P. Seidler, L.S. Wan, C. Fill, Formation, structure, and reactivity of amino-terminated organic films on silicon substrates, Journal of colloid and interface science, 329 (2009) 114-119.
[118] W. Bigelow, E. Glass, W. Zisman, Oleophobic monolayers. ii. temperature effects and energy of adsorption, Journal of colloid science, 2 (1947) 563-591.

[119] J. Brzoska, I.B. Azouz, F. Rondelez, Silanization of solid substrates: a step toward reproducibility, Langmuir, 10 (1994) 4367-4373.
[120] A.N. Parikh, D.L. Allara, I.B. Azouz, F. Rondelez, An intrinsic relationship between molecular structure in self-assembled n-alkylsiloxane monolayers and deposition temperature, The Journal of Physical Chemistry, 98 (1994) 7577-7590.
[121] W. Gao, L. Reven, Solid-state NMR studies of self-assembled monolayers, Langmuir, 11 (1995) 1860-1863.
[122] R.M. Pasternack, S. Rivillon Amy, Y.J. Chabal, Attachment of 3-(aminopropyl) triethoxysilane on silicon oxide surfaces: dependence on solution temperature, Langmuir, 24 (2008) 12963-12971.
[123] H. Brunner, T. Vallant, U. Mayer, H. Hoffmann, Formation of Ultrathin Films at the Solid–Liquid Interface Studied byIn SituEllipsometry, Journal of colloid and interface science, 212 (1999) 545-552.
[124] V. Hlady, R. VanWagenen, J. Andrade, J. Andrade, Surface and Interfacial Aspects of Biomedical Polymers, in: Protein Adsorption, Plenum Press New York, 1985, pp. 81-119.
[125] M. Mrksich, G.M. Whitesides, Using self-assembled monolayers to understand the interactions of man-made surfaces with proteins and cells, Annual review of biophysics and biomolecular structure, 25 (1996) 55-78.
[126] N. Faucheux, R. Schweiss, K. Lützow, C. Werner, T. Groth, Self-assembled monolayers with different terminating groups as model substrates for cell adhesion studies, Biomaterials, 25 (2004) 2721-2730.
[127] G. Toworfe, S. Bhattacharyya, R. Composto, C.S. Adams, I. Shapiro, P. Ducheyne, Effect of functional end groups of silane self-assembled monolayer surfaces on apatite formation, fibronectin adsorption and osteoblast cell function, J. Tissue Eng. Regen. Med., 3 (2009) 26-36.
[128] M.H. Lee, P. Ducheyne, L. Lynch, D. Boettiger, R.J. Composto, Effect of biomaterial surface properties on fibronectin–α 5 β 1 integrin interaction and cellular attachment, Biomaterials, 27 (2006) 1907-1916.
[129] P. Filippini, G. Rainaldi, A. Ferrante, B. Mecheri, G. Gabrielli, M. Bombace, P.L. Indovina, M.T. Santini, Modulation of osteosarcoma cell growth and differentiation by silane-modified surfaces, Journal of biomedical materials research, 55 (2001) 338-349.
[130] S. Lan, M. Veiseh, M. Zhang, Surface modification of silicon and gold-patterned silicon surfaces for improved biocompatibility and cell patterning selectivity, Biosensors and Bioelectronics, 20 (2005) 1697-1708.
[131] K. Webb, V. Hlady, P.A. Tresco, Relationships among cell attachment, spreading, cytoskeletal organization, and migration rate for anchorage-dependent cells on model surfaces, Journal of biomedical materials research, 49 (2000) 362.
[132] M.H. Lee, D.A. Brass, R. Morris, R.J. Composto, P. Ducheyne, The effect of non-specific interactions on cellular adhesion using model surfaces, Biomaterials, 26 (2005) 1721-1730.
[133] M. Franco, P.F. Nealey, S. Campbell, A.I. Teixeira, C.J. Murphy, Adhesion and proliferation of corneal epithelial cells on self-assembled monolayers, Journal of biomedical materials research, 52 (2000) 261-269.
[134] B. Spargo, M. Testoff, T. Nielsen, D. Stenger, J. Hickman, A. Rudolph, Spatially controlled adhesion, spreading, and differentiation of endothelial cells on self-assembled molecular monolayers, Proceedings of the National Academy of Sciences, 91 (1994) 11070-11074.

[135] R. Kapur, A.S. Rudolph, Cellular and cytoskeleton morphology and strength of adhesion of cells on self-assembled monolayers of organosilanes, Experimental cell research, 244 (1998) 275-285.
[136] C.F. Wertz, M.M. Santore, Effect of surface hydrophobicity on adsorption and relaxation kinetics of albumin and fibrinogen: single-species and competitive behavior, Langmuir, 17 (2001) 3006-3016.
[137] M. Zhang, T. Desai, M. Ferrari, Proteins and cells on PEG immobilized silicon surfaces, Biomaterials, 19 (1998) 953-960.
[138] A. Papra, N. Gadegaard, N.B. Larsen, Characterization of ultrathin poly (ethylene glycol) monolayers on silicon substrates, Langmuir, 17 (2001) 1457-1460.
[139] S. Sharma, R.W. Johnson, T.A. Desai, Ultrathin poly (ethylene glycol) films for silicon-based microdevices, Applied Surface Science, 206 (2003) 218-229.
[140] L.M. Pandey, S.K. Pattanayek, Hybrid surface from self-assembled layer and its effect on protein adsorption, Applied Surface Science, 257 (2011) 4731-4737.
[141] L.M. Pandey, S.K. Pattanayek, Properties of competitively adsorbed BSA and fibrinogen from their mixture on mixed and hybrid surfaces, Applied Surface Science, 264 (2013) 832-837.
[142] L.M. Pandey, S.K. Pattanayek, Relation between the wetting effect and the adsorbed amount of water-soluble polymers or proteins at various interfaces, Journal of Chemical & Engineering Data, 58 (2013) 3440-3446.
[143] R.O. Hynes, Integrins: bidirectional, allosteric signaling machines, Cell, 110 (2002) 673-687.
[144] E.F. Plow, T.A. Haas, L. Zhang, J. Loftus, J.W. Smith, Ligand binding to integrins, Journal of Biological Chemistry, 275 (2000) 21785-21788.
[145] M.A. Schwartz, M.D. Schaller, M.H. Ginsberg, Integrins: emerging paradigms of signal transduction, Annual review of cell and developmental biology, 11 (1995) 549-599.
[146] K. Lewandowska, E. Pergament, C.N. Sukenik, L.A. Culp, Cell-Type-Specific adhesion mechanisms mediated by fibronectin adsorbed to chemically derivatized substrata, Journal of biomedical materials research, 26 (1992) 1343-1363.
[147] C.N. Sukenik, N. Balachander, L.A. Culp, K. Lewandowska, K. Merritt, Modulation of cell adhesion by modification of titanium surfaces with covalently attached self-assembled monolayers, Journal of Biomedical Materials Research, 24 (1990) 1307-1323.
[148] R. Tzoneva, N. Faucheux, T. Groth, Wettability of substrata controls cell–substrate and cell–cell adhesions, Biochimica et Biophysica Acta (BBA)-General Subjects, 1770 (2007) 1538-1547.
[149] N. Faucheux, R. Tzoneva, M.-D. Nagel, T. Groth, The dependence of fibrillar adhesions in human fibroblasts on substratum chemistry, Biomaterials, 27 (2006) 234-245.
[150] J.E. Phillips, T.A. Petrie, F.P. Creighton, A.J. García, Human mesenchymal stem cell differentiation on self-assembled monolayers presenting different surface chemistries, Acta biomaterialia, 6 (2010) 12-20.
[151] L. Qian, W.M. Saltzman, Improving the expansion and neuronal differentiation of mesenchymal stem cells through culture surface modification, Biomaterials, 25 (2004) 1331-1337.
[152] D.S. Benoit, M.P. Schwartz, A.R. Durney, K.S. Anseth, Small functional groups for controlled differentiation of hydrogel-encapsulated human mesenchymal stem cells, Nature materials, 7 (2008) 816-823.

[153] B.G. Keselowsky, D.M. Collard, A.J. García, Surface chemistry modulates focal adhesion composition and signaling through changes in integrin binding, Biomaterials, 25 (2004) 5947-5954.
[154] K. Burridge, M. Chrzanowska-Wodnicka, Focal adhesions, contractility, and signaling, Annual review of cell and developmental biology, 12 (1996) 463-519.
[155] B. Geiger, A. Bershadsky, R. Pankov, K.M. Yamada, Transmembrane crosstalk between the extracellular matrix and the cytoskeleton, Nature Reviews Molecular Cell Biology, 2 (2001) 793-805.
[156] A.D. Bershadsky, N.Q. Balaban, B. Geiger, Adhesion-dependent cell mechanosensitivity, Annual review of cell and developmental biology, 19 (2003) 677-695.
[157] C.M. Franz, D.J. Müller, Analyzing focal adhesion structure by atomic force microscopy, Journal of cell science, 118 (2005) 5315-5323.
[158] W.-T. Chen, S. Singer, Immunoelectron microscopic studies of the sites of cell-substratum and cell-cell contacts in cultured fibroblasts, The Journal of cell biology, 95 (1982) 205-222.
[159] E.H. Danen, K.M. Yamada, Fibronectin, integrins, and growth control, Journal of cellular physiology, 189 (2001) 1-13.
[160] E. Hohenester, J. Engel, Domain structure and organisation in extracellular matrix proteins, Matrix biology, 21 (2002) 115-128.
[161] M. Mrksich, What can surface chemistry do for cell biology?, Current opinion in chemical biology, 6 (2002) 794-797.
[162] J.S. Hansen, C.H. Nielsen, R.S. Bartlett, S.L. Thibeault, ADVANCES IN BIOMIMETICS, 2011.
[163] J.O. Lee, P. Rieu, M.A. Arnaout, R. Liddington, Crystal structure of the A domain from the a subunit of integrin CR3 (CD11 b/CD18), Cell, 80 (1995) 631-638.
[164] J.-P. Xiong, T. Stehle, B. Diefenbach, R. Zhang, R. Dunker, D.L. Scott, A. Joachimiak, S.L. Goodman, M.A. Arnaout, Crystal structure of the extracellular segment of integrin αVβ3, Science, 294 (2001) 339-345.
[165] B.D. Adair, M. Yeager, Three-dimensional model of the human platelet integrin αIIbβ3 based on electron cryomicroscopy and x-ray crystallography, Proceedings of the National Academy of Sciences, 99 (2002) 14059-14064.
[166] R. Li, C.R. Babu, J.D. Lear, A.J. Wand, J.S. Bennett, W.F. DeGrado, Oligomerization of the integrin αIIbβ3: roles of the transmembrane and cytoplasmic domains, Proceedings of the National Academy of Sciences, 98 (2001) 12462-12467.
[167] O. Vinogradova, J. Vaynberg, X. Kong, T.A. Haas, E.F. Plow, J. Qin, Membrane-mediated structural transitions at the cytoplasmic face during integrin activation, Proceedings of the National Academy of Sciences, 101 (2004) 4094-4099.
[168] R.O. Hynes, Integrins: versatility, modulation, and signaling in cell adhesion, Cell, 69 (1992) 11-25.
[169] B. Menon, P. Sudhakaran, Actin binds to the cytoplasmic tail of alpha~ 1 subunit of integrin in hepatocytes, INDIAN JOURNAL OF BIOCHEMISTRY AND BIOPHYSICS, 37 (2000) 81-85.
[170] F.T. Bosman, Integrins: cell adhesives and modulators of cell function, The Histochemical journal, 25 (1993) 469-477.
[171] H. Gardner, A. Broberg, A. Pozzi, M. Laato, J. Heino, Absence of integrin alpha1beta1 in the mouse causes loss of feedback regulation of collagen synthesis in normal and wounded dermis, Journal of Cell Science, 112 (1999) 263-272.

[172] H. Gardner, J. Kreidberg, V. Koteliansky, R. Jaenisch, Deletion of integrin α1 by homologous recombination permits normal murine development but gives rise to a specific deficit in cell adhesion, Developmental biology, 175 (1996) 301-313.
[173] A. Pozzi, K.K. Wary, F.G. Giancotti, H.A. Gardner, Integrin α1β1 mediates a unique collagen-dependent proliferation pathway in vivo, The Journal of cell biology, 142 (1998) 587-594.
[174] K.L. Sarratt, H. Chen, M.M. Zutter, S.A. Santoro, D.A. Hammer, M.L. Kahn, GPVI and α2β1 play independent critical roles during platelet adhesion and aggregate formation to collagen under flow, Blood, 106 (2005) 1268-1277.
[175] T. Bengtsson, A. Aszodi, C. Nicolae, E.B. Hunziker, E. Lundgren-Åkerlund, R. Fässler, Loss of α10β1 integrin expression leads to moderate dysfunction of growth plate chondrocytes, Journal of cell science, 118 (2005) 929-936.
[176] C. Popov, T. Radic, F. Haasters, W. Prall, A. Aszodi, D. Gullberg, M. Schieker, D. Docheva, Integrins α2β1 and α11β1 regulate the survival of mesenchymal stem cells on collagen I, Cell death & disease, 2 (2011) e186.
[177] S.N. Popova, B. Rodriguez-Sánchez, Å. Lidén, C. Betsholtz, T. Van Den Bos, D. Gullberg, The mesenchymal α11β1 integrin attenuates PDGF-BB-stimulated chemotaxis of embryonic fibroblasts on collagens, Developmental biology, 270 (2004) 427-442.
[178] S.N. Popova, M. Barczyk, C.-F. Tiger, W. Beertsen, P. Zigrino, A. Aszodi, N. Miosge, E. Forsberg, D. Gullberg, α11β1 integrin-dependent regulation of periodontal ligament function in the erupting mouse incisor, Molecular and cellular biology, 27 (2007) 4306-4316.
[179] M. Pfaff, S. Liu, D.J. Erle, M.H. Ginsberg, Integrin β cytoplasmic domains differentially bind to cytoskeletal proteins, Journal of Biological Chemistry, 273 (1998) 6104-6109.
[180] D.A. Calderwood, R. Zent, R. Grant, D.J.G. Rees, R.O. Hynes, M.H. Ginsberg, The talin head domain binds to integrin β subunit cytoplasmic tails and regulates integrin activation, Journal of Biological Chemistry, 274 (1999) 28071-28074.
[181] J.T. Yang, H. Rayburn, R.O. Hynes, Embryonic mesodermal defects in alpha 5 integrin-deficient mice, Development, 119 (1993) 1093-1105.
[182] D. Taverna, M.-H. Disatnik, H. Rayburn, R.T. Bronson, J. Yang, T.A. Rando, R.O. Hynes, Dystrophic muscle in mice chimeric for expression of α5 integrin, The Journal of cell biology, 143 (1998) 849-859.
[183] B.L. Bader, H. Rayburn, D. Crowley, R.O. Hynes, Extensive vasculogenesis, angiogenesis, and organogenesis precede lethality in mice lacking all αv integrins, Cell, 95 (1998) 507-519.
[184] J.H. McCarty, A. Lacy-Hulbert, A. Charest, R.T. Bronson, D. Crowley, D. Housman, J. Savill, J. Roes, R.O. Hynes, Selective ablation of αv integrins in the central nervous system leads to cerebral hemorrhage, seizures, axonal degeneration and premature death, Development, 132 (2005) 165-176.
[185] U. Müller, D. Wang, S. Denda, J.J. Meneses, R.A. Pedersen, L.F. Reichardt, Integrin α8β1 is critically important for epithelial–mesenchymal interactions during kidney morphogenesis, Cell, 88 (1997) 603-613.
[186] A.L. Evans, U. Müller, Stereocilia defects in the sensory hair cells of the inner ear in mice deficient in integrin α8β1, Nature genetics, 24 (2000) 424-428.
[187] D. Tronik-Le Roux, V. Roullot, C. Poujol, T. Kortulewski, P. Nurden, G. Marguerie, Thrombasthenic mice generated by replacement of the integrin αIIb gene: demonstration that transcriptional activation of this megakaryocytic locus precedes lineage commitment, Blood, 96 (2000) 1399-1408.

[188] K. Holmbäck, M. Danton, T. Suh, C. Daugherty, J. Degen, Impaired platelet aggregation and sustained bleeding in mice lacking the fibrinogen motif bound by integrin alpha IIb beta 3, The EMBO journal, 15 (1996) 5760.
[189] M. Van der Vieren, H. Le Trong, C.L. Wood, P.F. Moore, T.S. John, D.E. Staunton, W.M. Gallatin, A novel leukointegrin, αdβ2, binds preferentially to ICAM-3, Immunity, 3 (1995) 683-690.
[190] H. Wu, J.R. Rodgers, X.-Y. Dai Perrard, J.L. Perrard, J.E. Prince, Y. Abe, B.K. Davis, G. Dietsch, C.W. Smith, C.M. Ballantyne, Deficiency of CD11b or CD11d results in reduced staphylococcal enterotoxin-induced T cell response and T cell phenotypic changes, The Journal of Immunology, 173 (2004) 297-306.
[191] M.P. Schön, A. Arya, E.A. Murphy, C.M. Adams, U.G. Strauch, W.W. Agace, J. Marsal, J.P. Donohue, H. Her, D.R. Beier, Mucosal T lymphocyte numbers are selectively reduced in integrin αE (CD103)-deficient mice, The Journal of Immunology, 162 (1999) 6641-6649.
[192] R. Schmits, T. Kündig, D.M. Baker, G. Shumaker, J. Simard, G. Duncan, A. Wakeham, A. Shahinian, A. Van Der Heiden, M.F. Bachmann, LFA-1-deficient mice show normal CTL responses to virus but fail to reject immunogenic tumor, The Journal of experimental medicine, 183 (1996) 1415-1426.
[193] Z.-M. Ding, J.E. Babensee, S.I. Simon, H. Lu, J.L. Perrard, D.C. Bullard, X.Y. Dai, S.K. Bromley, M.L. Dustin, M.L. Entman, Relative contribution of LFA-1 and Mac-1 to neutrophil adhesion and migration, The Journal of Immunology, 163 (1999) 5029-5038.
[194] U. O'doherty, M. Peng, S. Gezelter, W. Swiggard, M. Betjes, N. Bhardwaj, R. Steinman, Human blood contains two subsets of dendritic cells, one immunologically mature and the other immature, Immunology, 82 (1994) 487.
[195] H. Wu, R.M. Gower, H. Wang, X.-Y. Dai Perrard, R. Ma, D.C. Bullard, A.R. Burns, A. Paul, C.W. Smith, S.I. Simon, Functional role of CD11c+ monocytes in atherogenesis associated with hypercholesterolemia, Circulation, 119 (2009) 2708-2717.
[196] A.R. Rosenkranz, A. Coxon, M. Maurer, M.F. Gurish, K.F. Austen, D.S. Friend, S.J. Galli, T.N. Mayadas, Cutting edge: impaired mast cell development and innate immunity in Mac-1 (CD11b/CD18, CR3)-deficient mice, The Journal of Immunology, 161 (1998) 6463-6467.
[197] H. Lu, C.W. Smith, J. Perrard, D. Bullard, L. Tang, S.B. Shappell, M.L. Entman, A.L. Beaudet, C.M. Ballantyne, LFA-1 is sufficient in mediating neutrophil emigration in Mac-1-deficient mice, Journal of Clinical Investigation, 99 (1997) 1340.
[198] T. Tang, A. Rosenkranz, K.J. Assmann, M.J. Goodman, J.-C. Gutierrez-Ramos, M.C. Carroll, R.S. Cotran, T.N. Mayadas, A role for Mac-1 (CDIIb/CD18) in immune complex–stimulated neutrophil function in vivo: Mac-1 deficiency abrogates sustained Fcγ receptor–dependent neutrophil adhesion and complement-dependent proteinuria in acute glomerulonephritis, The Journal of experimental medicine, 186 (1997) 1853-1863.
[199] V. Wixler, E. Laplantine, D. Geerts, A. Sonnenberg, D. Petersohn, B. Eckes, M. Paulsson, M. Aumailley, Identification of novel interaction partners for the conserved membrane proximal region of α-integrin cytoplasmic domains, FEBS letters, 445 (1999) 351-355.
[200] J.A. Kreidberg, M.J. Donovan, S.L. Goldstein, H. Rennke, K. Shepherd, R.C. Jones, R. Jaenisch, Alpha 3 beta 1 integrin has a crucial role in kidney and lung organogenesis, Development, 122 (1996) 3537-3547.
[201] C.M. DiPersio, K.M. Hodivala-Dilke, R. Jaenisch, J.A. Kreidberg, R.O. Hynes, α3β1 integrin is required for normal development of the epidermal basement membrane, The Journal of cell biology, 137 (1997) 729-742.

[202] E. Georges-Labouesse, M. Mark, N. Messaddeq, A. Gansmüller, Essential role of α6 integrins in cortical and retinal lamination, Current Biology, 8 (1998) 983-S981.
[203] U. Mayer, G. Saher, R. Fässler, A. Bornemann, F. Echtermeyer, H. von der Mark, N. Miosge, E. Pösch, K. von der Mark, Absence of integrin α7 causes a novel form of muscular dystrophy, Nature genetics, 17 (1997) 318-323.
[204] S. Liu, S.M. Thomas, D.G. Woodside, D.M. Rose, W.B. Kiosses, M. Pfaff, M.H. Ginsberg, Binding of paxillin to α4 integrins modifies integrin-dependent biological responses, Nature, 402 (1999) 676-681.
[205] J.T. Yang, H. Rayburn, R.O. Hynes, Cell adhesion events mediated by alpha 4 integrins are essential in placental and cardiac development, Development, 121 (1995) 549-560.
[206] X. Huang, M. Griffiths, J. Wu, R.V. Farese, D. Sheppard, Normal development, wound healing, and adenovirus susceptibility in β5-deficient mice, Molecular and cellular biology, 20 (2000) 755-759.
[207] D.T. Loo, S.B. Kanner, A. Aruffo, Filamin Binds to the Cytoplasmic Domain of the β1-Integrin IDENTIFICATION OF AMINO ACIDS RESPONSIBLE FOR THIS INTERACTION, Journal of Biological Chemistry, 273 (1998) 23304-23312.
[208] C.A. Otey, G.B. Vasquez, K. Burridge, B.W. Erickson, Mapping of the alpha-actinin binding site within the beta 1 integrin cytoplasmic domain, Journal of Biological Chemistry, 268 (1993) 21193-21197.
[209] K.B. Reddy, P. Gascard, M.G. Price, E.V. Negrescu, J.E. Fox, Identification of an Interaction between the M-band Protein Skelemin and β-Integrin Subunits COLOCALIZATION OF A SKELEMIN-LIKE PROTEIN WITH β1-and β3-INTEGRINS IN NON-MUSCLE CELLS, Journal of Biological Chemistry, 273 (1998) 35039-35047.
[210] R. Sampath, P.J. Gallagher, F.M. Pavalko, Cytoskeletal Interactions with the Leukocyte Integrin β2 Cytoplasmic Tail ACTIVATION-DEPENDENT REGULATION OF ASSOCIATIONS WITH TALIN AND α-ACTININ, Journal of Biological Chemistry, 273 (1998) 33588-33594.
[211] G.A. Rezniczek, J.M. de Pereda, S. Reipert, G. Wiche, Linking integrin α6β4-based cell adhesion to the intermediate filament cytoskeleton: direct interaction between the β4 subunit and plectin at multiple molecular sites, The Journal of cell biology, 141 (1998) 209-225.
[212] F. Sanvito, S. Piatti, A. Villa, M. Bossi, G. Lucchini, P.C. Marchisio, S. Biffo, The β4 integrin interactor p27BBP/eIF6 is an essential nuclear matrix protein involved in 60S ribosomal subunit assembly, The Journal of cell biology, 144 (1999) 823-838.
[213] S.K. Alahari, J.W. Lee, R.L. Juliano, Nischarin, a novel protein that interacts with the integrin α5 subunit and inhibits cell migration, The Journal of cell biology, 151 (2000) 1141-1154.
[214] D. Calderwood, Talin controls integrin activation, Biochemical Society Transactions, 32 (2004) 434-437.
[215] R. Fässler, M. Meyer, Consequences of lack of beta 1 integrin gene expression in mice, Genes & development, 9 (1995) 1896-1908.
[216] L.E. Stephens, A.E. Sutherland, I.V. Klimanskaya, A. Andrieux, J. Meneses, R.A. Pedersen, C.H. Damsky, Deletion of beta 1 integrins in mice results in inner cell mass failure and peri-implantation lethality, Genes & development, 9 (1995) 1883-1895.
[217] J.P. Mizgerd, H. Kubo, G.J. Kutkoski, S.D. Bhagwan, K. Scharffetter-Kochanek, A.L. Beaudet, C.M. Doerschuk, Neutrophil emigration in the skin, lungs, and peritoneum: different

requirements for CD11/CD18 revealed by CD18-deficient mice, The Journal of experimental medicine, 186 (1997) 1357-1364.
[218] K. Scharffetter-Kochanek, H. Lu, K. Norman, N. Van Nood, F. Munoz, S. Grabbe, M. McArthur, I. Lorenzo, S. Kaplan, K. Ley, Spontaneous skin ulceration and defective T cell function in CD18 null mice, The Journal of experimental medicine, 188 (1998) 119-131.
[219] K.M. Hodivala-Dilke, K.P. McHugh, D.A. Tsakiris, H. Rayburn, D. Crowley, M. Ullman-Culleré, F.P. Ross, B.S. Coller, S. Teitelbaum, R.O. Hynes, β3-integrin–deficient mice are a model for Glanzmann thrombasthenia showing placental defects and reduced survival, Journal of Clinical Investigation, 103 (1999) 229.
[220] K.P. McHugh, K. Hodivala-Dilke, M.-H. Zheng, N. Namba, J. Lam, D. Novack, X. Feng, F.P. Ross, R.O. Hynes, S.L. Teitelbaum, Mice lacking β3 integrins are osteosclerotic because of dysfunctional osteoclasts, Journal of Clinical Investigation, 105 (2000) 433.
[221] R. Van Der Neut, P. Krimpenfort, J. Calafat, C.M. Niessen, A. Sonnenberg, Epithelial detachment due to absence of hemidesmosomes in integrin β4 null mice, Nature genetics, 13 (1996) 366-369.
[222] J. Dowling, Q.-C. Yu, E. Fuchs, Beta4 integrin is required for hemidesmosome formation, cell adhesion and cell survival, The Journal of cell biology, 134 (1996) 559-572.
[223] X.-Z. Huang, J.F. Wu, D. Cass, D.J. Erle, D. Corry, S.G. Young, R.V. Farese, D. Sheppard, Inactivation of the integrin beta 6 subunit gene reveals a role of epithelial integrins in regulating inflammation in the lung and skin, The Journal of cell biology, 133 (1996) 921-928.
[224] J.S. Munger, X. Huang, H. Kawakatsu, M.J. Griffiths, S.L. Dalton, J. Wu, J.-F. Pittet, N. Kaminski, C. Garat, M.A. Matthay, A mechanism for regulating pulmonary inflammation and fibrosis: the integrin αvβ6 binds and activates latent TGF β1, Cell, 96 (1999) 319-328.
[225] N. Wagner, J. Löhler, E.J. Kunkel, K. Ley, E. Leung, G. Krissansen, K. Rajewsky, W. Müller, Critical role for β7 integrins in formation of the gut-associated lymphoid tissue, (1996).
[226] G. Gorfu, J. Rivera-Nieves, K. Ley, Role of β7 integrins in intestinal lymphocyte homing and retention, Current molecular medicine, 9 (2009) 836.
[227] F. Ruggiero, J. Comte, C. Cabañas, R. Garrone, Structural requirements for alpha 1 beta 1 and alpha 2 beta 1 integrin mediated cell adhesion to collagen V, Journal of cell science, 109 (1996) 1865-1874.
[228] L. Camper, U. Hellman, E. Lundgren-Åkerlund, Isolation, cloning, and sequence analysis of the integrin subunit α10, a β1-associated collagen binding integrin expressed on chondrocytes, Journal of Biological Chemistry, 273 (1998) 20383-20389.
[229] K.-i. TASHIRO, A. MONJI, I. YOSHIDA, Y. HAYASHI, K. MATSUDA, N. TASHIRO, Y. MITSUYAMA, An IKLLI-containing peptide derived from the laminin α1 chain mediating heparin-binding, cell adhesion, neurite outgrowth and proliferation, represents a binding site for integrin α3β1 and heparan sulphate proteoglycan, Biochem. J, 340 (1999) 119-126.
[230] A. van der Flier, A. Sonnenberg, Function and interactions of integrins, Cell and tissue research, 305 (2001) 285-298.
[231] M.B. Srichai, R. Zent, Integrin structure and function, in: Cell-Extracellular Matrix Interactions in Cancer, Springer, 2010, pp. 19-41.
[232] J.D. Loike, B. Sodeik, L. Cao, S. Leucona, J.I. Weitz, P.A. Detmers, S.D. Wright, S.C. Silverstein, CD11c/CD18 on neutrophils recognizes a domain at the N terminus of the A alpha chain of fibrinogen, Proceedings of the National Academy of Sciences, 88 (1991) 1044-1048.

[233] M.D. Schaller, C.A. Borgman, B.S. Cobb, R.R. Vines, A.B. Reynolds, J.T. Parsons, pp125FAK a structurally distinctive protein-tyrosine kinase associated with focal adhesions, Proceedings of the National Academy of Sciences, 89 (1992) 5192-5196.
[234] S.K. Hanks, M.B. Calalb, M.C. Harper, S.K. Patel, Focal adhesion protein-tyrosine kinase phosphorylated in response to cell attachment to fibronectin, Proceedings of the National Academy of Sciences, 89 (1992) 8487-8491.
[235] J.-L. Guan, J.E. Trevithick, R. Hynes, Fibronectin/integrin interaction induces tyrosine phosphorylation of a 120-kDa protein, Cell regulation, 2 (1991) 951-964.
[236] L. Kornberg, H.S. Earp, J. Parsons, M. Schaller, R. Juliano, Cell adhesion or integrin clustering increases phosphorylation of a focal adhesion-associated tyrosine kinase, Journal of Biological Chemistry, 267 (1992) 23439-23442.
[237] S.K. Mitra, D.A. Hanson, D.D. Schlaepfer, Focal adhesion kinase: in command and control of cell motility, Nature reviews Molecular cell biology, 6 (2005) 56-68.
[238] Y. Furuta, S. Kanazawa, N. Takeda, K. Sobue, N. Nakatsuji, S. Nomura, J. Fujimoto, M. Okada, T. Yamamoto, S. Aizawa, Reduced cell motility and enhanced focal adhesion contact formation in cells from FAK-deficient mice, Nature, 377 (1995) 539-544.
[239] L. Tack, K. Schickle, F. Böke, H. Fischer, Immobilization of specific proteins to titanium surface using self-assembled monolayer technique, Dental Materials, 31 (2015) 1169-1179.
[240] Q. Liu, J. Ding, F.K. Mante, S.L. Wunder, G.R. Baran, The role of surface functional groups in calcium phosphate nucleation on titanium foil: a self-assembled monolayer technique, Biomaterials, 23 (2002) 3103-3111.
[241] L.M. Pandey, Effect of solid surface with self assembled monolayers on adsorption of proteins, in, 2012.
[242] J.A. Howarter, J.P. Youngblood, Optimization of silica silanization by 3-aminopropyltriethoxysilane, Langmuir : the ACS journal of surfaces and colloids, 22 (2006) 11142-11147.
[243] Y. Yang, A.M. Bittner, S. Baldelli, K. Kern, Study of self-assembled triethoxysilane thin films made by casting neat reagents in ambient atmosphere, Thin Solid Films, 516 (2008) 3948-3956.
[244] N. Aissaoui, L. Bergaoui, J. Landoulsi, J.-F. Lambert, S. Boujday, Silane layers on silicon surfaces: mechanism of interaction, stability, and influence on protein adsorption, Langmuir : the ACS journal of surfaces and colloids, 28 (2011) 656-665.
[245] R. Tian, O. Seitz, M. Li, W. Hu, Y.J. Chabal, J. Gao, Infrared Characterization of Interfacial Si− O Bond Formation on Silanized Flat SiO2/Si Surfaces, Langmuir : the ACS journal of surfaces and colloids, 26 (2010) 4563-4566.
[246] F. Zhang, M. Srinivasan, Self-assembled molecular films of aminosilanes and their immobilization capacities, Langmuir : the ACS journal of surfaces and colloids, 20 (2004) 2309-2314.
[247] L.M. Pandey, S.K. Pattanayek, D. Delabouglise, Properties of adsorbed bovine serum albumin and fibrinogen on self-assembled monolayers, The Journal of Physical Chemistry C, 117 (2013) 6151-6160.
[248] D.J. Michalak, S. Rivillon, Y.J. Chabal, A. Esteve, N.S. Lewis, Infrared spectroscopic investigation of the reaction of hydrogen-terminated,(111)-oriented, silicon surfaces with liquid methanol, The Journal of Physical Chemistry B, 110 (2006) 20426-20434.

[249] D. Flinn, D. Guzonas, R.-H. Yoon, Characterization of silica surfaces hydrophobized by octadecyltrichlorosilane, Colloids and Surfaces A: Physicochemical and Engineering Aspects, 87 (1994) 163-176.
[250] N. Tillman, A. Ulman, J.S. Schildkraut, T.L. Penner, Incorporation of phenoxy groups in self-assembled monolayers of trichlorosilane derivatives. Effects on film thickness, wettability, and molecular orientation, Journal of the American Chemical Society, 110 (1988) 6136-6144.
[251] D.R. Scheuing, Fourier transform infrared spectroscopy in colloid and interface science, American Chemical Society, 1990.
[252] C.-H. Chiang, H. Ishida, J.L. Koenig, The structure of γ-aminopropyltriethoxysilane on glass surfaces, Journal of Colloid and Interface Science, 74 (1980) 396-404.
[253] R. Pena-Alonso, F. Rubio, J. Rubio, J. Oteo, Study of the hydrolysis and condensation of γ-Aminopropyltriethoxysilane by FT-IR spectroscopy, Journal of materials science, 42 (2007) 595-603.
[254] D. Karpovich, G. Blanchard, Direct measurement of the adsorption kinetics of alkanethiolate self-assembled monolayers on a microcrystalline gold surface, Langmuir, 10 (1994) 3315-3322.
[255] S.M. Slack, T.A. Horbett, Changes in the strength of fibrinogen attachment to solid surfaces: an explanation of the influence of surface chemistry on the Vroman effect, Journal of Colloid and Interface Science, 133 (1989) 148-165.
[256] F.S. Damos, R.C. Luz, L.T. Kubota, Determination of thickness, dielectric constant of thiol films, and kinetics of adsorption using surface plasmon resonance, Langmuir, 21 (2005) 602-609.
[257] T. Ave, Physical Chemistry of Surfaces, Arthur W. Adamson and Alice P. Gast. John Wiley & Sons, 1nc., 605, in, Springer, 1998.
[258] T. Leitner, G. Friedbacher, T. Vallant, H. Brunner, U. Mayer, H. Hoffmann, Investigations of the growth of self-assembled octadecylsiloxane monolayers with atomic force microscopy, Microchimica Acta, 133 (2000) 331-336.
[259] S.-R. Yang, B.O. Kolbesen, A comparative study of the growth of octadecyltrichlorosilane and 3-mercaptopropyltrimethoxysilane self-assembled monolayers on hydrophilic silicon surfaces, Applied Surface Science, 255 (2008) 1726-1735.
[260] A. Hasan, L.M. Pandey, Kinetic studies of attachment and re-orientation of octyltriethoxysilane for formation of self-assembled monolayer on a silica substrate, Materials Science and Engineering: C, 68 (2016) 423-429.
[261] E. Ajami, K.-F. Aguey-Zinsou, Functionalization of electropolished titanium surfaces with silane-based self-assembled monolayers and their application in drug delivery, Journal of colloid and interface science, 385 (2012) 258-267.
[262] S.-H. Choi, B.-m. Zhang Newby, Alternative method for determining surface energy by utilizing polymer thin film dewetting, Langmuir, 19 (2003) 1419-1428.
[263] M. Holmberg, X. Hou, Competitive Protein Adsorption Multilayer Adsorption and Surface Induced Protein Aggregation, Langmuir, 25 (2009) 2081-2089.
[264] M. Holmberg, K.B. Stibius, N.B. Larsen, X. Hou, Competitive protein adsorption to polymer surfaces from human serum, Journal of Materials Science: Materials in Medicine, 19 (2008) 2179-2185.
[265] C.M. Alves, R.L. Reis, J.A. Hunt, The competitive adsorption of human proteins onto natural-based biomaterials, Journal of the Royal Society Interface, (2010) rsif20100022.

[266] J. Benesch, J.F. Mano, R.L. Reis, Analysing protein competition on self-assembled mono-layers studied with quartz crystal microbalance, Acta Biomater., 6 (2010) 3499-3505.
[267] R. Green, M. Davies, C. Roberts, S. Tendler, Competitive protein adsorption as observed by surface plasmon resonance, Biomaterials, 20 (1999) 385-391.
[268] J. Brash, D. Lyman, Adsorption of plasma proteins in solution to uncharged, hydrophobic polymer surfaces, Journal of Biomedical Materials Research Part A, 3 (1969) 175-189.
[269] H.P. Felgueiras, N.S. Murthy, S.D. Sommerfeld, M.M. Brás, V.r. Migonney, J. Kohn, Competitive adsorption of plasma proteins using a quartz crystal microbalance, ACS applied materials & interfaces, 8 (2016) 13207-13217.
[270] P. Ying, Y. Yu, G. Jin, Z. Tao, Competitive protein adsorption studied with atomic force microscopy and imaging ellipsometry, Colloids and Surfaces B: Biointerfaces, 32 (2003) 1-10.
[271] M. Deyme, A. Baszkin, J.E. Proust, E. Perez, G. Albrecht, M.M. Boissonnade, Collagen at interfaces II: competitive adsorption of collagen against albumin and fibrinogen, Journal of Biomedical Materials Research Part A, 21 (1987) 321-328.
[272] B. Lassen, M. Malmsten, Competitive protein adsorption at plasma polymer surfaces, Journal of colloid and interface science, 186 (1997) 9-16.
[273] Y.S. Tremsina, V.I. Sevastianov, S. Petrash, W. Dando, M.D. Foster, Competitive adsorption of human serum albumin and gamma-globulin from a binary protein mixture onto hexadecyltrichlorosilane coated glass, Journal of Biomaterials Science, Polymer Edition, 9 (1998) 151-161.
[274] Y. Jeyachandran, E. Mielczarski, B. Rai, J. Mielczarski, Quantitative and qualitative evaluation of adsorption/desorption of bovine serum albumin on hydrophilic and hydrophobic surfaces, Langmuir, 25 (2009) 11614-11620.
[275] Y.H. Tan, M. Liu, B. Nolting, J.G. Go, J. Gervay-Hague, G.-y. Liu, A nanoengineering approach for investigation and regulation of protein immobilization, ACS nano, 2 (2008) 2374-2384.
[276] L. Zhang, B. Casey, D.K. Galanakis, C. Marmorat, S. Skoog, K. Vorvolakos, M. Simon, M.H. Rafailovich, The influence of surface chemistry on adsorbed fibrinogen conformation, orientation, fiber formation and platelet adhesion, Acta biomaterialia, 54 (2017) 164-174.
[277] S. Tunc, M.F. Maitz, G. Steiner, L. Vázquez, M.T. Pham, R. Salzer, In situ conformational analysis of fibrinogen adsorbed on Si surfaces, Colloids Surf. B. Biointerfaces, 42 (2005) 219-225.
[278] I.E. Svendsen, O. Santos, J. Sotres, A. Wennerberg, K. Breding, T. Arnebrant, L. Lindh, Adsorption of HSA, IgG and laminin-1 on model hydroxyapatite surfaces–effects of surface characteristics, Biofouling, 28 (2012) 87-97.
[279] M. Ka, A. Carle, P. Thomsen, J. Olsson, P. Tengvall, Analysis of rat plasma proteins desorbed from gold and methyl-and hydroxyl-terminated alkane thiols on gold surfaces, Journal of Materials Science: Materials in Medicine, 11 (2000) 191-199.
[280] P. Milleding, A. Carlén, A. Wennerberg, S. Karlsson, Protein characterisation of salivary and plasma biofilms formed in vitro on non-corroded and corroded dental ceramic materials, Biomaterials, 22 (2001) 2545-2555.
[281] A. Singh, P. Datta, L.M. Pandey, Deciphering the mechanistic insight into the stoichiometric ratio dependent behavior of Cu (II) on BSA fibrillation, International journal of biological macromolecules, 97 (2017) 662-670.

[282] I. Sharma, S.K. Pattanayek, Effect of surface energy of solid surfaces on the micro-and macroscopic properties of adsorbed BSA and lysozyme, Biophysical Chemistry, 226 (2017) 14-22.
[283] H.T. Phan, S. Bartelt-Hunt, K.B. Rodenhausen, M. Schubert, J.C. Bartz, Investigation of bovine serum albumin (BSA) attachment onto self-assembled monolayers (SAMs) using combinatorial quartz crystal microbalance with dissipation (QCM-D) and spectroscopic ellipsometry (SE), PloS one, 10 (2015) e0141282.
[284] D.A. Barrett, G.M. Power, M.A. Hussain, I.D. Pitfield, P.N. Shaw, M.C. Davies, Protein interactions with model chromatographic stationary phases constructed using self-assembled monolayers, Journal of separation science, 28 (2005) 483-491.
[285] D.A. Smith, M.L. Wallwork, J. Zhang, J. Kirkham, C. Robinson, A. Marsh, M. Wong, The effect of electrolyte concentration on the chemical force titration behavior of ω-functionalized SAMs: evidence for the formation of strong ionic hydrogen bonds, The Journal of Physical Chemistry B, 104 (2000) 8862-8870.
[286] J. Zhang, J. Kirkham, C. Robinson, M.L. Wallwork, D.A. Smith, A. Marsh, M. Wong, Determination of the ionization state of 11-thioundecyl-1-phosphonic acid in self-assembled monolayers by chemical force microscopy, Analytical chemistry, 72 (2000) 1973-1978.
[287] J.-i. Anzai, B. Guo, T. Osa, Quartz-crystal microbalance and cyclic voltammetric studies of the adsorption behaviour of serum albumin on self-assembled thiol monolayers possessing different hydrophobicity and polarity, Bioelectrochemistry and bioenergetics, 40 (1996) 35-40.
[288] A. Kudelski, Influence of electrostatically bound proteins on the structure of linkage monolayers: adsorption of bovine serum albumin on silver and gold substrates coated with monolayers of 2-mercaptoethanesulphonate, Vibrational Spectroscopy, 33 (2003) 197-204.
[289] M. Rabe, D. Verdes, S. Seeger, Understanding protein adsorption phenomena at solid surfaces, Advances in colloid and interface science, 162 (2011) 87-106.
[290] M.M. Ouberai, K. Xu, M.E. Welland, Effect of the interplay between protein and surface on the properties of adsorbed protein layers, Biomaterials, 35 (2014) 6157-6163.
[291] B. Jachimska, K. Tokarczyk, M. Łapczyńska, A. Puciul-Malinowska, S. Zapotoczny, Structure of bovine serum albumin adsorbed on silica investigated by quartz crystal microbalance, Colloids and Surfaces A: Physicochemical and Engineering Aspects, 489 (2016) 163-172.
[292] J.F. FOSTER, Some aspects of the structure and conformational properties of serum albumin, in: Albumin: Structure, function and uses, Elsevier, 1977, pp. 53-84.
[293] K. Kubiak-Ossowska, K. Tokarczyk, B. Jachimska, P.A. Mulheran, Bovine Serum Albumin Adsorption at a Silica Surface Explored by Simulation and Experiment, The Journal of Physical Chemistry B, 121 (2017) 3975-3986.
[294] Q. Wei, T. Becherer, S. Angioletti-Uberti, J. Dzubiella, C. Wischke, A.T. Neffe, A. Lendlein, M. Ballauff, R. Haag, Protein interactions with polymer coatings and biomaterials, Angewandte Chemie International Edition, 53 (2014) 8004-8031.
[295] E.P. Vieira, S. Rocha, M. Carmo Pereira, H. Mohwald, M.A. Coelho, Adsorption and diffusion of plasma proteins on hydrophilic and hydrophobic surfaces: effect of trifluoroethanol on protein structure, Langmuir, 25 (2009) 9879-9886.
[296] I. Azpiazu, D. Chapman, Spectroscopic studies of fibrinogen and its plasmin-derived fragments, Biochimica et Biophysica Acta (BBA)-Protein Structure and Molecular Enzymology, 1119 (1992) 268-274.

[297] M.-J. Desroches, S. Omanovic, Adsorption of fibrinogen on a biomedical-grade stainless steel 316LVM surface: a PM-IRRAS study of the adsorption thermodynamics, kinetics and secondary structure changes, Physical Chemistry Chemical Physics, 10 (2008) 2502-2512.
[298] A. Zhmurov, O. Kononova, R.I. Litvinov, R.I. Dima, V. Barsegov, J.W. Weisel, Mechanical transition from α-helical coiled coils to β-sheets in fibrin (ogen), Journal of the American Chemical Society, 134 (2012) 20396-20402.
[299] B.R. Singh, M.P. Fuller, FT-IR in combination with the attenuated total reflectance technique: A very sensitive method for the structural analysis of polypeptides, Applied spectroscopy, 45 (1991) 1017-1021.
[300] C.E. Giacomelli, M.G. Bremer, W. Norde, ATR-FTIR study of IgG adsorbed on different silica surfaces, Journal of colloid and interface science, 220 (1999) 13-23.
[301] J. Buijs, W. Norde, J.W.T. Lichtenbelt, Changes in the secondary structure of adsorbed IgG and F (ab ‘) 2 studied by FTIR spectroscopy, Langmuir, 12 (1996) 1605-1613.
[302] A. Brown, Analysis of cooperativity by isothermal titration calorimetry, International journal of molecular sciences, 10 (2009) 3457-3477.
[303] F. Yin, R. Cao, A. Goddard, Y. Zhang, E. Oldfield, Enthalpy versus entropy-driven binding of bisphosphonates to farnesyl diphosphate synthase, Journal of the American Chemical Society, 128 (2006) 3524-3525.
[304] A. Hasan, V. Saxena, L. Pandey, Surface functionalization of Ti6Al4V via self-assembled monolayers for improved protein adsorption and fibroblast adhesion, Langmuir: the ACS journal of surfaces and colloids, (2018).
[305] Y. Arima, H. Iwata, Effects of surface functional groups on protein adsorption and subsequent cell adhesion using self-assembled monolayers, Journal of Materials Chemistry, 17 (2007) 4079-4087.
[306] L.M. Pandey, S. Le Denmat, D. Delabouglise, F. Bruckert, S.K. Pattanayek, M. Weidenhaupt, Surface chemistry at the nanometer scale influences insulin aggregation, Colloids and Surfaces B: Biointerfaces, 100 (2012) 69-76.
[307] A. Hasan, V. Saxena, L.M. Pandey, Surface Functionalization of Ti6Al4V via Self-assembled Monolayers for Improved Protein Adsorption and Fibroblast Adhesion, Langmuir, (2018).
[308] T. Groth, G. Altankov, Studies on cell-biomaterial interaction: role of tyrosine phosphorylation during fibroblast spreading on surfaces varying in wettability, Biomaterials, 17 (1996) 1227-1234.
[309] S.B. Kennedy, N.R. Washburn, C.G. Simon, E.J. Amis, Combinatorial screen of the effect of surface energy on fibronectin-mediated osteoblast adhesion, spreading and proliferation, Biomaterials, 27 (2006) 3817-3824.
[310] M. Hindié, E. Camand, R. Agniel, F. Carreiras, E. Pauthe, P. Van Tassel, Effects of human fibronectin and human serum albumin sequential adsorption on preosteoblastic cell adhesion, Biointerphases, 9 (2014) 029008.
[311] C.-T. Hsiao, H.-W. Cheng, C.-M. Huang, H.-R. Li, M.-H. Ou, J.-R. Huang, K.-H. Khoo, H.W. Yu, Y.-Q. Chen, Y.-K. Wang, Fibronectin in cell adhesion and migration via N-glycosylation, Oncotarget, 8 (2017) 70653.
[312] J.L. Bays, K.A. DeMali, Vinculin in cell–cell and cell–matrix adhesions, Cellular and Molecular Life Sciences, 74 (2017) 2999-3009.

[313] K. Ohashi, S. Fujiwara, K. Mizuno, Roles of the cytoskeleton, cell adhesion and rho signalling in mechanosensing and mechanotransduction, The Journal of Biochemistry, 161 (2017) 245-254.
[314] Y. Arima, H. Iwata, Preferential adsorption of cell adhesive proteins from complex media on self-assembled monolayers and its effect on subsequent cell adhesion, Acta biomaterialia, 26 (2015) 72-81.
[315] W. Tutak, G. Jyotsnendu, P. Bajcsy, C.G. Simon, Nanofiber scaffolds influence organelle structure and function in bone marrow stromal cells, Journal of Biomedical Materials Research Part B: Applied Biomaterials, 105 (2017) 989-1001.
[316] S. Grohmann, H. Rothe, K. Liefeith, Investigations on the secondary structure of polypeptide chains in polyelectrolyte multilayers and their effect on the adhesion and spreading of osteoblasts, Biointerphases, 7 (2012) 62.
[317] A. Nanci, J. Wuest, L. Peru, P. Brunet, V. Sharma, S. Zalzal, M. McKee, Chemical modification of titanium surfaces for covalent attachment of biological molecules, Journal of Biomedical Materials Research Part A, 40 (1998) 324-335.
[318] G. Mani, D.M. Johnson, D. Marton, M.D. Feldman, D. Patel, A.A. Ayon, C.M. Agrawal, Drug delivery from gold and titanium surfaces using self-assembled monolayers, Biomaterials, 29 (2008) 4561-4573.
[319] C. Pfaffenroth, A. Winkel, W. Dempwolf, L.J. Gamble, D.G. Castner, M. Stiesch, H. Menzel, Self-Assembled Antimicrobial and Biocompatible Copolymer Films on Titanium, Macromolecular bioscience, 11 (2011) 1515-1525.
[320] P.J. Majewski, G. Allidi, Synthesis of hydroxyapatite on titanium coated with organic self-assembled monolayers, Materials Science and Engineering: A, 420 (2006) 13-20.
[321] K.K. Nair, R. Kaur, N. Iqbal, A. Hasan, S. Alam, S. Raza, High yield, facile aqueous synthesis and characterization of C18 functionalized iron oxide nanoparticles, Materials Research Express, 2 (2015) 045014.
[322] M. Lorenzetti, I. Dogša, T.a. Stošicki, D. Stopar, M. Kalin, S. Kobe, S.a. Novak, The influence of surface modification on bacterial adhesion to titanium-based substrates, ACS applied materials & interfaces, 7 (2015) 1644-1651.
[323] A. Mahapatro, T.M.D. Negron, S.A. Arshanapalli, A.S. Gomes, L. Yao, Fabrication, biofunctionality and biocompatibility evaluations of octadecyltrichlorosilane nano coatings on magnesium alloy, Journal of Nanoengineering and Nanomanufacturing, 5 (2015) 294-303.
[324] D. Liu, P. Majewski, B. O'Neill, Y. Ngothai, C. Colby, The optimal SAM surface functional group for producing a biomimetic HA coating on Ti, Journal of Biomedical Materials Research Part A, 77 (2006) 763-772.
[325] N. Marín-Pareja, M. Cantini, C. González-García, E. Salvagni, M. Salmerón-Sanchez, M.-P. Ginebra, Different organization of type I collagen immobilized on silanized and nonsilanized titanium surfaces affects fibroblast adhesion and fibronectin secretion, ACS applied materials & interfaces, 7 (2015) 20667-20677.
[326] K. Kushiro, C.-H. Lee, M. Takai, Simultaneous characterization of protein–material and cell–protein interactions using dynamic QCM-D analysis on SAM surfaces, Biomaterials science, 4 (2016) 989-997.
[327] Y. Yan, E. Chibowski, A. Szcześ, Surface properties of Ti-6Al-4V alloy part I: Surface roughness and apparent surface free energy, Materials Science and Engineering: C, 70 (2017) 207-215.

[328] H. Fabre, D. Mercier, A. Galtayries, D. Portet, N. Delorme, J.-F. Bardeau, Impact of hydrophilic and hydrophobic functionalization of flat TiO2/Ti surfaces on proteins adsorption, Applied Surface Science, (2017).
[329] V. Vadillo-Rodríguez, M.A. Pacha-Olivenza, M.L. Gónzalez-Martín, J.M. Bruque, A.M. Gallardo-Moreno, Adsorption behavior of human plasma fibronectin on hydrophobic and hydrophilic Ti6Al4V substrata and its influence on bacterial adhesion and detachment, Journal of Biomedical Materials Research Part A, 101 (2013) 1397-1404.
[330] D.C. Carter, J.X. Ho, Structure of serum albumin, Advances in protein chemistry, 45 (1994) 153-203.
[331] S. Sugio, A. Kashima, S. Mochizuki, M. Noda, K. Kobayashi, Crystal structure of human serum albumin at 2.5 Å resolution, Protein engineering, 12 (1999) 439-446.
[332] C. Herranz-Diez, C. Mas-Moruno, S. Neubauer, H. Kessler, F.J. Gil, M. Pegueroles, J.M. Manero, J. Guillem-Marti, Tuning Mesenchymal Stem Cell Response onto Titanium–Niobium–Hafnium Alloy by Recombinant Fibronectin Fragments, ACS applied materials & interfaces, 8 (2016) 2517-2525.
[333] E. Pauthe, J. Pelta, S. Patel, D. Lairez, F. Goubard, Temperature-induced β-aggregation of fibronectin in aqueous solution, Biochimica et Biophysica Acta (BBA)-Protein Structure and Molecular Enzymology, 1597 (2002) 12-21.
[334] K.K. Chittur, FTIR/ATR for protein adsorption to biomaterial surfaces, Biomaterials, 19 (1998) 357-369.
[335] L. Baujard-Lamotte, S. Noinville, F. Goubard, P. Marque, E. Pauthe, Kinetics of conformational changes of fibronectin adsorbed onto model surfaces, Colloids and Surfaces B: Biointerfaces, 63 (2008) 129-137.
[336] Y. Tamada, Y. Ikada, Fibroblast growth on polymer surfaces and biosynthesis of collagen, Journal of Biomedical Materials Research Part A, 28 (1994) 783-789.
[337] H.-Y. Chang, C.-C. Huang, K.-Y. Lin, W.-L. Kao, H.-Y. Liao, Y.-W. You, J.-H. Lin, Y.-T. Kuo, D.-Y. Kuo, J.-J. Shyue, Effect of surface potential on NIH3T3 cell adhesion and Proliferation, The Journal of Physical Chemistry C, 118 (2014) 14464-14470.
[338] J. Rosales-Leal, M. Rodríguez-Valverde, G. Mazzaglia, P. Ramón-Torregrosa, L. Diaz-Rodriguez, O. Garcia-Martinez, M. Vallecillo-Capilla, C. Ruiz, M. Cabrerizo-Vílchez, Effect of roughness, wettability and morphology of engineered titanium surfaces on osteoblast-like cell adhesion, Colloids and Surfaces A: Physicochemical and Engineering Aspects, 365 (2010) 222-229.
[339] P.M. Davidson, M. Bigerelle, G. Reiter, K. Anselme, Different surface sensing of the cell body and nucleus in healthy primary cells and in a cancerous cell line on nanogrooves, Biointerphases, 10 (2015) 031004.
[340] A. Bourkoula, V. Constantoudis, D. Kontziampasis, P. Petrou, S. Kakabakos, A. Tserepi, E. Gogolides, Roughness threshold for cell attachment and proliferation on plasma micro-nanotextured polymeric surfaces: the case of primary human skin fibroblasts and mouse immortalized 3T3 fibroblasts, Journal of Physics D: Applied Physics, 49 (2016) 304002.
[341] H.P. Felgueiras, M.D. Evans, V. Migonney, Contribution of fibronectin and vitronectin to the adhesion and morphology of MC3T3-E1 osteoblastic cells to poly (NaSS) grafted Ti6Al4V, Acta biomaterialia, 28 (2015) 225-233.
[342] R. Pankov, K.M. Yamada, Fibronectin at a glance, Journal of cell science, 115 (2002) 3861-3863.

[343] S.-i. Aota, M. Nomizu, K.M. Yamada, The short amino acid sequence Pro-His-Ser-Arg-Asn in human fibronectin enhances cell-adhesive function, Journal of Biological Chemistry, 269 (1994) 24756-24761.
[344] M. Gao, D. Craig, V. Vogel, K. Schulten, Identifying unfolding intermediates of FN-III 10 by steered molecular dynamics, Journal of molecular biology, 323 (2002) 939-950.
[345] M.M. Gentleman, E. Gentleman, The role of surface free energy in osteoblast–biomaterial interactions, International Materials Reviews, 59 (2014) 417-429.
[346] X. Liu, J.Y. Lim, H.J. Donahue, R. Dhurjati, A.M. Mastro, E.A. Vogler, Influence of substratum surface chemistry/energy and topography on the human fetal osteoblastic cell line hFOB 1.19: phenotypic and genotypic responses observed in vitro, Biomaterials, 28 (2007) 4535-4550.
[347] Y. Yuan, M.P. Hays, P.R. Hardwidge, J. Kim, Surface characteristics influencing bacterial adhesion to polymeric substrates, RSC Advances, 7 (2017) 14254-14261.
[348] G. Bruinsma, H. Van der Mei, H. Busscher, Bacterial adhesion to surface hydrophilic and hydrophobic contact lenses, Biomaterials, 22 (2001) 3217-3224.
[349] I. Yoda, H. Koseki, M. Tomita, T. Shida, H. Horiuchi, H. Sakoda, M. Osaki, Effect of surface roughness of biomaterials on Staphylococcus epidermidis adhesion, BMC microbiology, 14 (2014) 234.
[350] F. Alam, K. Balani, Adhesion force of staphylococcus aureus on various biomaterial surfaces, Journal of the mechanical behavior of biomedical materials, 65 (2017) 872-880.
[351] R.E. Hancock, H.-G. Sahl, Antimicrobial and host-defense peptides as new anti-infective therapeutic strategies, Nature biotechnology, 24 (2006) 1551.
[352] P. Hamill, K. Brown, H. Jenssen, R.E. Hancock, Novel anti-infectives: is host defence the answer?, Current opinion in biotechnology, 19 (2008) 628-636.
[353] M. Zasloff, Antimicrobial peptides of multicellular organisms, nature, 415 (2002) 389.
[354] G. Diamond, N. Beckloff, A. Weinberg, K.O. Kisich, The roles of antimicrobial peptides in innate host defense, Current pharmaceutical design, 15 (2009) 2377-2392.
[355] A.K. Marr, W.J. Gooderham, R.E. Hancock, Antibacterial peptides for therapeutic use: obstacles and realistic outlook, Current opinion in pharmacology, 6 (2006) 468-472.
[356] B. Mojsoska, G. Carretero, S. Larsen, R.V. Mateiu, H. Jenssen, Peptoids successfully inhibit the growth of gram negative E. coli causing substantial membrane damage, Scientific reports, 7 (2017) 42332.
[357] N.P. Chongsiriwatana, J.A. Patch, A.M. Czyzewski, M.T. Dohm, A. Ivankin, D. Gidalevitz, R.N. Zuckermann, A.E. Barron, Peptoids that mimic the structure, function, and mechanism of helical antimicrobial peptides, Proceedings of the National Academy of Sciences, 105 (2008) 2794-2799.
[358] H. Jenssen, P. Hamill, R.E. Hancock, Peptide antimicrobial agents, Clinical microbiology reviews, 19 (2006) 491-511.
[359] R.F. Epand, L. Raguse, S.H. Gellman, R.M. Epand, Antimicrobial 14-helical β-peptides: potent bilayer disrupting agents, Biochemistry, 43 (2004) 9527-9535.
[360] E.A. Porter, B. Weisblum, S.H. Gellman, Mimicry of host-defense peptides by unnatural oligomers: antimicrobial β-peptides, Journal of the American Chemical Society, 124 (2002) 7324-7330.
[361] A. Ivankin, L. Livne, A. Mor, G.A. Caputo, W.F. DeGrado, M. Meron, B. Lin, D. Gidalevitz, Role of the conformational rigidity in the design of biomimetic antimicrobial compounds, Angewandte Chemie International Edition, 49 (2010) 8462-8465.

[362] B.C. Hamper, S.A. Kolodziej, A.M. Scates, R.G. Smith, E. Cortez, Solid phase synthesis of β-peptoids: N-substituted β-aminopropionic acid oligomers, The Journal of organic chemistry, 63 (1998) 708-718.
[363] A. Violette, M.C. Averlant-Petit, V. Semetey, C. Hemmerlin, R. Casimir, R. Graff, M. Marraud, J.-P. Briand, D. Rognan, G. Guichard, N, N ‘-Linked Oligoureas as Foldamers: Chain Length Requirements for Helix Formation in Protic Solvent Investigated by Circular Dichroism, NMR Spectroscopy, and Molecular Dynamics, Journal of the American Chemical Society, 127 (2005) 2156-2164.
[364] L. Arnt, G.N. Tew, New poly (phenyleneethynylene) s with cationic, facially amphiphilic structures, Journal of the American Chemical Society, 124 (2002) 7664-7665.
[365] R.N. Zuckermann, J.M. Kerr, S.B. Kent, W.H. Moos, Efficient method for the preparation of peptoids [oligo (N-substituted glycines)] by submonomer solid-phase synthesis, Journal of the American Chemical Society, 114 (1992) 10646-10647.
[366] S. Rotem, A. Mor, Antimicrobial peptide mimics for improved therapeutic properties, Biochimica et Biophysica Acta (BBA)-Biomembranes, 1788 (2009) 1582-1592.
[367] S.M. Miller, R.J. Simon, S. Ng, R.N. Zuckermann, J.M. Kerr, W.H. Moos, Proteolytic studies of homologous peptide and N-substituted glycine peptoid oligomers, Bioorganic & medicinal chemistry letters, 4 (1994) 2657-2662.
[368] C.W. Wu, K. Kirshenbaum, T.J. Sanborn, J.A. Patch, K. Huang, K.A. Dill, R.N. Zuckermann, A.E. Barron, Structural and spectroscopic studies of peptoid oligomers with α-chiral aliphatic side chains, Journal of the American Chemical Society, 125 (2003) 13525-13530.
[369] K. Kirshenbaum, A.E. Barron, R.A. Goldsmith, P. Armand, E.K. Bradley, K.T. Truong, K.A. Dill, F.E. Cohen, R.N. Zuckermann, Sequence-specific polypeptoids: a diverse family of heteropolymers with stable secondary structure, Proceedings of the National Academy of Sciences, 95 (1998) 4303-4308.
[370] P. Armand, K. Kirshenbaum, R.A. Goldsmith, S. Farr-Jones, A.E. Barron, K.T. Truong, K.A. Dill, D.F. Mierke, F.E. Cohen, R.N. Zuckermann, NMR determination of the major solution conformation of a peptoid pentamer with chiral side chains, Proceedings of the National Academy of Sciences, 95 (1998) 4309-4314.
[371] C.A. Olsen, Peptoid–peptide hybrid backbone architectures, ChemBioChem, 11 (2010) 152-160.
[372] J.E. Murphy, T. Uno, J.D. Hamer, F.E. Cohen, V. Dwarki, R.N. Zuckermann, A combinatorial approach to the discovery of efficient cationic peptoid reagents for gene delivery, Proceedings of the National Academy of Sciences, 95 (1998) 1517-1522.
[373] C. García-Martínez, M. Humet, R. Planells-Cases, A. Gomis, M. Caprini, F. Viana, E. De la Peña, F. Sanchez-Baeza, T. Carbonell, C. De Felipe, Attenuation of thermal nociception and hyperalgesia by VR1 blockers, Proceedings of the National Academy of Sciences, 99 (2002) 2374-2379.
[374] R.N. Zuckermann, E.J. Martin, D.C. Spellmeyer, G.B. Stauber, K.R. Shoemaker, J.M. Kerr, G.M. Figliozzi, D.A. Goff, M.A. Siani, R.J. Simon, Discovery of nanomolar ligands for 7-transmembrane G-protein-coupled receptors from a diverse N-(substituted) glycine peptoid library, Journal of medicinal chemistry, 37 (1994) 2678-2685.
[375] Z. Wu, M. Tan, X. Chen, Z. Yang, L. Wang, Molecular hydrogelators of peptoid–peptide conjugates with superior stability against enzyme digestion, Nanoscale, 4 (2012) 3644-3646.
[376] G.K. Olivier, A. Cho, B. Sanii, M.D. Connolly, H. Tran, R.N. Zuckermann, Antibody-mimetic peptoid nanosheets for molecular recognition, ACS nano, 7 (2013) 9276-9286.

[377] N.P. Chongsiriwatana, J.S. Lin, R. Kapoor, M. Wetzler, J.A. Rea, M.K. Didwania, C.H. Contag, A.E. Barron, Intracellular biomass flocculation as a key mechanism of rapid bacterial killing by cationic, amphipathic antimicrobial peptides and peptoids, Scientific reports, 7 (2017) 16718.
[378] A.M. Czyzewski, H. Jenssen, C.D. Fjell, M. Waldbrook, N.P. Chongsiriwatana, E. Yuen, R.E. Hancock, A.E. Barron, In vivo, in vitro, and in silico characterization of peptoids as antimicrobial agents, PloS one, 11 (2016) e0135961.
[379] R.A. Moore, N.C. Bates, R. Hancock, Interaction of polycationic antibiotics with Pseudomonas aeruginosa lipopolysaccharide and lipid A studied by using dansyl-polymyxin, Antimicrobial agents and chemotherapy, 29 (1986) 496-500.
[380] S. Fidai, S.W. Farmer, R.E. Hancock, Interaction of cationic peptides with bacterial membranes, in: Antibacterial Peptide Protocols, Springer, 1997, pp. 187-204.
[381] D. Dunn, S. Raghavan, R. Volz, Gentamicin sulfate attachment and release from anodized Ti-6Al-4V orthopedic materials, Journal of Biomedical Materials Research Part A, 27 (1993) 895-900.
[382] J. Pan, D. Thierry, C. Leygraf, Electrochemical and XPS studies of titanium for biomaterial applications with respect to the effect of hydrogen peroxide, Journal of biomedical materials research, 28 (1994) 113-122.
[383] C. Larsson, P. Thomsen, J. Lausmaa, M. Rodahl, B. Kasemo, L. Ericson, Bone response to surface modified titanium implants: studies on electropolished implants with different oxide thicknesses and morphology, Biomaterials, 15 (1994) 1062-1074.

LIST OF PUBLICATIONS

(A) Journal Publications from Thesis

1. **Abshar Hasan** and Lalit M. Pandey. Polymers, surface-modified polymers, and self-assembled monolayers as surface-modifying agents for biomaterials. Polymer-Plastics Technology and Engineering, 2015, 54, 1358-1378.
2. **Abshar Hasan** and Lalit M. Pandey. Kinetic studies of attachment and re-orientation of octyltriethoxysilane for formation of self-assembled monolayer on a silica substrate. Materials Science and Engineering: C, 2016, 68, 423-429.
3. **Abshar Hasan**, Varun Saxena and Lalit M. Pandey. Surface Functionalization of Ti6Al4V via Self-assembled Monolayers for Improved Protein Adsorption and Fibroblast Adhesion. Langmuir, 2018, 34, 3494–3506.
4. **Abshar Hasan**, Lalit M. Pandey. Chapter - Self-assembled monolayers in biomaterials. Book-Nanobiomaterials, 2017, 137-178.
5. **Abshar Hasan**, Lalit M. Pandey, Conformational and Organizational Insights into Serum Proteins during Competitive Adsorption on Self-Assembled Monolayers. Langmuir, 2018, 34, 8178−8194.
6. **Abshar Hasan**, Sudip K. Pattanayek, and Lalit M. Pandey. Effect of Functional Groups of Self-Assembled Monolayers on Protein Adsorption and Initial Cell Adhesion. ACS Biomater. Sci. Eng., 2018, 4, 3224−3233.

(B) Journal Publications from Miscellaneous Work

7. **Abshar Hasan**, Gyan Waibhaw, Sakshi Tiwari, K. Dharmalingam, Ishani Shukla, Lalit M. Pandey. Fabrication and characterization of chitosan, polyvinylpyrrolidone, and

cellulose nanowhiskers nanocomposite films for wound healing drug delivery application. Journal of Biomedical Materials Research Part A, 2017, 105, 2391-2404.

8. **Abshar Hasan**, Gyan Waibhaw, Varun Saxena, Lalit M. Pandey. Nano-biocomposite scaffolds of chitosan, carboxymethyl cellulose and silver nanoparticle modified cellulose nanowhiskers for bone tissue engineering applications. International journal of biological macromolecules, 2018, 111, 923-934.
9. Varun Saxena, **Abshar Hasan**, Lalit M. Pandey. Effect of Zn/ZnO integration with hydroxyapatite: a review Materials Technology, 2018, 33, 79-92.
10. Varun Saxena, **Abshar Hasan**, Swati Sharma and Lalit M. Pandey, Edible oil nanoemulsion: An organic nanoantibiotic as a potential biomolecule delivery vehicle. International Journal of Polymeric Materials, 2017, 10.1080/00914037.2017.1332625
11. Sakshi Tiwari, **Abshar Hasan**, Lalit M. Pandey. A novel bio-sorbent comprising encapsulated *Agrobacterium fabrum* (SLAJ731) and iron oxide nanoparticles for removal of crude oil co-contaminant, lead Pb(II). Journal of Environmental Chemical Engineering, 2017, 5, 442–452.
12. Swati Sharma, Sakshi Tiwari, **Abshar Hasan**, Varun Saxena, Lalit M. Pandey. Recent advances in conventional and contemporary methods for remediation of heavy metal-contaminated soils. 3 Biotech, 2018, 8, 216.
13. Rasmi R. Bahera, **Abshar Hasan**, Lalit M. Pandey and Mamilla R. Sankar. Laser cladding with HA and functionally graded TiO2-HA precursors on Ti-6Al-4V alloy for enhancing bioactivity and cyto-compatibility. Surface and Coatings Technology, 2018, 352, 420–436.

14. Sunayan Deka, Varun Saxena, **Abshar Hasan**, Pranjal Chandra and Lalit M. Pandey. Synthesis, characterization and in vitro analysis of α-Fe2O3-GdFeO3 biphasic materials as therapeutic agent for magnetic hyperthermia applications. Materials Science and Engineering C, 2018, 92, 932–941.
15. Swati Sharma, **Abshar Hasan**, Naveen. Kumar, Lalit M. Pandey. Removal of methylene blue dye from aqueous solution using immobilized *Agrobacterium fabrum* biomass along with iron-oxide nanoparticles as biosorbent. Environmental Science and Pollution Research, 2018, 25, 21605–15.

(C) Publications under preparation

16. **Abshar Hasan**, Lalit M. Pandey, and King H.A. Lau. Antifouling surface preparation using antimicrobial peptoids for biomedical applications.
17. **Abshar Hasan** and Lalit M. Pandey. Role of interfaces during surface-biological fluid interactions: Perspectives from protein behavior and cell adhesion processes.
18. **Abshar Hasan**, Lalit M. Pandey, and King H.A. Lau. Self assembled antibacterial micelles from amphiphilic lipopeptoids.
19. **Abshar Hasan** and Lalit M. Pandey. Integrin expression kinetics on Hybrid surfaces.

(D) Book Chapter(s)

1. **Abshar Hasan** and Lalit M. Pandey. Self-assembled monolayers in biomaterials, 137-178, In Nanobiomaterials- Nanostructured Materials for Biomedical Applications, Woodhead Publishing, Elsevier, 2018.

(E) Conferences Publications

1. **Abshar Hasan** and Lalit M. Pandey. Polymers, surface modified polymers and self-assembled monolayer as surface modifying agents for biomaterials, poster presented at "International Conference of Disease Biology and Therapeutics (ICDBT)" organized by Institute of Advanced Study in Science and Technology, Guwahati, December, 2014.
2. **Abshar Hasan** and Lalit M. Pandey. Kinetics of formation of self-assembled monolayers of octyltriethoxysilane (TEOS) on silica substrates, poster presented at "5th International conference on Advanced Nanomaterials and Nanotechnology (ICANN)" organized by Centre of Nanotechnology, IIT-Guwahati, December-2015.
3. **Abshar Hasan**, Ajeet Singh and Lalit M. Pandey. Study on competitive protein adsorption on mono, mixed and hybrid self-assembled monolayers" presented at "International Conference on "Advances in Biological Systems and Materials Science in NanoWorld" organized by Physics Department, IIT (BHU), from 19-23 February, 2017.
4. **Abshar Hasan**, Lalit M. Pandey and King H.A. Lau. Antibacterial surface modifications for biomedical applications presented at "Annual Strathwide Conference 2018" organized by University of Strathclyde, Glasgow, 6 June, 2018.
5. **Abshar Hasan**, Lalit M. Pandey, Michelle Maclean, Karen Faulds, and King H.A. Lau. Antifouling Surface Modification for Biomedical Applications presented at "8th International Meeting on Antimicrobial Peptides". Edinburgh, UK, 2-4 September, 2018.

(F) Awards

1. Received prestigious Commonwealth Split-site Fellowship-2018 for one year (October 2017 to September 2018) to work at Dr. King Hang Aaron Lau's lab, Dept. of Pure and Applied Chemistry at University of Strathclyde, UK.